THE UNIVERSITY OF OKLAHOMA
GRADUATE COLLEGE

MULTIDISCIPLINARY DESIGN OPTIMIZATION OF AIRCRAFT WING STRUCTURES WITH AEROELASTIC AND AEROSERVOELASTIC CONSTRAINTS

A DISSERTATION
SUBMITTED TO THE GRADUATE FACULTY
In partial fulfillment of the requirements for the
degree of
DOCTOR OF PHILOSOPHY

By
SANG-YOUNG JUNG
Norman, Oklahoma
1999

UMI Number: 9914421

MULTIDISCIPLINARY DESIGN OPTIMIZATION OF AIRCRAFT WING STRUCTURES WITH AEROELASTIC AND AEROSERVOELASTIC CONSTRAINTS

A DISSERTATION APPROVED FOR THE SCHOOL OF AEROSPACE AND MECHANICAL ENGINEERING

By

A. G. Striz

M. C. Altan

R. Parthasarathy

T. Trafalis

Acknowledgments

The author wishes to acknowledge with great appreciation and pleasure the invaluable advice, support, encouragement, and supervision given by his advisor, Dr. Alfred G. Striz, Professor, School of Aerospace and Mechanical Engineering, during the progress of this study. The author has been fortunate for having received full support from the other members of his advisory committee.

The author is thankful to Dr. Dudley E. Smith and Dr. Ramkumar Parthasarathy for their advice in the field of aerodynamics, to Dr. M. Cengiz Altan for his valuable suggestions and advice in the field of composite materials throughout the study, and to Dr. Theodore Trafalis for his suggestions in the field of optimization.

A large part of this dissertation was performed under a subcontract of a US AF/STTR Phase II contract (No. F33615-96-C-3217) to ZONA Technology, Inc. Thanks goes to Dr. Danny Liu, Dr. P. C. Chen, and Darius Sarhaddi of ZONA Technology, Inc., for their continual assistance with ZAERO and ASTROS* matters. They made this dissertation possible.

Special thanks is extended to the author's wife, Young-Hee Kwon, and to his two daughters, Suyeon and Sumin, for their understanding, support, and encouragement

TABLE OF CONTENTS

LIST OF TABLES

LIST OF FIGURES

NOMENCLATURE

[A], [B], [C], and [D]	: Matrices in State-Space Equation
a	: Speed of Sound
b	: Reference Length (Semi-chord), $b = c/2$
c	: Chord Length
C_L, C_m, C_δ	: Coefficients of Lift, Wing Moment, and Aileron Moment
$C_{L\alpha}$	: Slope of Lift Coefficient Curve
C_p	: Pressure Coefficient
G_j	: Gain Factor for j-th Actuator
$\mathbf{F}$	: Functionals in Multidisciplinary System
$\{F\}$	: Force Vector
g	: Structural Damping
$\mathbf{g}(\mathbf{x})$ or $g_i(\mathbf{x})$	: Inequality Constraint
$\mathbf{h}(\mathbf{x})$ or $h_i(\mathbf{x})$	: Equality Constraint
h	: Plunging Degree of Freedom
J	: Jacobian Transformation
k	: Reduced Frequency, $\omega b/V$
L_j	: Quantity Obtained from Sensor
M	: Freestream Mach Number

$[M]$, $[C]$, $[K]$	: Modal Mass, Damping, and Stiffness Matrices
$[m]$, $[c]$, $[k]$	: Mass, Damping, and Stiffness Matrices of Physical DOFs
$\{p\}$, $\{\bar{p}\}$	: Pressure and Pressure Amplitude, $p_t = \bar{p}_t e^{ikt}$
$[q]$	: Physical Coordinates and Dynamic Pressure
$\{Q\}$	: Generalized Aerodynamic Force Vector
s	: Span
s, $\bar{s}$	: Laplace Transform Variable, Non-dimensional Laplace Transform Variable
S	: Wing Area
t, τ	: Time and Nondimensional Time
$\{u\}$	: Actuator Input
$\{U\}$, $\{\bar{U}\}$	: Right and Left Eigenvectors
u, v, and w	: Flow Velocity
V	: Freestream Velocity
$\{w\}$, $\{\bar{w}\}$	: Downwash and Amplitude of Downwash, $w_t = \bar{w}_t e^{ikt}$
$\{X\}$	: Design Variable Vector
$\{x\}$	: State Vector
x, y, z	: Cartesian Coordinates
$\{Y\}$	: Intermediate Design Variable Vector
α	: Angle of Attack
β	: $(1-M^2)^{1/2}$

γ	: Ratio of Specific Heats
δ	: Control Surface Deflection
ϕ	: Velocity Potential
$\{\phi\}$ and $[\Phi]$	: Modal vector and Modal Matrix
$\{\phi_y\}$	: Sensor Output Vector
φ	: Phase Angle
μ	: Viscosity Coefficient or Air Mass Ratio
ρ	: Air Density
Λ	: Sweep Back Angle
τ	: Non-dimensional Time
ω	: Frequency of System
ω_n, ω_h, ω_α, ω_δ	: Natural Frequencies
ξ, η, and ζ	: Curvilinear Coordinates
$\{\eta\}$	: Modal Vector or Generalized Coordinate Vector
ζ	: Modal Damping Coefficient

Subscript or Superscript

c	: Control Surface
f	: Flutter Point
s	: Structure
x, y, z, t	: Differentiation with Respect to x, y, z, and t, Respectively

ABSTRACT

Design procedures for aircraft wing structures with control surfaces are presented using multidisciplinary design optimization. Several disciplines such as stress analysis, structural vibration, aerodynamics, and controls are considered simultaneously and combined for design optimization. Vibration data and aerodynamic data including those in the transonic regime are calculated by existing codes. Flutter analyses are performed using those data. A flutter suppression method is studied using control laws in the closed-loop flutter equation. For the design optimization, optimization techniques such as approximation, design variable linking, temporary constraint deletion, and optimality criteria are used. Sensitivity derivatives of stresses and displacements for static loads, natural frequency, flutter characteristics, and control characteristics with respect to design variables are calculated for an approximate optimization. The objective function is the structural weight. The design variables are the section properties of the structural elements and the control gain factors. Existing multidisciplinary optimization codes (ASTROS* and MSC/NASTRAN) are used to perform single and multiple constraint optimizations of fully built up finite element wing structures. Three benchmark wing models are developed and/or modified for this purpose. The models are tested extensively.

Chapter 1

INTRODUCTION

When designing aircraft structures, the most important and difficult efforts are the analysis and design of the wing structures. It should be verified that the wing structure of an aircraft is stable with regard to aeroservoelasticity as well as in strength and buckling. To analyze and design such aeroelastic systems with control surfaces, the interactions of several disciplines such as statics, structural vibration, aerodynamics, and control laws need to be considered. Several design procedures for wing structures with control surfaces are presented here by multidisciplinary design optimization.

The Automated STRuctural Optimization System (ASTROS) is a finite element based optimization code tailored to the preliminary design of aerospace structures (Ref. 1.1), but applicable to other industries involving light weight structural design coupled with other disciplines. As such it combines generality with the flexibility of multiple discipline integration. For the design of aircraft, spacecraft, or missiles, ASTROS can save design effort and time, improve flight performance, and reduce structural weight. Specifically, ASTROS was created to allow for the effective multidisciplinary interaction between aerodynamics, structures, controls, and other modules. Although today a well acclaimed, proven tool for MDO and multidisciplinary analysis, ASTROS still required further improvement in its capabilities in steady/unsteady aerodynamics, aeroelasticity, and aeroservoelasticity (e.g., Ref. 1.6).

While an enhancement of the aero*servo*elastic capabilities is in progress, the seamless integration of a unified aerodynamic module (ZAERO, developed by ZONA Technology, Inc.) for all Mach numbers with ASTROS has been completed. The new code is called ASTROS*. The present module ZAERO improves the capabilities of ASTROS* in several ways: it allows for the modeling, analysis, and optimization of realistic wing-body configurations, and it adds the nonlinear unsteady transonic/hypersonic flow regimes to the Mach number ranges already supported in ASTROS.

Specifically, the ZAERO module consists of four major steady/unsteady aerodynamic codes that jointly cover the complete flyable Mach number range, namely the subsonic code ZONA6, the transonic code ZTAIC, the supersonic code ZONA7, and the hypersonic code ZONA7U. Together they enhance the purely subsonic and supersonic capabilities for lifting surface type of configurations presently available in ASTROS. Thus, the ZAERO module serves as a general unified aerodynamic tool which can generate steady/unsteady aerodynamic data for general wing-body configurations throughout all Mach numbers by means of a unified AIC (Aerodynamic Influence Coefficient) approach, called UAIC. In detail, the different codes have the following capabilities:

- *ZONA6:* Subsonic steady/unsteady aerodynamics for arbitrary wing-body configurations with or without external stores including body wake effects.

- *ZTAIC:* Unsteady transonic AIC method using externally provided steady pressure input.
- *ZONA7:* Supersonic steady/unsteady aerodynamics for arbitrary wing-body configurations with or without external stores. ZONA51 is the wing/lifting surface option of ZONA7.
- *ZONA7U:* Unified hypersonic and supersonic steady/unsteady aerodynamics for arbitrary wing-body configurations with or without external stores.

The present objective is to present benchmarking and applications test cases for the validation of ASTROS* and to exercise some of its new capabilities in the unified Mach flight regime of subsonic-transonic-supersonic and hypersonic speeds with various wing planforms.

To perform structural design optimization, analyses are performed first and sensitivity data are calculated for the optimization. The accuracy of the design optimization closely depends on the exactness of the analysis. The FEM (Finite Element Method) is normally used to analyze large complex aircraft structures, and the properties of the respective elements are then used as design variables to perform weight optimization.

The structural analyses were performed here by the commercial FEM based optimization code ASTROS* (Ref. 1.1) and some by MSC/NASTRAN (Ref. 1.2). Static and normal modes analyses were performed first to check the FEM models, to understand their behavior, and to obtain the structural characteristics. Aeroelastic analysis and design begin with normal modes analysis. Normal modes data such as the natural frequencies, modes shapes, generalized mass, and generalized stiffness were calculated for various wing structures and those data were used to perform aeroelastic analyses.

Aerodynamic data are necessary to calculate the aeroelastic properties of a wing. Steady aerodynamic loads are normally used for static aeroelasticity and unsteady aerodynamic loads are required for flutter calculations. Steady aerodynamic pressure coefficients were required to calculate unsteady aerodynamic loads in transonic flow. Here, the steady aerodynamic pressure coefficients in the transonic regime were calculated by the CFD code, ENSAERO (Ref. 1.3). The steady and unsteady aerodynamic loads were then calculated by ASTROS* and some by MSC/NASTRAN for subsonic and supersonic flow, and by ZTAIC in ASTROS* for transonic flow. ZTAIC, using the Transonic Equivalent Method (TES), was recently incorporated into ASTROS* as mentioned above.

Aeroelastic analyses require structural and aerodynamic data. There are many fields in aeroelasticity as stated in Chapter 1 of Ref. 1.4. Static aeroelasticity and flutter were considered here. In static aeroelasticity, the trim parameters such as angle of attack, rotational velocity, rotational acceleration, control surface deflection angles, stability derivatives, and pressure distribution were calculated including the effects of the elastic deformation of the wing. The displacements and stresses of the wing were obtained at the trim condition. Static aeroelastic analysis and optimization were performed by ASTROS*.

Flutter is the dynamic instability of the structure under the interaction of aerodynamic, inertial, and elastic loads. In flutter analysis, the flutter speed, the flutter frequency, and the flutter mode shape were computed. Flutter analyses were performed by ASTROS* and some by MSC/NASTRAN by the k-method and the pk-method, respectively. Flutter speeds were also calculated by the root-locus method. The results from the three methods were compared.

For active control, the frequency domain method was used. The aerodynamic loads were approximated by the minimum-state method (Ref. 1.5). An actuator was added to the system and the loop was closed using a feedback control law. Output feedback was used here. The actuator parameters were designed such as to maximize the flutter speed.

Sensitivities of the objective function and the constraints with respect to the design variables are necessary to perform design optimization. Sensitivity derivatives of the flutter characteristics, such as flutter speed and flutter frequency, and of the stability margins, such as the gain margin and the phase margin, with respect to the design variables were calculated for flutter optimization and flutter suppression.

In the structural optimization of a wing, the objective function is the structural weight, and possible constraints are the displacements and stresses, natural frequencies, flutter speed, and gain margin requirements. The design variables are the properties of the structural elements and the control parameters. Here, for isotropic materials, the skin thicknesses and bar cross-sectional areas were the design variables. For composite materials, the thicknesses of the plies were the design variables.

Because actual wing structures are complex and require considerable CPU time, several optimization techniques such as approximate optimization, design variable linking, and temporary constraints deletion were used together with optimality criteria methods. In the design optimization sections, the analysis and design capabilities of the commercial codes ASTROS* and MSC/NASTRAN were used and were also combined with mathematical programming approaches in application to large and complex wing structures under aeroelastic constraints.

The mathematical optimization problems can be solved by one of many different optimizers such as NPSOL, ADS, DOT/DOC, the IMSL module in MS-FORTRAN, and the optimization module in MATLAB. Here, NPSOL was used in the complex structural optimization problem with the constraints of strength, displacement, the lowest natural frequency, and flutter speed, and IMSL was used in the simple unconstrained optimization problem of flutter suppression.

All of these design procedures were applied to the GAF (Generalized Advanced Fighter) wing, the DAST (Drones for Aerodynamic and Structural Testing) wing, and the AAW (ASTROS* Aeroelastic Wing) models. These three models were used to validate ASTROS* and to show its widened applicability in all Mach number ranges.

Chapter 2

STRUCTURAL ANALYSIS

2.1 Introduction

The finite element method is the most popular and powerful method to perform structural analysis. Many codes such as MSC/NASTRAN, ANSYS, I-DEAS, SAP90, ASTROS, ANALYZE, etc., have extensive capabilities for the analysis of complex structures. Here, MSC/NASTRAN and ASTROS were utilized to obtain structural characteristics. When using such codes for actual complex structures, e.g., aircraft, ground vehicles, or satellites, accurate FEM modeling is not easy and takes time. Solid knowledge of the finite element method and the coding format for each program is necessary together with knowledge about the behavior of the structure to use an FEM code effectively. To obtain acceptable results for advanced applications such as response analysis, flutter analysis, and structural design optimization, FEM models should first be checked carefully in static analysis and normal modes analysis.

In this chapter, the necessity and importance of static and vibration analysis in structural analysis and optimization using the finite element method are described. The basic govern equations of motion used in normal modes and response analysis are reviewed with the help of Refs. 2.1 and 2.2. Some explanations about normal modes analysis of aircraft wing structures by ASTROS* and MSC/NASTRAN are given in Section 2.3.4.

2.2 Static and Buckling Analysis

When aircraft wing structures are designed, the basic minimum sizes of areas or thicknesses are often determined such that the wings do not fail under applied static loads. Failure modes can be fracture, excessive displacements, and/or buckling of the structure. If a wing is unstable statically, structural design optimizations can be used to improve the design. This topic is not treated here in detail, but static analyses were performed by ASTROS* and MSC/NASTRAN to check out the FEM models.

2.3 Structural Vibration Analysis

2.3.1 Normal Modes Analysis

Flutter analysis starts with normal modes analysis. The infinite dimensional space required to represent the exact motion of an aeroelastic system can be reduced to a finite dimensional space by the technique of truncated normal modes (Ref. 1.4). Normal modes data such as natural frequencies, mode shapes, generalized masses, and generalized stiffnesses are used for flutter analysis or dynamic response analysis where the structural behavior is linear. The equations of motion for the calculation of natural frequencies and normal modes are (Refs. 2.1 and 2.2)

$$[m]\{\ddot{q}\}+[k]\{q\}=0 \tag{2.1}$$

where $\{q\}$ is the vector of physical displacements, $[m]$ is the physical mass matrix, and $[k]$ is the physical stiffness matrix of the structural system. To solve Eq. (2.1), the motion is assumed harmonic of the form

$$\{q\} = \{\phi\} \cdot e^{i\omega t} \tag{2.2}$$

where $\{\phi\}$ is the eigenvector or mode shape and ω is the circular frequency. If Eq. (2.2) is substituted into Eq. (2.1), the equation of motion is simplified to

$$\left[\ [k] - \omega^2 [m]\ \right]\{\phi\} = 0 \tag{2.3}$$

For a nontrivial solution of Eq. (2.3),

$$\left|\ [k] - \lambda [m]\ \right| = 0 \tag{2.4}$$

where $\lambda = \omega^2$ is called an eigenvalue. There exists a set of eigenvalues λ_i or ω_i^2 and eigenvectors $\{\phi_i\}$ corresponding to each eigenvalue. For the i-th eigenvalue, the related natural frequency is $f_i = \dfrac{\omega_i}{2\pi}$.

When a linear elastic structure is vibrating in free or forced vibration, its deflected shape at any given time is assumed as a linear combination of all of its normal modes

$$\{q(t)\} = \sum_i \{\phi_i\}\eta_i(t) = [\Phi]\{\eta\} \tag{2.5}$$

where $\{\phi_i\}$ is the i-th mode shape, $[\Phi] = [\phi_1, \phi_2, \cdots, \phi_n]$, and η_i is the i-th modal displacement. If $[k]$ and $[m]$ are symmetric and real,

$$\{\phi_i\}^T[m]\{\phi_j\} = 0,$$

$$\{\phi_i\}^T[k]\{\phi_j\} = 0 \qquad \text{if } i \neq j \tag{2.6}$$

and the i-th generalized mass and generalized stiffness are defined, respectively, as

$$M_i = \{\phi_i\}^T[m]\{\phi_i\},$$

$$K_i = \{\phi_i\}^T[k]\{\phi_i\} \tag{2.7}$$

Substituting Eq. (2.5) into Eq. (2.1) and premultiplying by $\{\phi_i\}^T$ results in

$$\sum_i \left(\{\phi_i\}^T[m]\{\phi_i\}\ddot{\eta}_i + \{\phi_i\}^T[k]\{\phi_i\}\eta_i \right) = 0 \tag{2.8}$$

with $\eta_i(t) = \overline{\eta}_i e^{j\omega_i t}$, Rayleigh's equation is obtained

$$\omega_i^2 = \frac{\{\phi_i\}^T[k]\{\phi_i\}}{\{\phi_i\}^T[m]\{\phi_i\}} \tag{2.9}$$

Because the scaling of normal modes is arbitrary, there exist several methods to normalize the modes. One of the methods scales each eigenvector to result in a unit value of generalized mass as

$$[M] = [\Phi]^T[m][\Phi] = [I],$$

$$[K] = [\Phi]^T[k][\Phi] = [\omega_i^2] \tag{2.10}$$

This is more convenient for flutter analysis than other methods.

2.3.2 Modal Frequency Response Analysis

Actually, flutter analysis is a sort of response analysis of forced vibrations generated by the air flow. To understand flutter calculations, response vibration analysis should be understood. There exist several methods to analyze forced vibration. The modal frequency method and the modal transient method are often used for this type of analysis. The appropriate equations of motion can be derived as follows (Refs. 2.1 and 2.2):

The damped forced vibration equation of motion in physical coordinates $\{q(t)\}$ is

$$[m]\{\ddot{q}(t)\}+[c]\{\dot{q}(t)\}+[k]\{q(t)\}=\{F(t)\} \tag{2.11}$$

When the excitation force is harmonic, this can be represented by

$$[m]\{\ddot{q}(t)\}+[c]\{\dot{q}(t)\}+[k]\{q(t)\}=\{F(\omega)\}e^{i\omega t} \tag{2.12}$$

A harmonic solution is assumed:

$$\{q(t)\}=\{q(\omega)\}e^{i\omega t} \tag{2.13}$$

Substituting Eq. (2.13) into Eq. (2.12) yields

$$-\omega^2[m]\{q(\omega)\}+i\omega[c]\{q(\omega)\}+[k]\{q(\omega)\}=\{F(\omega)\} \tag{2.14}$$

If we change the physical coordinates to modal coordinates

$$\{q(\omega)\}=[\Phi]\{\eta(\omega)\} \tag{2.15}$$

where $[\Phi]$ is the modal matrix, the equation of motion becomes

$$-\omega^2[m][\Phi]\{\eta(\omega)\}+i\omega[c][\Phi]\{\eta(\omega)\}+[k][\Phi]\{\eta(\omega)\}=\{F(\omega)\} \tag{2.16}$$

Premultiplying by $[\Phi]^T$, we can obtain the following form of the equation of motion

$$[\ -\omega^2[M]+i\omega[C]+[K]\ ]\{\eta(\omega)\}=\{Q(\omega)\} \tag{2.17}$$

where $[M]$, $[C]$, $[K]$, and $\{Q\}$ are modal (generalized) mass matrix, modal (generalized) damping matrix, modal (generalized) stiffness matrix, and modal (generalized) force vector, respectively, defined by

$$\begin{aligned} [M] &= [\Phi]^T[m][\Phi] \\ [C] &= [\Phi]^T[c][\Phi] \\ [K] &= [\Phi]^T[k][\Phi] \\ \{Q(\omega)\} &= [\Phi]^T[F(\omega)] \end{aligned} \tag{2.18}$$

Here, if the modal matrix is normalized as in Eq. (2.10), and uncoupled modal damping is used, $[M]$ is a unit matrix, $[C]$ is a diagonal matrix whose components are $2\omega_i\zeta_i$, and $[K]$ is a diagonal matrix whose components are ω_i^2.

2.3.3 Modal Transient Response Analysis

We can change the physical coordinates to modal coordinates in the time domain:

$$\{q(t)\}=[\Phi]\{\eta(t)\} \tag{2.19}$$

Substituting Eq. (2.19) into Eq. (2.11), and simplifying, the equations of motion are derived as

$$[M]\{\ddot{\eta}(t)\}+[C]\{\dot{\eta}(t)\}+[K]\{\eta(t)\}=\{Q(t)\} \tag{2.20}$$

where

$$[M] = [\Phi]^T [m][\Phi]$$

$$[C] = [\Phi]^T [c][\Phi]$$

$$[K] = [\Phi]^T [k][\Phi] \tag{2.21}$$

$$\{Q(t)\} = [\Phi]^T [F(t)]$$

2.3.4 Normal Modes Analysis by ASTROS and MSC/NASTRAN

MSC/NASTRAN and ASTROS use several methods to solve Eq. (2.4) such as the Inverse Power method, the Given's method, and the Lanczos method. ASET (analysis set) degrees of freedom are usually defined to reduce the matrix size of Eq. (2.4) and, thus, CPU time. The vertical translation DoFs are generally sufficient for the ASET for a simple wing structure because the stiffness components for the vertical displacement are weaker than those of any other DoFs, and the lift of the wing is, in general, only dependent on the vertical displacements. However, other translation DoFs may be necessary for complex wing structures having control surfaces and/or stores. For aircraft models using bar elements to the model the fuselage, their rotational DoFs should be included in the ASET. A half aircraft model is generally generated to reduce the number of DoFs. In this case, all analyses such as normal modes analysis, static aeroelastic analysis, vibration response analysis, and flutter analysis should be performed for both symmetric and anti-symmetric boundary conditions.

Chapter 3

AERODYNAMIC ANALYSIS

3.1 Introduction

3.1.1 Background

Unsteady aerodynamic load calculations are the most difficult part of flutter analysis. To calculate flutter speeds correctly, accurate unsteady aerodynamic loads are necessary. The methods to calculate these loads are different for different air speed ranges. Analytical methods for the subsonic and supersonic regimes are well developed. There are, however, no analytical methods for non-linear transonic flow. Nowadays, Computational Fluid Dynamics (CFD) is used to calculate transonic aerodynamics. The small-disturbance potential equation, Euler equations, and Navier-Stokes equations are used for the formulations of CFD.

3.1.2. Review of Previous Work

In References 1.4 and 1.7, previous work regarding the calculation of unsteady aerodynamic loads by analytical methods were reviewed. Wagner first studied the growth of lift on a two-dimensional airfoil in incompressible flow due to an impulsive change in the vertical velocity of the airfoil in 1925 (Ref. 1.4). Theodorsen (Ref. 3.1) calculated the lift on an oscillating airfoil and Garrick and Rubinow (Ref. 3.2) showed the relation between Wagner's solution and

Theodosen's solution. R. T. Jones (Ref. 3.3) first considered the aerodynamic forces on finite wings of non-uniform motion in incompressible flow. Mzelsky and Drischler (Ref. 3.4) and Drischler (Ref. 3.5) obtained approximations to the indicial lift and moment in plunging and pitching in compressible flow over two-dimensional airfoils. Miles (Ref. 3.6) considered transient loading on finite wings at supersonic speeds. In 1969, Djojodihardjo and Widnall (Ref. 3.7) presented a numerical technique for arbitrarily moving airfoils and lifting surfaces based on Green's representation theorem in potential theory. Several techniques have been developed for the calculation of aerodynamic loads for simple harmonically oscillating airfoils and lifting surfaces. Cunningham (Ref. 3.8) used the Kernel function technique. Chen and Liu (Ref. 3.9 and 3.10) calculated the unsteady aerodynamics by the Harmonic Gradient Method.

Aerodynamic loads are generally calculated by CFD codes. Borland and Rizzetta (Ref. 3.12), Guruswamy (Ref. 3.13), Batina et. al. (Refs. 3.14-15), Ballhaus, et. al. (Refs. 3.16-18), Nixon (Ref. 3.19), Fung and Chung (Ref. 3.20), and Landahl (Ref. 3.21) calculated aerodynamic loads by the nonlinear potential equation for 2-dimensional flow. Liu, Kao, and Fung (Ref. 3.22) and Landahl (Ref. 3.21) calculated aerodynamic loads by the nonlinear potential equation for 3-dimensional flow. Guruswamy used the Euler equations (Ref. 3.23) and then the Navier-Stokes equations (Refs. 1.3 and 3.24) to calculate the unsteady aerodynamic loads of wings. Other references using CFD include Refs. 3.25-28.

Albano and Rodden (Ref. 3.11) developed the Doublet-Lattice technique via the linear potential equation. Similar methods were installed in commercial FEM programs such as ASTROS and MSC/NASTRAN and have been used for aeroelastic analyses and optimizations of aircraft structures as shown in Table 3.1.

3.1.3 Scope of Research

Steady and unsteady airloads in the subsonic and supersonic regimes can be calculated by ASTROS* and MSC/NASTRAN. ZTAIC, using the transonic equivalent strip (TES) method, was recently installed in ASTROS*. This module calculates unsteady aerodynamic loads in the transonic regime. ZTAIC needs transonic steady aerodynamic pressure coefficients as input. ENSAERO (Ref. 1.3), a transonic CFD code, is used to calculate these coefficients. All basic equations for aerodynamics are reviewed in the following. The theoretical background and the capabilities of ASTROS*, MSC/NASTRAN, and ENSAERO to calculate steady and unsteady aerodynamic loads are reviewed, as well.

3.2 Basic Equations of Aerodynamics

3.2.1 Conservation Equations in Navier-Stokes Flow

The strong conservation law form of the Navier-Stokes equations is often used for shock-capturing purposes. The non-dimensionalized governing equations, including the thin-layer Navier-Stokes equations (Ref. 3.24), are described in a generalized body-conforming curvilinear coordinate system for three dimensions as

$$\partial_\tau \hat{Q} + \partial_\xi \hat{E} + \partial_\eta \hat{F} + \partial_\zeta \hat{G} = \mathrm{Re}^{-1}\, \partial_\zeta \hat{G}^v \tag{3.1}$$

where $\tau = t$, $\xi = \xi(x,y,z,t)$, $\eta = \eta(x,y,z,t)$, and $\zeta = \zeta(x,y,z,t)$. The vector of conserved quantities $\hat{Q}$ and the inviscid flux vectors $\hat{E}$, $\hat{F}$, and $\hat{G}$ are

$$\hat{Q} = \begin{bmatrix} \rho \\ \rho u \\ \rho v \\ \rho w \\ e \end{bmatrix},\ \hat{E} = \frac{1}{J}\begin{bmatrix} \rho\hat{V} \\ \rho u\hat{V} + \xi_x p \\ \rho v\hat{V} + \xi_y p \\ \rho w\hat{V} + \xi_z p \\ \rho H\hat{V} - \xi_t p \end{bmatrix},\ \hat{F} = \frac{1}{J}\begin{bmatrix} \rho\hat{V} \\ \rho u\hat{V} + \eta_x p \\ \rho v\hat{V} + \eta_y p \\ \rho w\hat{V} + \eta_z p \\ \rho H\hat{V} - \eta_t p \end{bmatrix},\ \hat{G} = \frac{1}{J}\begin{bmatrix} \rho\hat{V} \\ \rho u\hat{V} + \zeta_x p \\ \rho v\hat{V} + \zeta_y p \\ \rho w\hat{V} + \zeta_z p \\ \rho H\hat{V} - \zeta_t p \end{bmatrix} \tag{3.2}$$

where H is the total enthalpy and $\hat{V}$ is the contravariant velocity component. The time metric is related to the grid velocity as

$$\xi_t = -\xi_x x_t - \xi_y y_t - \xi_z z_t \tag{3.3a}$$

$$\eta_t = -\eta_x x_t - \eta_y y_t - \eta_z z_t \tag{3.3b}$$

$$\zeta_t = -\zeta_x x_t - \zeta_y y_t - \zeta_z z_t \tag{3.3c}$$

The Cartesian velocity components *u, v,* and *w* are non-dimensionalized by the free-stream speed of sound a_∞, the density ρ is non-dimensionalized by the free stream density ρ_∞, and the total energy e is non-dimensionalized by $\rho_\infty a_\infty^2$. The viscous flux vector $\hat{G}^v$ is given by

$$\hat{G}^v = \frac{1}{J}\begin{bmatrix} 0 \\ \mu m_1 u_\zeta + \frac{\mu}{3} m_2 \zeta_x \\ \mu m_1 v_\zeta + \frac{\mu}{3} m_2 \zeta_y \\ \mu m_1 w_\zeta + \frac{\mu}{3} m_2 \zeta_z \\ \mu m_1 m_3 + \frac{\mu}{3} m_2 (\zeta_x u + \zeta_y v + \zeta_z w) \end{bmatrix} \tag{3.4}$$

where

$$\begin{aligned} m_1 &= \zeta_x^2 + \zeta_y^2 + \zeta_z^2 \\ m_2 &= \zeta_x \mu_\zeta + \zeta_y v_\zeta + \zeta_z w_\zeta \\ m_3 &= \frac{1}{2}(u^2 + v^2 + w^2)_\zeta + \frac{1}{\Pr(\gamma - 1)}(a^2)_\zeta \end{aligned} \tag{3.5}$$

and Re is the Reynolds number, Pr is the Prandtl number, a is the speed of sound, and J is the transformation Jacobian. For a perfect gas, the pressure is represented by

$$p = (\gamma - 1)\{e - \frac{\rho}{2}(u^2 + v^2 + w^2)\}. \tag{3.6}$$

where ρ is the fluid density, γ is the ratio of specific heats, and e is the total energy per unit volume of the fluid. The viscosity coefficient μ is computed as the sum of $\mu_l + \mu_t$ where μ_l is taken from the free-stream laminar viscosity, assumed to be constant for transonic flows, and the turbulent viscosity μ_t is evaluated by the Baldwin-Lomax algebraic eddy-viscosity model (Ref. 3.32) using thin-layer approximation. In this approximation, the viscous terms in the streamwise or near streamwise directions are neglected. The thin-layer equations are similar to the classical boundary-layer equations with the main exception that the normal momentum equation is retained here. This prevents the occurrence of the usual boundary singularity at a separation point. The modification of the turbulence model originally developed for crossflow separation by Degani and Schiff (Ref. 3.33) can be applied.

In Ref 3.28, David Nixon stated about the boundary conditions of the Navier-Stokes equations:

"For the incompressible Navier-Stokes equations in two dimensions, it is necessary and sufficient to specify all the velocity components on the boundary. It is expected, but not proven, that these are also correct boundary conditions for incompressible three-dimensional flow. No rigorous set of boundary conditions for compressible Navier-Stokes equations has been derived.

In high-Reynolds-number flow, the effect of viscosity is usually confined to a thin shear layer near the trailing edge. The flow outside of the region can be regarded as inviscid. Splitting the flow field between the thin layer and an outer inviscid region is generally used in computational applications. However, this boundary layer approximation creates matching or coupling problems between the inviscid and viscous flows. Furthermore, near separation, the viscous boundary-layer equations can have undesirable critical behavior."

3.2.2 Conservation Equations in Euler Flow

For most aerodynamic flows, the Reynolds number is much greater than one and, except for thin viscous layers, the overall flow can generally be considered to be inviscid. The Eqs. (3.1), becomes the conservation equations of Euler flow if the right hand side is set to zero, i.e.,

$$\partial_\tau \hat{Q} + \partial_\xi \hat{E} + \partial_\eta \hat{F} + \partial_\zeta \hat{G} = 0 \tag{3.7}$$

Like the Navier-Stokes flow, the pressure p is related to the other variables by Eq. (3.6). The boundary conditions for the Euler equations require the specification of the normal and tangential velocities at the boundary. In addition to the boundary conditions, the Kutta-Joukowski condition and an entropy condition are necessary to close the problem.

3.2.3 Small-Disturbance Potential Equation

Assuming the small perturbation velocity potential such that

$$u = V(1+\phi_x)\text{, } v = V\phi_y\text{, and } w = V\phi_z \tag{3.8}$$

with u, v, and w as the velocity components in a Cartesian co-ordinate system, using non-dimensional coordinates, and non-dimensionalizing t by multiplying the physical time by V/c, Marten T. Landahl (Ref. 3.21) derived the following partial differential equation for ϕ:

$$\begin{aligned}
&(1-M^2)\phi_{xx} + \phi_{yy} + \phi_{zz} - 2M^2\phi_{xt} - M^2\phi_{tt} = \\
&\quad M^2\{\tfrac{1}{2}(\gamma-1)(2\phi_x + 2\phi_t + \phi_x^2 + \phi_y^2 + \phi_z^2)(\phi_{xx} + \phi_{yy} + \phi_{zz}) \\
&\quad + (2\phi_x + \phi_x^2)\phi_{xx} + \phi_y^2\phi_{yy} + 2\phi_y\phi_z\phi_{yz} + \phi_z^2\phi_{zz} \\
&\quad + 2(1+\phi_x)(\phi_y\phi_{yx} + \phi_z\phi_{zx}) + 2(\phi_x\phi_{xt} + \phi_y\phi_{yt} + \phi_z\phi_{zt})\}
\end{aligned} \tag{3.9}$$

The pressure coefficient is represented by

$$C_p = -2\phi_x - 2\phi_t - \phi_y{}^2 - \phi_z{}^2 \tag{3.10}$$

Neglecting 3rd order terms and small terms,

$$M^2(\phi_t + 2\phi_x)_t = \{(1-M^2)\phi_x + F\phi_x{}^2 + G\phi_y{}^2\}_x + (\phi_y + H\phi_x\phi_y)_y + \phi_{zz} \tag{3.11}$$

where $F = -\frac{1}{2}(\gamma+1)M^2$, $G = \frac{1}{2}(\gamma-3)M^2$, $H = -(\gamma-1)M^2$

This equation is strictly valid only for isentropic flow but is a good approximation for flows with weak shocks. Borland and Rizzetta (Ref. 3.12), Guruswamy (Ref. 3.13), and Batina et. al. (Refs. 3.14-15) used this equation to calculate unsteady transonic aerodynamics. Neglecting 2nd order terms except $\phi_x\phi_{xx}$ results in

$$\{(1 - M^2 - M^2(\gamma+1)\phi_x\}\phi_{xx} + \phi_{yy} + \phi_{zz} - 2M^2\phi_{xt} - M^2\phi_{tt} = 0 \tag{3.12}$$

Ballhaus et. al. (Refs. 3.16-18), Nixon (Ref. 3.19), Fung and Chung (Ref. 3.20), and Landahl (Ref. 3.21) for 2-D, and Lie et. al. (Ref. 3.22) and Landahl (Ref. 3.21) for 3-D used this equation to calculate unsteady transonic aerodynamics. Neglecting all non-linear terms results in

$$\{(1 - M^2\}\phi_{xx} + \phi_{yy} + \phi_{zz} - 2M^2\phi_{xt} - M^2\phi_{tt} = 0 \tag{3.13}$$

This is the linearized partial differential equation for unsteady, compressible flow. The Doublet-Lattice Method (DLM) installed in MSC/NASTRAN uses this equation (Ref. 3.11).

The non-dimensional aerodynamic pressure coefficient is represented by

$$C_p = -2\phi_x - 2\phi_t \tag{3.14}$$

For wing surfaces, the boundary conditions are

$$\phi = 0 \qquad \text{far upstream} \tag{3.15a}$$

$$\phi_x + \phi_t = 0 \qquad \text{far downstream} \tag{3.15b}$$

$$\phi_z = 0 \qquad \text{far above and below} \tag{3.15c}$$

$$\phi_y = 0 \qquad \text{far spanwise and at the wing root} \tag{3.15d}$$

$$\phi_z = f_x + f_t \qquad \text{on the wing surface,} \tag{3.15e}$$

across the trailing vortex sheet in the wake, defined by $z = 0$ for $x > x_{te}$,

$$\text{the jump of } \phi_z = 0 \text{ and the jump of } \phi_x + \phi_t = 0 \tag{3.15f}$$

and the initial conditions are

$$\phi(x, y, z, 0) = g(x, y, z) \tag{3.16a}$$

$$\phi_t(x, y, z, 0) = h(x, y, z) \tag{3.16b}$$

where $g(x, y, z)$ and $h(x, y, z)$ are initial distributions, respectively.

3.3 Steady Aerodynamic Analysis

3.3.1 Steady Aerodynamic Analysis by ENSAERO

ENSAERO is a multidisciplinary aeroelastic code based on the Euler/Navier-Stokes flow equations and modal finite-element structural equations (Ref. 1.4). This flow solver uses time-accurate central finite difference schemes with artificial viscosity based on the Beam-Warming algorithm (Ref. 3.29) and upwind schemes based on flux splitting in the streamwise direction (Ref. 3.30). The basic coding accommodates patched zonal grid techniques for the efficient modeling of full aircraft (Ref. 3.31). In the Navier-Stokes calculations, spanwise and normal viscous effects can be considered. The method proposed by Baldwin and Lomax (Ref. 3.32) is used for the turbulence model. Several methods such as the original Baldwin-Lomax model, free stream capturing, regeneration for control, and Degani-Schiff modeling are used for correction of the vortex flows. The steady aerodynamic results from ENSAERO were used here for the transonic flow code ZTAIC to calculate the unsteady aerodynamic loads.

3.3.2 Steady Aerodynamic Analysis by ASTROS* and MSC/NASTRAN

In the static aeroelastic analyses by ASTROS* and MSC/NASTRAN, the steady aerodynamic loads can be calculated for rigid and elastically deformed structures by linear theory in the subsonic and supersonic regime. Static aeroelastic analysis for the subsonic flows, transonic flows, low supersonic flows, and high supersonic/hypersonic flows can be performed using the methods in the flow codes ZONA6, ZTAIC, ZONA7, and ZONA7U in ASTROS*, respectively.

3.4. Unsteady Aerodynamic Analysis

3.4.1 Typical Section in 2-Dimensional Incompressible Flow

The unsteady aerodynamic forces acting on a thin two-dimensional airfoil by unsteady motion in a compressible fluid were obtained by Wagner, Küssner, von Karman, Sears, and others. The steady lift acting on a two-dimensional airfoil whose angle of attack is α radians as shown in Fig. 3.1 in an incompressible fluid is

$$L_{steady} = qC_L(2b)\alpha \tag{3.17}$$

If we define the vertical velocity component of the fluid on the airfoil as the downwash, $w = V\sin\alpha \cong V\alpha$, i.e., $\alpha = w/V$

$$L_{steady} = \frac{1}{2}\rho V^2(2\pi)(2b)\frac{w}{V} = 2\pi b\rho Vw \tag{3.18}$$

The unsteady lift due to circulation is

$$L_1 = L_{steady}\Phi(\tau) = 2\pi b\rho Vw\Phi(\tau) \tag{3.19}$$

where $\tau = Vt/b$ is non-dimensional time and $\Phi(\tau)$ is called Wagner's function. The exact form of $\Phi(\tau)$ is

$$\Phi(\tau) = 1 - \int_0^\infty \{(K_0 - K_1)^2 + \pi^2(I_0 + I_1)^2\}^{-1} e^{-x\tau} x^{-2} dx \tag{3.20}$$

There are many approximate expressions given in Ref. 1.7, pp. 207. When we consider a more general type of motion of an airfoil having two degrees of freedom, a vertical translation h, positive downward, and a rotation a, positive nose up about an axis located at a distance $a_h b$ from the mid-chord point (Fig. 3.1), the circulatory lift per unit span is calculated according to Ref. 1.7 as

$$L_1(\tau) = 2\pi b\rho U^2 \int_{-\infty}^{\tau} \Phi(\tau - \tau_0)\left[\alpha'(\tau_0) + \frac{1}{b}h''(\tau_0) + (\frac{1}{2} - a_h)\alpha''(\tau_0)\right]d\tau_0 \tag{3.21}$$

There are other non-circulatory forces, i.e., apparent mass forces, given by

$$L_2 = \rho\pi b^2(\ddot{h} - a_h b\ddot{\alpha}) = \rho\pi U^2(h'' - a_h b\alpha'') \tag{3.22}$$

$$L_3 = \rho\pi b^2 U\dot{\alpha} = \rho\pi bU^2\alpha' \tag{3.23}$$

and the apparent moment of inertia is

$$M_a = -\frac{\rho\pi b^4}{8}\ddot{\alpha} = -\frac{\rho\pi b^2 U^2}{8}\alpha'' \tag{3.24}$$

The total lift per unit span is

$$L = L_1 + L_2 + L_3 \tag{3.25}$$

The total moment per unit span about the elastic axis is

$$M = (\frac{1}{2} + a_h)bL_1 + a_h bL_2 - (\frac{1}{2} - a_h)bL_3 + M_a \tag{3.26}$$

3.4.2 Unsteady Aerodynamic Analysis by ENSAERO

ENSAERO computes aeroelastic responses by simultaneously integrating the Euler/Navier-Stokes equations and the structural equations of motion using an aeroelastically adaptive dynamic grid. ENSAERO has an option of computing unsteady flows over wings in oscillating and ramp motion. This code also has zonal grid capability which was developed earlier for steady computations and. extended to moving grids. The geometry capability in the code can handle general wing motions. For the unsteady pressure calculations on a rigid configuration in ramp motion, the pitch rate is defined as $\dot{\alpha}c / U_\infty$ where α is in radians. The responses of lift, moment, and drag for a given pitch rate are calculated. ENSAERO has the capability of computing aeroelastic responses associated with vortical/transonic/separated flows through the calculation of the interaction between the unsteady aerodynamics and the structural motions including control surface motions.

3.4.3 Unsteady Aerodynamic Analysis in ASTROS* and MSC/NASTRAN

In the flutter analyses by ASTROS* and MAC/NASTRAN, the unsteady aerodynamic loads can be calculated by linear theory in the subsonic and supersonic regime. The unsteady transonic aerodynamic loads can be calculated by nonlinear theory using ZTAIC in ASTROS*. This transonic unsteady aerodynamic code utilizes the Transonic Equivalent Strip (TES) method. While the transonic shock effects cannot be considered by linear theory, the shock effects are modeled here through the assumption that the strength and the position of the shock in steady flow are preserved by the shock in unsteady flow. Although the shock is not preserved perfectly in unsteady flow, this is an advanced method for incorporating shock effects in transonic flow. ZONA6 and ZONA7 in ASTROS* are used to calculate aerodynamic loads for arbitrary lifting surface-body combinations in the subsonic and supersonic flow regimes, respectively. ZONA7U in ASTROS* utilizing a unified hypersonic-supersonic lifting surface method is used to calculate aerodynamic loads for arbitrary lifting surfaces in the high supersonic/hypersonic flow regime. Here, the concept of piston theory was generalized and suitably integrated with the AIC (Aerodynamic Influence Coefficient) matrix due to supersonic lifting theory; thus, this unified method can account for the effects of wing thickness and/or flow incidence, upstream influence, and three-dimensionality for an arbitrary lifting surface system.

Table 3.1 Summary of Unsteady Lifting Surface Theories Applicable to Aeroservoelasticity and Multidisciplinary Design Optimization

Speed range	Methods	Installed in	Alias
Subsonic	DLM	MSC/NASTRAN ASTROS	
	USDA	ASTROS*	ZONA6
Transonic	TES	ASTROS*	ZTAIC
Supersonic	HGM	MSC/NASTRAN	ZONA51
	CPM	ASTROS	
	USDA	ASTROS*	ZONA7
Hypersonic	Piston theory	MSC/NASTRAN	
	USDA	ASTROS*	ZONA7U

DLM = Doublet Lattice Method

CPM = Constant Pressure Method

HGM = Harmonic Gradient Method

TES = Transonic Equivalent Strip Method

USDA = Unified S-Domain Aerodynamics

ASTROS* : ASTROS Containing ZAERO Module

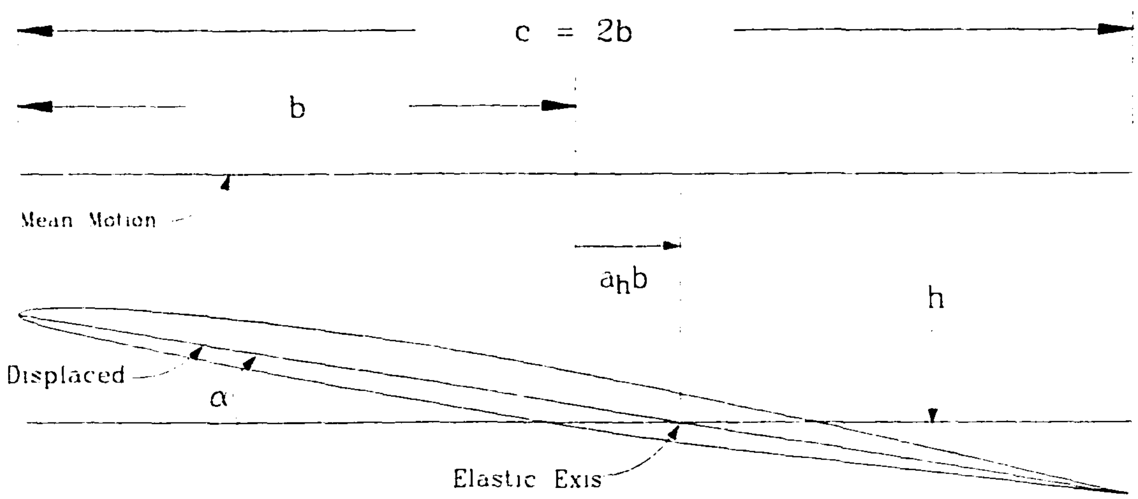

Figure 3.1 2-Dimensional Airfoil Motion

Chapter 4

AEROELASTIC ANALYSIS

4.1 Introduction

4.1.1 Background

Because an aircraft is composed of an elastic structure and is subjected to the airflow, aeroelastic effects have to be considered in detail. The field of elasticity is explained in Ref. 1.4. Static aeroelasticity and flutter are the most important phenomena in aeroelasticity. In static aeroelasticity, the lift, trim parameters, and stability parameters are calculated by considering the elastic effects of the structure. Flutter is a dynamic instability of an elastic body in an airflow occurring through the interactions of the structure and any unsteady aerodynamic loads.

When an aircraft is designed, it should be verified that the aircraft is free from flutter within the flight envelope. An increasing emphasis on fuel efficiency coupled with advances in aerodynamic and structural design techniques result in an increasing payload to structural weight ratio. This increased structural efficiency results in lower elastic mode frequencies, the modes are more easily excited, and flutter problems become more important. In general, flutter speed and flutter frequency can be calculated using structural vibration characteristics and unsteady aerodynamic loads of any lifting surfaces by the V-g method, the k-method, the pk-method, or the root-locus method.

Methods for conventional aeroelastic analysis in the linear subsonic and supersonic speed regimes are well developed. However, aeroelastic analyses involving complex nonlinear flows with local shocks, wing tip vortices, and flow separation in the transonic speed regime, as well as aerodynamic heating in the hypersonic speed regime are not as fully understood, yet. Computational methods are generally used for aeroelastic computations in nonlinear flow.

4.1.2 Review of Previous Work

Smilg and Wasserman originated the most popular technique, the V-g method in Ref. 4.1. Garrick and Rubinow (Ref. 4.2) calculated flutter speeds by the V-g method using aerodynamic influence coefficients in simple harmonic motion. Edwards (Ref 4.3) calculated flutter dynamic pressures by the root-locus method. Yang, Guruswamy, and Striz performed flutter analyses of various two-dimensional airfoils in transonic flow in Refs. 4.4-6. Karpel (Refs. 4.7-9) and Vepa (Ref. 4.10) calculated flutter dynamic pressures by the root-locus method using approximate rational functions for the unsteady aerodynamic influence coefficients and extended the approach to control analysis. Tiffany and Adams (Ref. 4.11), and Leishman and Crouse (Ref. 4.12) extended the rational function approximation method to compressible flows. Transonic flutter analyses in three-dimensional flow were performed in Refs. 4.13-17. In Refs. 4.13, 4.14, and 4.16, the effects of angle of attack were included. In general, flutter analyses can be performed by the FEM codes

ASTROS* and MSC/NASTRAN by linear theory. Transonic flutter analysis can now be performed by ZTAIC, recently installed in ASTROS*.

4.1.3 Scope of Research

In static aeroelasticity, stability derivatives, pressure distributions, and trim parameters such as angle of attack, pitch rate, pitch acceleration, and control surface deflection angles were calculated in the trim condition by ASTROS*. Static aeroelastic analyses were performed for the pitching case. All parameters were calculated for the rigid structure and for the deformed structure. Displacements and stresses were calculated at these trim conditions. In flutter analysis, several methods such as the V-g method, the root-locus method, and the time domain method to calculate flutter speed were reviewed. Flutter speeds and flutter frequencies were calculated for the models by ASTROS*, and V-g plots were drawn for subsonic, transonic, and supersonic flow cases. Finite state-space formulations for the aeroelastic system were used to code a program which will calculate approximate aerodynamic coefficients by the minimum-state method. Root loci were drawn to calculate the flutter speed. The results of the flutter analyses by ASTROS*, MSC/NASTRAN, and the root-locus method were compared.

4.2 Aeroelastic Equations of Motion

4.2.1 Second Order Formulation in Modal Coordinates

The common approach for analyzing an aeroelastic system is based on the second-order frequency domain formulation of the matrix equations of motion in modal coordinates (Ref 1.4). The equations of motion are often obtained by finite element modeling techniques. Using a Laplace transform, the open loop aeroelastic system equations of motion are

$$\left[\ [M]s^2+[C]s+[K]\ \right]\{\eta(s)\}=q[Q(s')]\{\eta(s)\} \tag{4.1}$$

where $[M]$, $[C]$, and $[K]$ are the modal mass, modal damping, and modal stiffness matrices, respectively, defined by Eq. (2.18), $q=\frac{1}{2}\rho V^2$ is the dynamic pressure, s is the Laplace variable, and

$$s'=sb/V \tag{4.2}$$

is the non-dimensionalized Laplace variable. The generalized aerodynamic influence coefficient matrix is calculated using unsteady aerodynamic methods such as the Doublet-Lattice Method (DLM), the Constant Pressure Method (CPM), or the Harmonic Gradient Method (HGM) for three-dimensional wings. ZONA6, ZTAIC, ZONA7, and ZONA7U of ASTROS* were used here to calculate these aerodynamic loads.

4.2.2 Finite State-Space Aeroelastic Formulation

To change the aeroelastic equations of motion (Eq. 4.1) into a state space equation. the generalized unsteady aerodynamic loads should be represented by rational functions (Ref. 1.5 and Refs. 4.7-9). If the loads are assumed in the rational function form of Eq. (4.3), Eq. (4.1) can be changed into a state space equation (4.10) by the following process as described in Ref. 1.5:

$$[\tilde{Q}(s')] = [A_0] + [A_1]s' + [A_2]s'^2 + [D][s'[I] - [R]]^{-1}[E]s' \tag{4.3}$$

where s' is the non-dimensional Laplace variable in the form

$$s' = sb / V \tag{4.4}$$

An augmented state vector is now defined by its Laplace transformation as

$$\{x_a(s)\} = (s'[I] - [R])^{-1}[E]\{\eta(s)\}s \tag{4.5}$$

$$s'[I]\{x_a(s)\} = s[E]\{\eta(s)\} + [R]\{x_a(s)\} \tag{4.6}$$

and, with the substitution of Eq. (4.4),

$$s\{x_a(s)\} = s[E]\{\eta(s)\} + \frac{V}{b}[R]\{x_a(s)\} \tag{4.7}$$

The substitution of Eq. (4.3) into Eq (4.1) and using Eq. (4.7) yields

$$([\overline{M}]s^2 + [\overline{C}]s + [\overline{K}])\{\eta\} - q[D]\{x_a\} = 0 \tag{4.8}$$

where

$$[\overline{M}] = [M] - \frac{\rho b^2}{2}[A_2],\ [\overline{C}] = [C] - \frac{\rho b^2}{2}[A_1],\ [\overline{K}] = [K] - \frac{\rho b^2}{2}[A_0] \tag{4.9}$$

The time-domain state-space open-loop equation is represented by

$$\{\dot{x}\} = [A]\{x\} \tag{4.10}$$

where

$$\{x\} = \begin{Bmatrix} \eta \\ \dot{\eta} \\ x_a \end{Bmatrix}, \quad [A] = \begin{bmatrix} 0 & [I] & 0 \\ -[\overline{M}]^{-1}[K + qA_0] & -[\overline{M}]^{-1}[C + \frac{qb}{V} A_1] & q[\overline{M}]^{-1}[D] \\ 0 & [E] & \frac{V}{b}[R] \end{bmatrix}$$

4.2.3 Minimum-State Method

The generalized unsteady aerodynamic coefficients $F(k) + iG(k)$ at k=0, 1, 2, ..., k_f have already been calculated. The next step is to determine the coefficients A_0, A_1, A_2, D, R, and E of Eq. (4.3) for $[\tilde{Q}(s')]$ to best fit $F(k) + iG(k)$. This minimum-state method has been presented in Refs. 4.7-9 as follows:

It is assumed that the data are matched at the points k =0 and k_f.

Then, at k = 0, $[\tilde{Q}(ik')] = F(0) + iG(0) = [A_0]$ and

at $k = k_f$, $[\tilde{Q}(ik')] = F(ik) + i(G(ik) = [A_0] + i[A_1]k - [A_2]k^2 + [D]\left[ik[I] - [R]\right]^{-1}[E]ik$

These are four equations, i.e., two real and two imaginary. Solving these equations with $G(0) = 0$ yields

$$[A_0] = [F(0)]$$

$$[A_1] = [G(k_f)]/k_f + [D](k_f^{\,2}[I] + [R]^2)^{-1}[R][E] \tag{4.11}$$

$$[A_2] = ([F(0)] - [F(k_f)])/k_f^{\,2} + [D](k_f^{\,2}[I] + [R]^2)^{-1}[R]$$

The next step is to determine [D], [E], and [R]. At the other points, $k = k_i$, Eqs. (4.3) and (4.11) can be used

$$[D][C(R,k_1)][E]=([F(k_1)]-[F(0)])/k_1^2-([F(k_f)]-[F(0)])/k_f^2$$

$$[D][C(R,k_1)][R][E]=[G(k_t)]/k_t-[G(k_1)]/k_1 \tag{4.12}$$

where $[C(R,k_1)]=(k_1^2[I]+[R]^2)^{-1}-(k_f^2[I]+[R]^2)^{-1}$

Then, [D], [R], and [E] can be obtained from Eqs. (4.12) by the least-squares method as in Ref. 1.5.

4. 3 Methods of Flutter Analysis

4.3.1. V-g Method

For a simple harmonic motion with frequency ω, the aeroelastic system equations of motion neglecting damping can be rewritten from Equation (4.1) as

$$\left[[M]-\frac{1}{\omega^2}[K]-\frac{\rho b^2}{2k^2}[Q(ik)]\right]\{\eta\}=0 \tag{4.13}$$

The velocity V and the frequency ω in a nontrivial solution of this equation are the flutter velocity and the flutter frequency, respectively. For given ρ and M, this equation is solved for several k. In the process, an artificial structural damping g is added so that Eq. (4.13) becomes

$$\left[[M]-\frac{1+ig}{\omega^2}[K]-\frac{\rho b^2}{2k^2}[Q(ik)]\right]\{\eta\}=0 \tag{4.14}$$

If we set

$$\Omega=(1+ig)/\omega^2 \tag{4.15}$$

Eq. (4.14) become

$$[K]^{-1}\left[[M]-\frac{\rho b^2}{2k^2}[Q(ik)]\right]\{\eta\}=\Omega\{\eta\} \tag{4.16}$$

Eq. (4.16) is a complex eigenvalue problem. If the Ω_i are obtained, the ω_i can be calculated by Eq. (4.15) and V_i can be calculated from the equation $k=b\omega_i/V_i$. As a result,

$$\omega_i=\sqrt{1/\mathrm{Re}(\Omega_i)},\ V_i=\omega_i b/k,\ g_i=\mathrm{Im}(\Omega_i)/\mathrm{Re}(\Omega_i) \tag{4.17}$$

ω and V are flutter frequency and flutter velocity at the point $g_i=0$.

4.3.2. Root-Locus Method

For a non-trivial solution to the Laplace-transformed, open loop, aeroelastic system equation of motion (4.1), roots s_i should exist for the following equation.

$$\left|\ [M]s^2+[C]s+[K]-q[Q(s')]\ \right|=0 \tag{4.18}$$

The system is unstable when the real part of one of the roots is positive. The main difficulty in solving Eq. (4.18) is that the $[Q(s')]$ usually contain non-rational terms. Eq. (4.18) is solved for various q, and root loci are plotted in the Laplace s plane. If the real part of a root is larger than zero, the aeroelastic system is unstable. Thus, the flutter dynamic pressure q_f is that q for which one root is purely imaginary. The flutter frequency is then

$$\omega_f=\mathrm{Im}(s_i)\quad\text{when}\quad\mathrm{Re}(s_i)=0 \tag{4.19}$$

In order to solve Eq. (4.18) by the methods of linear algebra, $[Q(s')]$ needs to be approximated using a rational function of s' as given in Eq. (4.3). The root-locus method provides correct vibration frequencies and damping ratios at any flight condition, while the V-g method is correct only on the flutter boundary. Moreover, because the air density ρ is not predetermined, the root-locus flutter dynamic pressure represents an actual flutter condition. The root-locus method is also used in the design for active control of an aeroelastic system,.

Here, the flutter speeds were calculated by changing Eq. (4.18) to a state-space formulation, and the generalized aerodynamic forces were approximated by the minimum-state method explained in Section 4.2.3. The aerodynamic forces were calculated by ZONA6, ZTAIC, ZONA7, and ZONA7U of ASTROS* for the subsonic, transonic, low supersonic, and high supersonic/hypersonic flight regimes, respectively.

4.3.3. Flutter Analysis by Time Domain Response

Flutter speeds are generally calculated by the V-g method and the root-locus method, using a Laplace transform to the frequency domain, in the subsonic and supersonic regimes where the aerodynamic forces are linear. These methods are not applicable if flight takes place in the transonic regime. Transonic aerodynamic loads with shocks are severely nonlinear. In this case, flutter analysis can be performed by time domain response. The governing aeroelastic equation of motion is

$$[M]\{\ddot{\eta}\} + [C]\{\dot{\eta}\} + [K]\{\eta\} = q\{Q\} \tag{4.20}$$

where

$$\{Q\} = [\Phi]^T [A]\{\Delta C_p\} \tag{4.21}$$

is the generalized aerodynamic force vector, $\{\eta\}$ represents the modal coordinates, $[\Phi]$ is the modal matrix, and $[A]$ is the diagonal area matrix of the aerodynamic control points. If we assume that the structural motion is linear, the physical motion can be represented by

$$\{q\} = [\Phi]\{\eta\} \tag{4.22}$$

The equation of motion can be solved by numerical time integration using the linear acceleration method. A step-by step integration procedure for the aeroelastic response can be obtained as follows: first, assume the free-stream conditions and the wing surface boundary conditions are obtained from a set of selected starting values. The aerodynamic coefficients are then calculated from the transonic aerodynamic equation of motion. The generalized aerodynamic forces $Q(t)$ at time t are calculated by Eq. (4.21). The generalized displacement, velocity, and acceleration vectors at time $t+\Delta t$ are computed by Eq. (4.20) The new boundary conditions on the wing are computed by Eq. (4.22). The process is repeated until the required response is obtained.

4.3.4. pk-Method of Flutter Solution in ASTROS* and MSC/NASTRAN

The fundamental equation for modal flutter analysis by the pk-method was derived in Ref. 4.18:

$$\left[Mp^2 + (B - \frac{1}{4}\rho c V Q^I / k)p + (K - \frac{1}{2}\rho V^2 Q^R) \right]\{\eta\} = 0 \tag{4.23}$$

where $\{\eta\}$ are the generalized modal coordinates, Q^I is the imaginary part of the generalized aerodynamic coefficient matrix, Q^R is the real part of the generalized aerodynamic coefficient matrix, $p = \omega(\gamma \pm i)$ is a complex eigenvalue, c is a reference length, and k is the reduced frequency $\frac{\omega c}{2V}$. Furthermore,

$$k = (c/2V)\,\mathrm{Im}(p) \tag{4.24}$$

The matrix terms in Eq. (4.23) are all real. Eq. (4.23) can be written in the state-space form as

$$[A - pI]\{\overline{\eta}\} = 0 \tag{4.25}$$

where

$$[A] = \begin{bmatrix} 0 & I \\ -M^{-1}[K - \frac{1}{2}\rho V^2 Q^R] & -M^{-1}[B - \frac{1}{4}\rho c V Q^I / k] \end{bmatrix}, \tag{4.26}$$

$$\text{and } \{\overline{\eta}\} = \begin{Bmatrix} \eta \\ \dot{\eta} \end{Bmatrix} \tag{4.27}$$

The eigenvalues of the matrix $[A]$ are either real ($k = 0$) or complex conjugate pairs ($k \neq 0$). Real roots indicate rigid body modes or structural divergence modes. When a velocity is given, the solution satisfying Eqs. (4.23) and (4.24) is obtained by an iterative method. For real roots, the iteration begins at $k = 0$. $Q^R(m,k)$ and $Q^I(m,k)/k$ are obtained by extrapolation from the values of $Q(m,k)$ calculated before. They are then substituted into Eq. (4.25), which is solved for the eigenvalues of matrix $[A]$. Only real roots (i.e., real eigenvalues of the matrix $[A]$) are roots of

Eq. (4.23) because only they can satisfy Eq. (4.24). For complex roots, the iteration begins with

$$k_1^{(0)} = \omega_{11}^{(0)}\left(\frac{c}{2V}\right), \tag{4.28}$$

for the first mode. $Q(m,k)$ is obtained by interpolation, and the complex eigenvalues are calculated as $p_{r1}^{(1)} = \omega_{r1}^{(1)}(\gamma_{r1}^{(1)} \pm i)$, where r denotes the oscillatory mode number ordered by frequency ($\omega_{11} < \omega_{21} < \ldots$). Then, the next estimate of the reduced frequency is $k_1^{(1)} = \omega_{11}^{(1)}\left(\frac{c}{2V}\right)$. The iteration is continued until convergence occurs. If the converged complex eigenvalues are $p_{r1}^{(c)} = \omega_{r1}^{(c)}(\gamma_{r1}^{(c)} \pm i)$, only $p_{11}^{(c)}$ satisfies Eqs. (4.23) and (4.24) because the associated reduced frequency is $k_1^{(c)} = \omega_{11}^{(c)}\left(\frac{c}{2V}\right)$. Otherwise Eq. (4.24) is not satisfied. The search for the second oscillatory mode begins with the first estimate of the next reduced frequency, $k_2^{(0)} = \omega_{21}^{(c)}\left(\frac{c}{2V}\right)$, and the iteration continues. This procedure continues for the higher modes. A convergence criterion is given by

$$\begin{aligned} \left| \, k_s^{(j)} - k_s^{(j-1)} \, \right| &\le \varepsilon \qquad \text{for } k_s^{(j-1)} \le 1.0 \\ &\le \varepsilon k_s^{(j-1)} \qquad \text{for } k_s^{(j-1)} \ge 1.0 \end{aligned} \tag{4.29}$$

where ε is a user input with a default value of 0.001, s is the number of the oscillatory mode under investigation, and j is the iteration number.

Chapter 5

AEROSERVOELASTICITY

5.1 Introduction

5.1.1 Background

When installing an aeroelastic control system, aircraft maneuverability, ride comfort, and service life can be increased for a given structural layout through gust alleviation, and the flight envelope can be expanded through flutter suppression.

Aeroservoelasticity deals with the interactions between the structural, aerodynamic, and control system characteristics of a flight vehicle. Structural dynamic motions are sensed by control sensors, feedback is provided to the control surface actuators through a control transfer function, and the actuators change the motion of the structure via the control surfaces. This closed aeroservoelastic loop can be used for gust alleviation and flutter suppression.

In gust alleviation, the response of an aircraft to a gust input is minimized or lowered to a required level by changing the parameters of the control system. In flutter suppression, the flutter speed is increased to a required level by changing the parameters of the control system by the pole assignment method or same numerical optimization method. The loss of a flutter suppression control system may result in almost immediate major structural failure and loss of the aircraft. Thus, active control systems must be highly reliable, and structural stability should be ensured in the entire flight envelope.

The classical approach to flutter (Ref 1.4) is based on aerodynamic influence coefficient matrices computed for simple harmonic motion at discrete values of reduced frequencies. However, in various modern control design techniques, the equations of motion represented by a linear time-invariant state-space form are used. The aerodynamic loads are transformed into the Laplace domain (s-plane).

Most of these approaches focus on linear control laws based on state feedback or output feedback. In the case of design optimization for full state feedback control, a sequential approach is usually adopted in which the control gains are determined by solving Riccati equations corresponding to the changing structural system during a design iteration. In the case of output feedback, the structural dimensions and the control gains are treated as strictly independent design variables in the optimization problem.

There are other methods where the aerodynamic and structural equations of motion are simultaneously integrated by a time-accurate numerical scheme.

5.1.2 Review of Previous Work

Early analytical study for flutter suppression was performed by Abel (Ref. 5.1). Flight tests in the transonic regime with both full-scale aircraft and remotely piloted drones were reported in Ref. 5.2 and Ref. 5.3 and proved the possibility of aeroelastic control. Newsom, Abel, and Dunn (Refs. 5.4 and 5.5) designed control laws and evaluated their performance through wind tunnel test. Mukhopadhyay, Newsom, and Abel (Ref. 5.6) performed control optimization via reduced order control laws. Karpel (Refs. 5.7-9) performed flutter suppression and gust alleviation by output feed-back using rational approximate aerodynamic loads. Guruswamy (Ref. 5.10) integrated the aerodynamic and structural equations of motion simultaneously by a time-accurate numerical scheme. Recently, aeroservo-elastic analysis and test results were reported in Refs. 5.11 and 5.12

5.1.3 Scope of Research

The finite state-space approach for general structures in physical coordinates is presented in Section 5.2. The finite state-space approach for aeroservoelasticity in modal coordinates is first reviewed in Section 5.3. Actuator models, controller models, and sensor output equations were then formulated. By augmentation of the actuator states and controller states, the open-loop and closed-loop system matrices for an aeroelastic control system were formulated. For these open-loop and closed-loop aeroelastic control systems, flutter speed and control margins were also defined and are presented in Section 5.3. The sensitivities of the flutter speed and the control margins with respect to the control system parameters were formulated and are given in Section 5.4. Using the optimization module of IMSL in Microsoft FORTRAN, flutter speed was maximized considering the control parameters as design variables.

Finally, a time-accurate numerical scheme for active control presented by Guruswamy (Ref. 5.10) is reviewed.

5.2 Finite State-Space Formulation Using Physical Coordinates

The following derivation is based on that in Reference 5.4. The equation of motion based on the finite element formulation for physical coordinates is given by

$$[m]\{\ddot{q}\}+[c]\{\dot{q}\}+[k]\{q\}=\{F\} \tag{5.1}$$

where $\{q\}$ is the vector of the physical degrees of freedom (DOF). The load vector $\{F\}$ can be represented as

$$\{F\}=[b]\{u\}+[e]\{f\} \tag{5.2}$$

where $\{u\}$ is the actuator force vector and $\{f\}$ is a vector of external disturbances (noises). Eq. (5.1) can be written as

$$[m]\{\ddot{q}\}+[c]\{\dot{q}\}+[k]\{q\}=[b]\{u\}+[e]\{f\} \tag{5.3}$$

If we define a state-space as

$$\{x\}=\begin{Bmatrix} q \\ \dot{q} \end{Bmatrix} \tag{5.4}$$

Eq. (5.3) can be transformed to a first-order state space equation

$$\{\dot{x}\}=[A_0]\{x\}+[B]\{u\}+[E]\{f\} \tag{5.5}$$

where

$$[A_0]=\begin{bmatrix} [0] & [I] \\ -[m]^{-1}[k] & -[m]^{-1}[c] \end{bmatrix} \tag{5.6}$$

$$[B]=\begin{bmatrix} [0] \\ [m]^{-1}[b] \end{bmatrix} \tag{5.7}$$

$$[E]=\begin{bmatrix} [0] \\ [m]^{-1}[e] \end{bmatrix} \tag{5.8}$$

Here, if the number of DOFs is n, the number of actuators is m, and the number of external disturbances is l, then the dimensions of $\{x\}$, $[A_0]$, $[B]$, and $[E]$ are $2n$ x 1, $2n$ x m, and $2n$ x l, respectively.

If linear full state feedback is chosen for the control $\{u\}$,

$$\{u\} = -[H]\{x\} = -\begin{bmatrix}[H_p] & [H_v]\end{bmatrix}\begin{Bmatrix} q \\ \dot{q} \end{Bmatrix} \tag{5.9}$$

where $[H_p]$ and $[H_v]$ are the sub-matrices containing position and velocity components of the m x $2n$ feedback gain matrix $[H]$, respectively. If external disturbances are neglected, the closed-loop state equation is

$$\{\dot{x}\} = [A]\{x\} + [E]\{f\} \tag{5.10}$$

where the closed system matrix $[A]$ is

$$\begin{aligned} [A] &= [A_0] - [B][H] \\ &= \begin{bmatrix} [0] & [I] \\ -[m]^{-1}([k]+[b][H_p] & -[m]^{-1}([c]+[b][H_v]] \end{bmatrix} \end{aligned} \tag{5.11}$$

5.3 Finite State-Space Aeroservoelastic Modeling

The following derivations are based on the works by Karpel (Refs. 1.5 and 5.7-9).

5.3.1 Finite State-Space Aeroservoelastic Formulation Using Modal Coordinates

A Laplace transform of the open-loop aeroservoelastic system equation of motion, excited by control surface motion, is given by separation of the elastic modes and the control surface modes in Ref. 5.9 as

$$\left[\, [M_s]s^2 + [C_s]s + [K_s] - Q_{ss}(s) \,\right]\{\eta(s)\} + \left[\, [M_{sc}]s^2 - Q_{sc}(s) \,\right]\{\delta(s)\} = 0 \quad (5.12)$$

where $[M_s]$, $[C_s]$, and $[K_s]$ are the generalized structural mass, damping, and stiffness matrices, respectively, $[M_{sc}]$ is the coupling mass matrix between the control and the structural modes, $\{\eta\}$ is the generalized structural displacement vector, $\{\delta\}$ is the vector of control surface command deflections, namely the actuator outputs in radians, $[Q_{ss}]$ and $[Q_{sc}]$ are the unsteady aerodynamic force matrices associated with the modes of the structure and the control surfaces, and q is the dynamic pressure. The total hinge moment vector including aerodynamic and inertia forces is

$$\{T_c(s)\} = (q[Q_{cs}(s)] - [M_{sc}]^T s^2)\{\eta(s)\} + (q[Q_{cc}(s)] - [M_{cc}]s^2)\{\delta(s)\} \qquad (5.13)$$

where $[M_{cc}]$ is a diagonal matrix of control surface moments of inertia about the hinge line. $[Q_{cs}]$ and $[Q_{cc}]$ are the unsteady aerodynamic force matrices associated with the modes of the structure and the control surfaces, respectively. The aerodynamic influence coefficient matrices were approximated by the minimum-state method as in Eq. (4.3) by

$$[\tilde{Q}(s')] = [A_0] + [A_1]s' + [A_2]s'^2 + [D]\left[s'[I] - [R]\right]^{-1}[E]s' \qquad (5.14)$$

The real-valued approximation matrices of Eq. (5.14) are partitioned into structural and control related terms as

$$[A_i] = \begin{bmatrix} A_{si} & A_{sci} \\ A_{csi} & A_{ci} \end{bmatrix} \text{ for } i = 0,\ 1, \text{ and } 2 \qquad (5.15)$$

$$[D]=\begin{bmatrix}D_s\\D_c\end{bmatrix} \tag{5.16}$$

$$[E]=\begin{bmatrix}E_s & E_c\end{bmatrix} \tag{5.17}$$

As in the case without control surfaces, an augmented state vector is now defined by its Laplace transformation as

$$\{x_a(s)\}=(s'[I]-[R])^{-1}([E_s]\{\eta(s)\}+[E_c]\{\delta_c(s)\})s' \tag{5.18}$$

$$s'[I]\{x_a(s)\}=s'[E_s]\{\eta(s)\}+s'[E_c]\{\delta_c(s)\}+[R]\{x_a(s)\} \tag{5.19}$$

and, with the substitution of Eq. (4.6)

$$s\{x_a(s)\}=s[E_s]\{\eta(s)\}+s[E_c]\{\delta_c(s)\}+\frac{V}{b}[R]\{x_a(s)\} \tag{5.20}$$

The substitution of Eq. (5.14) into Eq (5.12) and using Eq. (5.20) yields

$$([\overline{M}_s]s^2+[\overline{C}_s]s+[\overline{K}_s])\{\eta\}-q[D_s]\{x_a\}=(-[\overline{M}_{sc}]s^2+[\overline{C}_{sc}]s+[\overline{K}_{sc}])\{\delta_c(s)\} \tag{5.21}$$

where

$$[\overline{M}_s]=[M_s]-\frac{\rho b^2}{2}[A_{s2}],\ [\overline{C}_s]=[C_s]-\frac{\rho b^2}{2}[A_{s1}],\ [\overline{K}_s]=[K_s]-\frac{\rho b^2}{2}[A_{s0}]$$

$$[\overline{M}_{sc}]=[M_{sc}]-\frac{\rho b^2}{2}[A_{sc2}],\ [\overline{C}_{sc}]=-\frac{\rho b^2}{2}[A_{sc1}],\ [\overline{K}_s]=-\frac{\rho b^2}{2}[A_{sc0}] \tag{5.22}$$

Thus, the resulting time domain, state-space, open-loop aeroelastic plant equation of motion is

$$\{\dot{x}_p\}=[A_p]\{x_p\}+[B_p]\{u_p\} \tag{5.23}$$

where

$$[x_p] = \begin{Bmatrix} \eta \\ \dot{\eta} \\ x_a \end{Bmatrix}, \quad [u_p] = \begin{Bmatrix} \delta \\ \dot{\delta} \\ \ddot{\delta} \end{Bmatrix}, \tag{5.24}$$

$$[A_p] = \begin{bmatrix} 0 & [I] & 0 \\ -[\overline{M}_s]^{-1}[K_s - qA_{s0}] & -[\overline{M}_s]^{-1}[C_s - \frac{qb}{V}A_{s1}] & q[\overline{M}_s]^{-1}[D_s] \\ 0 & [E_s] & \frac{V}{b}[R] \end{bmatrix}, \tag{5.25}$$

and

$$[B_p] = \begin{bmatrix} 0 & 0 & 0 \\ -q[\overline{M}_s]^{-1}[A_{sc0}] & -\frac{qb}{V}[\overline{M}_s]^{-1}[A_{sc1}] & -[\overline{M}_s]^{-1}[M_{sc} - \frac{qb^2}{V}A_{sc2}] \\ 0 & [E_s] & 0 \end{bmatrix} \tag{5.26}$$

where $[\overline{M}_s] = [M_s] - \frac{qb^2}{V^2}[A_{s2}]$ and $\{x_a\}$ is the vector of aerodynamic states.

5.3.2 Actuator Model

To include the effect of actuator dynamics, an actuator model is described in state-state form and then interconnected to the basic vehicle equations. Actuator models are generally represented by transfer functions. Consider an actuator transfer function of the following form.

$$\frac{\delta(s)}{\delta_c(s)} = \frac{b_0}{s^n + a_{n-1}s^{n-1} + \cdots + a_0} \tag{5.27}$$

where $\delta(s) = \{u_p\} = \begin{Bmatrix} \delta \\ \dot{\delta} \\ \ddot{\delta} \end{Bmatrix}$ is the output of the actuator and $\delta_c(s) = \{u\}$ is the input command for one actuator. The coefficients a_i and b_o are defined by the equations of motion of an actuator system and are functions of the stiffness and inertia properties of the actuator system. The actuator transfer function can be expressed in a state-space form as

$$[\dot{x}_{ac}] = [A_{ac}]\{x_{ac}\} + \{B_{ac}\}\{u\}$$

$$\{u_p\} = [C_{ac}]\{x_{ac}\} \tag{5.28}$$

where $x_{ac} = \begin{Bmatrix} \delta \\ \dot{\delta} \\ \vdots \\ \dfrac{d^{n-1}\delta}{dt^{n-1}} \end{Bmatrix}$, and

$$[A_{ac}] = \begin{bmatrix} 0 & 1 & 0 & \dots & 0 \\ 0 & 0 & 1 & \cdots & 0 \\ \vdots & \vdots & \vdots & \ddots & \vdots \\ 0 & 0 & 0 & 0 & 1 \\ -a_0 & -a_1 & -a_2 & \cdots & -a_n \end{bmatrix}, \{B_{ac}\} = \begin{Bmatrix} 0 \\ 0 \\ \vdots \\ b_0 \end{Bmatrix}, \text{and } [C_{ac}] = \begin{bmatrix} 1 & 0 & 0 & \cdots & 0 \\ 0 & 1 & 0 & \dots & 0 \\ 0 & 0 & 1 & \dots & 0 \\ \vdots & \vdots & \vdots & \ddots & \vdots \\ 0 & 0 & 0 & 0 & 0 \end{bmatrix} \tag{5.29}$$

are the dynamic matrix, the control distribution, and the output matrix of an actuator, respectively. From Fig. 5.1, since $\{x_{ac}\} = \{u_p\}$, the plant vector $\{x_p\}$ of Eq. (5.23) can be augmented by the actuator states $\{x_{ac}\}$ of Eq. (5.28) which yields

$$[\dot{x}] = [A]\{x\} + \{B\}\{u\}$$

$$\{y\} = [C]\{x\} \tag{5.30}$$

where

$$\{x\} = \begin{Bmatrix} x_p \\ x_{ac} \end{Bmatrix} = \begin{Bmatrix} \eta \\ \dot{\eta} \\ x_a \\ x_{ac} \end{Bmatrix},\ [A] = \begin{bmatrix} A_p & B_p C_{ac} \\ 0 & A_{ac} \end{bmatrix},\ \{B\} = \begin{Bmatrix} 0 \\ \{B_{ac}\} \end{Bmatrix}, \tag{5.31}$$

and $\{y\}$ is the sensor reading vector. This equation is the starting point for designing a control system that can be augmented by the state vector.

5.3.3 Sensor Output Equation

When a sensor reads an acceleration, the output equation can be expressed as

$$\{y\} = [\phi_y]\{\ddot{\eta}\} = [C_p]\{x_p\} + [D_p]\{u_p\} = \left[[C_p] \quad [D_p]\right]\begin{Bmatrix} x_p \\ x_{ac} \end{Bmatrix} = [C]\{x\}, \tag{5.32}$$

because $\{x_{ac}\} = \{u_p\}$. $[\phi_y]$ is a modal vector at the sensor location. From Eq. (5.23),

$$[C_p] = [\phi_y][\overline{M}]^{-1}\left([K_s + qA_{s0}] \quad [C_s + \frac{qb}{V}A_{s1}] \quad q[D_s]\right),$$

$[D_p] = [\phi_y][\overline{M}]^{-1}\left(q[A_{c0}] \quad \frac{qb}{V}[A_{c1}] \quad [M_c + \frac{qb^2}{V^2}A_{c2}]\right)$, thus, $[C]$ is now represented by

$$[C] = \left|[C_p] \quad [D_p]\right| \tag{5.33}$$

5.3.4 Controller Model

A transfer function $T(s)$ can be realized in state-space form only when the order of the numerator is not larger than the order of the denominator. A general transfer function from input u_c to output y_c is expressed by a ratio of polynomials of s as

$$T(s) \equiv \frac{y_c(s)}{u_c(s)} = \frac{b_{c0}s^n + b_{c1}s^{n-1} + \cdots + b_{ccn}}{s^n + a_{c1}s^{n-1} + \cdots + a_{cn}} \tag{5.34}$$

The controller canonical form realization of Eq. (5.34) is

$$\begin{aligned} [\dot{x}_c] &= [A_c]\{x_c\} + \{B_c\}u_c \\ y_c &= [C_c]\{x_c\} + D_c u_c \end{aligned} \tag{5.35}$$

where $[A_c] = \begin{bmatrix} 0 & 1 & 0 & \cdots & 0 \\ 0 & 0 & 1 & \cdots & 0 \\ \vdots & \vdots & \vdots & \ddots & \vdots \\ 0 & 0 & 0 & 0 & 1 \\ -a_{c0} & -a_{c1} & -a_{c2} & \cdots & -a_{cn} \end{bmatrix}$, $\{B_c\} = \begin{Bmatrix} 0 \\ 0 \\ \vdots \\ 1 \end{Bmatrix}$,

$$[C_c] = \lfloor (b_{cn} - b_{c0}a_{cn}) \quad (b_{c(n-1)} - b_{c0}a_{c(n-1)}) \quad \cdots \quad (b_{c1} - b_{c0}a_{c1}) \rfloor$$

$$[D_c] = b_{c0}$$

The number of controller states in $\{x_c\}$ is equal to the order of the denominator polynomial in Eq. (5.34).

When two controllers are connected in series, and the input of controller 1 is the output of controller 2 as shown in Fig. 3.2 for the general case, the realization of $T(s)=T_2(s) \cdot T_1(s)$ is performed by using $u_{c1} = y_{c2}$, which yields Eqs. (5.35) with

$$[A_c] = \begin{bmatrix} [A_{c1}] & \{B_{c1}\}[C_{c2}] \\ 0 & [A_{c2}] \end{bmatrix}, \qquad \{B_c\} = \begin{Bmatrix} \{B_{c1}\}D_{c2} \\ \{B_{c2}\} \end{Bmatrix},$$

$$[C_c] = [[C_{c1}] \quad D_{c1}[C_{c2}]] \qquad D_c = D_{c1}D_{c2} \tag{5.36}$$

The assembly of the n_c independent control cascades (each one to be connected to its own actuator) has a multi-input-multi-output block-diagram form. For two control surfaces, for example, the entire state-space open-loop electronic control system is

$$\begin{aligned} [\dot{x}_c] &= [A_c]\{x_c\} + [B_c]\{u_c\} \\ \{y_c\} &= [C_c]\{x_c\} + [D_c]\{u_c\} \end{aligned} \tag{5.37}$$

where

$$[A_c] = \begin{bmatrix} [A_c^{(1)}] & 0 \\ 0 & [A_c^{(2)}] \end{bmatrix} \qquad [B_c] = \begin{bmatrix} \{B_c^{(1)}\} & 0 \\ 0 & \{B_c^{(2)}\} \end{bmatrix}$$

$$[C_c] = \begin{bmatrix} [C_c^{(1)}] & 0 \\ 0 & [C_c^{(2)}] \end{bmatrix} \qquad [D_c] = \begin{bmatrix} D_c^{(1)} & 0 \\ 0 & D_c^{(2)} \end{bmatrix} \tag{5.38}$$

and (1) and (2) represent the matrices for control surface 1 and control surface 2, respectively. The plant and actuator states of Eq. (5.30) are augmented by the control states of Eq. (5.37) by connecting $\{u_{ac}\} = \{y_c\}$ (See Fig. 5.1) which yields

$$\begin{Bmatrix} \dot{x}_p \\ \dot{x}_{ac} \\ \dot{x}_c \end{Bmatrix} = \begin{bmatrix} [A_p] & [B_p][C_{ac}] & 0 \\ 0 & [A_{ac}] & [B_{ac}][C_c] \\ 0 & 0 & A_c \end{bmatrix} \begin{Bmatrix} x_p \\ x_{ac} \\ x_c \end{Bmatrix} + \begin{bmatrix} 0 \\ [B_{ac}][D_c] \\ [B_c] \end{bmatrix} \{u_c\} \tag{5.39}$$

The structures of $[B_{ac}]$, Eq. (5.31), and $[C_c]$ and $[D_c]$, Eq. (5.38), allow for one-by one augmentation of the controller state, where $T_1^{(i)}(s)$ is augmented first, $T_2^{(i)}(s)$ second, for each control surface i. The sensor measurement equation (5.27) becomes

$$\{y\} = [C]\begin{Bmatrix} x_p \\ x_{ac} \\ x_c \end{Bmatrix} = \begin{bmatrix} [C_p] & [D_p] & 0 \end{bmatrix}\begin{Bmatrix} x_p \\ x_{ac} \\ x_c \end{Bmatrix} \tag{5.40}$$

5.3.5 Closed Loop Equations

Equations (5.30) and (5.32), when the control system is based on actuators and gains only, or the extended Eqs. (5.39) and (5.40) have the open-loop control form

$$[\dot{x}] = [A]\{x\} + [B]\{u\} \tag{5.41a}$$

$$\{y\} = [C]\{x\} \tag{5.41b}$$

where {x} contains $2n_m+m+3n_c+n_e$ states where n_m is the number of structural modes, m is the order of the aerodynamic state space, n_c is the number of actuators, and n_e is the total order of the electronic control system. $\{u\}$ contains n_c inputs, and $\{y\}$ contains n_s outputs where n_s is the number of sensors. The aeroservoelastic loop is closed by connecting the inputs to the outputs through a gain matrix $[G]$ as

$$\{u\} = [G]\{y\} \tag{5.42}$$

Substituting Eq. (5.41b) and Eq. (5.42) into Eq.(5.41a), the closed-loop equation is

$$[\dot{x}] = [\bar{A}]\{x\} \tag{5.43}$$

where $[\bar{A}] = [A] + [B][G][C]$. The block diagram of the active control system are shown in Fig. 5.1.

5.4 Definition of Flutter and Control Margins

Eq. (5.43) is the closed-loop system equation of motion with no process noise. For no flutter in the flight envelope, all the eigenvalues of $[\bar{A}]$ should have negative real parts over the entire range of Mach number and dynamic pressure q. Thus, the flutter dynamic pressure q_f is the lowest q for which the real part of any eigenvalue Re(λ_f) crosses the imaginary axis from the left side of the Laplace domain. For a system with m_m measurements and m_c commands, there are m_m x m_c gains in $[G]$. The gains should be designed so that the flight vehicle satisfies the flutter margin, the gain margin, and the phase margin required by Part 25 of the FAR regulation or Mil-Specs. The flutter margin (FM) is defined as

$$FM = (q_f - q_d) / q_d \tag{5.44}$$

where q_f and q_d are the dynamic pressures of flutter and design, respectively. At $q = q_d$, the magnitude of the gain G_{ij} is increased or decreased from its nominal value G_{ij_n} until instability occurs at G_{ij}^*. The gain margin (GM) is then defined as

$$GM_{ij} = 20 \log(G_{ij}^* / G_{ij}) \tag{5.45}$$

A phase margin for each non-zero gain is found by setting $q = q_d$ and $G_{ij} = G_{ij} e^{i\theta_{ij}}$ and by calculating root loci while increasing or decreasing the magnitudes of the phase shift until instability occurs at $\theta = \theta_{ij}^{*}$. The phase margin (*PM*) is then defined by

$$PM_{ij} = -(360/2\pi)\theta_{ij}^{*} \tag{5.46}$$

Flutter margins, gain margins, and phase margins as required by FAR regulations are different for different airplane types. Here, the constraint values are the same as those used in Ref. 5.19:

$$FM \geq 0.44\,,\ |\ GM_{ij}\ | \geq 6.0dB\,,\ \text{and}\ |\ PM_{ij}\ | \geq 60\,\text{deg} \tag{5.47}$$

5.5 Flutter Derivatives with Respect to Control System Parameters (Ref. 5.9)

5.5.1 Flutter Derivatives

Here, the actuator parameters were designed to maximize the flutter speed. To do this, the derivatives of the flutter dynamic pressure with respect to the actuator parameters were required. The derivatives of the flutter dynamic pressure with respect to design variables can be calculated like Ref. 5.19. Once the flutter dynamic pressure q_f and the flutter eigenvalue $\lambda_f = i\omega_f$ are known, the right eigenvector and the left eigenvector can be represented as

$$\left([\overline{A}(q_f)] - \lambda_f [I]\right)\{U_f\} = \{0\} \tag{5.48}$$

$$\{\overline{U}_f\}^T\left([\overline{A}(q_f)] - \lambda_f [I]\right) = \{0\}^T \tag{5.49}$$

The differentiation of Eq. (5.48) with respect to a design parameter X_i, pre-multiplied by $\{\overline{U}_f\}^T$, yields

$$\{\bar{U}_f\}^T\left(\frac{[\bar{A}(q_f)]}{\partial X_i}-\frac{\lambda_f}{\partial X_i}[I]\right)\{U_f\}+\{\bar{U}_f\}^T\left([\bar{A}(q_f)]-\lambda_f[I]\right)\frac{\{\partial U_f\}}{\partial X_i}=\{0\}.$$

The second term of this equation is zero from Eq. (5.49) and the eigenvalue derivative with respect to the design variables is

$$\frac{\partial\lambda_f}{\partial X_i}=\frac{\{\bar{U}_f\}^T\left.\frac{\partial[\bar{A}(q)]}{\partial X_i}\right|_{q=q_f}\{U_f\}}{\{\bar{U}_f\}^T\{U_f\}} \tag{5.50}$$

Similarly, the eigenvalue derivative with respect to the dynamic pressure is

$$\frac{\partial\lambda_f}{\partial q}=\frac{\{\bar{U}_f\}^T\left.\frac{\partial[\bar{A}(q)]}{\partial q}\right|_{q=q_f}\{U_f\}}{\{\bar{U}_f\}^T\{U_f\}} \tag{5.51}$$

where $\frac{\partial[\bar{A}(q)]}{\partial q}$ is the system matrix derivative with respect to the dynamic pressure.

The differential increment of λ due to simultaneous incremental changes in q and in X_i is

$$d\lambda_f=\frac{\partial\lambda_f}{\partial q}dq+\frac{\partial\lambda_f}{\partial X_i}dX_i \tag{5.52}$$

Equation (5.52) is a complex equation. When $d\lambda_f$ is purely imaginary ($d\lambda_f=id\omega_f$), dq is the incremental change in q_f. The real part of Eq. (5.52) in this case yields the flutter dynamic pressure derivatives

$$\frac{\partial q_f}{\partial X_i}=-\frac{\mathrm{Re}(\partial\lambda_f/\partial X_i)}{\mathrm{Re}(\partial\lambda_f/q)} \tag{5.53}$$

5.5.2 System Matrix Derivatives with Respect to Dynamic Pressure

For Eqs. (5.30) and (5.52), when the control system is based on actuators and gains only, the system matrix derivatives in Eqs. (5.50) and (5.51) are calculated as follows (see Ref. 5.9). The closed-loop state matrix $[\bar{A}]$ can be partitioned, for convenience, as

$$[\bar{A}] = \begin{bmatrix} A^{(1)} \\ A^{(2)} \\ A^{(3)} \\ A^{(4)} + B_{ac}GC \end{bmatrix} \tag{5.54}$$

where $A^{(1)} = \begin{bmatrix} 0 & I & 0 & 0 & 0 & 0 \end{bmatrix}$, $A^{(3)} = \begin{bmatrix} 0 & E_s & \frac{V}{b}R & 0 & E_c & 0 \end{bmatrix}$,

$$[A^{(2)}] = -[\bar{M}_s]^{-1} \begin{bmatrix} K_s + qA_{s0} & B_s + \frac{qb}{V}A_{s1} & qD & qA_{c0} & \frac{qb}{V}A_{c1} & \bar{M}_c + \frac{qb^2}{V^2}A_{c2} \end{bmatrix},$$

and $A^{(4)} = \begin{bmatrix} 0 & 0 & 0 & A_{ac} \end{bmatrix}$.

Only $[A^{(2)}]$ is a function of q and can be expressed as

$$[A^{(2)}] = -[\bar{M}_s]^{-1}[\tilde{A}^{(2)}] \tag{5.55}$$

where $[\bar{M}_s] = [M_s] - \frac{qb^2}{V^2}[A_{s2}]$ from Eq. (5.22) and where

$$[\tilde{A}^{(2)}] = \begin{bmatrix} K_s + qA_{s0} & B_s + \frac{qb}{V}A_{s1} & qD & q\tilde{A}_{c0} & \frac{qb}{V}\tilde{A}_{c1} & \bar{M}_c + \frac{qb^2}{V^2}\tilde{A}_{c2} \end{bmatrix} \tag{5.56}$$

The differentiation of Eq. (5.55) with respect to q yields

$$\frac{\partial[A^{(2)}]}{\partial q} = -[\bar{M}_s]^{-2}\frac{\partial[\bar{M}_s]}{\partial q}[\tilde{A}^{(2)}] - [\bar{M}_s]^{-1}\frac{\partial[\tilde{A}^{(2)}]}{\partial q}$$

$$= -[\overline{M}_s]^{-1}(-\frac{b^2}{V^2})[A_{s2}][\overline{M}_s]^{-1}[\widetilde{A}^{(2)}] - [\overline{M}_s]^{-1}\frac{\partial[\widetilde{A}^{(2)}]}{\partial q}$$

and with Eq. (5.55),

$$\frac{\partial[A^{(2)}]}{\partial q} = -[\overline{M}_s]^{-1}\left(-\frac{b^2}{V^2}[A_{s2}][A^{(2)}] + \frac{\partial[\widetilde{A}^{(2)}]}{\partial q}\right) \tag{5.57}$$

where $$\frac{\partial[\widetilde{A}^{(2)}]}{\partial q} = \begin{bmatrix} A_{s0} & \frac{b}{V}A_{s1} & D & \widetilde{A}_{c0} & \frac{b}{V}\widetilde{A}_{c1} & \frac{b^2}{V^2}\widetilde{A}_{c2} \end{bmatrix} \tag{5.58}$$

From Eq. (5.54), since $A^{(1)}$, $A^{(3)}$, and $A^{(4)}$ are not functions of q, and $[C] = \{\phi_y\}[A^{(2)}]$ from Eq. (5.33), the derivative of $[\overline{A}]$ with respect to q is

$$\frac{\partial[\overline{A}]}{\partial q} = \begin{bmatrix} 0 \\ \partial A^{(2)} / \partial q \\ 0 \\ B_{ac}G\phi_y \partial A^{(2)} / \partial q \end{bmatrix} \tag{5.59}$$

The system matrix derivatives with respect to the dynamic pressure can, thus, be calculated analytically from Eq.(5.57), the control system parameters, and the sensor output as shown in Eq. (5.59)

5.5.3 System Matrix Derivatives with Respect to Control System Parameters

As shown in Ref. 5.9, the sensor locations were assumed fixed, and the control system parameters were the control gains G_{ij} and the actuator parameters in $[A_{ac}]$ and $[B_{ac}]$. The derivatives of $[\overline{A}]$ with respect to a control gain G_{ij} which connects the i-th actuator with the j-th sensor can be obtained easily as

$$\frac{\partial[\bar{A}]}{\partial G_{ij}} = \begin{bmatrix} 0 \\ 0 \\ 0 \\ B_{aci}C_j \end{bmatrix} \qquad [5.60]$$

where B_{aci} is the i-th column of $[B_{ac}]$ and C_j is the j-th row of $[C]$. The derivative of $[\bar{A}]$ with respect to a control system dynamic parameter X_{aci}, i.e., a_i and b_0 in Eq. (5.29), is

$$\frac{\partial[\bar{A}]}{\partial X_{aci}} = \begin{bmatrix} 0 \\ 0 \\ 0 \\ \begin{bmatrix} 0 & \frac{\partial A_{ac}}{\partial X_{aci}} \end{bmatrix} + \frac{\partial B_{ac}}{\partial X_{aci}} GC \end{bmatrix} \qquad (5.61)$$

The structures of $[A_{ac}]$ and $[B_{ac}]$ depend on the specific nature of the control component and the associated state-space modeling technique. Here, for one actuator with the transfer function as represented by Eq. (5.27), the derivatives of $[\bar{A}]$ with respect to the actuator parameters a_i and b_0 can be obtained easily from Eq. (5.54). $[A_{ac}]$ is a function of a_i only, $[B_{ac}]$ is a function of b_0 only, and G and C are not functions of a_i nor b_0, thus,

$$\frac{\partial[\bar{A}]}{\partial a_i} = \begin{bmatrix} 0 \\ 0 \\ 0 \\ \begin{bmatrix} 0 & \frac{\partial A_{ac}}{\partial a_i} \end{bmatrix} \end{bmatrix}, \text{ for } i = 0,1,2,\ldots \text{ and } \frac{\partial[\bar{A}]}{\partial b_0} = \begin{bmatrix} 0 \\ 0 \\ 0 \\ \begin{bmatrix} 0 & \frac{\partial B_{ac}}{\partial b_0} GC \end{bmatrix} \end{bmatrix}, \qquad (5.62)$$

5.6 Active Flutter Suppression

The flutter speed was maximized, and the actuator parameters were calculated at the optimum flutter speed by using the IMSL module of Microsoft FORTRAN, specifically the subroutine DUMIDH. It is rather simple to use than NPSOL. Here, a function of N variables is minimized using a modified Newton method. This is an unconstrained optimization problem. The objective function was the negative of the flutter speed because the objective function is minimized in the program. The design variables were the control system parameters. The gradients of the objective and constraint functions were the results of the sensitivity analyses as described in the previous section. The Hessian was calculated by the finite difference method in the program. The method of flutter analysis in the program was the root-locus method. The structure was left unchanged in this optimization.

5.7 Time Accurate Numerical Scheme

Most analytical aeroelastic studies with active control surfaces are restricted to the linear subsonic and supersonic regimes. Aeroelastic characteristics of wings are especially sensitive in the transonic regime because of flow nonlinearity and the presence of moving shock waves. The influence of the control surfaces on the aeroelastic performance of wings is also more pronounced in the transonic regime. A method for the calculation of active controls in the time domain as presented by

P. Guruswamy (Ref. 5.10) is touched on in this section. A typical control law in the time domain can be assumed as

$$\delta(t) = \sum G_j L_j(t) e^{i\varphi_j} \tag{5.63}$$

where $\delta(t)$ is the control surface deflection at time t, G_j is the gain factor for the j-th term, L_j is a selected quantity obtained from the response analysis such as wing deflection, angle of attack, or generalized displacement, velocity, and acceleration at t, and φ_j is the phase angle for the j-th term. This approach was not used here.

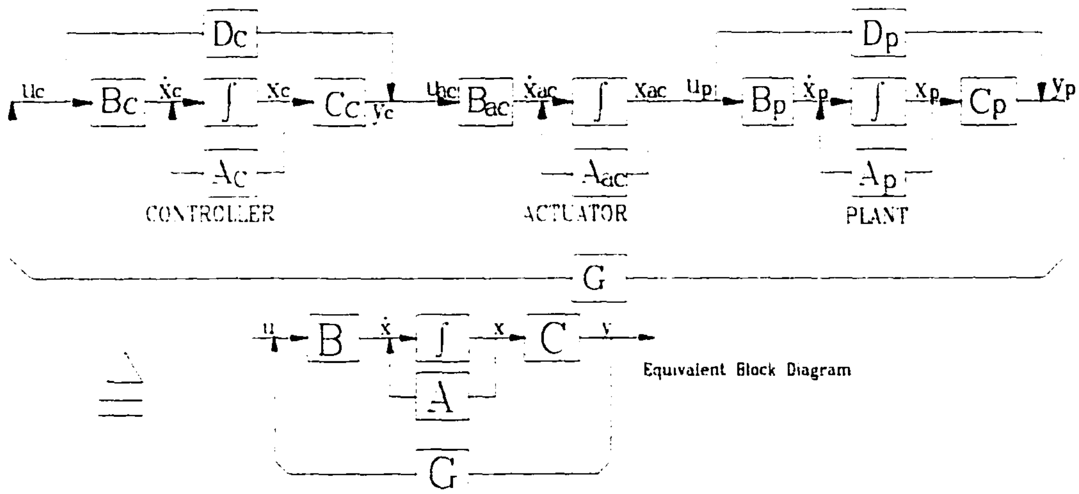

Figure 5.1 Block Diagram of Control System

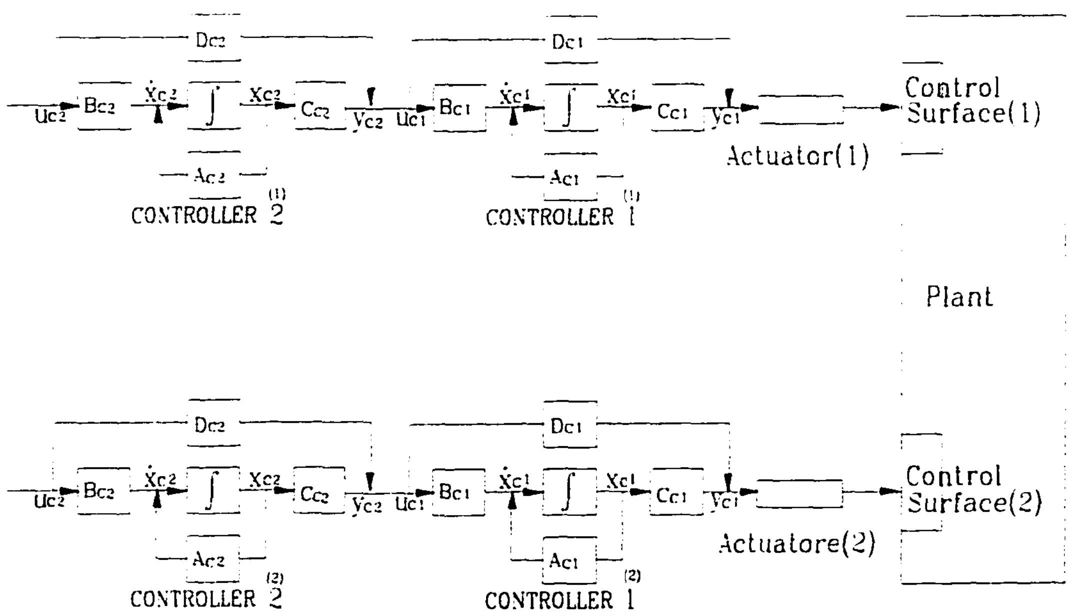

Figure 5.2 Block Diagrams for Two Controllers and Two Control Surfaces

Chapter 6

SENSITIVITY ANALYSIS AND STRUCTURAL DESIGN OPTIMIZATION

6.1 Introduction

6.1.1 Background

Modern high performance control augmented aircraft may exhibit strong coupling between the structural and control systems through aeroelastic effects. This calls for a multidisciplinary optimization process in which the structural and control variables are modified simultaneously (Refs. 6.1, 6.2). Constraints or performance measures can be the aerodynamic pressure distribution, the ratio of total lift to drag, stresses, displacements, control surface travel, hinge moments, flutter speed, control margins, aeroservoelastic poles, gust response, and aircraft maneuver parameters. The design variables can be wing planform data, wing thickness, section properties of structural elements, gain factors, actuator power, and sensor positions. In conventional design, the design variables are optimized in each discipline. If there are conflicts between the disciplines, there have to be trade-offs, and the optimization procedures are iterated. In general, the application of multidisciplinary design optimization techniques can provide new designs that would not have been developed using a conventional approach.

Until now, the practical application capabilities of structural design optimization were limited when compared to the level of existing structural analysis capabilities. However, structural design optimization can be performed by combining the powerful existing analysis tools with mathematical programming methods. The cost of such an optimization of a complex structure is not low. Thus, several optimization techniques such as design variable linking, approximate optimization, temporary constraint deletion, and the use of optimality criteria are needed to reduce the size of the optimization.

In the optimization using numerical solution methods such as direct search methods, the sensitivities of the objective function and of the constraints with respect to the design variables are needed. For any complex problems, these sensitivities can be calculated by finite difference methods. However, sensitivity calculations by the finite difference method need excessive CPU time and make it difficult to obtain accurate results. If sensitivities can be obtained by analytical methods, the optimization process becomes much easier and faster. However, for complex systems, it is often difficult, if not impossible, to find such analytical sensitivities.

A methodology has been presented in Ref. 6.3 to apply optimization to a complex system such as a total aircraft. In this method, the system is divided into many subsystems, the derivatives of each subsystem are calculated, and the optimization of the total system is performed. This methodology is called complete multidisciplinary design optimization.

6.1.2 Review of Previous Work

Early research in flutter-constrained optimization was performed by Turner (Ref. 6.5) and Rudisill and Bhatia (Ref. 6.6). The latter used a second order-formulation to develop expressions for exact derivatives of the flutter speed with respect to the structural design variables. Structural design optimizations for sizing the finite elements of aircraft structures were performed for strength and flutter requirements in Refs. 6.7-8. In Ref. 6.7, Wilkinson and Lerner used energy principles, optimality criteria, and numerical search techniques to achieve minimum weight design. In Ref 6.8, Wilkinson, Markowitz, Lerner, and George achieved minimum weight designs for metal and composite structures. Sensitivity derivatives of the flutter dynamic pressure and the stability margin with respect to the design variables were developed by Karpel (Ref. 5.20) for aeroservoelastic systems. Multidisciplinary optimization of aeroservoelastic systems were performed by Karpel (Refs. 6.9-10) with simultaneous optimal design of the structural and control components. There are many references relating structural optimization with aeroelastic constraints, such as Refs. 6.11, 6.12, 6.13, and 6.14.

Numerical optimization methods which can be applied to the optimization of large structures were presented by Gabriele and Ragsdell (Ref. 6.15) and Vanderplaats (Ref. 6.16). Several methods such as approximate concepts and optimality criteria to be applied to such complex structures were presented in Refs. 6.17-19.

A method for decomposing the optimization problem for coupled systems was developed by Sobieszczanski-Sobieski (Refs. 6.3-4) and the method was applied to aircraft design by Logan (Ref. 6.1), Malone and Mason (Ref. 6.2), and Arslan and Carlson (Ref. 6.20). However, they did not apply this method in the field of dynamic aeroelasticity.

Design sensitivity analyses and structural optimizations can be performed by multidisciplinary codes such as ASTROS* and MSC/NASTRAN (Ref. 6.21) for statics, normal modes, static aeroelasticity, and flutter by approximate methods. In these codes, powerful analysis capabilities are combined with numerical optimization approaches.

6.1.3 Scope of Research

The main process of design optimization as used here applied iterations of analysis, approximation, and optimization as shown in Fig. 6.1. In this method, the disciplinary analyses were performed first. The derivatives of the objective function and the constraints with respect to the given design variables were formulated, and the objective function and the constraints were approximated by Taylor's series expansions. The next design point was calculated by solving the approximate optimization problem using numerical optimizer NPSOL. The iterations were continued until convergence requirements were satisfied.

The objective function, the constraints, and the design variables used for the design optimization of airplane wings are defined in Section 6.2. Several optimization techniques to reduce the number of analyses are reviewed in Section 6.3. The mathematical programming techniques utilized here were design variable linking, approximate optimization, temporary constraint deletion, and the use of optimality criteria such as duality and fully stressed design methods. The sensitivity analyses are formulated in Section 6.4. The derivatives for statics and normal modes were formulated, as were the derivatives of flutter speed and control margins with respect to the design variables. The flutter sensitivity analysis methods used in ASTROS* and MSC/NASTRAN were reviewed. The global sensitivity equations of coupled systems as presented by Sobieszczanski-Sobieski were reviewed, as well.

6.2 Definition of Design Optimization of Airplane Wings with Control Surfaces

6.2.1 Objective Function

The objective function for structural design optimization of aircraft is rather simple. The total weight of all elements to be designed is generally used

$$W = \sum_{k=1}^{n_d} \rho_k X_k A_k \tag{6.1}$$

where ρ is density, X is skin thickness or section area of a bar, A is skin area or bar length, and n_d is the total number of design variables. Here, A and ρ were fixed in the FEM model and X was considered as the set of design variables. The objective function was a linear equation.

6.2.2 Constraints

The calculation of the constraints for the structural design optimization of an aircraft is complex. The constraints used here were the stress requirements of each element and the wing tip displacements due to static loads in statics or static aeroelasticity in the trim condition, a flutter speed requirement, and gain margin requirements in the control system.

If the applied stresses in the elements are σ_i, and the maximum displacements at the wing tip are u_i, then the constraints for static loading are

$$\{g_1\} = \frac{\sigma_i}{\sigma_{all}} - 1 \le 0 \tag{6.2}$$

$$\{g_2\} = \frac{u_i}{u_{all}} - 1 \le 0 \tag{6.3}$$

where σ_{all} and u_{all} are the allowable stress in the elements and the largest allowable displacement of the structure, respectively. In normal modes optimization, the lower limit of the first natural frequency was required to be a certain value, here:

$$g_3 = \frac{f_D}{f_1} - 1 \le 0 \tag{6.4}$$

where f_D is the required design frequency and f_1 is the first natural frequency calculated at the current design point. The flutter requirement was

$$g_4 = \frac{V_D}{V_F} - 1 \le 0 \tag{6.5}$$

where V_D is the design flutter velocity of the aircraft and V_F is the flutter velocity calculated at the current design point. The design flutter velocity of an aircraft is often required to be 1.15 times the limit velocity of the aircraft in FAR aviation regulations. Additional safety margins are required when a control system is involved. The requirements for control gain margins were given in Eq. (5.47). The inequality constraints for positive gain margins were chosen to be

$$\{g_5\} = \frac{6.0}{PGM_{ij}} - 1 \leq 0 \tag{6.6}$$

and the inequality constraints for negative gain margins were

$$\{g_6\} = \frac{-6.0}{NGM_{ij}} - 1 \leq 0 \tag{6.7}$$

where PMG_{ij} and NMG_{ij} are the positive gain margins and negative gain margins, respectively. The inequality constraints for positive phase margins were

$$\{g_7\} = \frac{60.0}{PPM_{ij}} - 1 \leq 0 \tag{6.8}$$

and the inequality constraint of negative gain margins were

$$\{g_8\} = \frac{-60.0}{NPM_{ij}} - 1 \leq 0 \tag{6.9}$$

where PPG_{ij} and NPG_{ij} are the positive gain margins and negative gain margins, respectively. All inequality equations were scaled to the range from –1 to zero to use the method of temporary constraint deletion which will be explained in Section 6.3.2.

6.2.3 Design Variables

From an aerodynamic point of view, plan form configurations such as aspect ratio, taper ratio, and sweep back angle together with wing thickness can be considered. However, these were not considered here. Instead, the design variables were the section properties of the elements and the control gains.

$$\{X\} = \begin{Bmatrix} T_i \\ G_{ij} \end{Bmatrix} \tag{6.10}$$

where T_i are skin the thicknesses, the ply thicknesses for composite materials, or the stiffener areas, and G_{ij} are the control gains.

6.3 Design Optimization Methodologies for Complex Structures

6.3.1 Approximate Structural Design Optimization

With information acquired from the structural analysis and a subsequent sensitivity analysis, an approximate optimization problem can be formulated. In this approach, the optimization problem is combined with the analysis program. This method is very simple and can be applied to any problem before a designer uses more complex methods to solve his/her design problems. In general, an optimization problem is posed as follows:

$$\text{Minimize} \quad f(\mathbf{Y}(\mathbf{X})) \tag{6.11}$$

$$\text{subject to } g_j(\mathbf{Y}(\mathbf{X})) \le 0 \quad j = 1, 2, \cdots, n_c \tag{6.12}$$

$$\text{with bounds } \; X_L \le X_i \le X_U, \;\; i = 1, 2, \ldots, n_d \tag{6.13}$$

where **X** is the vector of design variables (n_d x 1), **Y** is the vector of intermediate design variables (n_{id} x 1), and g_j is the j-th inequality constraint. This problem can be modified to an approximate design problem as

Minimize

$$\tilde{f}(\mathbf{Y}(\mathbf{X})) = \tilde{f}(\mathbf{Y}(\mathbf{X}_0)) + \sum_{k=1}^{n_{id}} \frac{\partial f(\mathbf{Y}(\mathbf{X}_0))}{\partial X_k}(Y_k(\mathbf{X}) - Y_k(\mathbf{X}_0)) \tag{6.14}$$

subject to

$$\tilde{g}_j(\mathbf{Y}(\mathbf{X})) = g_j(\mathbf{Y}(\mathbf{X}_0)) + \sum_{k=1}^{n_{id}} \frac{\partial g_j(\mathbf{Y}(\mathbf{X}_0))}{\partial X_k}(Y_k(\mathbf{X}) - Y_k(\mathbf{X}_0)) \quad j = 1, 2, \cdots, n_c \tag{6.15}$$

with bounds

$$X_L \le X_i \le X_U, \quad i = 1, 2, \ldots, n_d \tag{6.16}$$

In the design of wing structures, the objective function is not required to be approximated by Eq. (6.14) because the weight is represented by a simple explicit linear function.

6.3.2 Temporary Constraint Deletion

Before solving the optimization problem, we can reduce the number of constraints by deleting those constraints whose values are lower than given cutoff values at the design point. For example, values of the constraints in Eq. 6.2 or 6.9 lower than -0.5 at a design point can be deleted before optimizing. To apply this method, the constraints should be scaled to values between -1 and 0.

6.3.3. Design Variable Linking

When design variables are related to each other, the number of independent design variables can be reduced. Here, the section properties of the elements, the design variables, are represented as a linear sum of vectors as

$$\{X\} = \sum_{i=1}^{m} \{T_i\} a_i = [T]\{a\} \tag{6.17}$$

where the number of design variables is n, the number of independent linked variables is m, the number of design variables is reduced from n to m. In ASTROS* and MSC/NASTRAN, $\{X\}$ are called local design variables and a_i are called global design variables. Practically, there are two approaches to apply this method. In the first approach, elements are being designed to the same geometrical property for manufacturing reasons, based on structural symmetry or on designer decisions. This approach, for example, when $n = 8$ and $m = 4$, can be expressed in the form.

$$\begin{Bmatrix} X_1 \\ X_2 \\ X_3 \\ X_4 \\ X_5 \\ X_6 \\ X_7 \\ X_8 \end{Bmatrix} = \begin{bmatrix} 1 & 0 & 0 & 0 \\ 1 & 0 & 0 & 0 \\ 0 & 1 & 0 & 0 \\ 0 & 0 & 1 & 0 \\ 0 & 0 & 1 & 0 \\ 0 & 0 & 0 & 1 \\ 0 & 0 & 0.5 & 0 \\ 0 & 0.5 & 0 & 0 \end{bmatrix} \begin{Bmatrix} a_1 \\ a_2 \\ a_3 \\ a_4 \end{Bmatrix} \tag{6.18}$$

In this case, the local design variables X_1 and X_2 are the same as the global design variable a_1, and X_4 and X_5 are the same as a_3. In the second approach, each column of $[T]$ is an independent basis vector, called the shape function for the global design variable similar to the modal approach in vibration analysis. a_i are reduced sets of the generalized design variables. Practically, for structural design optimization problems, it is very difficult to find these vectors, especially in multidisciplinary design optimization while still satisfying all constraints.

Here, the gradient of a property $F(a_i)$ is represented as

$$\frac{\partial F(a_i)}{\partial a_i} = T^T \frac{\partial F(X_i)}{\partial X_i} \tag{6.19}$$

6.3.4 Optimality Criteria Methods

In optimality criteria methods, an algebraic or a differential equation which forms the optimality condition is used to solve the optimization problem unlike direct search methods. In Chapter 8 of Ref. 6.19, Haftka states that a simple optimality condition is the requirement that the first derivatives of the objective function are zero. The Euler-Lagrange equation which is used when the objective function is a functional and the Kuhn-Tucker conditions are optimality criteria. The dual method and the fully stressed design method which are used for structural optimization and available in ASTROS* are reviewed in the following.

a. Dual Methods

In the simplest linear problems, if the primal problem is written as

$$\begin{aligned} &\text{Minimize} \quad c^T X \\ &\text{subject to} \quad AX - b \geq 0 \end{aligned} \tag{6.20}$$

$X \geq 0$

then, the dual formulation in terms of the Lagrange multipliers is

$$\text{Maximize } \lambda^T b$$
$$\text{subject to } \lambda^T A - c \leq 0 \tag{6.21}$$
$$\lambda \geq 0$$

When the number of design variables is small and the number of constraints is large, the problem can be simplified by interchanging the number of design variables and the number of constraints. For non-linear problems,

$$\text{Minimize } f(X)$$
$$\text{subject to } g_j(X) \geq 0, \; j = 1,..,n_g \tag{6.22}$$

Falk's dual formulation is given in Chapter 8 of Ref. 6.19

$$\text{Maximize } \mathsf{L}_m(\lambda)$$
$$\text{such that } \lambda_j \geq 0, \; j = 1,..,n_g, \tag{6.23}$$

where

$$\mathsf{L}_m(\lambda) = \min_{X \in C} \mathsf{L}(X, \lambda), \tag{6.24}$$

and where

$$\mathsf{L}(X, \lambda) = f(X) - \sum_{j=1}^{n_g} \lambda_j g_j(X) \tag{6.25}$$

and C is some closed convex set introduced to ensure the well conditioning of the problem. A function is convex if

$f(\alpha x_2 + (1-\alpha)x_1) \leq \alpha f(x_2) + (1-\alpha) f(x_1)$, $0 \leq \alpha \leq 1$

where $x_1, x_2 \in S$, $\alpha x_1+(1-\alpha x_2) \in S$, $0 \le \alpha \le 1$, where S is a feasible domain. A function of n variables is convex if its Hessian is positive semi-definite.

b. Fully Stressed Design

Fully stressed design is a powerful optimality criteria method used in structural optimization. It is an intuitive condition which is different from the rigorous mathematical statements such as the Kuhn-Tucker conditions. But this technique is applicable to structures that are subject only to stress and minimum gage constraints. In Ref. 6.19, the FSD optimality criterion has been stated as follows:

"For the optimum design, each member of the structure that is not at its minimum gage is fully stressed under at least one of the design load conditions."

The FSD technique is usually complemented by a resizing algorithm based on the assumption that the load distribution in the structure is independent of member size. For truss structures, where the design variables are the cross-sectional areas, the force in any member is σA where σ is the axial stress and A is the cross-sectional area. Assuming that σA is constant leads to the stress ratio resizing technique

$$A_{new} = A_{old} \frac{\sigma}{\sigma_0} \tag{6.26}$$

where σ_0 is the allowable stress. For plate elements of uniform thickness, one can assume that $\sigma_{ij}t$ is constant, where t is the local thickness and σ_{ij} are the membrane stress components. The stress constraint is often expressed in terms of an equivalent stress σ_e as

$$\sigma_e = f(\sigma_{ij}) \leq \sigma_0 \tag{6.27}$$

For the von Mises stress constraint in a plane-stress problem,

$$\sigma_e^2 = \sigma_x^2 + \sigma_y^2 - \sigma_x \sigma_y + 3\tau_{xy}^2 \leq \sigma_0^2 \tag{6.28}$$

In this case, the stress ratio technique becomes

$$t_{new} = t_{old} \frac{\sigma}{\sigma_0} \tag{6.29}$$

6.3.5 Convergence Criteria

There are two sets of convergence criteria for two step iterations, where the first step contains the iterations in the inner phase where the approximate optimization problem is solved, and the second step the outer iterations of larger cycles which include analyses. In both steps in ASTROS* and MSC/NASTRAN, absolute and relative convergence criteria are used for the objective function, the constraints, and the side constraints on the design variables. When both sets of criteria for the objective function and the constraints are satisfied, the optimization problem is converging to a unique design. When the objective function convergence criteria are satisfied and the constraint convergence criteria are not satisfied, a best compromise infeasible design point can be found, if the side constraints on the design variables are satisfied. In flutter optimization, the convergence decision for the first step was done in NPSOL, and the convergence decision for the second step was performed after the flutter analysis by ASTROS* and the root-locus method at the given design point when the objective function, the flutter speed, met given convergence criteria. For the case of flutter suppression, which was unconstrained problem solved using IMSL, the absolute convergence criteria on the design variables and the objective function were applied.

6.4 Sensitivity Analysis

In order to obtain search directions or to generate approximate problems, the derivatives of the responses with respect to the design variables must be made available. The derivatives can be obtained analytically or by the finite difference method. To calculate the derivatives of responses, the derivatives of $[M]$, $[C]$, and $[K]$ with respect to the structural variables are frequently used. Many FEM codes have built-in modules to calculate these derivatives.

6.4.1 Sensitivity Derivatives for Statics

The derivatives of the static responses such as stresses, $\dfrac{\partial \sigma_j}{\partial X_i}$, and displacements, $\dfrac{\partial q_k}{\partial X_i}$, with respect to the design variables should be calculated to use in design optimization. The displacement responses due to the applied loads are computed by a displacement-based linear static analysis. The other static responses such as the stresses or strains are function of the displacements in the form

$$r = r(\bar{q}) \tag{6.30}$$

while the displacements are functions of the design variables

$$\bar{q} = \bar{q}(\bar{X}) \tag{6.31}$$

Thus, the static responses are implicit functions of the design variables implicitly as well as the displacements of the form

$$\bar{r} = \bar{r}\{\bar{q}(\bar{X})\} \tag{6.32}$$

In MSC/NASTRAN, as stated in Ref. 6.21, the sensitivities of these responses with respect to the design variables are approximated using first forward finite differences such as

$$\frac{\partial r_j}{\partial X_i} = \frac{r_j(\bar{X}^0 + \Delta X_i, \bar{q}^0 + \Delta\bar{q}) - r_j(\bar{X}^0, \bar{q}^0)}{\Delta X_i} \tag{6.33}$$

where r_j is the j-th design response. To calculate this equation, $\Delta\bar{q}$ should be known and is represented by

$$\Delta\bar{q} = \frac{\partial\bar{q}}{\partial X_i} \times \Delta X_i \tag{6.34}$$

Eq. (6.34) requires the displacement sensitivities. These can be computed by differentiating the equations of static equilibrium

$$[k]\{q\} = \{P\} \tag{6.35}$$

to obtain

$$[k]\frac{\partial\{q\}}{\partial X_i} = \frac{\partial\{P\}}{\partial X_i} - \frac{\partial[k]}{\partial X_i}\{q\} \tag{6.36}$$

The first term on the right side can be calculated by the finite difference method although it is usually zero. The displacements $\{q\}$ can be calculated via an analysis at the current design point. $[k]$ is the physical stiffness matrix and can be calculated by the FEM program. The second term on the right side becomes

$$\frac{\partial[k]}{\partial X_i}=\frac{\partial[k_i]}{\partial X_i} \tag{6.37}$$

where $[k_i]$ is the increase of the stiffness matrix due to an increase in the design variable X_i where the other elements of $[k]$ are independent of X_i. For linear systems,

$$\frac{\partial[k_i]}{\partial X_i}=\frac{[k_i]}{X_i} \tag{6.38}$$

This can be easily calculated in the FEM program. With Eqs. (6.37) and (6.38), displacement sensitivities can be calculated from Eq. (6.36) and the other static response sensitivities can be calculated with Eqs. (6.33) and (6.34)

6.4.2 Sensitivity Derivatives for Normal Modes

Eigenvalue sensitivities are calculated in the normal modes discipline like Ref. 6.21. The eigenvalue equation is

$$([k]-\lambda_j[m])\{\phi_j\}=0 \tag{6.39}$$

where λ_j and ϕ_j are the j-th eigenvalue and eigenvector, respectively. Eq. (6.39) can be differentiated with respect to the j-the design variable X_i to yield

$$([k]-\lambda_j[m])\frac{\partial\{\phi_j\}}{\partial X_i}+\left(\frac{\partial[k]}{\partial X_i}-\lambda_j\frac{\partial[m]}{\partial X_i}\right)\{\phi_j\}=\frac{\partial\lambda_j}{\partial X_i}[m]\{\phi_j\} \tag{6.40}$$

When Eq. (6.40) is pre-multiplied by ϕ_j^T, the first term is zero. Eq. (6.40) can be solved for the eigenvalue derivatives

$$\frac{\partial \lambda_j}{\partial X_i} = \frac{\{\phi_j\}^T \left(\frac{\partial [k]}{\partial X_i} - \lambda_j \frac{\partial [m]}{\partial X_i} \right) \{\phi_j\}}{\{\phi_j\}^T [m] \{\phi_j\}} \tag{6.41}$$

In Eq. (6.41), the derivatives of the stiffness matrix can be calculated by Eqs. (6.37) and (6.38), and the derivatives of the mass matrix can be calculated by the same method.

6.4.3 Flutter Derivatives for Aeroelastic Systems

The derivatives of the flutter speed with respect to the design variables can be calculated from Eq. (4.1), the second order differential equation, as stated in Ref. 6.7. By neglecting damping and using $s = i\omega$ and $k = b\omega / V$, Eq. (4.1) becomes

$$\left[[K] - \lambda([M] - \frac{\rho b^2}{2k^2}[Q(ik)]) \right] \{\eta_r\} = 0 \tag{6.42}$$

If we set $[A] = \frac{\rho b^2}{2k^2}[Q(ik)]$, the flutter sensitivities can be derived similar to Ref. 6.7.

$$\frac{\partial V_f}{\partial X_i} = -\frac{b\omega}{k^2}(\frac{\partial k}{\partial X_i}) + \frac{b}{2k\omega}(\frac{\partial \lambda}{\partial X_i}) \tag{6.43}$$

where

$$\frac{\partial k}{\partial X_i} = \frac{R_1 I_3 - I_1 R_3}{R_2 I_3 - I_2 R_3} \tag{6.44}$$

$$\frac{\partial\lambda}{\partial X_i} = \frac{(R_1 - R_2 \dfrac{\partial k}{\partial X_i})R_3 + (I_1 - I_2 \dfrac{\partial k}{\partial X_i})I_3}{R_3{}^2{}_3 - I_3{}^2} \tag{6.45}$$

and

$$R_1 + iI_1 = \{\eta_l\}^T (\frac{\partial[K]}{\partial X_i} - \lambda \frac{\partial[M]}{\partial X_i})\{\eta_r\} \tag{6.46}$$

$$R_2 + iI_2 = \lambda\{\eta_l\}^T (\frac{\partial[A]}{\partial k})\{\eta_r\} \tag{6.47}$$

$$R_3 + iI_3 = \{\eta_l\}^T ([M] + [A])\{\eta_r\} \tag{6.48}$$

Here, $\{\eta_r\}$ and $\{\eta_l\}$ are the left-handed and right-handed eigenvectors of Eq. (6.42),

$$[M] = [\Phi]^T [m][\Phi] \qquad \text{(6.49a\}}$$

$$[K] = [\Phi]^T [k][\Phi], \qquad \text{(6.49b\}}$$

and

$$\frac{\partial[M]}{\partial X_i} = \frac{[\Phi]^T [m_i][\Phi]}{X_i} \tag{6.50}$$

$$\frac{\partial[K]}{\partial X_i} = \frac{[\Phi]^T [k_i][\Phi]}{X_i} \tag{6.51}$$

where $[M_i]$ and $[K_i]$ are null matrices except for the terms associated with X_i. It was assumed that $[m]$ and $[k]$ were linear functions of X_i.

6.4.4 Sensitivity Derivatives for Aeroservoelastic Systems (Ref. 5.9)

Using the system matrix of Eq. (5.43) for an aeroservoelastic system, the derivative of the flutter dynamic pressure with respect to a design variable, X_i, the system matrix derivative with respect to the dynamic pressure, q, and the system matrix derivatives with respect to the actuator parameters were derived in Section 5.5.1, Section 5.5.2, and Section 5.5.3, respectively.

The derivatives of the system matrix, $[\bar{A}]$, with respect to a structural design variable, X_k, are

$$\frac{\partial[\bar{A}]}{\partial X_k} = \begin{bmatrix} 0 \\ \partial A^{(2)} / \partial X_k \\ 0 \\ B_{ac} G \phi_y \partial A^{(2)} / \partial X_k \end{bmatrix} \tag{6.52}$$

where

$$\frac{\partial[A^{(2)}]}{\partial X_k} = -[\bar{M}]^{-1}\left(\frac{\partial[M_s]}{\partial X_k}[A^{(2)}] + \begin{bmatrix} \frac{\partial[K_s]}{\partial X_k} & 0 & 0 & 0 & 0 & \frac{\partial[M_c]}{\partial X_k} \end{bmatrix} \right) \tag{6.53}$$

The derivatives of $[\bar{A}]$ with respect to the control gain G_{ij}, which connects the i-th actuator with the j-th sensor, are

$$\frac{\partial[\bar{A}]}{\partial G_{ij}} = \begin{bmatrix} 0 \\ 0 \\ 0 \\ B_{ac_i} C_j \end{bmatrix} \tag{6.54}$$

where B_{ac_i} is the i-th column of $[B_{ac}]$ and C_j is the j-th row of $[C]$.

The calculation of the derivative of a gain margin with respect to a gain, G_{ij}, was derived in Ref. 5.19 as follows: The value G_{ij}^{*} which causes flutter at $q_f^{*} = q_d$ and the gain margin GM_{ij} are calculated by Eq. (5.45). Since G_{ij}^{*} is not a function of G_{ij} itself, the differentiation of Eq. (5.45) with respect to G_{ij} yields:

$$\frac{\partial GM_{ij}}{\partial G_{ij}} = -\frac{20/\ln 10}{G_{ij\,n}} \tag{6.55}$$

The differentiation of Eq. (5.39) with respect to a design variable yields:

$$\frac{\partial GM_{ij}}{\partial X_i} = -\frac{20/\ln 10}{G_{ij}^{*}}\frac{\partial G_{ij}^{*}}{\partial X_i} \tag{6.56}$$

The calculation of the derivatives of a phase margin with respect to the G_{ij} starts with finding the phase shift $\theta_{ij} = \theta_{ij}^{*}$, which causes flutter at $q_f^{*} = q_d$. The differentiation of Eq. (5.40) with respect to X_i yields

$$\frac{\partial PM_{ij}}{\partial X_i} = -\frac{360}{2\pi}\frac{\partial \theta_{ij}^{*}}{\partial X_i} \tag{6.57}$$

6.4.5 Sensitivity Analysis by ASTROS* and MSC/NASTRAN

In ASTROS* and MSC/NASTRAN, the flutter design capability uses the pk-flutter method and the factor that the design response is the decay coefficient γ for a given design velocity or Mach number. The eigenvalue problem for flutter was given in Eq. (4.1) as

$$\begin{aligned}&\left[\mathbf{M}p^2+(\mathbf{C}-\frac{1}{4}\rho cVQ^I/k)p+(\mathbf{K}-\frac{1}{2}\rho V^2\mathbf{Q}^R)\right]\{\eta_r\}\\&=[F_{hh}]\{\eta_r\}\\&=[\Phi]^T[F_{gg}][\Phi]\{\eta_r\}=0\end{aligned} \tag{6.58}$$

where F_{gg} is the counterpart of F_{hh} for physical coordinates. The complex eigenvalue is

$$p=\omega(\gamma+i)=p_R+ip_I \tag{6.59}$$

From the relations $\gamma=p_R/\omega$ and $p_I=\omega$, the differential increment is expressed in terms of the real and imaginary parts of the eigenvalues as

$$\Delta\gamma=\frac{1}{\omega}(\Delta p_R-\gamma\Delta p_I) \tag{6.60}$$

To calculate Δp_P and Δp_I, the formulation of the left-handed and right-handed eigenvector in the global set (physical coordinates) is used:

$$\{v\}=[\Phi]\{\{\eta_l\} \tag{6.61}$$

$$\{u\}=[\Phi]\{\{\eta_r\} \tag{6.62}$$

Eq. (6.58) becomes

$$\begin{aligned}&\{v\}^T\left[p^2\Delta\mathbf{m}+p\Delta\mathbf{c}+\Delta\mathbf{k}+(2p\mathbf{m}+\mathbf{c})\Delta p\right]\{\eta_r\}\\&-\{v\}^T\left[\frac{1}{8}\rho c^2 p\Delta p_R\frac{\partial\mathbf{Q}^I}{\partial k}+\frac{1}{4}\rho cV\mathbf{Q}^I\Delta p+\frac{1}{4}\rho cV\Delta p\frac{\partial\mathbf{Q}^R}{\partial k}\right]\{\eta_r\}=0\end{aligned}\tag{6.63}$$

From this complex equation, the complex Δp can be calculated.

6.4.6 Global Sensitivity Equations of Coupled Systems

A system can be decomposed with coupled subsystems and represented as a set of simultaneous coupled equations as in Ref. 6.3 by

$$\begin{aligned}&\mathbf{f}_\alpha[(\mathbf{X},\mathbf{R}_\beta,\mathbf{R}_\gamma),\mathbf{R}_\alpha]=\mathbf{0}\\&\mathbf{f}_\beta[(\mathbf{X},\mathbf{R}_\gamma,\mathbf{R}_\alpha),\mathbf{R}_\beta]=\mathbf{0}\\&\mathbf{f}_\gamma[(\mathbf{X},\mathbf{R}_\alpha,\mathbf{R}_\beta),\mathbf{R}_\gamma]=\mathbf{0}\end{aligned}\tag{6.64}$$

where α, β, and γ mean symbols of the subsystems, **X** are the independent variables, and **R** are dependent variables. Each of the subsystems represents a distinct and separate analysis. Sensitivity derivatives of the solution **R** with respect to the independent variables **X** can be calculated using finite-difference techniques. However, this may be costly if the system analyses are nonlinear or iterative, and inaccurate to the point of producing meaningless results as the effects of small perturbations in **X** may drown in the noise of the iterative solution of the system. Sobieszczanski-Sobieski in Ref. 6.3 derived another method to calculate the sensitivity derivatives of the system solution **R** with respect to the independent variables **X**.

The implicit function theorem of functional analysis states that a set of governing equations

$$\mathbf{F}(\mathbf{R}.\mathbf{X}) = 0 \tag{6.65}$$

$$\mathbf{R} = \mathbf{f}(\mathbf{X}) \tag{6.66}$$

has the following sensitivity equation

$$\left[\frac{\partial \mathbf{F}}{\partial \mathbf{R}}\right]\left\{\frac{\partial \mathbf{R}}{\partial \mathbf{X}_k}\right\} = -\left\{\frac{\partial \mathbf{F}}{\partial \mathbf{X}_k}\right\} \tag{6.67}$$

The sensitivity equations are always linear, simultaneous, and algebraic, regardless of the mathematical nature of the governing equations of the system. The matrix of coefficients is a Jacobian matrix of the partial derivatives with respect to the dependent variables, and the right side vector contains the partial derivatives with respect to a particular independent variable. When applied to the partitioned system in Eq. (6.64), the sensitivity equation becomes

$$\begin{bmatrix} \dfrac{\partial \mathbf{f}_\alpha}{\partial \mathbf{R}_\alpha} & \dfrac{\partial \mathbf{f}_\alpha}{\partial \mathbf{R}_\beta} & \dfrac{\partial \mathbf{f}_\alpha}{\partial \mathbf{R}_\gamma} \\ \dfrac{\partial \mathbf{f}_\beta}{\partial \mathbf{R}_\alpha} & \dfrac{\partial \mathbf{f}_\beta}{\partial \mathbf{R}_\beta} & \dfrac{\partial \mathbf{f}_\beta}{\partial \mathbf{R}_\gamma} \\ \dfrac{\partial \mathbf{f}_\gamma}{\partial \mathbf{R}_\alpha} & \dfrac{\partial \mathbf{f}_\gamma}{\partial \mathbf{R}_\beta} & \dfrac{\partial \mathbf{f}_\gamma}{\partial \mathbf{R}_\gamma} \end{bmatrix} \begin{Bmatrix} \dfrac{\partial \mathbf{R}_\alpha}{\partial \mathbf{X}_k} \\ \dfrac{\partial \mathbf{R}_\beta}{\partial \mathbf{X}_k} \\ \dfrac{\partial \mathbf{R}_\gamma}{\partial \mathbf{X}_k} \end{Bmatrix} = -\begin{Bmatrix} \dfrac{\partial \mathbf{f}_\alpha}{\partial \mathbf{X}_k} \\ \dfrac{\partial \mathbf{f}_\beta}{\partial \mathbf{X}_k} \\ \dfrac{\partial \mathbf{f}_\gamma}{\partial \mathbf{X}_k} \end{Bmatrix} \tag{6.68}$$

A multidisciplinary optimization process can be made more concurrent by use of global sensitivity equations. Such equations were derived for internally coupled systems by Sobieszczanski-Sobieski (Ref. 6.3). In designing aircraft, many conflicting design features in each discipline or level can be integrated. Logan (Ref. 6.1) decomposed the aircraft system. For wing design as treated in Ref. 6.1, the conventional design process and a multidisciplinary design process are shown in Figs. 6.2 and 6.3.

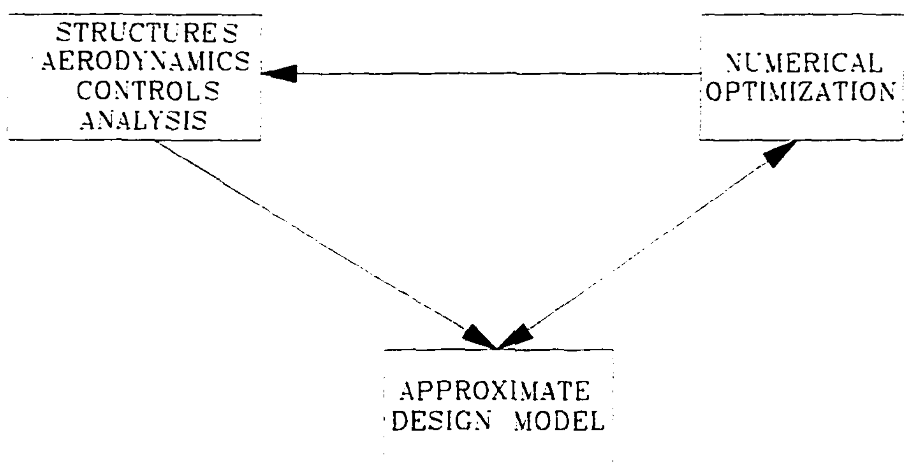

Figure 6.1 Relationship of Analysis and Approximate Design Optimization

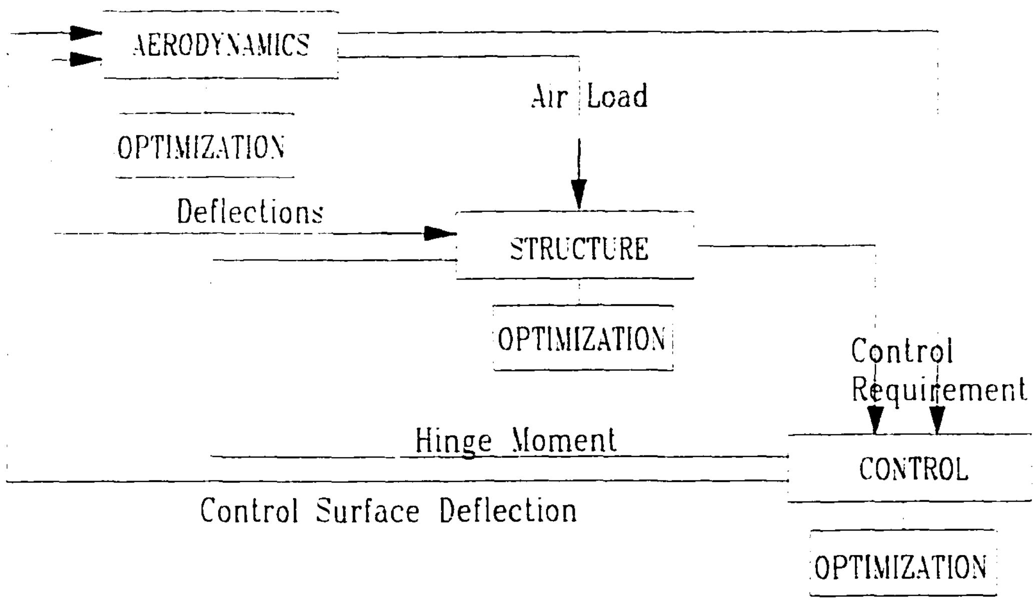

Figure 6.2 A Conventional Design Optimization Process

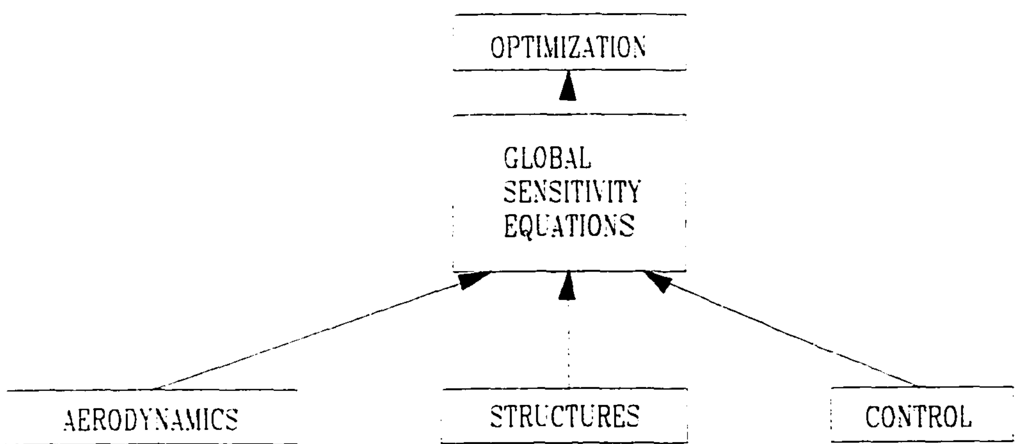

Figure 6.3 Multidisciplinary Design Optimization Process

Chapter 7

APPLICATIONS TO ACTUAL MODELS

7.1 Development of Benchmarking Models

A new aerodynamic module, ZAERO, was recently installed in ASTROS, creating ASTROS*, which contains the aerodynamic codes ZONA6, ZTAIC, ZONA7, and ZONA7U. Aerodynamic loads can now be calculated in the complete speed regime from subsonic over transonic to supersonic and hypersonic flow (Ref. 1.6). For verification of the accuracy, ease of use, and practical application capabilities of the new programs, benchmarking and testing is necessary.

In order to test and benchmark the aerodynamic, structural, and aeroelastic analysis as well as structural design optimization capabilities in ASTROS* for multiple disciplines, three different wing models were used: the GAF wing model, the DAST wing model, and the AAW model. GAF stands for "Generalized Advanced Fighter" wing and AAW stands for ASTROS* Aeroelastic Wing. This wing model was generated from MSC/NASTRAN data, obtained from P.C. Chen of ZONA Technology, Inc. (Ref. 7.1). The DAST model was developed from a supercritical wing model used to analyze a drone, flown in a flight test facility (Ref 5.3). The ASTROS* and MSC/NASTRAN data for this model were generated from Engineering Analysis Language (EAL, Ref. 7.3) data, obtained from NASA Langley Research Center. The AAW model or "ASTROS* Aeroelastic Wing" model represents a derivative of a MSC/NASTRAN model supplied by Ed Pendleton of AFRL/WPAFB (Ref. 7.2-3).

For benchmarking and testing of the models, static and normal modes analyses were performed by ASTROS*, and some of the analysis results and the calculated weight data were compared with results from MSC/NASTRAN. The data format of the ASTROS* case control deck is different from that of MSC/NASTRAN but the format of the bulk data deck is almost the same. The entries for optimization are different between the two codes. However, there was no difficulty in converting the data format, and reasonable comparisons were obtained for the GAF model. The DAST EAL model was a skin-spar-rib type wing. The spaces between the ribs of the original structural model were rather large, thus, the wing skin panels deformed easily, and the airfoil shape was hard to preserve. Many local modes were experienced in the wing panels for the normal modes analysis. Because of these local instabilities of the structure, reasonable results could not be obtained in the static aeroelastic and flutter analyses. Thus, more ribs were added to the original structure to prevent these local vibration modes.

The GAF and AAW wing models represent fighter wings, thus, were a good choice to test ZONA6 and ZTAIC at Mach number $M = 0.85$. Based on the results of the steady aerodynamic analysis by ENSAERO (Figs. 7.4a and 7.46a), the wings were in transonic flow at this speed. Since the DAST model had a supercritical wing which was thicker than the other two wings, it was transonic at Mach = 0.8 (Fig. 7.32c), and was used to test ZONA6 and ZTAIC at Mach = 0.8. The GAF and AAW wing models were used to test ZONA7 in the supersonic regime; however, the DAST wing was too thick for supersonic flow. Although none of the three models represented hypersonic wings, ZONA7U was tested on the GAF and AAW models at $M = 3.0$, in the high supersonic/hypersonic regime. The skins of the DAST wing are made of composite material and each layer of the skin was used as a design variable. The fuselage was included in the AAW model, and its structural and aerodynamic effects were considered.

7.2 Benchmarking and Testing of Codes

ASTROS* now includes the aerodynamic modules ZONA6, ZTAIC, ZONA7, and ZONA7U from ZONA Technology, Inc., to calculate the aerodynamic loads for static aeroelastic and flutter analysis. ZONA6 and ZONA7 use linear aerodynamic theory in the subsonic and supersonic regimes, respectively. ZTAIC uses TES (Transonic Equivalent Strip theory) to calculate the nonlinear aerodynamic loads in the transonic regime. ZONA7U uses a unified hypersonic/supersonic lifting surface method to compute the aerodynamic loads in the hypersonic regime. These modules have only recently been installed in ASTROS*. Thus, they were tested in the present research. Some results from ZONA6 and ZTAIC in ASTROS* were compared to the linear results of MSC/NASTRAN for the GAF model at Mach 0.85, and the DAST model at Mach 0.8. For ZONA7, results of static aeroelastic and flutter analyses were compared to those from MSC/NASTRAN for the GAF wing model at Mach numbers M = 1.15. For ZONA7U, results of static aeroelastic and flutter analyses were compared to the linear results from MSC/NASTRAN for the GAF model at Mach 3.0, even though this model was not a hypersonic wing model.

Then, structural design optimizations for individual disciplines and for multiple disciplines, i.e., statics and normal modes, were performed by ASTROS*. For these individual disciplines, reasonable results were obtained when some of the results for the final design values were compared to MSC/NASTRAN results. For the multiple discipline optimization, the results could not be compared because MSC/NASTRAN did not have a multidisciplinary design optimization capability until Version 70. However, for design optimization problems, accuracy can still be checked by performing final analyses in both ASTROS* and MSC/NASTRAN even though it cannot be known whether the final design from ASTROS* is truly a global optimum.

Structural design optimizations with a flutter constraint and multidisciplinary design optimizations including a flutter constraint could not be performed by ASTROS* and MSC/NASTRAN. Convergence could not be achieved using the pk-method in ASTROS*. In Version 69 of MSC/NASTRAN, the results were wrong when checked by a final analysis and, in Version 70, results could not be obtained because of a system error. Such flutter optimizations were performed, however, by an approximate design optimization method for the GAF model. The aerodynamic loads were obtained by ZONA6 of ASTROS*. The generalized unsteady aerodynamic coefficients were approximated by the minimum-state method, and the root-locus method was used to calculate the flutter speed. The structural sensitivities were calculated using the high level language MAPOL in ASTROS*. The approximate mathematical optimization problem was solved by NPSOL.

Flutter suppression was then performed by obtaining the parameters of the actuator and gain margins to maximize the flutter speed. The root-locus method was used to calculate the flutter speed, and the sensitivities of the flutter dynamic pressure with respect to the design variables were calculated analytically as shown in Chapter 5. Since this was an unconstrained optimization problem, and the Newton method in the IMSL module of MS-FORTRAN was used to solve the problem

7.3 Applications to Models

In the aerodynamic analyses, the pressure coefficients were calculated for the GAF and DAST models in the transonic regime, and for the AAW model in the transonic and supersonic regimes for Navier-Stokes flow by the CFD code, ENSAERO.

In the structural analyses, normal modes analyses, and flutter analyses were performed for the GAF model, and static aeroelastic analyses, normal mode analyses, and flutter analyses were performed for the DAST and AAW models. In the structural design optimizations, the structural weight of each respective wing model was minimized for the mentioned disciplines singly and simultaneously.

The wings were modeled by large and complex finite element models, and the thicknesses and areas of the elements of the FEM models were used as the design variables in the design optimizations. The numbers of elements of the FEM models were 530, 1680, and over 2000, for the GAF, DAST, and AAW models, respectively. The numbers Dgree of Freedom (DoF) of analysis set of the FEM models were 101, 1429, and over 1700, for the GAF, DAST, and AAW models, respectively. The numbers of global design variables were 52, 230, and over 100 for the GAF, DAST, and AAW models, respectively, and the numbers of local design variables were up to 1,000. The local design variables were reduced to global design variables by design variable linking.

Static aeroelastic and flutter analyses and optimizations were performed in the subsonic, transonic, low supersonic and high supersonic/hypersonic aerodynamic regimes. ZONA6 and ZTAIC of ASTROS* were used to calculate the aerodynamic loads in the transonic regime, and ZONA7 and ZONA7U were used to calculate aerodynamic loads in the low supersonic regime and high supersonic/hypersonic regimes, respectively.

The objective function was the total structural weight of the elements to be designed. The constraints were requirements on wing tip displacement, maximum stress, lower bound of the first natural frequency, and flutter speed. The design variables were the thicknesses of skins of isotropic material, the ply thicknesses of composite material plates, and the section areas of the spar caps

For the fixed cantilever-type GAF wing model, the wing tip displacements and maximum stresses of elements for static loads were calculated by static analysis, natural frequencies and normal modes were calculated by normal mode analysis, and flutter speeds were obtained by flutter analysis. The results from the analyses were used as constraints in the multidisciplinary design optimizations with the disciplines statics, normal modes, and flutter. The design variables were the skin thicknesses.

The DAST model is a wing model but has free boundary conditions and can maneuver like a full airplane. Wing tip displacement and stresses of elements were calculated by static aeroelastic analysis in a 10g pull-up maneuver trim condition. In static aeroelastic analysis, stability derivatives and trim parameters such as angle of attack and control surface deflection angles including the elastic effects of the structure were calculated. Displacement and stresses were also calculated in the trim condition including elastic deflection effects. Natural frequencies and normal modes were calculated by normal modes analysis, and flutter speeds were obtained by flutter analysis. The results obtained in the analyses were used as constraints in the multidisciplinary design optimizations including static aeroelasticity and normal modes. The design variables were the ply thicknesses of the composite material skins and the areas of the spar caps. The asymmetric stacking sequence of the ply was assumed to be [90,±45,0]

The AAW is a full airplane model with free boundary conditions. The wing tip displacements and maximum stresses were computed for a 7g pull-up maneuver trim condition. In static aeroelastic analysis, stability derivatives and trim parameters such as angle of attack and control surface deflection angles including the elastic effects of the structure were calculated. Displacement and stresses were calculated in the trim condition including elastic deflection effects. Natural frequencies and normal modes were calculated by normal mode analysis, and flutter speeds were obtained by flutter analysis. The results obtained in the analyses were used as constraints in the multidisciplinary design optimizations including static aeroelasticity and normal modes as for the DAST model. The design variables of the AAW were the thicknesses of the upper and lower skins of the inboard wing made of isotropic material.

All analysis and optimization cases are summarized in Table 7.1.

7.4 GAF (Generalized Advanced Fighter) Wing Model

7.4.1 Structural and Aerodynamic Analysis

7.4.1.1 Structural Configuration and Static Analysis

The GAF model is an aircraft wing model composed of skins, spars and ribs. A leading edge flap and a trailing edge control surface are attached to the main wing box. The wing is fixed at the root. The structural configuration of the wing in the form of a FEM model is shown in Fig. 7.1. Skins, spars, and ribs were modeled by QUAD4 elements, and CELAS2 elements were used to connect the control surfaces to the wing box. A summary of the number of elements and grid points is shown in the following:

NUMBER OF GRID POINTS		288
ELEMENTS PROCESSED		
	CROD	136
	CELAS2	2
	CQUAD4	371
	RBE2	21
TOTAL NUMBER OF ELEMENTS		530

A static analysis was performed for applied static loads, distributed at given grid points, in the vertical direction, using FORCE cards. The wing was fixed as a cantilever by SPC cards. The identification number the of FORCE cards in the bulk data deck was called by a STATIC card and the ID number of the SPC cards in the bulk data deck was called by a BOUNDARY card in the case control deck. Displacements at grid points and stresses in elements were calculated, and the output print of these data was controlled by a PRINT card in the case control deck.

The weight of this structure was 671.60 *lbs*, and the associated data of the initial structure are shown in Table 7.2. To print out these weight data, a GPWG card was entered in the bulk data deck, and the associated ID number was called in the PRINT card of the case control deck. The six components of the displacement were printed. The maximum vertical displacement at the wing tip was 27.068 *in* All stress components and the principal stresses were printed. The maximum principal stress in all elements was 64,000 *psi.* The data were used later as constraints in the structural design optimizations. The deformed shape of the structure is shown in Fig. 7.2.

7.4.1.2 Aerodynamic Configuration and Analysis by ENSAERO

Aerodynamic analyses of the wing were performed by the CFD code, ENSAERO. The steady aerodynamic pressure coefficients calculated here will be used as input data for ZTAIC of ASTROS*. The steady aerodynamic pressure coefficients were calculated for Euler flow and also for Navier-Stokes flow, with the results of the Euler flow, via a RESTART statement. For all cases, the Reynolds number was 10,000,000 and spanwise and normal viscous terms were used. For turbulence, the Baldwin-Lomax turbulence model was used, and, for correction for vortex flow, Degani-Schiff modeling was used. Iteration indices were less than 1.0E-09 and iteration numbers were about 500 for the Euler flow and then more than 500 additional iterations for the Navier-Stokes flow. The aerodynamic configuration of the wing is shown in Fig. 7.3. The total number of grid points was 151 x 44 x 34 in the x-, y-, and z- directions, respectively. The number of grid points on the wing was 61 x 34 on both lower and upper surfaces. The total number of iterations for Euler flow plus Navier-Stokes flow was about 1000, and the total CPU time on the CRAY computer was about 2 hours. In the transonic region belonged M = 0.85, convergence was slower than in the other regions, and more iterations were needed.

Two Mach number cases, M = 0.85 and M = 0.90, and two angle of attack cases, α = 0.0° and α = 5.0°, total of four cases were investigated. The results of the calculated aerodynamic pressure coefficients for Euler flow and for Navier-Stokes flow are shown in Fig. 7.4. In Euler flow, the strength of the shock was larger than in Navier-Stokes flow. This seems to come about because of the viscous effects in the Navier-Stokes flow. The computed points were as follows:

(1) M = 0.85, AoA = 0.0° (Navier-Stokes Flow)

(2) M = 0.85, AoA = 5.0° (Navier-Stokes Flow)

(3) M = 0.90, AoA = 0.0° (Navier-Stokes Flow)

(4) M = 0.90, AoA = 5.0° (Navier-Stokes Flow)

Fig. 7.4 shows that the flows were in the transonic regime at M = 0.85 and M = 0.90.

7.4.1.3 Normal Modes Analysis by ASTROS*

Natural frequencies, the associated modes shapes, and the generalized stiffness and mass matrices were calculated in the normal modes discipline. For the calculation of the eigenvalues, the INV (Inverse Power) method was used. This method was selected via the EIGR card and the ID number of this card was called by METHOD in the BOUNDARY card in the case control deck. ASET cards were used to save computing time and neglect motions other than vertical. Mode normalization was used in MASS because it was convenient that the components of the generalized mass were unity.

Normal modes data for 8 modes from the lowest mode up to 90.0 *Hz* were calculated. The lowest eight natural frequencies of the GAF model were 10.22, 30.97, 35.89, 49.74, 58.04, 65.51, 76.09, and 84.75 *Hz*. The results are shown in Table 7.3 and the mode shapes are presented in Fig. 7.5. The first and second modes were bending modes and the third mode was the first torsion mode, These data were later used in the flutter calculations. The lowest natural frequency, 10.22 *Hz*, was used as a constraint in normal modes design optimization.

7.4.1.4 Flutter Analysis

Flutter analyses were performed by the k-method in ASTROS*, the p-k-method in MSC/NASTRAN, and the root-locus method outside of these codes. Flutter analyses were performed in three aerodynamic regimes, transonic, low supersonic, and high supersonic/hypersonic. Mach numbers M = 0.85, 1.15, and 3.0 were selected to calculate flutter speeds. ZONA6 and ZTAIC of ASTROS* were used to calculate generalized unsteady aerodynamic loads at M = 0.85, and ZONA7 and ZONA7U were used for M = 1.15 and M = 3.0, respectively. The results are compared with those for MSC/NASTRAN and the root-locus method in Table 7.4. The generalized unsteady aerodynamic loads calculated by ASTROS* were used in the root-locus method. Two CAERO7 cards were used: the CAERO7, 100001 card represents the wing, and the number of associated aerodynamic boxes was 15 x 11. The CAERO7, 200001 card represented the fuselage region and the number of aerodynamic boxes was 15 x 2.

The generalized unsteady aerodynamic loads at M = 0.85 were calculated by ZONA6. There are 8 x 8 generalized aerodynamic coefficient terms, Q_{ij}, for each reduced frequency k. The plots of the real and imaginary parts of Q_{1j} and Q_{2j} (j = 1, 2,..., 8) versus k are shown in Figs. 7.6. Generalized unsteady aerodynamic loads were also approximated by the minimum-state method at M = 0.85. In Figs. 7.7, the Q_{1j} and Q_{2j} calculated by ZONA6 are shown as real part versus imaginary part by black and solid lines and the approximate Q_{1j} and Q_{2j} calculated by the minimum-state method are shown by color and dotted lines. The V-f and V-g plots for the results by ZONA6 of ASTROS* are shown in Fig. 7.8. The flutter speed was 17,337 *in/sec* and the flutter frequency was 14.3 *Hz*. The root-locus plot to calculate the flutter speed is shown in Fig. 7.9. The flutter speed was 15,888 *in/sec* and the flutter frequency was 17.3 *Hz*. The plots of Figs. 7.10 - 7.13 are for the results by ZTAIC at $M = 0.85$. The flutter speed was 18,172 *in/sec* and the flutter frequency was 18.1 *Hz* by the k-method, and the flutter speed was 16,581 *in/sec* and the flutter frequency was 15.6 *Hz* by the root-locus method. It is normally expected that the nonlinear flutter speed is lower than the linear flutter speed in the transonic regime. However, for the case of the GAF model, the nonlinear flutter speed was slightly higher than the linear flutter speed. The plots of Figs. 7.14 - 7.17 are for the results by ZONA7 at $M = 1.15$. The flutter speed was 20,776 *in/sec* and the flutter frequency was 19.8 *Hz* by the k-method, while a divergence speed 14,170 *in/sec* was obtained by the root-locus method instead. The plots of Figs. 7.18 - 7.21 are for the results by ZONA7U at $M = 3.0$. The flutter speed was 31,743 *in/sec* and the flutter frequency was 21.1 *Hz* by the k-method, and the flutter speed was 33,536 *in/sec* and the flutter frequency was 21.3 *Hz* by the root-locus method. For the results in subsonic flow at $M = 0.85$ and in supersonic flow at $M = 1.15$, root-locus results were close to the MSC/NASTRAN results as shown in Table 7.4.

7.4.2 Structural Design Optimization

7.4.2.1 Static Optimization

Static structural design optimization was performed. The design variables were the thicknesses of all skin elements. The objective function was the total weight of the skins. The constraints were the requirements for wing tip displacement and the stresses in the skins. The required wing tip displacement, 27.07 *in*, was the same as the result in the analysis of the original wing model. The required stress of 64,000 *psi* was the maximum stress in the same analysis. The number of global design variables was 52, and the design variables and their numbering are shown in Fig. 7.22.

The design variables were defined by DESVARP cards, which converted the properties of the elements into design variables. The upper and lower skins had the same property numbers and, thus, were the same design variables. This had the effect of linking the design variables of the upper and lower skins. The lower boundary of the design variables was the minimum material size, 0.118 *in*.

As a result of the static design optimization, the weight was reduced from 343.49 *lbs* to 313.37 *lbs*. In this optimization, the thicknesses of all skins started from their minimum basic material sizes. The iteration history of the design optimization is shown in Fig. 7.23 and Table 7.5. The required CPU time was

1 minute 55.5 seconds. A 8.8 % weight reduction was achieved for this short CPU time in 15 iterations. The convergence was excellent.

7.4.2.2 Normal Modes Optimization

In the normal modes optimization, the lower bound of the first frequency was used as a constraint. The required frequency of 10.22 *Hz* was the same as the result from the original analysis of the model.

As a result of the normal modes design optimization, the weight was reduced from the original weight of 343.49 *lbs* to 312.26 *lbs*. The iteration history of the design optimization is also shown in Fig. 7.23 and in Table 7.6. The required CPU time was 2 minute 48.3 seconds. A 9.1 % weight reduction was achieved for this short CPU time in 15 iterations. The convergence was excellent for this case with a structural design optimization and only one constraint.

7.4.2.3 Design Optimization for Static Loads and Normal Modes

Design optimization for static loads and normal modes was then performed. Displacements, stresses, and the lowest frequency were used as constraints. The constraint values, the required wing tip displacement of 27.07 *in*, the required maximum stress of 64,000 *psi*, and the required lowest frequency of 10.22 *Hz*, were the same as resulted from the original analyses.

As a result of the design optimization for the disciplines of statics and normal modes, the weight was reduced from 343.49 *lbs*, the weight of the original structure, to 313.28 *lbs*, for a reduction of about 10 %. More weight could still be taken off for smaller minimum basic sizes. The iteration history of the design optimization is again shown in Fig. 7.23 and in Table 7.7. The final design variable values are given in Table 7.8. In this optimization, the initial design variable values were the minimum basic sizes not those from the original structure. This means that the design optimization can be performed easily without any initial sizing calculations either manually or by CAD.

7.4.2.4 Flutter Optimization

Structural design optimization with only a flutter speed constraint was performed for the GAF model at $M = 0.85$. ZONA6 in ASTROS* was used for calculating the aerodynamic loads. The constrained flutter speed was 16,107.8 *in/sec*. Flutter sensitivities with respect to design variables were calculated, the flutter constraints were formulated by linear approximation, and the optimization problem was solved using the optimizer NPSOL. The derivatives of the mass matrix and the stiffness matrix, necessary to calculate the flutter sensitivities, were obtained by modifying the MAPOL language in ASTROS* for the static and normal modes disciplines. An iteration history of the design optimization for flutter speed is shown in Fig. 7.24 and in Table 7.9. As a result of the design optimization for the flutter discipline, the weight was reduced from 343.49 *lbs*, the weight of the original structure, to 333.15 *lbs*, by 12 iterations. In this case, the lengthy set of iterations was stopped without applying the convergence criteria since the intent was only to show the convergence behavior.

7.4.2.5 Multidisciplinary Design Optimization of Statics, Normal Modes, and Flutter

With flutter speed, static strength, and frequency constraints, the multidisciplinary design optimization was performed for the GAF model. The objective function was the total structural weight. The approximate optimization problem was calculated by NPSOL. The sensitivities of the static strength and frequency constraints, as well as the derivatives of the mass and stiffness matrices that are necessary to calculate the flutter sensitivities were obtained via the MAPOL programming language in ASTROS* from the static and normal modes disciplines. The sensitivity of the objective function, the total structural weight, was also obtained via MAPOL. The constraint values were the required wing tip displacement of 27.07 *in*, the required maximum stress of 64,000 *psi*, the required lowest frequency of 10.22 *Hz*, and the required flutter speed of 16,108 *in/sec*. An iteration history of the multidisciplinary optimization with strength, displacement, natural frequency, and flutter speed constraints is shown in Fig. 7.25 and Table 7.10. The final design variable values are given in Table 7.11. A weight reduction of 15.57 *lbs* was achieved compared with the weight of the original model, 343.49 *lbs*; this was a 4.5 % weight reduction in 6 iterations. The GAF model was an actual aircraft wing model supposed to be well designed at the outset, and the material minimum basic sizes were quite thick. Thus, a 4.5 % weight reduction in this small number of iterations can be considered a good result since strength, displacement, normal modes, and flutter constraints were considered simultaneously.

7.4.3 Flutter Suppression

Up to this point, the structure was designed for minimum weight under constraints of strength, displacement, natural frequency, and flutter speed. For the next step, the flutter speed was to be increased by the augmentation of a control system. The actuator parameters were determined to maximize the flutter speed for the GAF model. Eight modes were used. It was assumed that the sensor was attached at GRID 264, near the wing tip at the trailing edge. The root-locus plots for the open loop and closed loop cases are shown in Fig. 7.26 and Fig. 7.27, respectively. The flutter speeds was 16,106.2 *in/sec* and the flutter frequencies was 103.27 *rad/sec* for the open loop. For the closed-loop configurations, divergence occurred at 17,755.8 *in/sec* and, thus, the lowest unstable speed was increased by 10 %. When the flutter or divergence speed was a maximum, the actuator parameters were $a_0 = 103.88$, $a_1 = 1199.42$, $a_2 = 102.19$, $b_0 = 0.0722$, and the gain was 0.5238.

7.5 DAST (Drones for Aerodynamic and Structural Testing) Wing Model

7.5.1 Structural and Aerodynamic Analysis

7.5.1.1 Structural Configuration and Static Aeroelastic Analysis

The DAST wing model is a structural model of a supercritical wing used on a drone in a flight test facility (Ref 5.3). The ASTROS* and MSC/NASTRAN data for the DAST model were obtained by converting data from an EAL (Engineering Analysis Language) model. The DAST model is a skin-spar-rib type wing made of composite material. To avoid an excessive number of local modes in the normal modes analysis and to improve performance of the model in the static aeroelastic and flutter analyses, ribs were added to the original structure. The stacking sequence of the composite skin panels was changed to a more realistic [90/±45/0], from the original stacking sequence [90/0].

Analyses and structural design optimizations of a composite wing model were the specific goal here. The boundary condition of the structure was free at the root, and its behavior was thought to be the same as that of a full aircraft. A fuselage weight of 1177.2 *lbs* was added to the wing root by a CONM2 entry, and the total weight of the model became 1250.0 *lbs*, half the weight of the DAST model in Ref. 5.3. The wing had two trailing edge control surfaces. Steady flight in the trim condition with control surface deflections was assumed. The skins were modeled by plate elements, composed of four plies. The material coordinates are shown in the following:

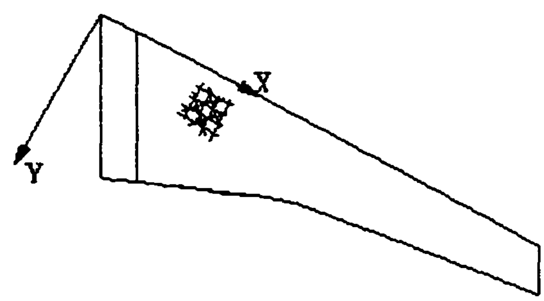

The lamina material of the composite was assumed to be AS/3501 graphite/epoxy. The stiffness and strength of each lamina are given below:

Lamina Stiffness:

$E_1 = 1.8 \times 10^6$ (*psi*)

$E_2 = 0.86 \times 10^6$ (*psi*)

$\upsilon_{12} = 0.3$

$G_{12} = G_{1z} = G_{2z} = 0.46 \times 10^6$ (*psi*)

$\rho = 0.057$ (*lbs/in*^{3})

Lamina Strength:

$S_L^{(+)} = 210{,}000$ (*psi*)

$S_L^{(-)} = 170{,}000$ (*psi*)

$S_T^{(+)} = 7{,}000$ (*psi*)

$S_T^{(-)} = 36{,}000$ (*psi*)

$S_{LT} = 9{,}000$ (*psi*)

The skins were modeled by QUAD4 and TRIA3 elements and the spar caps by BAR elements. The property cards for the QUAD4 and TRIA3 elements were PCOMP entries. The structural configuration of the FEM model is shown in Fig. 7.28. A summary of the number of grid points and elements is shown in the following.

NUMBER OF GRID POINTS	428
ELEMENTS PROCESSED	
CROD	432
CONM2	449
CBAR	172
CQUAD4	623
CTRIA3	4
TOTAL NUMBER OF ELEMENTS	1680

Two CAERO7 cards were used to generate the aerodynamic panels because the trailing edge consisted of two separate straight lines. The inboard wing was composed of 15 x 7 panels and the outboard wing of 15 x 10 panels, thus, the total number of panels was 275.

Symmetric static aeroelastic analysis was performed and the trim parameters, angle of attack and control surface deflection angle, were calculated under a 10g pull-up condition with zero pitching rate and zero pitching acceleration at Mach

M = 0.80. The inboard control surface was assumed to be fixed. The trim parameters were calculated when the structure was rigid and when the structure had elastic deformation. The displacements at the GRID points and the stresses in each ply of the plate elements were calculated at this trim condition. ZONA6 was used to calculate the aerodynamics.

The weight data output is shown in Table 7.12 including fuselage weight. The longitudinal stability derivatives of the aircraft for both the rigid and elastic cases are shown in Table 7.13. The calculated trim parameters for both the rigid and flexible structure at the trim condition are given in Table 7.14. The calculated angle of attack, 4.06° for the rigid case, was reasonable and a large deflection angle, -45.98°, of the control surface was necessary to obtain trim since no horizontal tail was included. The steady pressure distributions as attributed to each parameter such as thickness, camber, angle of attack, pitching rate, pitching acceleration, and control surface deflection are shown in Table 7.15. The steady pressure distributions in the trim condition for all trim parameters are shown in Fig. 7.29. The vertical displacement at GRID point 415 on the wing tip was 5.506 *in*, and the deflection shape in the trim condition is presented in Fig. 7.30. This value was later used as constraint in the structural design optimization. The required CPU time was 9 minutes 25.0 seconds

7.5.1.2 Aerodynamic Configuration and Analysis by ENSAERO

The aerodynamic analysis of the wing was performed by the CFD code, ENSAERO. The aerodynamic configuration of the wing is shown in Fig. 7.31. The input data for this model were nearly the same as those for the GAF model. Steady aerodynamic pressure coefficients were calculated for Navier-Stokes flow. For all cases, the Reynolds number was 10,000,000, and spanwise and normal viscous terms were used. For turbulence, the Baldwin-Lomax turbulence model was used and, for correction for vortex flow, Degani-Schiff modeling. The iteration indices were less than 1.0E-09, and there were about 500 iterations for Euler flow and then another 500+ iterations for Navier-Stokes flow. The total size of the grid was 151 x 44 x 34 in the x-, y-, and z- directions, respectively. The number of grid points on the wing was 61 x 34 on both the lower and upper surfaces. The results of the calculated aerodynamic pressure coefficients for Navier Stokes flow are shown in Fig. 7.32 for four cases:

(1) $M = 0.70$, AoA = 0.0°, (Navier-Stokes Flow)

(2) $M = 0.70$, AoA = 5.0°, (Navier-Stokes Flow)

(3) $M = 0.80$, AoA = 0.0°, (Euler Flow)

(4) $M = 0.80$, AoA = 0.0°, (Navier-Stokes Flow)

Fig. 7.32 shows that the DAST model was just entering the transonic regime at Mach 0.7 when the angle of attack was 0.0° and was in the transonic regime at

Mach 0.8. The strength of the shock in Euler flow was larger than that in Navier-Stokes flow.

7.5.1.3 Normal Modes Analysis by ASTROS*

Natural frequencies, the associated modes shapes, and the generalized stiffness and mass matrices were calculated in the normal modes discipline as for the GAF model. To calculate eigenvalues, the INV (Inverse Power) method was used. Normal modes data for 10 modes from the lowest to 200.0 *Hz* were calculated for a symmetric boundary condition. The axial direction of the fuselage was fixed. The first two modes were the rigid body modes, vertical translation and pitching rotation. The lowest seven natural frequencies of the elastic modes were 11.3, 48.7, 55.7, 103.3, 130.8, 147.8, and 199.0 *Hz*. The required CPU time was 2 minutes 11.0 seconds.

The results of the computations are shown in Table 7.16, and the mode shapes are plotted in Fig. 7.33. These data were later used in the flutter analysis. The lowest natural frequency, 10.22 *Hz*, was used as a constraint in the normal modes design optimization.

7.5.1.4 Flutter Analysis

Flutter analyses were performed by the k-method in ASTROS* and by the root-locus method for a Mach number of $M = 0.80$ using ZONA6 and ZTAIC. The results from ASTROS* and the root-locus method were compared and are shown in Table 7.17. The generalized unsteady aerodynamic loads calculated in ASTROS* were used in the root-locus method.

These generalized unsteady aerodynamic loads at $M = 0.85$ calculated by ZONA6 in ASTROS* are shown in Fig. 7.34. The generalized unsteady aerodynamic loads calculated by ZONA6 and approximated by the minimum-state method at $M = 0.85$ are presented in Fig. 7.35. The V-f and V-g plots for the flutter results by ZONA6 in ASTROS* are shown in Fig. 7.36 and the root-locus plots to calculate the flutter speed using the aerodynamics of ZONA6 in ASTROS* are given in Figs. 7.37. The V-f and V-g plots for the flutter results by ZTAIC in ASTROS* are shown in Fig. 7.38 and the root-locus plots to calculate the flutter speed using the aerodynamics of ZTAIC in ASTROS* are given in Figs. 7.39. The flutter speed and frequency calculated by the k-method and ZONA6 were 14,358 *in/sec* and 48.67 *Hz*, respectively. The flutter speed and frequency calculated by the root-locus method and ZONA6 were 13,490 *in/sec* and 36.3 *Hz*, respectively. The flutter speed and frequency calculated by the k-method and ZTAIC were 11,800 *in/sec* and 56.01 *Hz*, respectively. The flutter speed and frequency calculated by the root-locus method and ZTAIC were 12,892 in/sec and 49.30 *Hz*, respectively. The required CPU time by the k-method and ZONA6 of ASTROS* was 13 minutes 13.5 seconds, and the required CPU time by the k-method and ZTAIC of ASTROS* was 5 hours 22 minutes 31.4 seconds. The required CPU time is closely dependent on the number of the reduced frequency calculations. The total number and points of the reduced frequency calculations are also important for the accuracy of the flutter speed.

7.5.2 Structural Design Optimization

7.5.2.1 Static Aeroelastic Optimization

Static aeroelastic structural design optimization was performed in the 10*g* pull-up trim condition. The total weight of the wing skins and the spar caps was optimized. At the final design point, the trim parameters angle of attack and control surface deflection angle were required to match those of the analysis. The design variables were the ply thicknesses of the composite material skins and the areas of the spar caps. The minimum thicknesses of the plies were assumed to be 0.01 *in.* A displacement constraint at the wing tip, 5.506 *in*, was the same as the displacement from the original analysis. The Tsai-Wu failure criteria were used as strength constraints for the composite material. The Tsai-Wu criteria and the material parameters used in these criteria were as follows.

$$F_{11}\sigma_1^{\,2} + F_{22}\sigma_2^{\,2} + F_{66}\sigma_6^{\,2} + F_1\sigma_1 + F_2\sigma_2 + 2F_{12}\sigma_1\sigma_2 = 1$$

where

$$F_{11} = \frac{1}{S_L^{(+)} S_L^{(-)}} = 2.8011 \times 10^{-11}, \quad F_1 = \frac{1}{S_L^{(+)}} - \frac{1}{S_L^{(-)}} = -1.1204 \times 10^{-5},$$

$$F_{22} = \frac{1}{S_T^{(+)} S_T^{(-)}} = 3.9683 \times 10^{-9}, \quad F_2 = \frac{1}{S_T^{(+)}} - \frac{1}{S_T^{(-)}} = 1.1508 \times 10^{-4}$$

$$F_{12} = -\frac{(F_{11}F_{22})^{1/2}}{2} = -1.6670 \times 10^{-10} \text{ (Tsai-Hahn)},$$

The required stresses in the BAR elements were taken to be the von Mises stresses.

The design variables were defined by DESVARP entries, and each ply thickness was a design variable. Then, the properties of some of the elements were defined to the same design variables, with the effect of linking the variables. The number of properties to be determined was 989 and the number of global design variables was 254. The design variables and their numbering are shown in Fig. 7.40.

As a result of the design optimization for static aeroelasticity, the wing weight was reduced from 89.49 *lbs* to 10.96 *lbs* in only 18 iteration. This result shows that the capability of ASTROS* to design optimization is excellent. The iteration history of the design optimization is shown in Table 7.18. The results from the final analysis satisfied the constraints. Required CPU time was 2 hours 40 minutes 33.3 seconds

7.5.2.2 Normal Modes Optimization

In the normal modes optimization, the constraint was a lower bound on the first elastic natural frequency of the structure. The required frequency was 11.288 *Hz*, the same as that calculated in the analysis of the original structure.

As a result, the weight was reduced from 89.49 *lbs* to 9.43 *lbs*. This result was obtained in only 9 iterations. The iteration history of the design optimization is shown in Table 7.19. The required CPU time was 18 minutes 34.0 seconds

7.5.2.3 Multidisciplinary Design Optimization for Static Aeroelasticity and Normal Modes

Multidisciplinary design optimization for static aeroelasticity and normal modes was performed simultaneously. The displacements and stresses in a 10*g* trim condition and the lowest natural frequency were again used as the constraints.

As a result, the weight was reduced from 89.49 *lbs* to 10.86 *lbs*. The good result was obtained in only 11 iterations. The CPU time was 2 hours 53 minutes 42.3 seconds. The iteration history of the design optimization is shown in Table 7.20 and in Fig. 7.41. The final design variables are presented in Table 7.21. In the layer list, 1, 2, 3, and 4 identify the 90° +45°, -45°, and 0° directions of the skin layers. As a result, the thicknesses of the layers in the 0° direction with layer list number 4 in the spar direction were larger than those of the other layers.

7.6 AAW (ASTROS* Aeroelastic Wing) Model

7.6.1 Structural and Aerodynamic Analysis

7.6.1.1 Static Aeroelastic Analysis and Structural Configuration

The AAW model is a full aircraft model composed of wing, horizontal tail, vertical tail, and fuselage. The model was a derivative of a MSC/NASTRAN model. The airfoil section of this model is that of a supersonic fighter. It was used to test ZONA6 in the subsonic regime, ZTAIC in the transonic regime, and ZONA7 in the low supersonic regime. It is not a hypersonic wing model, but was used, nevertheless, to also test ZONA7U at $M = 3.0$

The main wing model is a fully built-up wing made of isotropic material. There are two control surfaces at the leading edge and two control surfaces at the trailing edge. The FEM representation of the skins, spars, and ribs were made by QUAD4 plate elements while those of the horizontal tail, vertical tail, and fuselage were made by BAR elements. The structural configuration in terms of the FEM model is shown in Fig. 7.42. There were nearly 800 grid points and over 2000 elements in the model.

The aerodynamic panels of the wing, the horizontal tail, and the vertical tail were generated using CAERO7 cards. Horizontal and vertical panels were generated separately for the fuselage, using 43 CAERO7 cards, as well. A total of 730 boxes and 1146 aerodynamic grid points were used to calculate the aerodynamic loads for the AAW model. The aerodynamic panels are shown in Fig. 7.45

Symmetric static aeroelastic analysis was performed and the trim parameters angle of attack and horizontal control surface deflection angle were calculated under a 7g pull-up trim condition with zero pitching rate and zero pitching acceleration at Mach number 0.85, 1.15, and 3.0. The main wing flaps were assumed to be fixed. The trim parameters were calculated for the rigid structure and when the structure had elastic deformation. The displacements at the GRID points and the stresses in each element were calculated at this trim condition. ZONA6, ZTAIC, ZONA7, and ZONA7U were used to calculate the aerodynamic data at Mach numbers 0.85, 0.85, 1.15, and 3.0, respectively.

The stability derivatives of the aircraft for both the rigid and elastic case are shown in Table 7.22, Table 7.23, Table 7.24, and Table 7.25 for M = 0.85 by ZONA6, M = 0.85 by ZTAIC, M = 1.15 by ZONA7, and M = 3.0 by ZONA7U, respectively. The calculated trim parameters for both the rigid and flexible structure at the trim condition are shown in Table 7.26, Table 7.27, Table 7.28, and Table 7.29, for M = 0.85 by ZONA6, M = 0.85 by ZTAIC, M = 1.15 by ZONA7, and M = 3.0 by ZONA7U, respectively. The steady pressure distributions on the main wing in the trim condition at M = 0.85 are presented in Fig. 7.43. The maximum vertical displacement on the wing tip in the trim condition at M = 0.85 of wing tip was 16.194 *in* by ZONA6, and this value was used later as constraint in the static aeroelastic design optimization. The deflection shape in the trim condition at $M = 0.85$ is shown in Fig. 7.44. The required CPU time was 1 hour 10 minutes 6.6 seconds, 6 hours 4 minutes 10.6 seconds, 47 minutes 47.5 seconds, and 49 minutes 59.2 seconds for ZONA7, ZTAIC, ZONA7, and ZONA7U, respectively.

7.6.1.2 Aerodynamic Configuration and Analysis by ENSAERO

Aerodynamic analyses of the main wing of the AAW model were performed using the CFD code, ENSAERO. The aerodynamic configuration of the wing is displayed in Fig. 7.45. The input data of this model were very similar to those for the GAF model. Steady aerodynamic pressure coefficients were calculated for Navier-Stokes flow. In all cases, the Reynolds number was 10,000,000, and spanwise and normal viscous terms were used. For turbulence, the Baldwin-Lomax turbulence model was used and, for correction for vortex flow, Degani-Schiff modeling. Iteration indices were less than 1.0E-09, and those were about 500 iteration for Euler flow and then another 500+ additional iterations for Navier-Stokes flow. The model consists of 151 x 44 x 34 points in the x-, y-, and z- directions, respectively. The number of grid points on the wing was 61 x 34 on both the lower and upper surfaces. The results for the calculated aerodynamic pressure coefficients in Navier Stokes flow are shown in Fig. 7.46. for the following cases:

(1) $M = 0.85$, AoA = 0.0° (Navier-Stokes Flow)

(2) $M = 0.85$, AoA = 8.6° (Navier-Stokes Flow)

(3) $M = 0.95$, AoA = 0.0° (Navier-Stokes Flow)

(4) $M = 1.05$, AoA = 0.0° (Navier-Stokes Flow)

Fig. 4.46 shows that the flows were transonic at Mach 0.85 and 0.95.

7.6.1.3 Normal Modes Analysis by ASTROS*

The natural frequencies, associated normal modes, and generalized stiffness and mass matrices were calculated in the normal modes discipline as for the GAF model. These data were later utilized for flutter analysis. To calculate the eigenvalues, the INV (Inverse Power) method was used, and the modes were normalized to 1.0 for all generalized masses. Normal modes data for 10 modes from the lowest frequency to 200.0 *Hz* for a symmetric boundary condition were calculated. The translation component in axial direction of fuselage was fixed. The first two modes were rigid body modes, vertical translation and pitching rotation. The lowest eight natural frequencies of the elastic mode were 5.47, 9.29, 1.27, 13.67, 15,76, 15.86, 17.45, and 19.72 *Hz*.

The results of these calculations are shown in Table 7.30 and the mode shapes are given in Fig. 7.47. These data were used in the subsequent flutter calculations. The lowest elastic natural frequency, 5.47 *Hz*, was used as a constraint in the normal modes design optimization. The required CPU time was 6 minutes 2.7 seconds

7.6.1.4 Flutter Analysis

Flutter analyses were performed by the k-method in ASTROS* and by the root-locus method for three aerodynamic regimes, high subsonic, low supersonic, and high supersonic/hypersonic. Mach numbers 0.85, 1.15, and 3.0 were selected to calculate flutter speeds. ZONA6 and ZTAIC of ASTROS* were used to calculate generalized unsteady aerodynamic loads at $M = 0.85$, and ZONA7 and ZONA7U were used at $M = 1.15$ and $M = 3.0$, respectively. The comparable results from ASTROS* and the root-locus method are listed in Table 7.31. The generalized unsteady aerodynamic loads calculated by ASTROS* were used in the root-locus method.

The V-f and V-g plots, and the root-locus plots for the flutter speed determination at $M = 0.85$ by ZONA6 are shown in Figs. 7.48 and 7.49. The plots by ZTAIC are given in Figs. 7.50 and 7.51, the plots by ZONA7 in Figs. 7.52-53, and the plots by ZONA7U in Figs. 7.54 and 7.55. The flutter speed and flutter frequency by the k-method and ZONA6 were 11,281 *in/sec* and 14.80 *Hz*, respectively. The required CPU time was 56 minutes 41.7 seconds. The flutter speed and flutter frequency by the root-locus method and ZONA6 were 10,979 *in/sec* and 14.77 *Hz*, respectively. The flutter speed and flutter frequency by the k-method and ZTAIC were 10,714 *in/sec* and 14.96 *Hz*, respectively. The required CPU time was 6 hours 59 minutes 52.9 seconds. The flutter speed and flutter frequency by the root-locus method and ZTAIC were 10,538 *in/sec* and 14.73 *Hz*, respectively. The flutter speed and flutter frequency by the k-method and ZONA7 were 11,088 *in/sec* and 14.90 *Hz*, respectively. The required CPU time was 39 minutes 57.2 seconds. The flutter speed and flutter frequency by the root-locus method and ZONA7 were 11,308 *in/sec* and 14.93 *Hz*, respectively. The flutter speed and flutter frequency by the k-method and ZONA7 were 58,768 *in/sec* and 8.55 *Hz*, respectively. The required CPU time was 29 minutes 44.4 seconds. There was no flutter until 50,000 *in/sec* by the root-locus method and ZONA7U.

7.6.2 Structural Design Optimization

7.6.2.1 Static Aeroelastic Optimization

A static aeroelastic structural design optimization was performed at the 7*g* pull-up trim condition. The total weight of the skins of the inboard wing rather than the total wing was optimized to reduce CPU time. For the optimal structure, the trim parameters angle of attack and control surface deflection angle were calculated. The required strengths in the skin elements were given by the von Mises stresses. The design variables and their numbering are shown in Fig. 7.56. The static aeroelastic optimization was performed for M = 0.85 by ZONA6 in ASTROS*. The iteration history of the design optimization is shown in Table 7.32. As a result, at M = 0.85 by ZONA6, the weight was reduced from 587.0 *lbs* to 528.9 *lbs* and the required CPU time was 8 hours 36 minutes 40.6 seconds. At M = 1.15 by ZONA7, the weight was reduced from 587.0 *lbs* to 519.9 *lbs* and the required CPU time was 3 hours 33 minutes 33.4 seconds. The iterations did not converge for ZTAIC and ZONA7U.

7.6.2.2 Normal Modes Optimization

In normal modes optimization, a constraint was set as the lower bound of the first natural frequency of the structure. This required frequency was 5.4706 *Hz* which was the same as the result calculated in the analysis of the original structure.

As a result, the weight was reduced from 587.0 *lbs* to 511.0 *lbs*, and the required CPU time was 1 hour 32 minutes 32.7 seconds. The iteration history of the design optimization is given in Table 7.33.

7.6.2.3 Multidisciplinary Design Optimization for Static Aeroelasticity and Normal Modes

Multidisciplinary design optimization for static aeroelasticity and normal modes was performed simultaneously. The required displacement, stress, and frequency constraints were those values obtained for the original model in the $7g$ pull-up trim condition.

As a result, at $M = 0.85$ with ZONA6, the weight was reduced from 587.0 *lbs* to 546.8 *lbs*, and the required CPU time was 5 hour 48 minutes 46.7 seconds. A 7.0 % weight reduction was achieved in 7 iterations. The iteration history of the design optimization is shown in Fig. 7.57 and Table 7.34, and the final design variables are given in Table 7.35. At $M = 1.15$ with ZONA7, the weight was reduced from 587.0 *lbs* to 535.4 *lbs*, and the required CPU time was 4 hour 8 minutes 14.2 seconds. A 8.9 % weight reduction was achieved in 7 iterations. The iteration history of the design optimization is shown in Fig. 7.58 and Table 7.36. The AAW model was a realistic aircraft model supposed to be well designed at the outset. Thus, such a 7 % weight reduction in this small number of iterations can be considered a good result even if only the steady aeroelastic and normal modes constraints were considered.

Table 7.1 Summary of Analyses and Design Optimizations of Aircraft Wing Models

	GAF Model	DAST Model	AAW Model
Aerodynamic Analysis By ENSAERO	• $M = 0.85$, $\alpha = 0.0°$ • $M = 0.90$, $\alpha = 0.0°$ • $M = 0.85$, $\alpha = 5.0°$ • $M = 0.90$, $\alpha = 5.0°$	• $M = 0.70$, $\alpha = 0.0°$ • $M = 0.70$, $\alpha = 5.0°$ • $M = 0.80$, $\alpha = 0.0°$ • $M = 0.80$, $\alpha = 5.0°$	• $M = 0.80$, $\alpha = 0.0°$ • $M = 0.85$, $\alpha = 0.0°$ • $M = 0.85$, $\alpha = 8.6°$ • $M = 0.90$, $\alpha = 0.0°$ • $M = 0.95$, $\alpha = 0.0°$ • $M = 1.05$, $\alpha = 0.0°$ • $M = 1.20$, $\alpha = 0.0°$ • $M = 1.20$, $\alpha = 18.8°$ • $M = 1.30$, $\alpha = 0.0°$
Structural Analysis	• Statics • Normal Modes • Flutter - With ZONA6 - With ZTAIC - With ZONA7 - With ZONA7U	• Static Aeroelasticity - With ZONA6 - With ZTAIC • Normal Modes • Flutter - With ZONA6 - With ZTAIC	• Static Aeroelasticity - With ZONA6 - With ZTAIC - With ZONA7 - With ZONA7U • Normal Modes • Flutter - With ZONA6 - With ZTAIC - With ZONA7 - With ZONA7U
Structural Design Optimization	• Statics • Normal Modes • Statics +Normal Modes • Flutter - With ZONA6 • Statics + Flutter + Normal Modes	• Static Aeroelasticity - With ZONA6 • Normal Modes • Static Aeroelasticity +Normal Modes	• Static Aeroelasticity - With ZONA6 - With ZTAIC - With ZONA7 - With ZONA7U • Normal Modes • Static Aeroelasticity +Normal Modes
Flutter Suppression	With ZONA6		

Table 7.2 Weight Data Output of GAF Model

OUTPUT FROM GRID POINT WEIGHT GENERATOR
REFERENCE POINT = 1
XO = 3.685130E+01, YO = 0.000000E+00, ZO = 2.084700E+00

M O

*	6.7160E+02	0.000E+00	0.0000E+00	0.0000E+00	-1.405E+03	-4.1995E+04	*
*	0.0000E+00	6.716E+02	0.0000E+00	1.4051E+03	0.000E+00	2.8357E+04	*
*	0.0000E+00	0.000E+00	6.7160E+02	4.1995E+04	-2.835E+04	0.0000E+00	*
*	0.0000E+00	1.405E+03	4.1995E+04	3.6085E+06	-2.140E+06	5.7740E+04	*
*	-1.4051E+03	0.000E+00	-2.8357E+04	-2.1406E+06	1.635E+06	8.8539E+04	*
*	-4.1995E+04	2.835E+04	0.0000E+00	5.7740E+04	8.853E+04	5.2324E+06	*

S

*	1.00000E+00	0.00000E+00	0.00000E+00	*
*	0.00000E+00	1.00000E+00	0.00000E+00	*
*	0.00000E+00	0.00000E+00	1.00000E+00	*

DIRECTION MASS AXIS SYSTEM (S)	MASS	X-C.G.	Y-C.G.	Z-C.G.
X	6.71602E+02	0.00000E+00	6.25301E+01	-2.09224E+00
Y	6.71602E+02	4.22239E+01	0.00000E+00	-2.09224E+00
Z	6.71602E+02	4.22239E+01	6.25301E+01	0.00000E+00

Table 7.3 Results of Normal Modes Analysis of GAF Model

Mode	Eigenvalue (*rad/s²*)	Freq. (*Hz.*)	Generalized Mass	Generalized Stiffness
1	4.12692E+03	1.02243E+01	1.00000E+00	4.12692E+03
2	3.78674E+04	3.09708E+01	1.00000E+00	3.78674E+04
3	5.08536E+04	3.58906E+01	1.00000E+00	5.08536E+04
4	9.76608E+04	4.97371E+01	1.00000E+00	9.76608E+04
5	1.32991E+05	5.80406E+01	1.00000E+00	1.32991E+05
6	1.69421E+05	6.55094E+01	1.00000E+00	1.69421E+05
7	2.28595E+05	7.60945E+01	1.00000E+00	2.28595E+05
8	2.83559E+05	8.47504E+01	1.00000E+00	2.83559E+05

Table 7.4 Results of Flutter Analyses of GAF Model

No	Mach	Method	Flutter Speed (*in/sec*)	F. Freq. (*Hz*)	CPU Time (Minute)
1	0.85	ZONA6 (k-Method)	17,336	14.3	8.9
		ZTAIC (k-Method)	18,172	18.1	498.3
		MSC/NASTRAN	15,800	16.7	
		Root-locus (ZONA6)	15,888	17.3	
		Root–locus (ZTAIC)	16,581	15.6	
2	1.15	ZONA7 (k-Method)	20,776	19.8	4.0
		MSC/NASTRAN	14,500	0.0	
		Root-locus (ZONA7)	14,170	0.0	
3	3.0	ZONA7U (k-Method)	31,743	21.1	2.8
		MSC/NASTRAN	36,100	22.0	
		Root-locus (ZONA7U)	33,536	21.3	

Table 7.5 Design Iteration History of GAF Model: Structural Optimization for Static Loads

Iteration Number	Objective Function	Function Evaluation	Gradient Evaluation	Retained Constraints	Active Constraints	Approximate Convergence
1	2.19373E+02	(Initial Function Value)				
2	2.86841E+02	90	21	45	27	not Converged
3	3.50363E+02	100	8	32	14	not Converged
4	3.40345E+02	36	11	18	6	not Converged
5	3.35738E+02	21	4	16	16	not Converged
6	3.32504E+02	41	3	18	17	not Converged
7	3.21375E+02	22	7	16	4	not Converged
8	3.18522E+02	22	7	17	10	not Converged
9	3.17345E+02	25	3	20	4	not Converged
10	3.16361E+02	23	3	20	4	not Converged
11	3.15494E+02	18	2	17	3	not Converged
12	3.14714E+02	18	3	18	3	not Converged
13	3.14138E+02	19	3	19	3	not Converged
14	3.13609E+02	20	3	19	6	not Converged
15	3.13368E+02	14	2	19	3	Converged

The Final Objective Function Value is: Designed = 3.13368E+02

Table 7.6 Design Iteration History of GAF Model: Structural Optimization for Normal Modes by ASTROS*

Iteration Number	Objective Function	Function Evaluation	Gradient Evaluation	Retained Constraints	Active Constraints	Approximate Convergence
1	2.19373E+02	(Initial Function Value)				
2	2.71428E+02	90	21	1	1	not Converged
3	3.30081E+02	93	21	1	1	not Converged
4	3.50735E+02	88	7	1	1	not Converged
5	3.35437E+02	31	6	1	1	not Converged
6	3.26556E+02	23	5	1	1	not Converged
7	3.21226E+02	23	5	1	1	not Converged
8	3.18468E+02	24	5	1	1	not Converged
10	3.15728E+02	37	3	1	1	not Converged
11	3.14820E+02	22	4	1	1	not Converged
12	3.13932E+02	22	4	1	1	not Converged
13	3.13314E+02	18	3	1	1	not Converged
14	3.12698E+02	22	4	1	1	not Converged
15	3.12255E+02	26	2	1	1	Converged

The Final Objective Function Value is: Designed = 3.12255E+02

Table 7.7 Design Iteration History of GAF Model: Structural Optimization for Statics and Normal Modes by ASTROS*

Iteration Number	Objective Function	Function Evaluation	Gradient Evaluation	Retained Constraints	Active Constraints	Approximate Convergence
1	2.19373E+02	(Initial Function Value)				
2	2.96459E+02	N/A FSD	N/A FSD	163	N/A FSD	not Converged
3	3.06451E+02	N/A FSD	N/A FSD	163	N/A FSD	not Converged
4	3.04878E+02	N/A FSD	N/A FSD	163	N/A FSD	not Converged
8	3.16221E+02	15	4	35	3	not Converged
9	3.15302E+02	18	3	35	3	not Converged
10	3.14613E+02	18	3	34	3	not Converged
11	3.14112E+02	10	3	34	4	not Converged
12	3.13653E+02	30	2	34	13	not Converged
13	3.13341E+02	16	2	34	3	not Converged
14	3.13282E+02	14	2	36	3	Converged

The Final Objective Function Value is: Designed = 3.13282E+02

Table 7.8 Final Design Variables of GAF Model: Structural Optimization for Statics and Normal Modes by ASTROS*

Design Variable	Design Value	Minimum Value	Maximum Value	Objective Sensitivity
102	1.00000E+00	1.00000E+00	2.63158E+01	6.17620D+01
501	1.00000E+00	1.00000E+00	1.00000E+01	2.40229D+00
502	1.00000E+00	1.00000E+00	1.00000E+01	2.37495D+00
503	6.32244E+00	1.00000E+00	1.00000E+01	2.39868D+00
504	1.00000E+00	1.00000E+00	1.00000E+01	2.79464D+00
505	1.00000E+00	1.00000E+00	1.00000E+01	1.80651D+00
506	1.00000E+00	1.00000E+00	1.00000E+01	4.44667D+00
507	1.00000E+00	1.00000E+00	1.00000E+01	4.39610D+00
508	5.62066E+00	1.00000E+00	1.00000E+01	4.43999D+00
509	1.00000E+00	1.00000E+00	1.00000E+01	5.17293D+00
510	1.00000E+00	1.00000E+00	1.00000E+01	3.34383D+00
511	1.00000E+00	1.00000E+00	1.00000E+01	3.96945D+00
512	1.00000E+00	1.00000E+00	1.00000E+01	3.92430D+00
513	4.27849E+00	1.00000E+00	1.00000E+01	3.96349D+00
514	1.00000E+00	1.00000E+00	1.00000E+01	4.61772D+00
515	1.00000E+00	1.00000E+00	1.00000E+01	2.98490D+00
516	1.00000E+00	1.00000E+00	1.00000E+01	3.49222D+00
517	1.11060E+00	1.00000E+00	1.00000E+01	3.45248D+00
518	2.29648E+00	1.00000E+00	1.00000E+01	3.48694D+00
519	1.00000E+00	1.00000E+00	1.00000E+01	8.12499D+00
520	1.00000E+00	1.00000E+00	1.00000E+01	2.62597D+00
521	1.00000E+00	1.00000E+00	1.00000E+01	3.01498D+00
522	1.11721E+00	1.00000E+00	1.00000E+01	2.98071D+00
523	1.43451E+00	1.00000E+00	1.00000E+01	3.01046D+00
524	1.00000E+00	1.00000E+00	1.00000E+01	7.01463D+00
525	1.00000E+00	1.00000E+00	1.00000E+01	2.26705D+00
526	1.00000E+00	1.00000E+00	1.00000E+01	2.53777D+00
527	1.00000E+00	1.00000E+00	1.00000E+01	2.50890D+00
528	1.00000E+00	1.00000E+00	1.00000E+01	2.53393D+00
529	1.00000E+00	1.00000E+00	1.00000E+01	5.90423D+00
530	1.00000E+00	1.00000E+00	1.00000E+01	1.90813D+00
531	1.00000E+00	1.00000E+00	1.00000E+01	2.06054D+00
532	1.00000E+00	1.00000E+00	1.00000E+01	2.03709D+00
533	1.00000E+00	1.00000E+00	1.00000E+01	2.05740D+00
534	1.00000E+00	1.00000E+00	1.00000E+01	4.79383D+00
535	1.00000E+00	1.00000E+00	1.00000E+01	1.54923D+00
536	1.00000E+00	1.00000E+00	1.00000E+01	1.58330D+00

537	1.00000E+00	1.00000E+00	1.00000E+01	1.56532D+00
538	1.00000E+00	1.00000E+00	1.00000E+01	1.58091D+00
539	1.00000E+00	1.00000E+00	1.00000E+01	3.68346D+00
540	1.00000E+00	1.00000E+00	1.00000E+01	1.19032D+00
541	1.00000E+00	1.00000E+00	1.00000E+01	6.12696D-01
542	1.00000E+00	1.00000E+00	1.00000E+01	6.05731D-01
543	1.00000E+00	1.00000E+00	1.00000E+01	6.11756D-01
544	1.00000E+00	1.00000E+00	1.00000E+01	1.42533D+00
545	1.00000E+00	1.00000E+00	1.00000E+01	4.60569D-01

Table 7.9 Design Iteration History of GAF Model: Structural Optimization with Flutter Constraint at $M = 0.85$

Iteration No.	Weight (*lbs*)	Flutter Speed (*in/sec*)	Flutter Frequeny (*rad/sec*)
1	343.78	16107.9 (Const.)	105.74
2	324.12	16029.3	103.21
3	348.26	16200.6	103.85
4	315.77	15979.9	102.46
5	339.22	16158.3	103.13
6	315.77	15979.0	102.46
7	327.59	16076.0	102.86
8	339.76	16162.0	103.03
9	327.47	16077.4	102.78
10	333.61	16121.0	102.90
11	328.68	16085.8	102.82
12	333.15	16104.1	102.85

Table 7.10 Design Iteration History of GAF Model: Multidisciplinary Design Optimization (Stress + Displacement + Natural Frequency +Flutter Speed) at $M = 0.85$

Iteration No.	Weight (*lbs*)	F. Speed (*in/sec*)	F.freq. (*Hz*)	Tip Disp. (*in*)	M. Stress (*psi*)	1^{st} Freq. (*Hz*)
Required		16,107.8		27.38	64,000	10.208
1	219.37	15,232.2	13.72	63.38	164,000	6.00
2	324.61	16,086.6	14.38	37.20	125,000	8.07
3	386.50	16,517.5	14.42	25.57	76,260	9.32
4	366.36	16,492.7	16.42	25.29	64,260	10.28
5	339.64	16,267.7	16.60	26.44	62,550	10.32
6	328.86	16,112.3	16.45	26.44	62,480	10.32
7	327.92	16,106.2	16.44	26.80	63,650	10.27

Table 7.11 Final Design Variable Values of GAF Model: Multidisciplinary Design Optimization (Stress + Displacement + Natural Frequency +Flutter Speed) At $M = 0.85$

Variable	State	Value	L. bound	U. bound	Lagr multip.
VARBL 1	LL	1.0000	1.0000	1.0100	61.60661
VARBL 2	LL	1.3210	1.3210	1.3476	2.417356
VARBL 3	LL	3.0350	3.0350	3.0960	2.413862
VARBL 4	LL	5.0275	5.0275	5.1286	2.405284
VARBL 5	LL	1.0000	1.0000	1.0100	2.803832
VARBL 6	LL	1.0000	1.0000	1.0100	1.755699
VARBL 7	LL	1.3176	1.3176	1.3441	4.126373
VARBL 8	LL	2.8860	2.8860	2.9441	4.255834
VARBL 9	LL	4.3147	4.3147	4.4014	4.670451
VARBL 10	LL	1.0000	1.0000	1.0100	5.299779
VARBL 11	LL	1.0000	1.0000	1.0100	3.263696
VARBL 12	LL	1.1785	1.1785	1.2022	3.411701
VARBL 13	LL	2.1322	2.1322	2.1751	2.354970
VARBL 14	FR	3.4188	3.4037	3.4721	.000000
VARBL 15	LL	1.0000	1.0000	1.0100	4.830757
VARBL 16	LL	1.0000	1.0000	1.0100	2.668114
VARBL 17	LL	1.3602	1.3602	1.3876	2.827459
VARBL 18	LL	1.7225	1.7225	1.7571	2.866750
VARBL 19	LL	1.6573	1.6573	1.6906	3.743286
VARBL 20	LL	1.0000	1.0000	1.0100	8.890014
VARBL 21	LL	1.0000	1.0000	1.0100	2.52555
VARBL 22	LL	1.1280	1.1280	1.1507	2.982377
VARBL 23	LL	1.3032	1.3032	1.3294	3.038492
VARBL 24	LL	1.2682	1.2682	1.2937	3.038216
VARBL 25	LL	1.0000	1.0000	1.0100	7.012024
VARBL 26	LL	1.0000	1.0000	1.0100	2.286383
VARBL 27	LL	1.0000	1.0000	1.0100	2.525305
VARBL 28	LL	1.0221	1.0221	1.0427	2.497412
VARBL 29	LL	1.0000	1.0000	1.0100	2.541466
VARBL 30	LL	1.0000	1.0000	1.0100	5.922578
VARBL 31	LL	1.0000	1.0000	1.0100	1.907490
VARBL 32	LL	1.0000	1.0000	1.0100	2.060489
VARBL 33	LL	1.0000	1.0000	1.0100	2.033227
VARBL 34	LL	1.0000	1.0000	1.0100	2.053379
VARBL 35	LL	1.0000	1.0000	1.0100	4.786958
VARBL 36	LL	1.0000	1.0000	1.0100	1.548409
VARBL 37	LL	1.0000	1.0000	1.0100	1.582935

VARBL 38	LL	1.0000	1.0000	1.0100	1.565027
VARBL 39	LL	1.0000	1.0000	1.0100	1.580414
VARBL 40	LL	1.0000	1.0000	1.0100	3.682065
VARBL 41	LL	1.0000	1.0000	1.0100	1.189650
VARBL 42	LL	1.0000	1.0000	1.0100	.611605
VARBL 43	LL	1.0000	1.0000	1.0100	.605568
VARBL 44	LL	1.0000	1.0000	1.0100	.611541
VARBL 45	LL	1.0000	1.0000	1.0100	1.424990
VARBL 46	LL	1.0000	1.0000	1.0100	.460554
VARBL 47	LL	1.4474	1.4474	1.4765	4.104928
VARBL 48	LL	2.8321	2.8321	2.8890	4.009018
VARBL 49	LL	4.4457	4.4457	4.5350	3.914433
VARBL 50	LL	1.3709	1.3709	1.3985	4.135922
VARBL 51	LL	2.8615	2.8615	2.9190	3.974858
VARBL 52	LL	4.3594	4.3594	4.4470	3.893831

Table 7.12 Weight Data Output of DAST Model

```
OUTPUT FROM GRID POINT WEIGHT GENERATOR
                    REFERENCE POINT =        1

         XO = 2.417731E+02, YO = 1.805970E+01, ZO = 5.992480E+01

                         M O
* 1.3002E+03  0.0000E+00  0.0000E+00  0.0000E+00  -1.258E+03  6.7508E+03 *
* 0.0000E+00  1.3002E+03  0.0000E+00  1.2586E+03  0.000E+00   2.6715E+04 *
* 0.0000E+00  0.0000E+00  1.3002E+03  -6.7508E+03 -2.671E+04  0.0000E+00 *
* 0.0000E+00  1.2586E+03 -6.7508E+03  3.3057E+05  5.025E+04   2.8499E+04 *
* -1.2586E+03 0.0000E+00 -2.6715E+04  5.0253E+04  8.815E+05   1.1363E+03 *
* 6.7508E+03  2.6715E+04  0.0000E+00  2.8499E+04  1.136E+03   1.1457E+06 *

 DIRECTION
AXIS SYSTEM (S)   MASS          X-C.G.         Y-C.G.         Z-C.G.
     X         1.300231E+03  0.000000E+00 -5.192037E+00 -9.680215E-01
     Y         1.300231E+03  2.054661E+01  0.000000E+00 -9.680215E-01
     Z         1.300231E+03  2.054661E+01 -5.192037E+00  0.000000E+00

                   I(Q)
        *  5.62043E+05                    *
        *             2.22358E+05         *
        *                        4.03149E+05 *
```

Table 7.13 Non-Dimensional Longitudinal Stability Derivatives of DAST Model: 10g Pull-up Maneuver, $M = 0.8$, by ZONA6 of ASTROS*, for Rigid and Flexible Structure

TRIM IDENTIFICATION = 1 REFERENCE GRID = 446
REFERENCE AREA = 2.8236E+03 REFERENCE CHORD = 4.0000E+01

	<< LIFT >>			<< PITCHING MOMENT >>		
	RIGID	RIGID	FLEX.	RIGID	RIGID	FLEXIBLE
PARAMETER	DIRECT	SPLINED		DIRECT	SPLINED	
Thickness/Camber	0.9860	0.9876	0.9097	-0.5291	-0.5291	-0.4653
Angle of Attack (1/*deg*)	0.2222	0.2224	0.2193	-0.0821	-0.0822	-0.0751
Angle of Attack (1/*rad*)	12.7330	12.7418	12.5669	-4.7045	-4.7117	-4.3015
Pitch Rate (s/*deg*)	0.3004	0.3007	0.2889	-0.1578	-0.1579	-0.1427
Pitch Rate (s/*rad*)	17.2142	17.2293	16.5505	-9.0398	-9.0457	-8.1754
Control Surface 1 (1/*deg*)	0.0255	0.0255	0.0241	-0.0119	-0.0119	-0.0110
Control Surface 1 (1/*rad*)	1.4584	1.4597	1.3820	-0.6799	-0.6804	-0.6292
Control Surface 2 (1/*deg*)	0.0105	0.0105	0.0086	-0.0104	-0.0104	-0.0085
Control Surface 2 (1/*rad*)	0.6039	0.6039	0.4951	-0.5945	-0.5945	-0.4863

Table 7.14 Trim Parameters of DAST Model: 10g Pull-up Maneuver, $M = 0.80$, by ZONA6 of ASTROS*, for Rigid and Flexible Structure

TRIM RESULTS FOR TRIM SET 1 OF TYPE PITCH
MACH NUMBER 8.00000E-01
DYNAMIC PRESSURE 6.55000E+00
VELOCITY 1.02700E+04
TRIM PARAMETERS:

DEFINITION	LABEL	FLEXIBLE	RIGID	
LOAD FACTOR	"NZ"	3.86399E+03	3.86399E+03	(Input)
PITCH ACCELERATION	"QACCEL"	0.00000E+00	0.00000E+00 rad/s^2	(Input)
ANGLE OF ATTACK	"ALPHA"	4.03914E+00	4.06115E+00 *deg*	(Computed)
CONTROL SURFACE	"AIL1"	0.00000E+00	0.00000E+00 *deg*	(Input)
CONTROL SURFACE	"AIL2"	-4.50767E+01	-4.59823E+01 *deg*	(Computed)
PITCH RATE	"QRATE"	0.00000E+00	0.00000E+00 *deg/s*	(Input)
THICKNESS/CAMBER	"THKCAM"	1.00000E+00	1.00000E+00	(Input)

Table 7.15 Pressure Distribution of DAST Model: 10g Pull-up Maneuver, $M = 0.80$, by ZONA6 of ASTROS*, for Rigid Structure

***** STEADY RIGID AERODYNAMIC PRESSURE OF TRIM PARAMETERS, MACH = 0.8

	NZ	/ QACCEL	/ THKCAM	/ ALPHA	/ QRATE	/ AIL1	/ AIL2 /
EXT ID	1.00000	1.00000	1.00000	1.00000	1.00000	1.00000	1.00000
100001	0.000E+00	0.0000E+00	0.1187E+01	0.3902E+00	0.1944E+02	0.1130E-01	0.1297E-02
100002	0.000E+00	0.0000E+00	0.3618E-02	0.1648E+00	0.5510E+02	0.5688E-02	0.6083E-03
100003	0.000E+00	0.0000E+00	0.3257E+00	0.1358E+00	0.7387E+02	0.5331E-02	0.5410E-03
100004	0.000E+00	0.0000E+00	0.3145E+00	0.1146E+00	0.8996E+02	0.5203E-02	0.4977E-03
100005	0.000E+00	0.0000E+00	0.2030E+00	0.9709E-01	0.1070E+03	0.5334E-02	0.4711E-03
100006	0.000E+00	0.0000E+00	0.1223E+00	0.8566E-01	0.1186E+03	0.5604E-02	0.4587E-03
100007	0.000E+00	0.0000E+00	0.1675E+00	0.7631E-01	0.1269E+03	0.5946E-02	0.4493E-03
100008	0.000E+00	0.0000E+00	0.2747E+00	0.6763E-01	0.1321E+03	0.6348E-02	0.4390E-03
100010	0.000E+00	0.0000E+00	0.3706E+00	0.5213E-01	0.1314E+03	0.7075E-02	0.4055E-03
100011	0.000E+00	0.0000E+00	0.5720E+00	0.4458E-01	0.1249E+03	0.7226E-02	0.3770E-03
100012	0.000E+00	0.0000E+00	0.7607E+00	0.3684E-01	0.1134E+03	0.7027E-02	0.3366E-03
100013	0.000E+00	0.0000E+00	0.8239E+00	0.2910E-01	0.9704E+02	0.6332E-02	0.2843E-03
100014	0.000E+00	0.0000E+00	0.7120E+00	0.2675E-01	0.9062E+02	0.5954E-02	0.2648E-03
100095	0.000E+00	0.0000E+00	0.1553E+00	0.1345E+00	0.1924E+03	0.1359E-01	0.1047E-02
100096	0.000E+00	0.0000E+00	0.3246E+00	0.1135E+00	0.1798E+03	0.1395E-01	0.9832E-03
100097	0.000E+00	0.0000E+00	0.3363E+00	0.9745E-01	0.1695E+03	0.1480E-01	0.9392E-03
100098	0.000E+00	0.0000E+00	0.3187E+00	0.8368E-01	0.1593E+03	0.1623E-01	0.9021E-03
100099	0.000E+00	0.0000E+00	0.3592E+00	0.7209E-01	0.1489E+03	0.1820E-01	0.8664E-03
100100	0.000E+00	0.0000E+00	0.4803E+00	0.6178E-01	0.1373E+03	0.2069E-01	0.8246E-03
100101	0.000E+00	0.0000E+00	0.6898E+00	0.5213E-01	0.1240E+03	0.2341E-01	0.7692E-03
100102	0.000E+00	0.0000E+00	0.9059E+00	0.4272E-01	0.1080E+03	0.2483E-01	0.6926E-03
100103	0.000E+00	0.0000E+00	0.1037E+01	0.3365E-01	0.8960E+02	0.2183E-01	0.5918E-03
100104	0.000E+00	0.0000E+00	0.9455E+00	0.3095E-01	0.8326E+02	0.1956E-01	0.5533E-03
100105	0.000E+00	0.0000E+00	0.4757E+00	0.1950E-01	0.5492E+02	0.1143E-01	0.3741E-03
200001	0.000E+00	0.0000E+00	0.1347E+01	0.6808E+00	0.7119E+03	0.4181E-01	0.4223E-02
200002	0.000E+00	0.0000E+00	0.6021E+00	0.2752E+00	0.3165E+03	0.1890E-01	0.1857E-02
200003	0.000E+00	0.0000E+00	0.4546E+00	0.2171E+00	0.2684E+03	0.1633E-01	0.1574E-02
200004	0.000E+00	0.0000E+00	0.3411E+00	0.1745E+00	0.2343E+03	0.1468E-01	0.1382E-02
200005	0.000E+00	0.0000E+00	0.1682E+00	0.1392E+00	0.2075E+03	0.1374E-01	0.1245E-02
200006	0.000E+00	0.0000E+00	0.3490E+00	0.1173E+00	0.1910E+03	0.1351E-01	0.1175E-02
200007	0.000E+00	0.0000E+00	0.3562E+00	0.1005E+00	0.1777E+03	0.1358E-01	0.1127E-02
200008	0.000E+00	0.0000E+00	0.3296E+00	0.8611E-01	0.1650E+03	0.1378E-01	0.1088E-02
200009	0.000E+00	0.0000E+00	0.3721E+00	0.7399E-01	0.1524E+03	0.1393E-01	0.1049E-02
200010	0.000E+00	0.0000E+00	0.4953E+00	0.6319E-01	0.1392E+03	0.1375E-01	0.1002E-02
200141	0.000E+00	0.0000E+00	0.1783E+00	0.5911E-01	0.1498E+03	0.2110E-02	0.1439E-01
200142	0.000E+00	0.0000E+00	0.1566E+00	0.4419E-01	0.1179E+03	0.1622E-02	0.1467E-01
200143	0.000E+00	0.0000E+00	0.1282E+00	0.3330E-01	0.9427E+02	0.1258E-02	0.1525E-01
200144	0.000E+00	0.0000E+00	0.1625E+00	0.2552E-01	0.7700E+02	0.9911E-03	0.1575E-01
200145	0.000E+00	0.0000E+00	0.2705E+00	0.1968E-01	0.6344E+02	0.7840E-03	0.1564E-01
200146	0.000E+00	0.0000E+00	0.4903E+00	0.1504E-01	0.5200E+02	0.6138E-03	0.1425E-01
200147	0.000E+00	0.0000E+00	0.6968E+00	0.1123E-01	0.4173E+02	0.4692E-03	0.1147E-01
200148	0.000E+00	0.0000E+00	0.8203E+00	0.8135E-02	0.3242E+02	0.3474E-03	0.8347E-02
200149	0.000E+00	0.0000E+00	0.6733E+00	0.7355E-02	0.2975E+02	0.3151E-03	0.7491E-02
200150	0.000E+00	0.0000E+00	0.2064E+00	0.4303E-02	0.1867E+02	0.1880E-03	0.4241E-02

Table 7.16 Results of Normal Modes Analysis of DAST Model

MODE	EXTRACTION ORDER	EIGENVALUE $(rad/sec)^2$	FREQUENCY (*Hz*)	GENERALIZED MASS	GENERALIZED STIFFNESS
1	1	0.00000E+00	0.00000E+00	1.00000E+00	0.00000E+00
2	2	0.00000E+00	0.00000E+00	1.00000E+00	0.00000E+00
3	7	5.03062E+03	1.12884E+01	1.00000E+00	5.03062E+03
4	6	9.34976E+04	4.86654E+01	1.00000E+00	9.34976E+04
5	4	1.22573E+05	5.57209E+01	1.00000E+00	1.22573E+05
6	3	4.21470E+05	1.03325E+02	1.00000E+00	4.21470E+05
7	5	6.75673E+05	1.30824E+02	1.00000E+00	6.75673E+05
8	8	8.62662E+05	1.47822E+02	1.00000E+00	8.62662E+05
9	9	1.56335E+06	1.98998E+02	1.00000E+00	1.56335E+06

Table 7.17 Results of Flutter Analyses of DAST Model

No.	Mach	Method	Flutter Speed (*in/sec*)	Flutter Freq. (*Hz*)	CPU Time (Minute)
1	0.80	k-method (ZONA6)	14,357.3	48.67	13.2
2	0.80	Root-locus (ZOZA6)	13,489.5	36.30	
3	0.80	k-method (ZTAIC)	11,800.0	56.01	322.5
4	0.80	Root–locus (ZTAIC)	12,892.0	49.30	

Table 7.18 Design Iteration History of DAST Model: Structural Optimization for Static Aeroelasticity, 10*g* Pull-up Maneuver, $M = 0.8$, by ZONA6 of ASTROS*

Iteration Number	Objective Function	Function Evaluation	Gradient Evaluation	Retained Constraints	Active Constraints	Approximate Convergence
1	8.94951E+01	(Initial Function Value)				
2	1.13956E+01	N/A FSD	N/A FSD	812	N/A FSD	not Converged
3	1.26949E+01	N/A FSD	N/A FSD	812	N/A FSD	not Converged
4	1.43839E+01	N/A FSD	N/A FSD	812	N/A FSD	not Converged
5	2.07644E+01	96	21	90	17	not Converged
10	3.82994E+01	74	7	81	1	not Converged
11	2.70619E+01	57	8	81	81	not Converged
12	1.95782E+01	52	6	81	69	not Converged
13	1.45880E+01	86	11	81	25	not Converged
14	1.18083E+01	128	11	82	33	not Converged
15	1.11908E+01	57	10	125	61	not Converged
16	1.09201E+01	70	9	189	65	not Converged
17	1.08636E+01	12	4	213	57	Converged

The Final Objective Function Value is: Designed = 1.08636E+01

Table 7.19 Design Iteration History of DAST Model: Structural Optimization for Normal Modes

Iteration Number	Objective Function	Function Evaluation	Gradient Evaluation	Retained Constraints	Active Constraints	Approximate Convergence
1	8.94951E+01	(Initial Function Value)				
2	5.96634E+01	12	2	299	0	not Converged
3	3.97756E+01	8	2	299	0	not Converged
4	2.65171E+01	8	2	299	0	not Converged
5	1.76780E+01	8	2	299	0	not Converged
6	1.18357E+01	71	6	299	1	not Converged
7	9.56212E+00	66	5	247	1	not Converged
8	9.46601E+00	50	4	139	1	Converged
9	9.43376E+00	34	3	191	1	Converged

The Final Objective Function Value is: Designed = 9.43376E+00

Table 7.20 Design Iteration History of DAST Model: Multidisciplinary Design Optimization (Static Aeroelasticity + Normal Modes) at $M = 0.80$

Iteration Number	Objective Function	Function Evaluation	Gradient Evaluation	Retained Constraints	Active Constraints	Approximate Convergence
1	8.94951E+01	(Initial Function Value)				
2	1.13956E+01	N/A FSD	N/A FSD	812	N/A FSD	not Converged
3	1.26949E+01	N/A FSD	N/A FSD	812	N/A FSD	not Converged
4	1.43839E+01	N/A FSD	N/A FSD	812	N/A FSD	not Converged
5	2.07644E+01	96	21	91	17	not Converged
6	2.70584E+01	87	21	82	1	not Converged
7	3.28609E+01	100	21	82	1	not Converged
8	4.15089E+01	99	21	82	1	not Converged
10	3.82994E+01	74	7	82	1	not Converged
11	2.70619E+01	57	8	82	82	not Converged
12	1.95782E+01	52	6	82	67	not Converged
13	1.45880E+01	86	11	82	26	not Converged
14	1.18087E+01	118	10	75	33	not Converged
15	1.11916E+01	57	10	126	59	not Converged
16	1.09214E+01	85	11	190	65	not Converged
17	1.08601E+01	13	5	214	65	Converged

The Final Objective Function Value is: Designed = 1.08601E+01

Table 7.21 Final Design Variable Values of DAST Model: Multidisciplinary Design Optimization (Static Aeroelasticity + Normal Modes) at $M = 0.80$

Design Variable	Design Value	Minimum Value	Maximum Value	Objective Sensitivity	Layer List
1	1.00000E-01	1.00000E-01	2.00000E+00	1.05124D+00	1
2	1.00000E-01	1.00000E-01	2.00000E+00	1.05124D+00	2
3	1.00000E-01	1.00000E-01	2.00000E+00	1.05124D+00	3
4	2.28423E-01	1.00000E-01	2.00000E+00	1.05124D+00	4
5	1.00000E-01	1.00000E-01	2.00000E+00	6.82000D-01	1
6	1.00000E-01	1.00000E-01	2.00000E+00	6.82000D-01	2
7	1.00000E-01	1.00000E-01	2.00000E+00	6.82000D-01	3
8	2.09535E-01	1.00000E-01	2.00000E+00	6.82000D-01	4
11	1.00000E-01	1.00000E-01	2.00000E+00	3.58901D-01	1
12	2.96067E-01	1.00000E-01	2.00000E+00	3.58901D-01	2
13	1.82035E-01	1.00000E-01	2.00000E+00	3.58901D-01	3
14	1.55974E+00	1.00000E-01	2.00000E+00	3.58901D-01	4
15	1.00000E-01	1.00000E-01	2.00000E+00	3.55142D-01	1
16	1.00000E-01	1.00000E-01	2.00000E+00	3.55142D-01	2
17	1.00000E-01	1.00000E-01	2.00000E+00	3.55142D-01	3
18	1.04790E-01	1.00000E-01	2.00000E+00	3.55142D-01	4
21	1.00000E-01	1.00000E-01	2.00000E+00	9.56914D-01	1
22	1.00000E-01	1.00000E-01	2.00000E+00	9.56914D-01	2
23	1.00000E-01	1.00000E-01	2.00000E+00	9.56914D-01	3
24	1.00000E-01	1.00000E-01	2.00000E+00	9.56914D-01	4
25	1.00000E-01	1.00000E-01	2.00000E+00	5.99842D-01	1
26	1.00000E-01	1.00000E-01	2.00000E+00	5.99842D-01	2
27	1.00000E-01	1.00000E-01	2.00000E+00	5.99842D-01	3
28	1.00000E-01	1.00000E-01	2.00000E+00	5.99842D-01	4
31	1.00000E-01	1.00000E-01	2.00000E+00	3.35104D-01	1
32	1.22199E-01	1.00000E-01	2.00000E+00	3.35104D-01	2
33	1.00000E-01	1.00000E-01	2.00000E+00	3.35104D-01	3
34	2.84548E-01	1.00000E-01	2.00000E+00	3.35104D-01	4
35	1.00000E-01	1.00000E-01	2.00000E+00	3.29375D-01	1
36	1.00000E-01	1.00000E-01	2.00000E+00	3.29375D-01	2
37	1.00000E-01	1.00000E-01	2.00000E+00	3.29375D-01	3
38	1.95734E-01	1.00000E-01	2.00000E+00	3.29375D-01	4
41	1.00000E-01	1.00000E-01	2.00000E+00	8.67215D-01	1
42	1.00000E-01	1.00000E-01	2.00000E+00	8.67215D-01	2

43	1.00000E-01	1.00000E-01	2.00000E+00	8.67215D-01	3
44	1.00000E-01	1.00000E-01	2.00000E+00	8.67215D-01	4
45	1.00000E-01	1.00000E-01	2.00000E+00	3.56964D-01	1
46	1.00000E-01	1.00000E-01	2.00000E+00	3.56964D-01	2
47	1.00000E-01	1.00000E-01	2.00000E+00	3.56964D-01	3
48	1.00000E-01	1.00000E-01	2.00000E+00	3.56964D-01	4
51	1.00000E-01	1.00000E-01	2.00000E+00	3.11536D-01	1
52	1.00000E-01	1.00000E-01	2.00000E+00	3.11536D-01	2
53	1.00000E-01	1.00000E-01	2.00000E+00	3.11536D-01	3
54	1.08439E-01	1.00000E-01	2.00000E+00	3.11536D-01	4
55	1.00000E-01	1.00000E-01	2.00000E+00	3.04165D-01	1
56	1.00000E-01	1.00000E-01	2.00000E+00	3.04165D-01	2
57	1.00000E-01	1.00000E-01	2.00000E+00	3.04165D-01	3
58	1.05724E-01	1.00000E-01	2.00000E+00	3.04165D-01	4
61	1.00000E-01	1.00000E-01	2.00000E+00	7.88873D-01	1
62	1.00000E-01	1.00000E-01	2.00000E+00	7.88873D-01	2
63	1.00000E-01	1.00000E-01	2.00000E+00	7.88873D-01	3
64	1.00000E-01	1.00000E-01	2.00000E+00	7.88873D-01	4
65	1.00000E-01	1.00000E-01	2.00000E+00	3.80607D-01	1
66	1.00000E-01	1.00000E-01	2.00000E+00	3.80607D-01	2
67	1.00000E-01	1.00000E-01	2.00000E+00	3.80607D-01	3
68	1.00000E-01	1.00000E-01	2.00000E+00	3.80607D-01	4
71	1.00000E-01	1.00000E-01	2.00000E+00	2.86918D-01	1
72	1.00000E-01	1.00000E-01	2.00000E+00	2.86918D-01	2
73	1.00000E-01	1.00000E-01	2.00000E+00	2.86918D-01	3
74	1.00000E-01	1.00000E-01	2.00000E+00	2.86918D-01	4
75	1.00000E-01	1.00000E-01	2.00000E+00	2.78862D-01	1
76	1.00000E-01	1.00000E-01	2.00000E+00	2.78862D-01	2
77	1.00000E-01	1.00000E-01	2.00000E+00	2.78862D-01	3
78	1.00000E-01	1.00000E-01	2.00000E+00	2.78862D-01	4
81	1.00000E-01	1.00000E-01	2.00000E+00	3.67613D-01	1
82	1.00000E-01	1.00000E-01	2.00000E+00	3.67613D-01	2
83	1.00000E-01	1.00000E-01	2.00000E+00	3.67613D-01	3
84	1.00000E-01	1.00000E-01	2.00000E+00	3.67613D-01	4
85	1.00000E-01	1.00000E-01	2.00000E+00	1.71286D-01	1
86	1.00000E-01	1.00000E-01	2.00000E+00	1.71286D-01	2
87	1.00000E-01	1.00000E-01	2.00000E+00	1.71286D-01	3
88	1.00000E-01	1.00000E-01	2.00000E+00	1.71286D-01	4
91	1.00000E-01	1.00000E-01	2.00000E+00	1.33777D-01	1
92	1.00000E-01	1.00000E-01	2.00000E+00	1.33777D-01	2

93	1.00000E-01	1.00000E-01	2.00000E+00	1.33777D-01	3
94	1.00000E-01	1.00000E-01	2.00000E+00	1.33777D-01	4
95	1.00000E-01	1.00000E-01	2.00000E+00	1.30096D-01	1
96	1.00000E-01	1.00000E-01	2.00000E+00	1.30096D-01	2
97	1.00000E-01	1.00000E-01	2.00000E+00	1.30096D-01	3
98	1.00000E-01	1.00000E-01	2.00000E+00	1.30096D-01	4
101	1.00000E-01	1.00000E-01	2.00000E+00	3.49838D-01	1
102	1.00000E-01	1.00000E-01	2.00000E+00	3.49838D-01	2
103	1.00000E-01	1.00000E-01	2.00000E+00	3.49838D-01	3
104	1.00000E-01	1.00000E-01	2.00000E+00	3.49838D-01	4
106	1.00000E-01	1.00000E-01	2.00000E+00	1.63135D-01	2
107	1.00000E-01	1.00000E-01	2.00000E+00	1.63135D-01	3
108	1.00000E-01	1.00000E-01	2.00000E+00	1.63135D-01	4
111	1.00000E-01	1.00000E-01	2.00000E+00	1.27431D-01	1
112	1.00000E-01	1.00000E-01	2.00000E+00	1.27431D-01	2
113	1.00000E-01	1.00000E-01	2.00000E+00	1.27431D-01	3
114	1.00000E-01	1.00000E-01	2.00000E+00	1.27431D-01	4
115	1.00000E-01	1.00000E-01	2.00000E+00	1.23935D-01	1
116	1.00000E-01	1.00000E-01	2.00000E+00	1.23935D-01	2
117	1.00000E-01	1.00000E-01	2.00000E+00	1.23935D-01	3
118	1.00000E-01	1.00000E-01	2.00000E+00	1.23935D-01	4
121	1.00000E-01	1.00000E-01	2.00000E+00	6.46313D-01	1
122	1.00000E-01	1.00000E-01	2.00000E+00	6.46313D-01	2
123	1.00000E-01	1.00000E-01	2.00000E+00	6.46313D-01	3
124	1.00000E-01	1.00000E-01	2.00000E+00	6.46313D-01	4
125	1.00000E-01	1.00000E-01	2.00000E+00	3.01834D-01	1
126	1.00000E-01	1.00000E-01	2.00000E+00	3.01834D-01	2
127	1.00000E-01	1.00000E-01	2.00000E+00	3.01834D-01	3
128	1.00000E-01	1.00000E-01	2.00000E+00	3.01834D-01	4
131	1.00000E-01	1.00000E-01	2.00000E+00	2.35825D-01	1
132	1.00000E-01	1.00000E-01	2.00000E+00	2.35825D-01	2
133	1.00000E-01	1.00000E-01	2.00000E+00	2.35825D-01	3
134	1.00000E-01	1.00000E-01	2.00000E+00	2.35825D-01	4
135	1.00000E-01	1.00000E-01	2.00000E+00	2.29360D-01	1
136	1.00000E-01	1.00000E-01	2.00000E+00	2.29360D-01	2
137	1.00000E-01	1.00000E-01	2.00000E+00	2.29360D-01	3
138	1.00000E-01	1.00000E-01	2.00000E+00	2.29360D-01	4
141	1.00000E-01	1.00000E-01	2.00000E+00	5.75088D-01	1
142	1.17946E-01	1.00000E-01	2.00000E+00	5.75088D-01	2
143	1.36251E-01	1.00000E-01	2.00000E+00	5.75088D-01	3

144	1.06661E-01	1.00000E-01	2.00000E+00	5.75088D-01	4
145	1.00000E-01	1.00000E-01	2.00000E+00	2.25171D-01	1
146	1.00000E-01	1.00000E-01	2.00000E+00	2.25171D-01	2
147	1.00000E-01	1.00000E-01	2.00000E+00	2.25171D-01	3
148	1.00000E-01	1.00000E-01	2.00000E+00	2.25171D-01	4
151	1.00000E-01	1.00000E-01	2.00000E+00	2.10394D-01	1
152	1.00000E-01	1.00000E-01	2.00000E+00	2.10394D-01	2
153	1.00000E-01	1.00000E-01	2.00000E+00	2.10394D-01	3
154	1.00000E-01	1.00000E-01	2.00000E+00	2.10394D-01	4
155	1.00000E-01	1.00000E-01	2.00000E+00	2.04631D-01	1
156	1.00000E-01	1.00000E-01	2.00000E+00	2.04631D-01	2
157	1.00000E-01	1.00000E-01	2.00000E+00	2.04631D-01	3
158	1.00000E-01	1.00000E-01	2.00000E+00	2.04631D-01	4
161	1.00000E-01	1.00000E-01	2.00000E+00	4.46490D-01	1
162	1.00000E-01	1.00000E-01	2.00000E+00	4.46490D-01	2
163	1.00000E-01	1.00000E-01	2.00000E+00	4.46490D-01	3
164	1.00000E-01	1.00000E-01	2.00000E+00	4.46490D-01	4
165	1.00000E-01	1.00000E-01	2.00000E+00	1.69649D-01	1
166	1.00000E-01	1.00000E-01	2.00000E+00	1.69649D-01	2
167	1.00000E-01	1.00000E-01	2.00000E+00	1.69649D-01	3
168	1.00000E-01	1.00000E-01	2.00000E+00	1.69649D-01	4
171	1.00000E-01	1.00000E-01	2.00000E+00	1.86520D-01	1
172	1.00000E-01	1.00000E-01	2.00000E+00	1.86520D-01	2
173	1.00000E-01	1.00000E-01	2.00000E+00	1.86520D-01	3
174	1.00000E-01	1.00000E-01	2.00000E+00	1.86520D-01	4
175	1.00000E-01	1.00000E-01	2.00000E+00	1.81490D-01	1
176	1.00000E-01	1.00000E-01	2.00000E+00	1.81490D-01	2
177	1.00000E-01	1.00000E-01	2.00000E+00	1.81490D-01	3
178	1.00000E-01	1.00000E-01	2.00000E+00	1.81490D-01	4
181	1.00000E-01	1.00000E-01	2.00000E+00	5.64183D-01	1
182	1.00000E-01	1.00000E-01	2.00000E+00	5.64183D-01	2
183	1.00000E-01	1.00000E-01	2.00000E+00	5.64183D-01	3
184	1.95856E-01	1.00000E-01	2.00000E+00	5.64183D-01	4
185	1.00000E-01	1.00000E-01	2.00000E+00	3.59374D-01	1
186	2.13487E-01	1.00000E-01	2.00000E+00	3.59374D-01	2
187	2.55090E-01	1.00000E-01	2.00000E+00	3.59374D-01	3
188	1.65567E+00	1.00000E-01	2.00000E+00	3.59374D-01	4
191	1.00000E-01	1.00000E-01	2.00000E+00	3.55309D-01	1
192	1.00000E-01	1.00000E-01	2.00000E+00	3.55309D-01	2
193	1.00000E-01	1.00000E-01	2.00000E+00	3.55309D-01	3

194	1.08876E-01	1.00000E-01	2.00000E+00	3.55309D-01	4
195	1.00000E-01	1.00000E-01	2.00000E+00	6.00242D-01	1
196	1.00000E-01	1.00000E-01	2.00000E+00	6.00242D-01	2
197	1.00000E-01	1.00000E-01	2.00000E+00	6.00242D-01	3
198	1.00000E-01	1.00000E-01	2.00000E+00	6.00242D-01	4
201	1.00000E-01	1.00000E-01	2.00000E+00	3.35389D-01	1
202	1.00000E-01	1.00000E-01	2.00000E+00	3.35389D-01	2
203	1.24392E-01	1.00000E-01	2.00000E+00	3.35389D-01	3
204	2.92392E-01	1.00000E-01	2.00000E+00	3.35389D-01	4
205	1.00000E-01	1.00000E-01	2.00000E+00	3.29343D-01	1
206	1.00000E-01	1.00000E-01	2.00000E+00	3.29343D-01	2
207	1.00000E-01	1.00000E-01	2.00000E+00	3.29343D-01	3
208	2.14306E-01	1.00000E-01	2.00000E+00	3.29343D-01	4
211	1.00000E-01	1.00000E-01	2.00000E+00	3.58983D-01	1
212	1.00000E-01	1.00000E-01	2.00000E+00	3.58983D-01	2
213	1.00000E-01	1.00000E-01	2.00000E+00	3.58983D-01	3
214	1.00000E-01	1.00000E-01	2.00000E+00	3.58983D-01	4
215	1.00000E-01	1.00000E-01	2.00000E+00	3.11969D-01	1
216	1.00000E-01	1.00000E-01	2.00000E+00	3.11969D-01	2
217	1.00000E-01	1.00000E-01	2.00000E+00	3.11969D-01	3
218	1.22438E-01	1.00000E-01	2.00000E+00	3.11969D-01	4
221	1.00000E-01	1.00000E-01	2.00000E+00	3.04128D-01	1
222	1.00000E-01	1.00000E-01	2.00000E+00	3.04128D-01	2
223	1.00000E-01	1.00000E-01	2.00000E+00	3.04128D-01	3
224	1.23405E-01	1.00000E-01	2.00000E+00	3.04128D-01	4
225	1.00000E-01	1.00000E-01	2.00000E+00	3.83608D-01	1
226	1.00000E-01	1.00000E-01	2.00000E+00	3.83608D-01	2
227	1.00000E-01	1.00000E-01	2.00000E+00	3.83608D-01	3
228	1.00000E-01	1.00000E-01	2.00000E+00	3.83608D-01	4
231	1.00000E-01	1.00000E-01	2.00000E+00	2.87848D-01	1
232	1.00000E-01	1.00000E-01	2.00000E+00	2.87848D-01	2
233	1.00000E-01	1.00000E-01	2.00000E+00	2.87848D-01	3
234	1.00000E-01	1.00000E-01	2.00000E+00	2.87848D-01	4
235	1.00000E-01	1.00000E-01	2.00000E+00	4.51979D-01	1
236	1.00000E-01	1.00000E-01	2.00000E+00	4.51979D-01	2
237	1.00000E-01	1.00000E-01	2.00000E+00	4.51979D-01	3
238	1.00000E-01	1.00000E-01	2.00000E+00	4.51979D-01	4
245	1.00000E-01	1.00000E-01	2.00000E+00	1.34223D-01	1
246	1.00000E-01	1.00000E-01	2.00000E+00	1.34223D-01	2
247	1.00000E-01	1.00000E-01	2.00000E+00	1.34223D-01	3

248	1.00000E-01	1.00000E-01	2.00000E+00	1.34223D-01	4
251	1.00000E-01	1.00000E-01	2.00000E+00	1.30169D-01	1
252	1.00000E-01	1.00000E-01	2.00000E+00	1.30169D-01	2
253	1.00000E-01	1.00000E-01	2.00000E+00	1.30169D-01	3
254	1.00000E-01	1.00000E-01	2.00000E+00	1.30169D-01	4
255	1.00000E-01	1.00000E-01	2.00000E+00	1.64721D-01	1
256	1.00000E-01	1.00000E-01	2.00000E+00	1.64721D-01	2
257	1.00000E-01	1.00000E-01	2.00000E+00	1.64721D-01	3
258	1.00000E-01	1.00000E-01	2.00000E+00	1.64721D-01	4
261	1.00000E-01	1.00000E-01	2.00000E+00	1.27836D-01	1
262	1.00000E-01	1.00000E-01	2.00000E+00	1.27836D-01	2
263	1.00000E-01	1.00000E-01	2.00000E+00	1.27836D-01	3
264	1.00000E-01	1.00000E-01	2.00000E+00	1.27836D-01	4
265	1.00000E-01	1.00000E-01	2.00000E+00	1.23987D-01	1
266	1.00000E-01	1.00000E-01	2.00000E+00	1.23987D-01	2
267	1.00000E-01	1.00000E-01	2.00000E+00	1.23987D-01	3
268	1.00000E-01	1.00000E-01	2.00000E+00	1.23987D-01	4
271	1.00000E-01	1.00000E-01	2.00000E+00	4.28677D-01	1
272	1.00000E-01	1.00000E-01	2.00000E+00	4.28677D-01	2
273	1.00000E-01	1.00000E-01	2.00000E+00	4.28677D-01	3
274	1.00000E-01	1.00000E-01	2.00000E+00	4.28677D-01	4
275	1.00000E-01	1.00000E-01	2.00000E+00	2.36503D-01	1
276	1.20179E-01	1.00000E-01	2.00000E+00	2.36503D-01	2
277	1.00000E-01	1.00000E-01	2.00000E+00	2.36503D-01	3
278	1.01198E-01	1.00000E-01	2.00000E+00	2.36503D-01	4
281	1.00000E-01	1.00000E-01	2.00000E+00	2.29397D-01	1
282	1.14907E-01	1.00000E-01	2.00000E+00	2.29397D-01	2
283	1.00000E-01	1.00000E-01	2.00000E+00	2.29397D-01	3
284	1.08398E-01	1.00000E-01	2.00000E+00	2.29397D-01	4
285	1.00000E-01	1.00000E-01	2.00000E+00	2.27539D-01	1
291	1.00000E-01	1.00000E-01	2.00000E+00	2.10926D-01	1
292	1.00000E-01	1.00000E-01	2.00000E+00	2.10926D-01	2
293	1.00000E-01	1.00000E-01	2.00000E+00	2.10926D-01	3
294	1.01179E-01	1.00000E-01	2.00000E+00	2.10926D-01	4
295	1.00000E-01	1.00000E-01	2.00000E+00	2.04613D-01	1
296	1.00000E-01	1.00000E-01	2.00000E+00	2.04613D-01	2
297	1.00000E-01	1.00000E-01	2.00000E+00	2.04613D-01	3
298	1.00666E-01	1.00000E-01	2.00000E+00	2.04613D-01	4
301	1.00000E-01	1.00000E-01	2.00000E+00	1.71867D-01	1
302	1.00000E-01	1.00000E-01	2.00000E+00	1.71867D-01	2

303	1.00000E-01	1.00000E-01	2.00000E+00	1.71867D-01	3
304	1.00000E-01	1.00000E-01	2.00000E+00	1.71867D-01	4
305	1.00000E-01	1.00000E-01	2.00000E+00	1.86993D-01	1
306	1.00000E-01	1.00000E-01	2.00000E+00	1.86993D-01	2
307	1.00000E-01	1.00000E-01	2.00000E+00	1.86993D-01	3
308	1.00000E-01	1.00000E-01	2.00000E+00	1.86993D-01	4
311	1.00000E-01	1.00000E-01	2.00000E+00	1.81448D-01	1
312	1.00000E-01	1.00000E-01	2.00000E+00	1.81448D-01	2
313	1.00000E-01	1.00000E-01	2.00000E+00	1.81448D-01	3
314	1.00000E-01	1.00000E-01	2.00000E+00	1.81448D-01	4
315	1.00000E-01	1.00000E-01	2.00000E+00	3.88795D+00	
316	1.37788E-01	1.00000E-01	2.00000E+00	2.30795D+00	

Table 7.22 Non-Dimensional Longitudinal Stability Derivatives of AAW Model: *7g* Pull-up Maneuver, $M = 0.85$, by ZONA6 of ASTROS*, for Rigid and Flexible Structure

TRIM IDENTIFICATION = 1 REFERENCE GRID = 12
REFERENCE AREA = 2.8800E+04 REFERENCE CHORD = 1.3827E+02

PARAMETER	<< LIFT >>			<<PITCHING MOMENT>>>		
	RIGID DIRECT	RIGID SPLINED	FLEX.	RIGID DIRECT	RIGID SPLINED	FLEXIBLE
THICKNESS/CAMBER	-0.1315	-0.1275	-0.1757	-0.0042	-0.0080	-0.0008
ANGLE OF ATTACK (°)	0.1922	0.1951	0.2194	-0.0125	-0.0167	-0.0124
PITCH RATE (*s/deg*)	0.3618	0.3740	0.2978	-0.2907	-0.3132	-0.2474
CONTROL SURFACE (°)	-0.0318	-0.0349	-0.0231	0.0426	0.0474	0.0311

Table 7.23 Non-Dimensional Longitudinal Stability Derivatives of AAW Model: 7*g* Pull-up Maneuver, $M = 0.85$, by ZTAIC of ASTROS*, for Rigid and Flexible Structure

TRIM IDENTIFICATION = 1 REFERENCE GRID = 12
REFERENCE AREA = 2.8800E+04 REFERENCE CHORD = 1.3827E+02

	<< LIFT >>			<<PITCHING MOMENT>>		
	RIGID	RIGID	FLEX.	RIGID	RIGID	FLEX.
PARAMETER	DIRECT	SPLINED		DIRECT	SPLINED	
THICKNESS/CAMBER	-1.3162	-0.8979	-2.5215	0.1914	0.2819	2.7592
ANGLE OF ATTACK *1/deg*	0.1922	0.1951	0.2194	-0.0125	-0.0167	-0.0124
ANGLE OF ATTACK *1/rad*	11.0101	11.1810	12.5715	-0.7141	-0.9591	-0.7103
PITCH RATE *s/deg*	0.3618	0.3740	0.2978	-0.2907	-0.3132	-0.2474
PITCH RATE *s/rad*	20.7310	21.4259	17.0639	-16.6565	-17.9477	-14.1748
CONTROL SURFACE *1/deg*	-0.0318	-0.0349	-0.0231	0.0426	0.0474	0.0311
CONTROL SURFACE *1/rad*	-1.8210	-2.0022	-1.3244	2.4398	2.7150	1.7797

Table 7.24 Non-Dimensional Longitudinal Stability Derivatives of AAW Model: 7*g* Pull-up Maneuver, $M = 1.15$, by ZONA7 of ASTROS*, for Rigid and Flexible Structure

TRIM IDENTIFICATION = 2 REFERENCE GRID = 12
REFERENCE AREA = 2.8800E+04 REFERENCE CHORD = 1.3827E+02

	<< LIFT >>			<<PITCHING MOMENT>>		
	RIGID	RIGID	FLEX.	RIGID	RIGID	FLEX.
PARAMETER	DIRECT	SPLINED		DIRECT	SPLINED	
THICKNESS/CAMBER	-0.1803	-0.1792	-0.4983	0.0290	0.0289	0.1797
ANGLE OF ATTACK *1/deg*	0.2237	0.2271	0.3043	-0.0753	-0.0818	-0.0984
ANGLE OF ATTACK *1/rad*	12.8143	13.0099	17.4378	-4.3130	-4.6869	-5.6362
PITCH RATE *s/deg*	0.3803	0.3817	0.1726	-0.4394	-0.4462	-0.2510
PITCH RATE *s/rad*	21.7869	21.8725	9.8885	-25.1751	-25.5648	-14.3812
CONTROL SURFACE *1/deg*	-0.0309	-0.0324	-0.0155	0.0493	0.0521	0.0236
CONTROL SURFACE *1/rad*	-1.7716	-1.8570	-0.8877	2.8252	2.9847	1.3525

Table 7.25 Non-Dimensional Longitudinal Stability Derivatives of AAW Model: 7*g* Pull-up Maneuver, *M* = 3.0, by ZONAU7 of ASTROS*, for Rigid and Flexible Structure

	<< LIFT	>>		<<PITCHING	MOMENT>>	
	RIGID	RIGID	FLEX.	RIGID	RIGID	FLEX.
PARAMETER	DIRECT	SPLINED		DIRECT	SPLINED	
THICKNESS/CAMBER	-0.0631	-0.0595	-0.2173	0.0196	0.0159	0.0855
ANGLE OF ATTACK *1/deg*	0.0844	0.0804	0.0426	-0.0297	-0.0257	-0.0109
ANGLE OF ATTACK *1/rad*	4.8369	4.6085	2.4389	-1.7022	-1.4731	-0.6258
PITCH RATE *s/deg*	0.0779	0.0676	0.0821	-0.1581	-0.1432	-0.1067
PITCH RATE *s/rad*	4.4609	3.8715	4.7017	-9.0591	-8.2030	-6.1153
CONTROL SURFACE *1/deg*	-0.0105	-0.0088	-0.0031	0.0172	0.0142	0.0037
CONTROL SURFACE *1/rad*	-0.6008	-0.5047	-0.1757	0.9873	0.8114	0.2095

Table 7.26 Trim Parameters of AAW Model: 7*g* Pull-up Manuever, *M* = 0.85, by ZONA6 of ASTROS*, for Rigid and Flexible Structure

TRIM RESULTS FOR TRIM SET 1 OF TYPE PITCH
MACH NUMBER 8.50000E-01
DYNAMIC PRESSURE 7.38000E+00, VELCITY .13780E+04

TRIM PARAMETERS:	LABEL	FLEXIBLE	RIGID	
LOAD FACTOR	"NZ "	2.70479E+03	2.7047E+03	(Input)
PITCH ACCELERATION	"QACCEL"	0.00000E+00	0.0000E+00 rad/s^2	(Input)
ANGLE OF ATTACK	"ALPHA"	6.26928E+00	6.9735E+00 *deg*	(Computed)
PITCH RATE	"QRATE"	0.00000E+00	0.0000E+00 *deg/s*	(Input)
CONTROL SURFACE	"STBLTR"	2.34365E+00	2.5108E+00 *deg*	(Computed)
THICKNESS/CAMBER	"THKCAM"	1.00000E+00	1.0000E+00	(Input)

Table 7.27 Trim Parameters of AAW Model: 7*g* Pull-up Maneuver, *M* = 0.85, by ZTAIC of ASTROS*, for Rigid and Flexible Structure

TRIM RESULTS FOR TRIM SET 1 OF TYPE PITCH
MACH NUMBER 0.85, DYNAMIC PRESSURE 0.738, VELOCITY 11,378

TRIM PARAMETER	LABEL	FLEXIBLE	RIGID	
LOAD FACTOR	"NZ "	2.70479E+03	2.70479E+03	(Input)
PITCH ACCELERATION	"QACCEL"	0.00000E+00	0.0000E+00 rad/s^2	(Input)
ANGLE OF ATTACK	"ALPHA"	7.65822E+00	1.0018E+01 *deg*	(Computed)
PITCH RATE	"QRATE"	0.00000E+00	0.0000E+00 *deg/s*	(Input)
CONTROL SURFACE	"STBLTR"	-8.5954E+01	-2.5315E+00 *deg*	(Computed)
THICKNESS/CAMBER	"THKCAM"	1.0000E+00	1.0000E+00	(Input)

Table 7.28 Trim Parameters of AAW Model: 7g Pull-up Maneuver, $M = 1.15$, by ZONA7 of ASTROS*, for Rigid and Flexible Structure

MACH NUMBER 1.15000E+00
DYNAMIC PRESSURE 1.35400E+01, VELOCITY 1.54100E+04

TRIM PARAMETER	LABEL	FLEXIBLE	RIGID	
LOAD FACTOR	"NZ "	2.70479E+03	2.70479E+03	(Input)
PITCH ACCELERATION	"QACCEL"	0.00000E+00	0.00000E+00 *rad/^{2}*	(Input)
ANGLE OF ATTACK	"ALPHA"	4.18166E+00	4.4486E+00 *deg*	(Computed)
PITCH RATE	"QRATE"	0.00000E+00	0.0000E+00 *deg/s*	(Input)
CONTROL SURFACE	"STBLTR"	9.67603E+00	6.37018E+00 *deg*	(Computed)
THICKNESS/CAMBER	"THKCAM"	1.00000E+00	1.00000E+00	(Input)

Table 7.29 Trim Parameters of AAW Model: 7g Pull-up Maneuver, $M = 3.0$, by ZONA7U of ASTROS*, for Rigid and Flexible Structure

TRIM RESULTS FOR TRIM SET 3 OF TYPE PITCH
MACH NUMBER 3.00000E+00
DYNAMIC PRESSURE 9.21200E+01, VELOCITY 4.02000E+04

TRIM PARAMETERS	LABEL	FLEXIBLE	RIGID	
LOAD FACTOR	"NZ"	2.70479E+03	2.7047E+03	(Input)
PITCH ACCELERATION	"QACCEL"	0.00000E+00	0.0000E+00 *rad/s^2*	(Input)
ANGLE OF ATTACK	"ALPHA"	7.09505E+00	2.1903E+00 *deg*	(Computed)
PITCH RATE	"QRATE"	0.00000E+00	0.0000E+00 *deg/s*	(Input)
CONTROL SURFACE	"STBLTR"	-2.32463E+00	2.8218E+00 *deg*	(Computed)
THICKNESS/CAMBER	"THKCAM"	1.00000E+00	1.0000E+00	(Input)

Table 7.30. Results of Normal Modes Analysis of AAW Model

MODE	EXT. ORDER	EIGENVALUE *(rad/sec)*^{2}	FREQUENCY *(Hz)*	GENERALIZED MASS	GENERALIZED STIFFNESS
1	1	0.00000E+00	0.00000E+00	1.00000E+00	0.00000E+00
2	2	0.00000E+00	0.00000E+00	1.00000E+00	0.00000E+00
3	8	1.18195E+03	5.47166E+00	1.00000E+00	1.18195E+03
4	5	3.40450E+03	9.28638E+00	1.00000E+00	3.40450E+03
5	3	6.37910E+03	1.27116E+01	1.00000E+00	6.37910E+03
6	4	7.37361E+03	1.36666E+01	1.00000E+00	7.37361E+03
7	6	9.80147E+03	1.57567E+01	1.00000E+00	9.80147E+03
8	7	9.92482E+03	1.58556E+01	1.00000E+00	9.92482E+03
9	9	1.20184E+04	1.74479E+01	1.00000E+00	1.20184E+04
10	10	1.53511E+04	1.97192E+01	1.00000E+00	1.53511E+04
11	11	2.04324E+04	2.27499E+01	1.00000E+00	2.04324E+04

Table 7.31 Results of Flutter Analyses of AAW Model

No.	Mach No.	Aerodynamic Module	F. Method	Flutter Speed (*in*/sec)	Flutter Freq. (*Hz*)
1	0.85	ZONA6	k-method	11,281.4	14.80
			Root–locus	10,978.9	14.77
2	0.85	ZTAIC	k-method	10,713.7	14.96
			Root-locus	10,537.6	14.73
3	1.15	ZONA7	k-method	11,087.9	14.90
			Root–locus	11,308.3	14.93
4	3.0	ZONA7U	k-method	58,768.0	8.55
			Root–locus	No Flutter	

Table 7.32 Design Iteration History of AAW Model: Structural Optimization for Static Aeroelasticity: 7g Pull-up Maneuver, $M = 0.85$, by ZONA6 of ASTROS*

Iteration Number	Objective Function	Function Evaluation	Gradient Evaluation	Retained Constraints	Active Constraints	Approximate Convergence
1	5.86976E+02 (Initial Function Value)					
2	3.86589E+02	N/A FSD	N/A FSD	160	N/A FSD	not Converged
3	3.85472E+02	N/A FSD	N/A FSD	160	N/A FSD	not Converged
4	3.88594E+02	N/A FSD	N/A FSD	160	N/A FSD	not Converged
5	5.82891E+02	102	21	68	1	not Converged
6	5.58810E+02	41	7	33	3	not Converged
9	5.35176E+02	17	4	33	8	not Converged
10	5.32730E+02	24	4	33	8	not Converged
11	5.31184E+02	16	3	33	11	not Converged
12	5.30271E+02	18	3	33	10	not Converged
13	5.29567E+02	18	3	33	11	not Converged
14	5.29048E+02	14	2	33	11	not Converged
15	5.28862E+02	13	2	33	11	Converged

Final Objective Function Value is: Designed = 5.28862E+02

Table 7.33 Design Iteration History of AAW Model: Structural Optimization for Normal Modes

Iteration Number	Objective Function	Function Evaluation	Gradient Evaluation	Retained Constraints	Active Constraints	Approximate Convergence
1	5.86976E+02 (Initial Function Value)					
2	5.61598E+02	37	4	1	1	not Converged
3	5.46746E+02	30	4	1	1	not Converged
4	5.35543E+02	27	4	1	1	not Converged
5	5.26827E+02	38	6	1	1	not Converged
10	5.13924E+02	19	3	1	1	not Converged
11	5.13499E+02	10	2	1	1	not Converged
12	5.12416E+02	18	3	1	1	not Converged
13	5.11963E+02	13	2	1	1	not Converged
14	5.11807E+02	10	2	1	1	not Converged
15	5.11653E+02	11	2	1	1	not Converged
16	5.11501E+02	10	2	1	1	Converged

Final Objective Function Value is: Designed = 5.11501E+02

Table 7.34 Design Iteration History of AAW Model: Multidisciplinary Optimization (Static Aeroelasticity + Normal Modes), $M = 0.85$, by ZONA6 of ASTROS*

Iteration Number	Objective Function	Function Evaluation	Gradient Evaluation	Retained Constraints	Active Constraints	Approximate Convergence
1	5.86976E+02 (Initial Function Value)					
2	3.86589E+02	N/A FSD	N/A FSD	160	N/A FSD	not Converged
3	3.85472E+02	N/A FSD	N/A FSD	160	N/A FSD	not Converged
4	3.88594E+02	N/A FSD	N/A FSD	160	N/A FSD	not Converged
5	5.82768E+02	98	21	69	2	not Converged
6	5.59573E+02	46	7	33	4	not Converged
7	5.46785E+02	17	6	33	8	not Converged
8	5.46793E+02	13	2	33	1	Converged

Final Objective Function Value is: Designed = 5.46793E+02

Table 7.35 Final Design Variable Values of AAW Model: Multidisciplinary Optimization (Static Aeroelasticity + Normal Modes), $M = 0.85$, by ZONA6 of ASTROS*

Design Variable	Design Value	Minimum Value	Maximum Value	Objective Sensitivity
1701	1.22058E+00	5.00000E-01	5.00000E+00	1.74016D+00
1702	1.60513E+00	5.00000E-01	5.00000E+00	1.77430D+00
1703	7.95815E-01	5.00000E-01	5.00000E+00	8.70047D+00
1704	7.57608E-01	5.00000E-01	5.00000E+00	1.08802D+01
1705	8.45186E-01	5.00000E-01	5.00000E+00	3.85550D+00
1706	7.20742E-01	5.00000E-01	5.00000E+00	6.39913D+00
1707	1.04533E+00	5.00000E-01	5.00000E+00	3.04685D+00
1708	1.03217E+00	5.00000E-01	5.00000E+00	2.35767D+00
1709	1.13811E+00	5.00000E-01	5.00000E+00	4.82027D+00
1710	7.18104E-01	5.00000E-01	5.00000E+00	4.16019D+00
1711	7.57840E-01	5.00000E-01	5.00000E+00	5.07441D+00
1712	1.70811E+00	5.00000E-01	5.00000E+00	1.00477D+00
1713	1.01334E+00	5.00000E-01	5.00000E+00	3.28584D+00
1714	1.24860E+00	5.00000E-01	5.00000E+00	5.92739D+00
1715	1.10802E+00	5.00000E-01	5.00000E+00	6.77305D+00
1716	9.19356E-01	5.00000E-01	5.00000E+00	2.80967D+00
1717	1.20391E+00	5.00000E-01	5.00000E+00	4.66995D+00
1718	1.81623E+00	5.00000E-01	5.00000E+00	3.11335D+00
1719	1.86799E+00	5.00000E-01	5.00000E+00	1.87446D+00
1720	1.79343E+00	5.00000E-01	5.00000E+00	4.27074D+00
1721	1.09471E+00	5.00000E-01	5.00000E+00	4.13102D+00
1722	1.01616E+00	5.00000E-01	5.00000E+00	5.28995D+00
1723	2.03646E+00	5.00000E-01	5.00000E+00	1.10335D+00
1724	1.47628E+00	5.00000E-01	5.00000E+00	4.04877D+00
1725	1.70998E+00	5.00000E-01	5.00000E+00	6.62340D+00
1726	1.43939E+00	5.00000E-01	5.00000E+00	7.48039D+00
1727	1.48071E+00	5.00000E-01	5.00000E+00	3.07621D+00
1728	1.55908E+00	5.00000E-01	5.00000E+00	5.33289D+00
1729	1.45407E+00	5.00000E-01	5.00000E+00	4.43926D+00
1730	1.55623E+00	5.00000E-01	5.00000E+00	2.38329D+00
1731	1.72700E+00	5.00000E-01	5.00000E+00	5.07280D+00
1732	1.24940E+00	5.00000E-01	5.00000E+00	1.70193D+00
1733	1.26331E+00	5.00000E-01	5.00000E+00	1.86622D+00
1734	1.15086E+00	5.00000E-01	5.00000E+00	2.22035D+00
1735	1.42646E+00	5.00000E-01	5.00000E+00	4.75506D+00
1736	9.34999E-01	5.00000E-01	5.00000E+00	8.70663D+00

1737	8.26596E-01	5.00000E-01	5.00000E+00	8.97545D+00
1738	7.55591E-01	5.00000E-01	5.00000E+00	3.66347D+00
1739	8.16538E-01	5.00000E-01	5.00000E+00	5.16857D+00
1740	6.93052E-01	5.00000E-01	5.00000E+00	5.06523D+00
1741	6.96326E-01	5.00000E-01	5.00000E+00	3.08955D+00
1742	9.45179E-01	5.00000E-01	5.00000E+00	3.39517D+00
1743	9.35337E-01	5.00000E-01	5.00000E+00	1.56717D+00
1744	7.72785E-01	5.00000E-01	5.00000E+00	2.53572D+00
1745	7.56979E-01	5.00000E-01	5.00000E+00	3.18882D+00
1746	1.03175E+00	5.00000E-01	5.00000E+00	4.65414D+00
1757	1.00094E+00	5.00000E-01	5.00000E+00	4.47074D+00
1758	7.69823E-01	5.00000E-01	5.00000E+00	9.87355D-01
1759	6.82903E-01	5.00000E-01	5.00000E+00	1.85035D+01
1769	7.43817E-01	5.00000E-01	5.00000E+00	9.80553D-01
1770	6.59264E-01	5.00000E-01	5.00000E+00	8.06593D-01
1781	5.00000E-01	5.00000E-01	5.00000E+00	4.90527D-01
1782	8.72983E-01	5.00000E-01	5.00000E+00	8.17501D+00
1783	7.90637E-01	5.00000E-01	5.00000E+00	1.00029D+01
1784	6.92899E-01	5.00000E-01	5.00000E+00	4.04138D+00
1785	6.85072E-01	5.00000E-01	5.00000E+00	6.91639D+00
1786	7.31669E-01	5.00000E-01	5.00000E+00	5.60300D+00
1787	8.38961E-01	5.00000E-01	5.00000E+00	3.77051D+00
1788	8.55981E-01	5.00000E-01	5.00000E+00	8.42925D+00
1791	8.51278E-01	5.00000E-01	5.00000E+00	3.10291D+00
1792	5.00000E-01	5.00000E-01	5.00000E+00	1.07651D+01
1793	9.37030E-01	5.00000E-01	5.00000E+00	6.51065D+00
1794	1.01890E+00	5.00000E-01	5.00000E+00	6.55478D+00
1795	6.72597E-01	5.00000E-01	5.00000E+00	7.61272D+00
1796	5.70086E-01	5.00000E-01	5.00000E+00	1.28009D+01
1797	1.00423E+00	5.00000E-01	5.00000E+00	6.49647D+00
1798	1.06266E+00	5.00000E-01	5.00000E+00	3.91175D+00
1799	7.59363E-01	5.00000E-01	5.00000E+00	1.30907D+01
1800	8.26111E-01	5.00000E-01	5.00000E+00	4.22861D+00
1801	7.98238E-01	5.00000E-01	5.00000E+00	5.28934D+00
1802	1.82031E+00	5.00000E-01	5.00000E+00	1.13463D+00
1803	1.58645E+00	5.00000E-01	5.00000E+00	3.87084D+00
1804	1.52330E+00	5.00000E-01	5.00000E+00	7.22828D+00
1805	1.21068E+00	5.00000E-01	5.00000E+00	7.91604D+00
1806	5.67002E-01	5.00000E-01	5.00000E+00	1.07664D+01
1807	1.36037E+00	5.00000E-01	5.00000E+00	5.42275D+00
1808	1.05276E+00	5.00000E-01	5.00000E+00	2.86677D+01
1815	8.70374E-01	5.00000E-01	5.00000E+00	8.93814D+00

1816	7.62127E-01	5.00000E-01	5.00000E+00	9.60091D+00
1817	7.23239E-01	5.00000E-01	5.00000E+00	4.25357D+00
1818	6.86500E-01	5.00000E-01	5.00000E+00	6.71715D+00
1819	9.12321E-01	5.00000E-01	5.00000E+00	4.05310D+00
1820	8.28862E-01	5.00000E-01	5.00000E+00	2.62631D+00
1821	8.67128E-01	5.00000E-01	5.00000E+00	8.61160D+00
1824	1.10600E+00	5.00000E-01	5.00000E+00	1.74421D+00
1825	1.01462E+00	5.00000E-01	5.00000E+00	4.66375D+00
1826	1.01394E+00	5.00000E-01	5.00000E+00	6.82308D+00
1827	7.27502E-01	5.00000E-01	5.00000E+00	9.90440D+00
1828	5.64714E-01	5.00000E-01	5.00000E+00	4.45509D+00
1829	5.41270E-01	5.00000E-01	5.00000E+00	7.72091D+00
1830	7.95036E-01	5.00000E-01	5.00000E+00	4.11063D+00
1831	7.27085E-01	5.00000E-01	5.00000E+00	3.26568D+00
1832	8.26841E-01	5.00000E-01	5.00000E+00	4.91151D+00
1833	7.42066E-01	5.00000E-01	5.00000E+00	1.89184D+00
1834	7.26199E-01	5.00000E-01	5.00000E+00	2.01049D+00
1835	8.90492E-01	5.00000E-01	5.00000E+00	2.00697D+00
1836	9.94744E-01	5.00000E-01	5.00000E+00	4.38660D+00
1837	7.90668E-01	5.00000E-01	5.00000E+00	5.95469D-01
1848	7.71484E-01	5.00000E-01	5.00000E+00	7.63867D-01
1849	8.82981E-01	5.00000E-01	5.00000E+00	4.92393D-01
1860	6.96603E-01	5.00000E-01	5.00000E+00	3.81880D-01

Table 7.36 Design Iteration History of AAW Model: Multidisciplinary Optimization (Static Aeroelasticity + Normal Modes), $M = 1.15$, by ZONA7 of ASTROS*

Iteration Number	Objective Function	Function Evaluation	Gradient Evaluation	Retained Constraints	Active Constraints	Approximate Convergence
1	5.86976E+02 (Initial Function Value)					
2	3.82909E+02	N/A FSD	N/A FSD	160	N/A FSD	not Converged
3	3.69848E+02	N/A FSD	N/A FSD	160	N/A FSD	not Converged
4	3.70292E+02	N/A FSD	N/A FSD	160	N/A FSD	not Converged
5	5.55220E+02	101	21	67	2	not Converged
6	5.51907E+02	49	8	33	3	not Converged
7	5.41261E+02	21	6	33	8	not Converged
8	5.35403E+02	25	5	33	8	not Converged
9	5.35410E+02	14	2	33	7	Converged

Final Objective Function Value is: Designed = 5.35410E+02

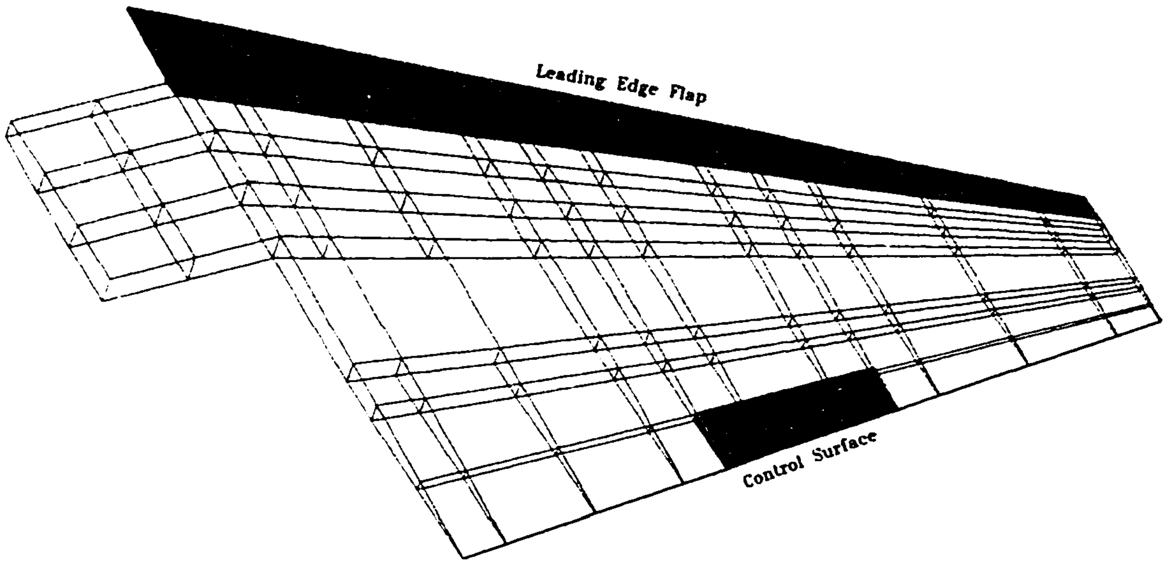

Figure 7.1 Structural Configuration of GAF Model by FEM

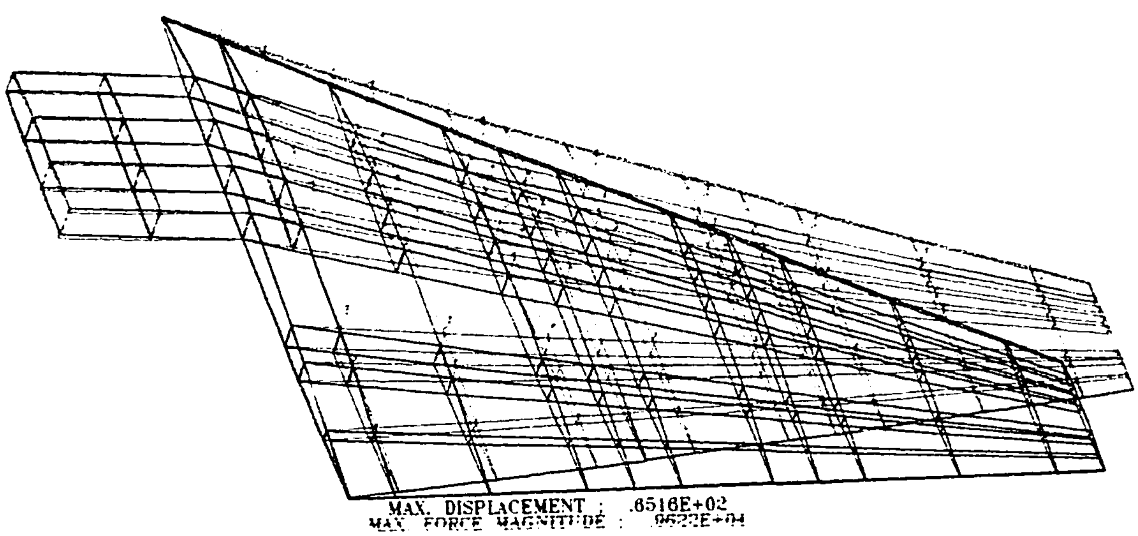

Figure 7.2 Deflection Shape of GAF Model for Static Loads

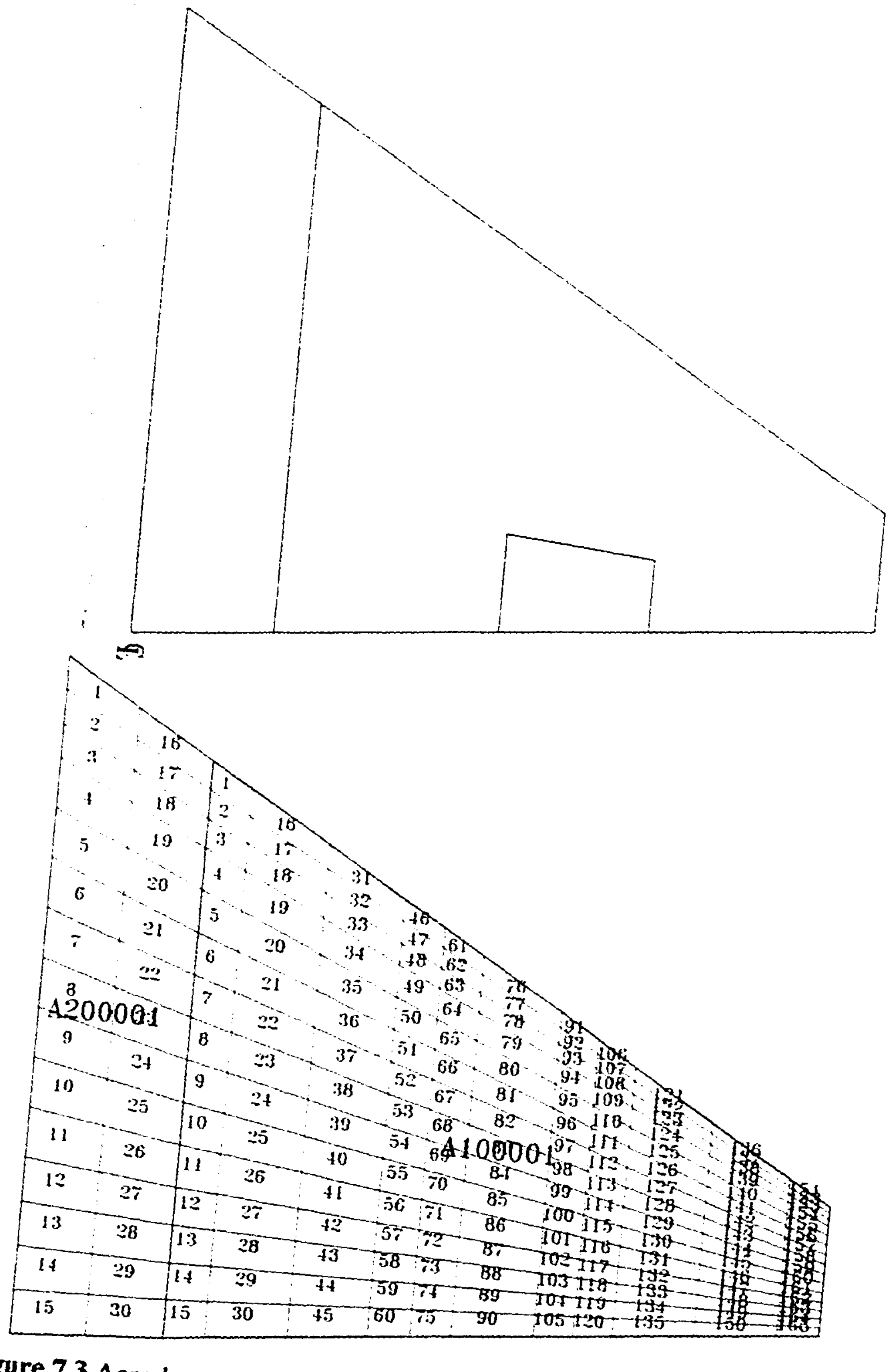

Figure 7.3 Aerodynamic Configuration of GAF Model and Aerodynamic Panels

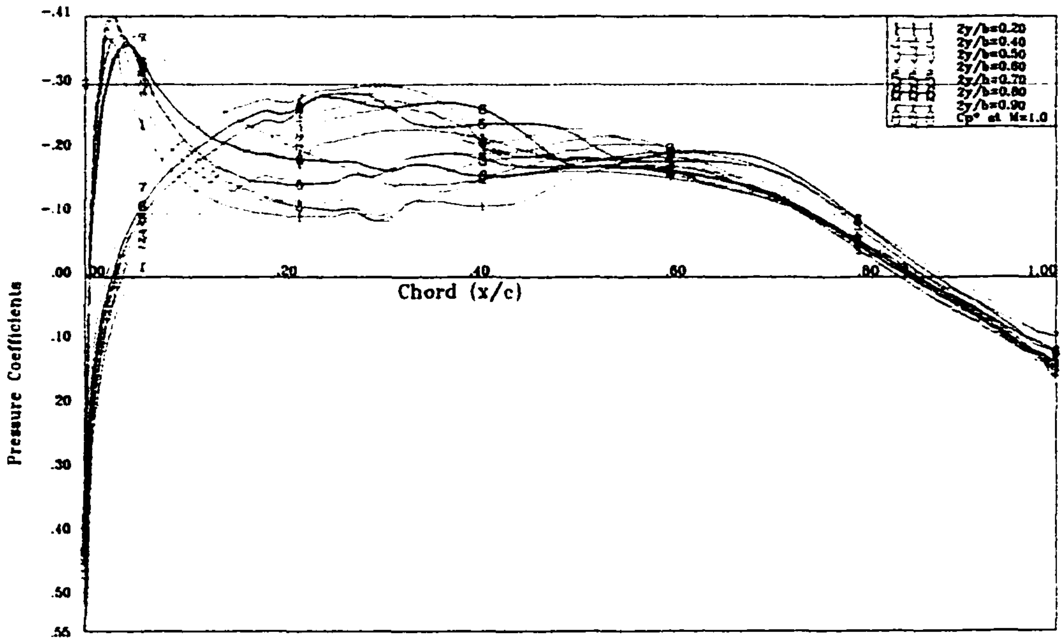

Figure 7.4a Aerodynamic Pressure Coefficients of GAF Model for Navier-Stokes Flow: $M = 0.85$, AoA = 0.0°, by ENSAERO

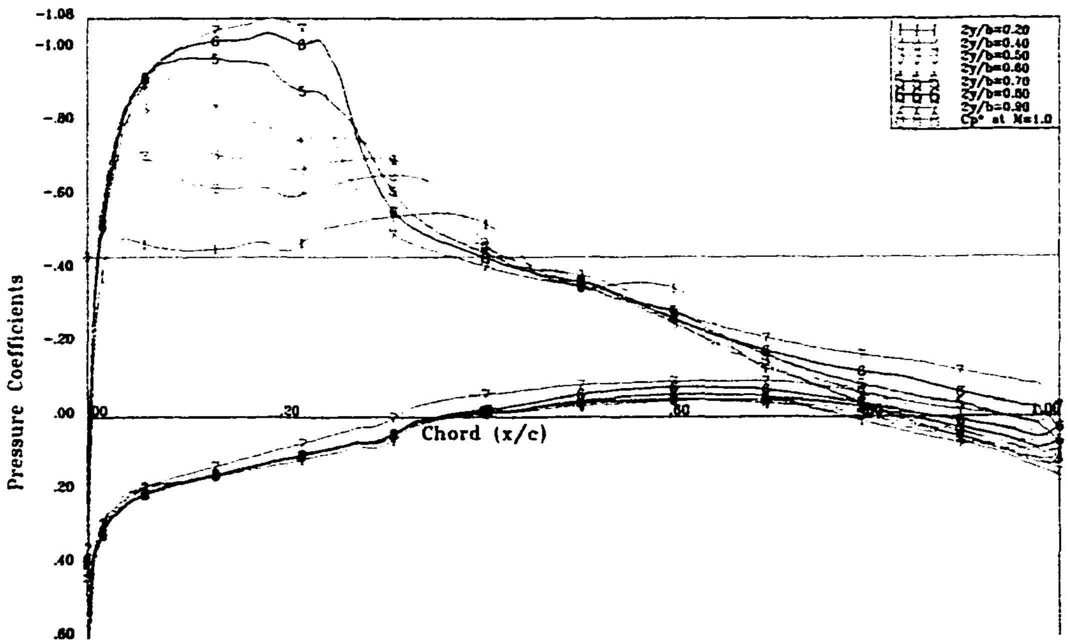

Figure 7.4b Aerodynamic Pressure Coefficients of GAF Model for Navier-Stokes Flow: $M = 0.85$, AoA = 5.0°, by ENSAERO

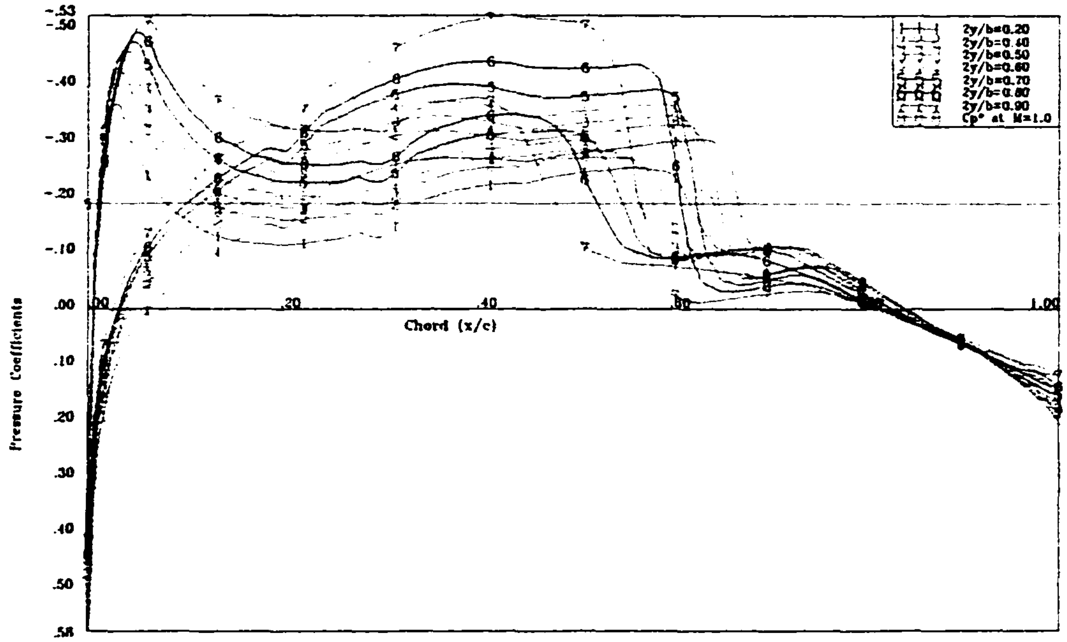

Figure 7.4c Aerodynamic Pressure Coefficients of GAF Model for Navier-Stokes Flow: $M = 0.90$, AoA = 0.0°, by ENSAERO

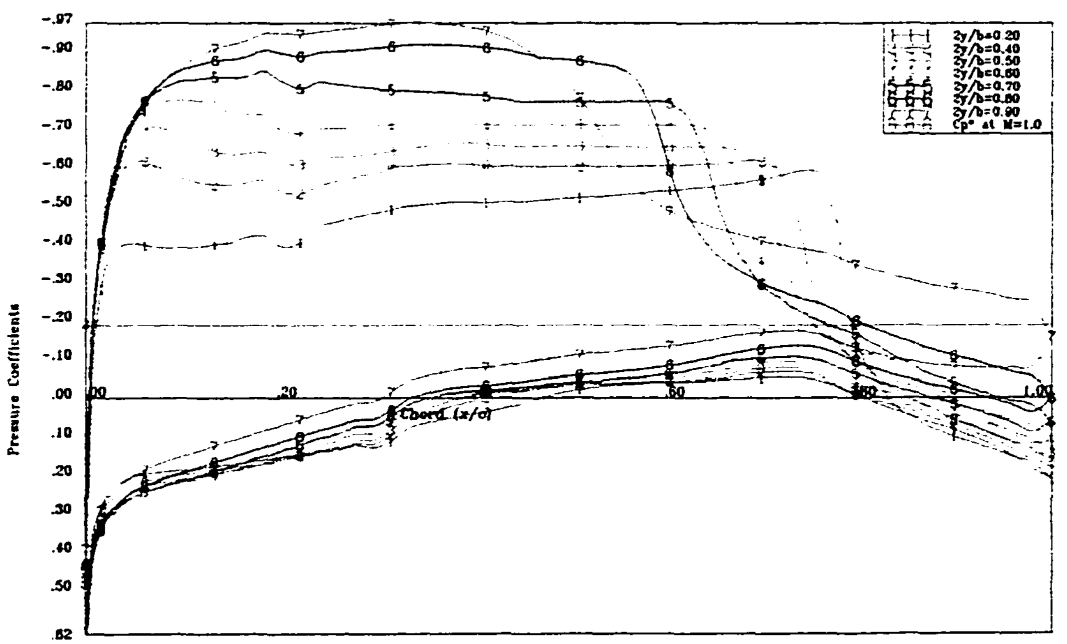

Figure 7.4d Aerodynamic Pressure Coefficients of GAF Model for Navier-Stokes Flow: $M = 0.90$, AoA = 5.0°, by ENSAERO

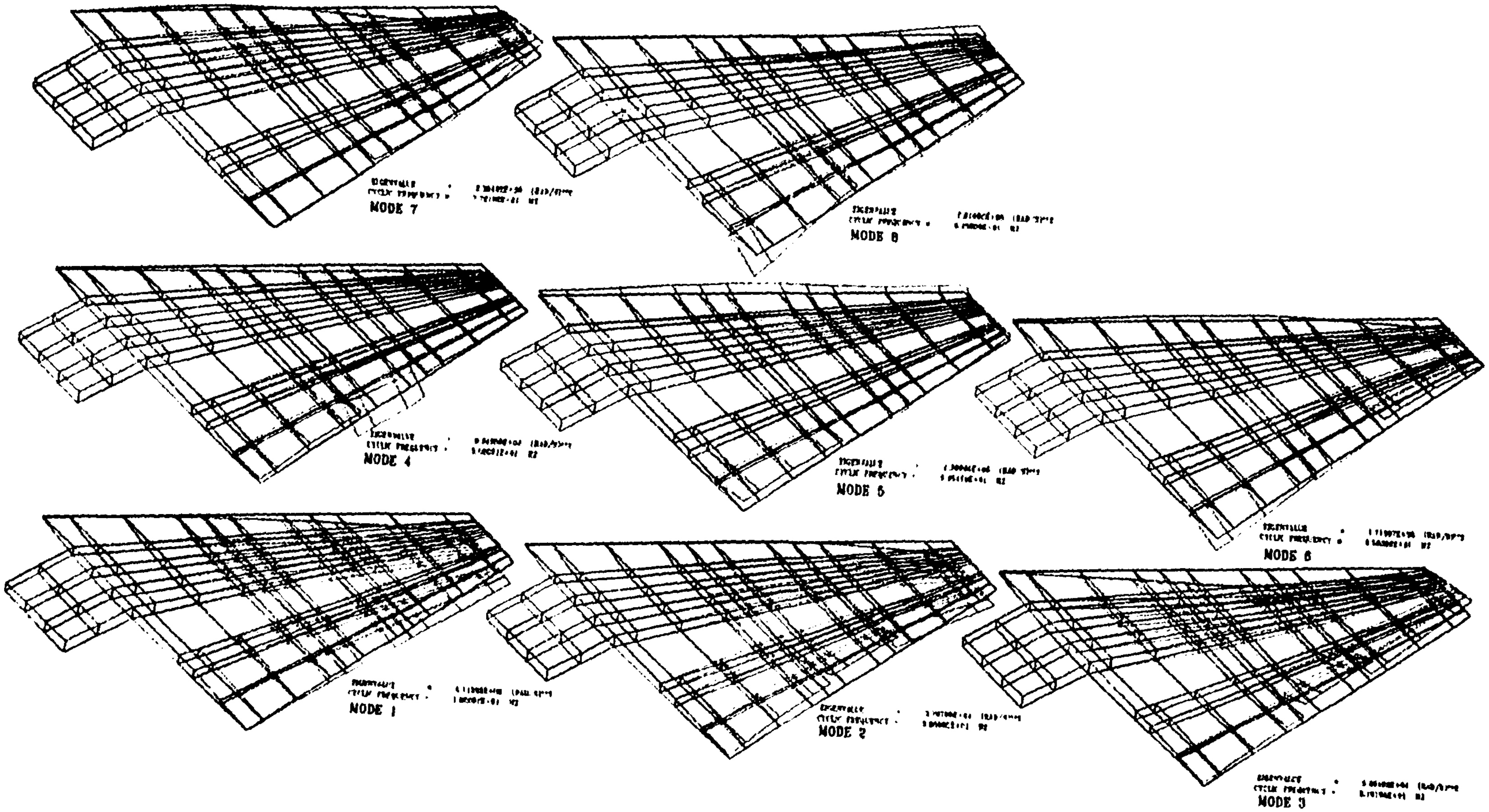

Figure 7.5 Normal Modes of GAF Model

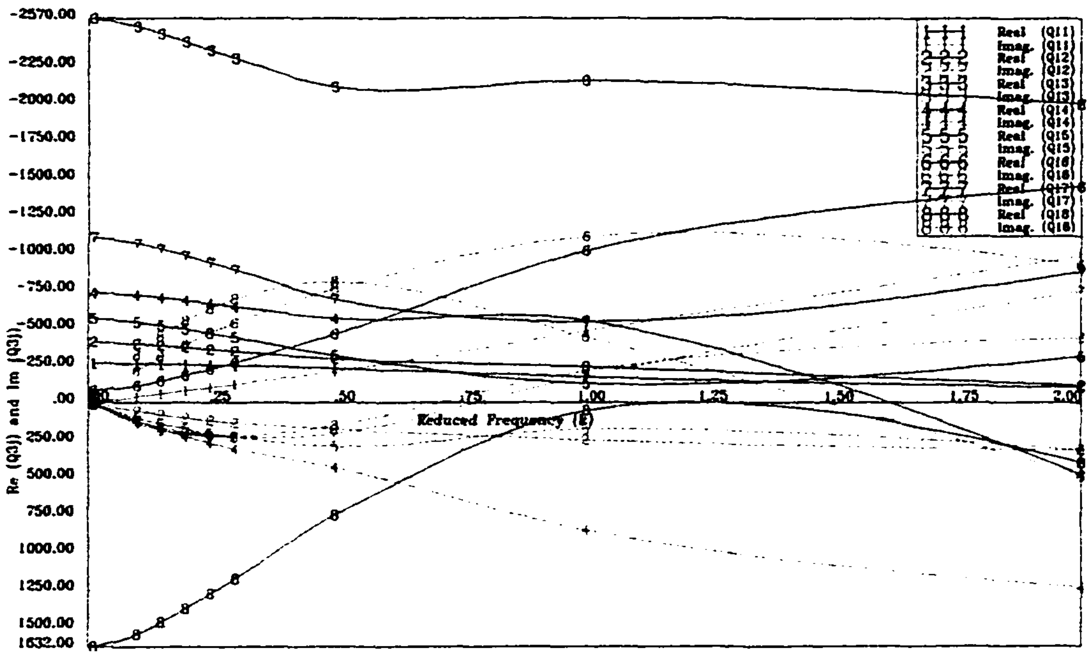

Figure 7.6a Generalized Unsteady Aerodynamic Coefficients Q_{1j} of GAF Model: $M = 8.5$, by ZONA6 of ASTROS*

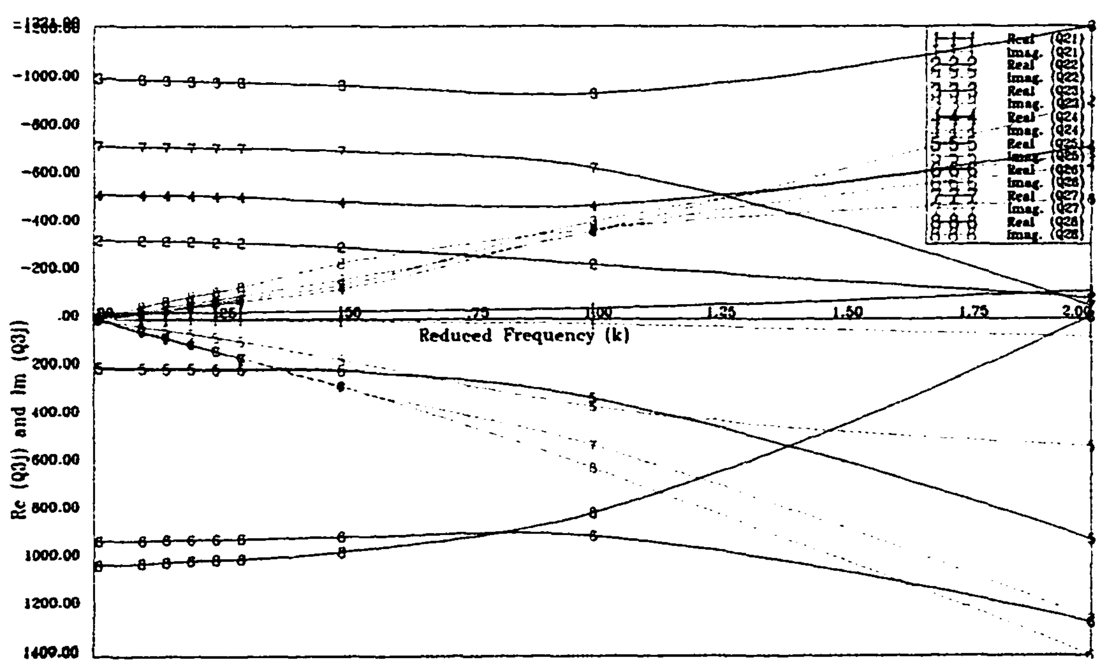

Figure 7.6b Generalized Unsteady Aerodynamic Coefficients Q_{2j} of GAF Model: $M = 8.5$, by ZONA6 of ASTROS*

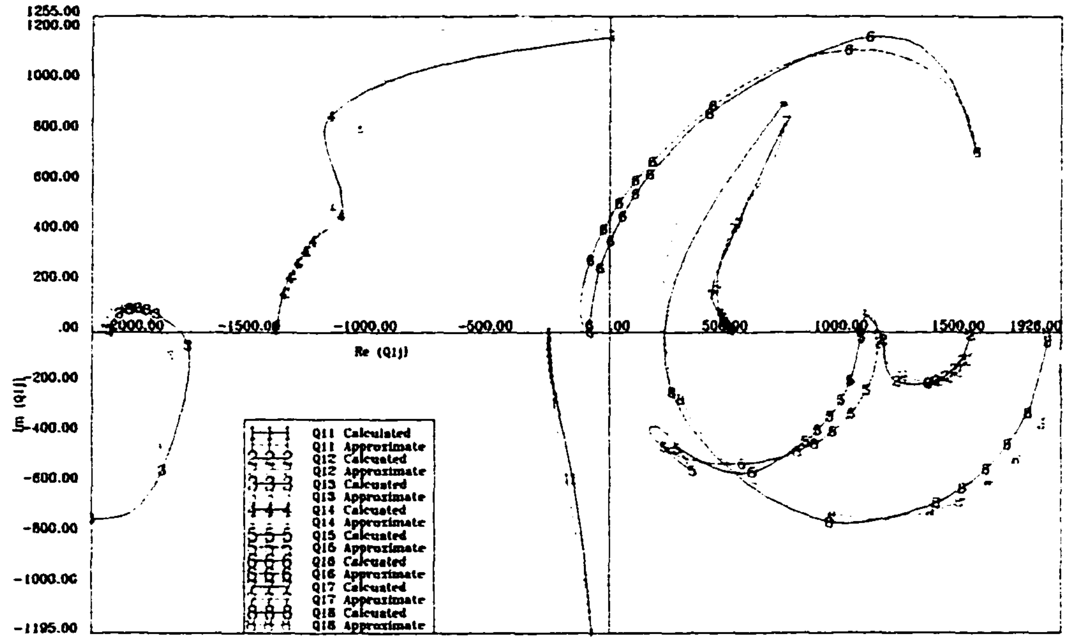

Figure 7.7a Generalized Unsteady Aerodynamic Coefficients Q_{1j} of GAF Model: $M = 8.5$, by ZONA6 of ASTROS* and Approximated by Minimum-State Method

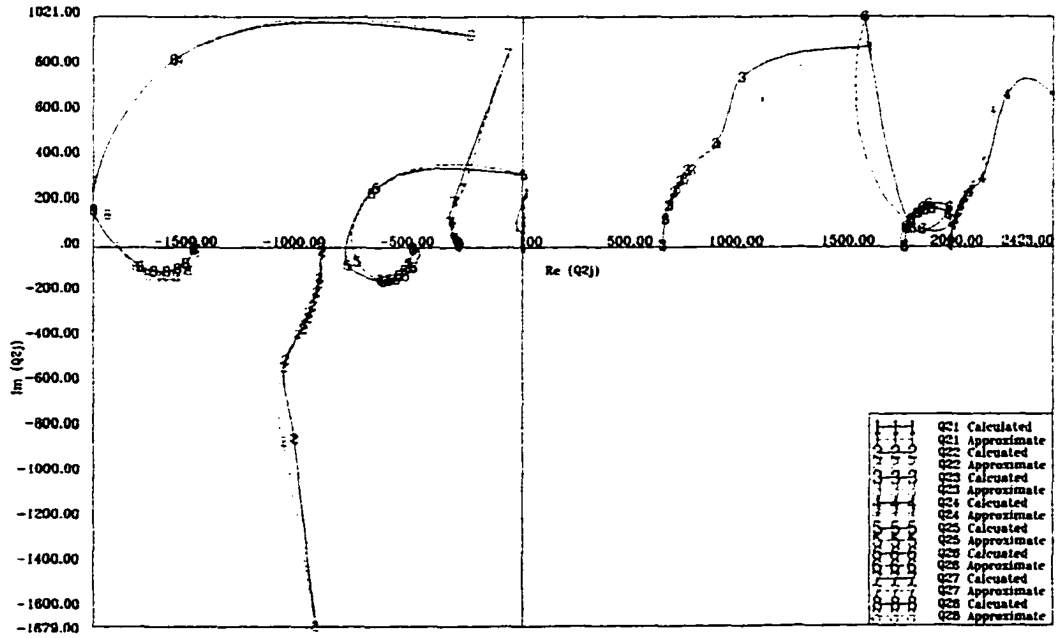

Figure 7.7b Generalized Unsteady Aerodynamic Coefficients Q_{2j} of GAF Model: $M = 8.5$, by ZONA6 of ASTROS* and Approximated by Minimum-State Method

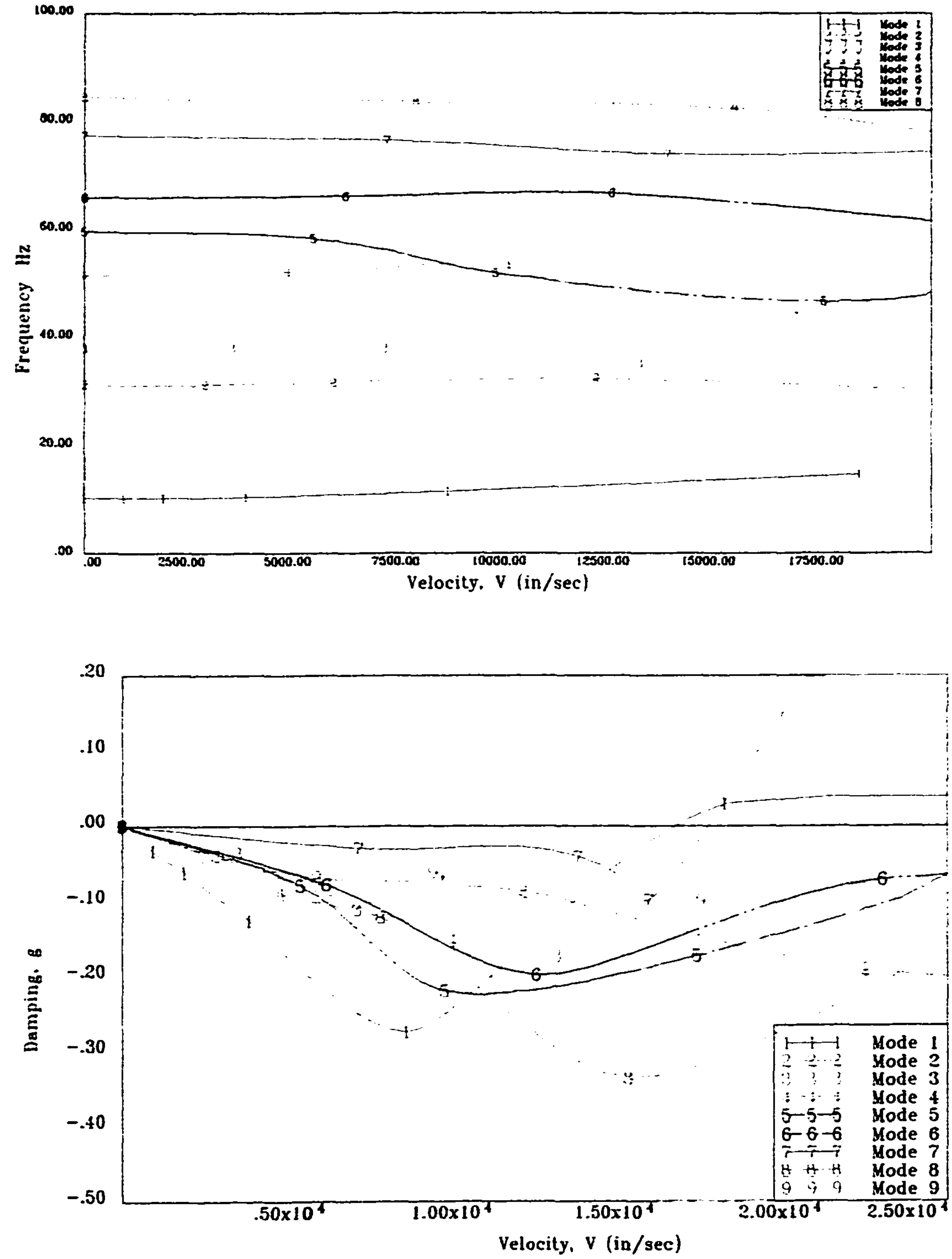

Figure 7.8 V-f and V-g Plots of GAF Model: $M = 0.85$, by ZONA6 of ASTROS*
(Flutter Speed = 17,337 *in/sec*, Flutter Frequency = 14.3 *Hz.*)

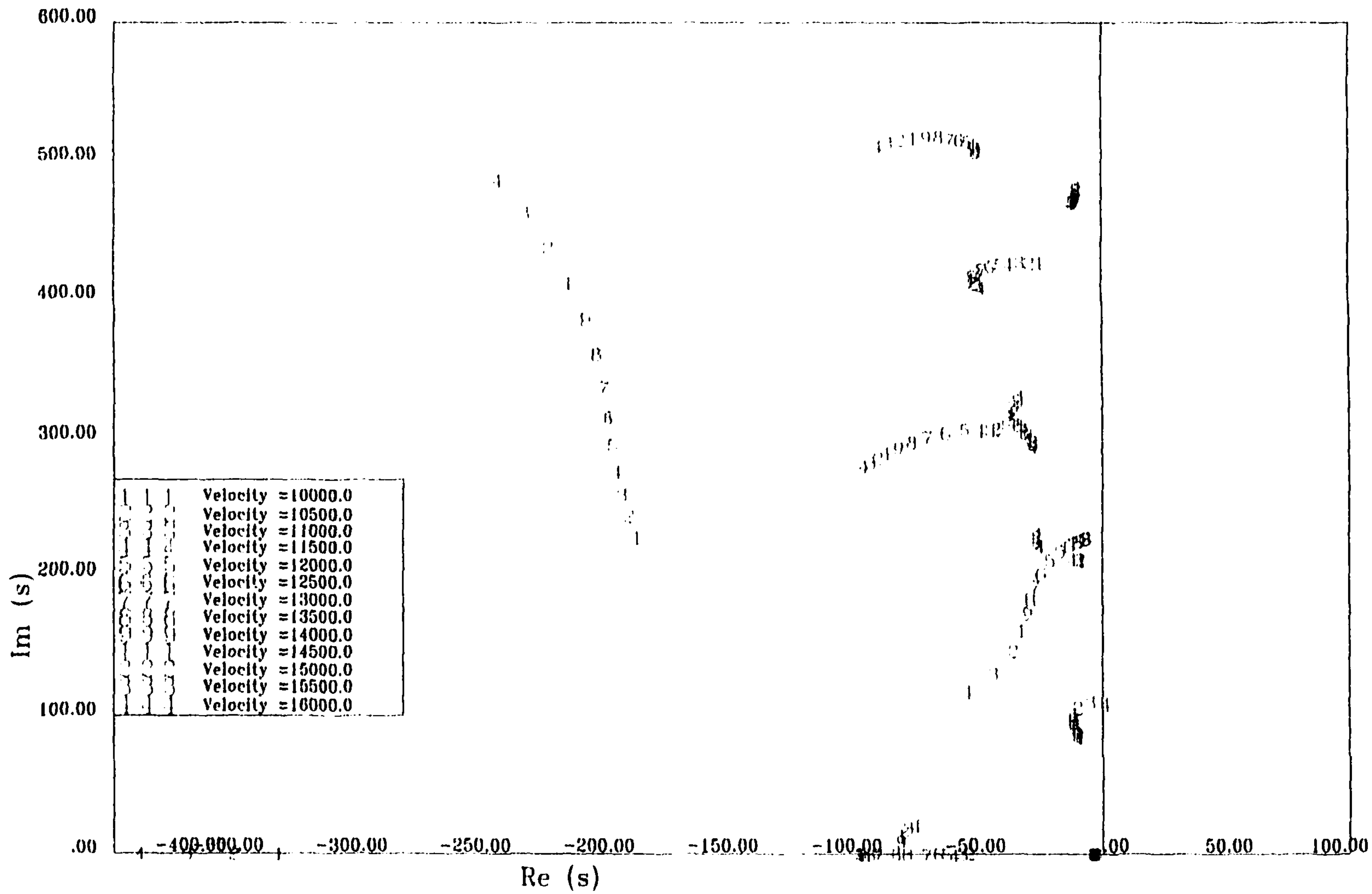

Figure 7.9 Root-locus Plot of GAF Model; M= 0.85, ZONA6 of ASTROS' (Flutter Speed = 15,888 in/sec, Flutter Frequency = 17.3 Hz.)

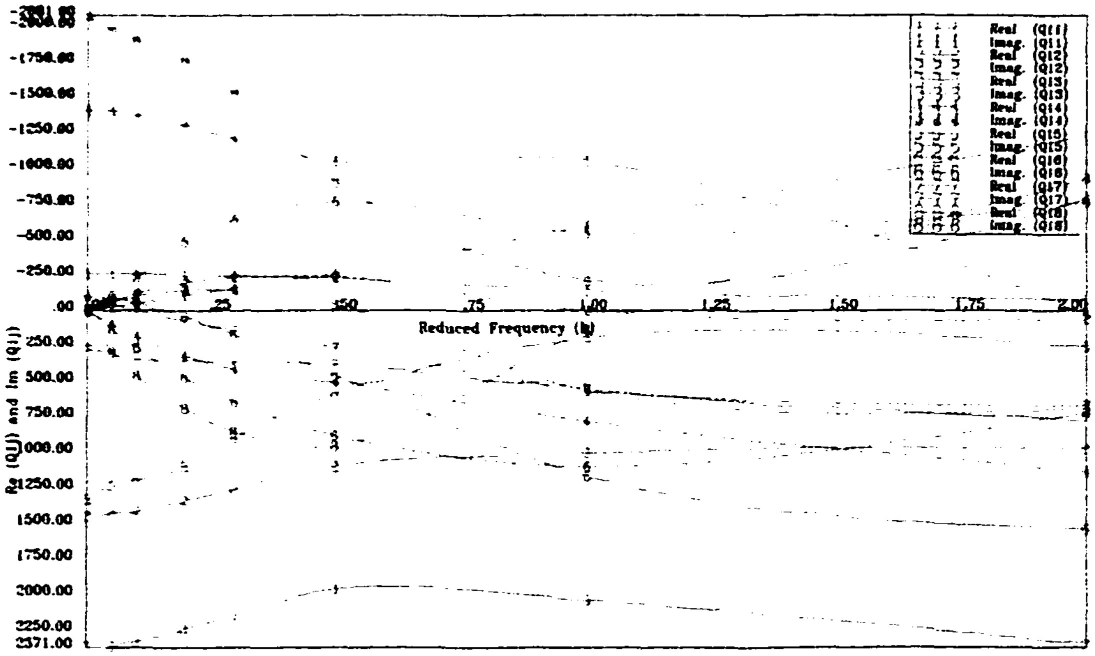

Figure 7.10a Generalized Unsteady Aerodynamic Coefficients Q_{1j} of GAF Model: $M = 0.85$, by ZTAIC of ASTROS*

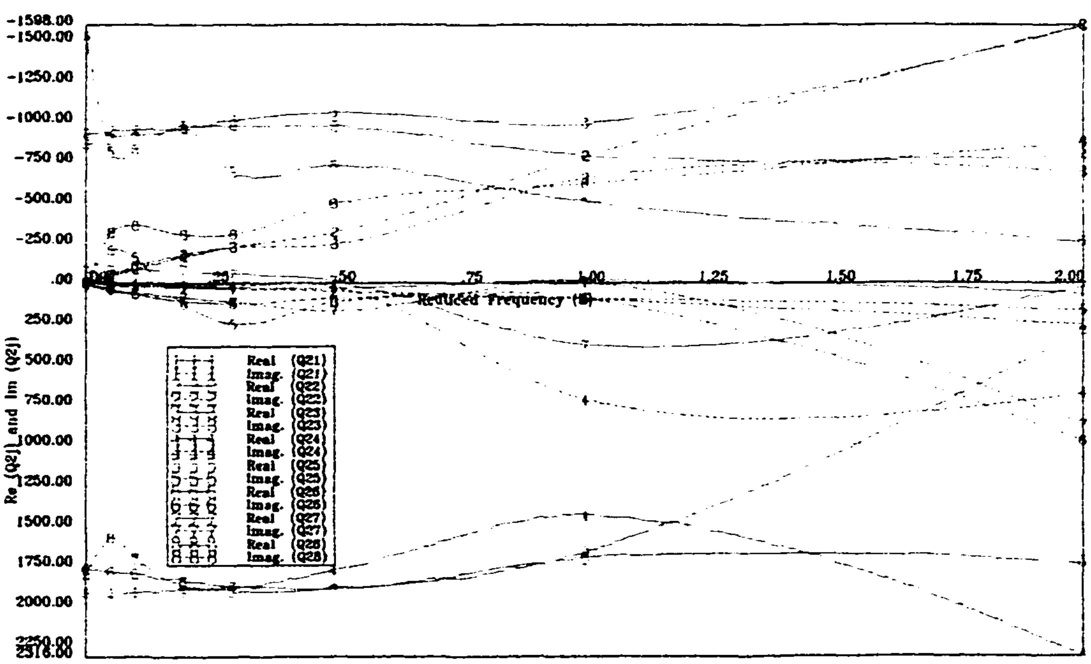

Figure 7.10b Generalized Unsteady Aerodynamic Coefficients Q_{2j} of GAF Model: $M = 0.85$, by ZTAIC of ASTROS*

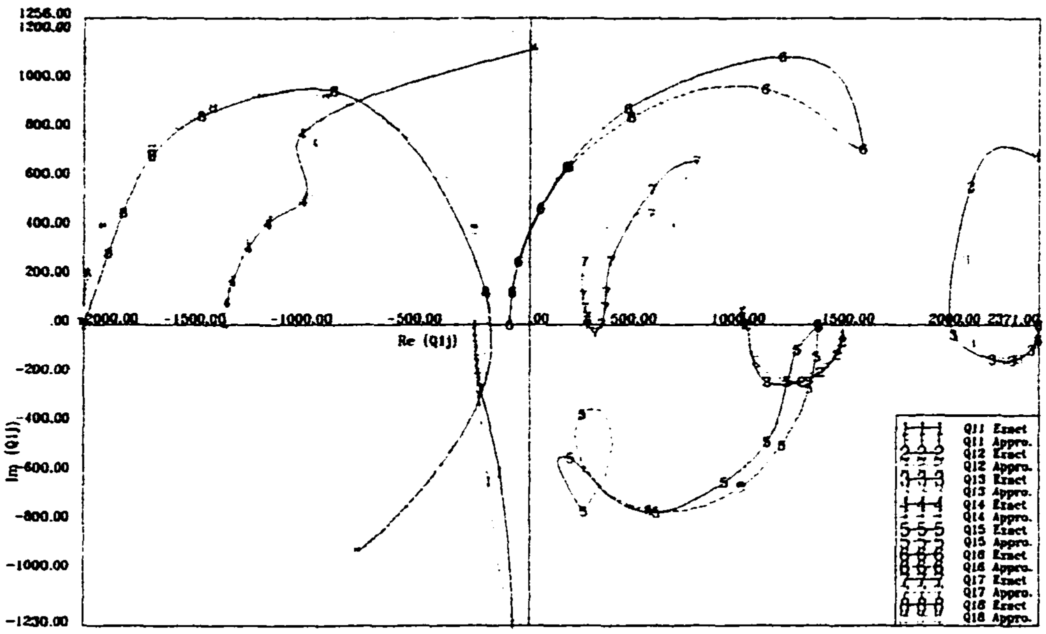

Figure 7.11a Generalized Unsteady Aerodynamic Coefficients Q_{1j} of GAF Model: $M = 0.85$, by ZTAIC of ASTROS* and Approximated by Minimum-State Method

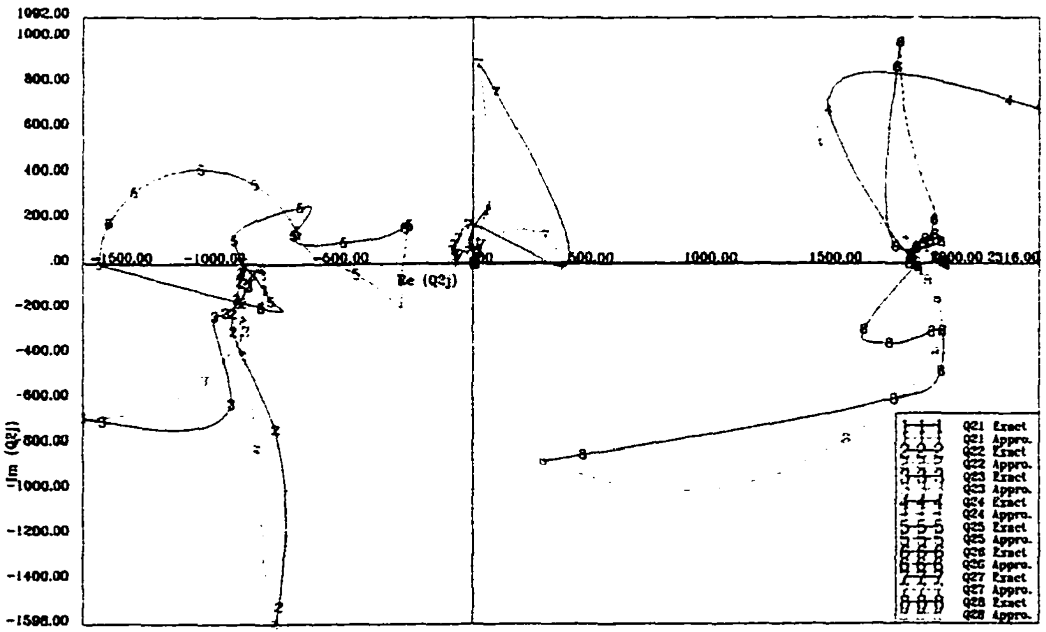

Figure 7.11b Generalized Unsteady Aerodynamic Coefficients Q_{2j} of GAF Model: $M = 0.85$, by ZTAIC of ASTROS* and Approximated by Minimum-State Method

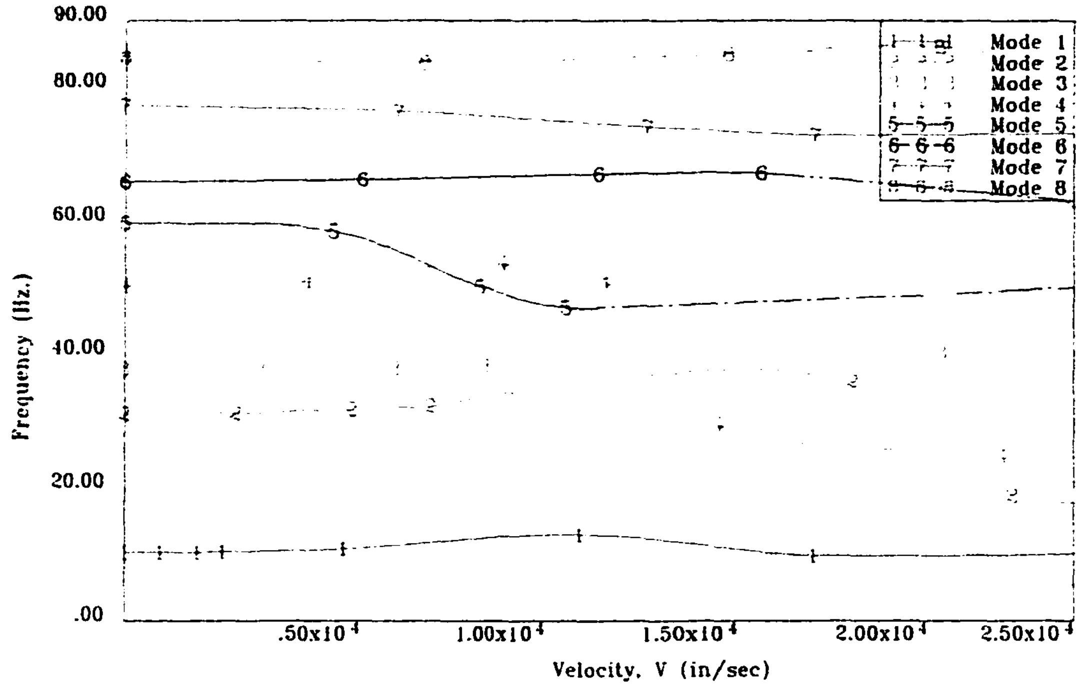

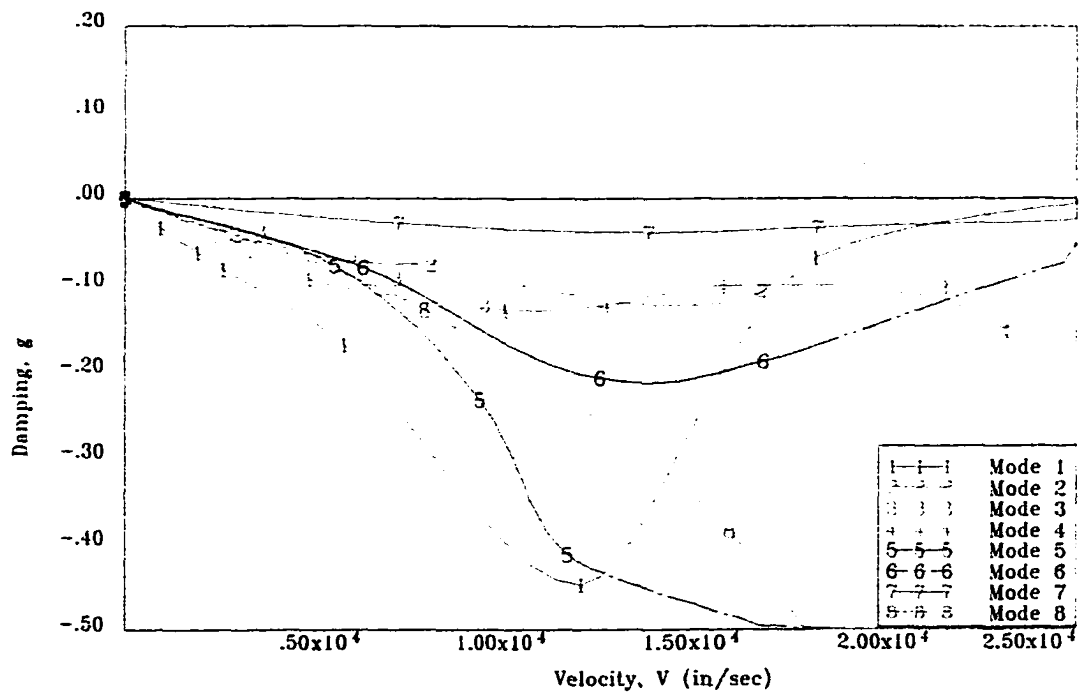

Figure 7.12 V-f and V-g Plots of GAF Model: $M = 0.85$, by ZTAIC of ASTROS*
(Flutter Speed = 18,172 *in/sec*, Flutter Frequency = 18.1 *Hz.*)

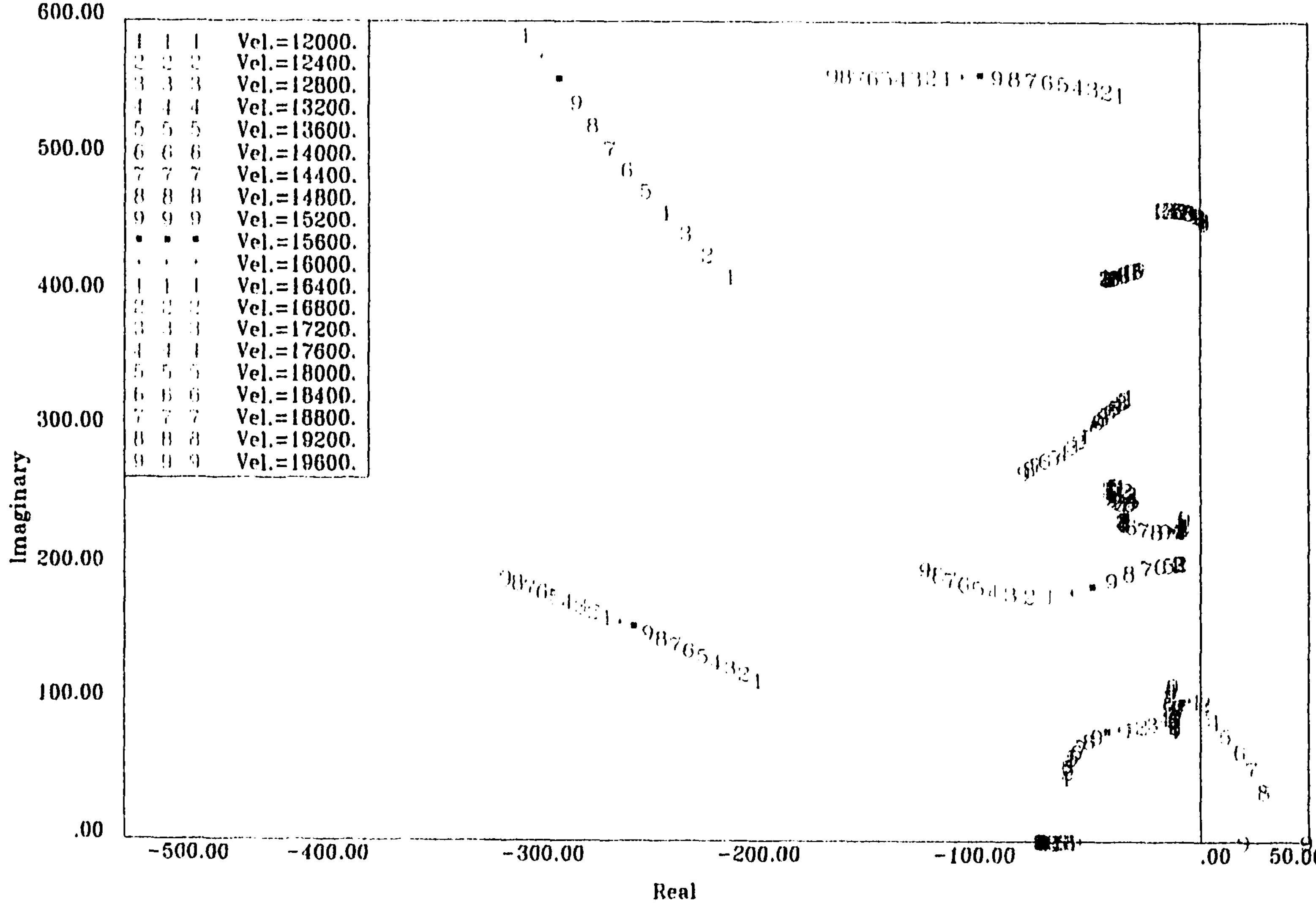

Figure 7.13 Root-Locus Plot of GAF Model: M = 0.85, by ZTAIC of ASTROS*
(Flutter Speed = 16,581 in/sec, Flutter Frequency = 15.6 Hz.)

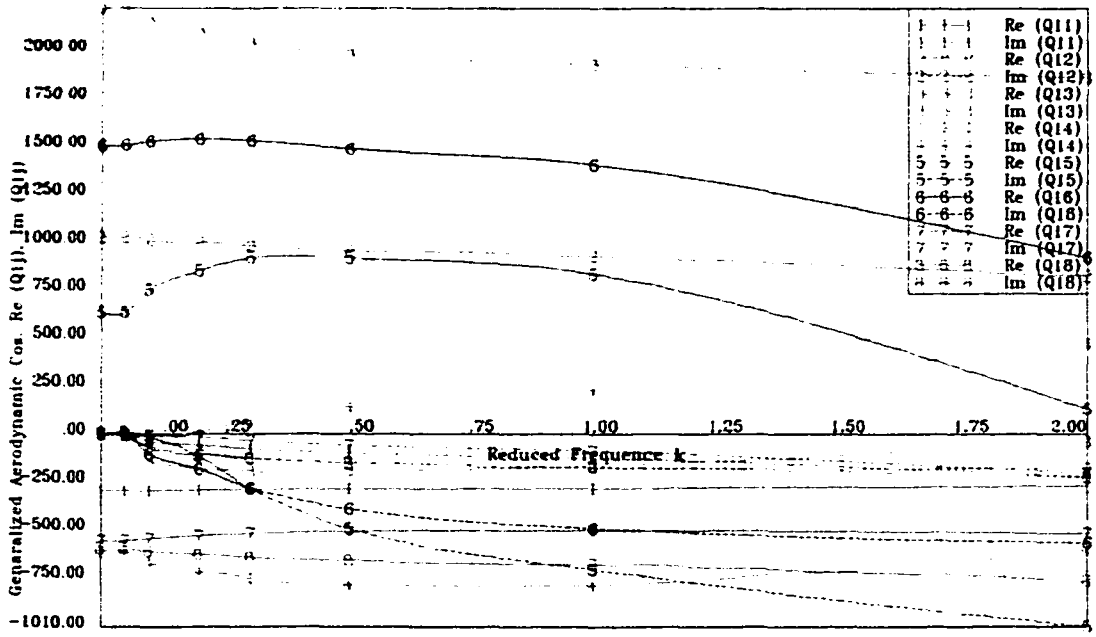

Figure 7.14 Generalized Unsteady Aerodynamic Coefficients Q_{1j} of GAF Model: $M = 1.15$, by ZONA7 of ASTROS*

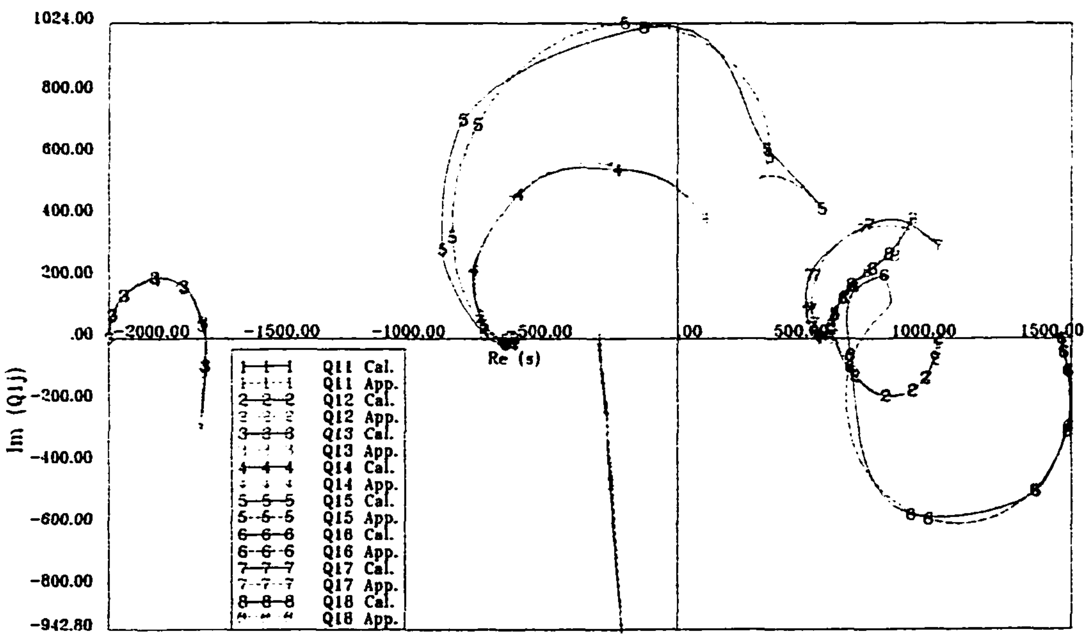

Figure 7.15 Generalized Unsteady Aerodynamic Coefficients Q_{1j} of GAF Model: $M = 1.15$, by ZONA7 of ASTROS* and Approximated by Minimum-State Method

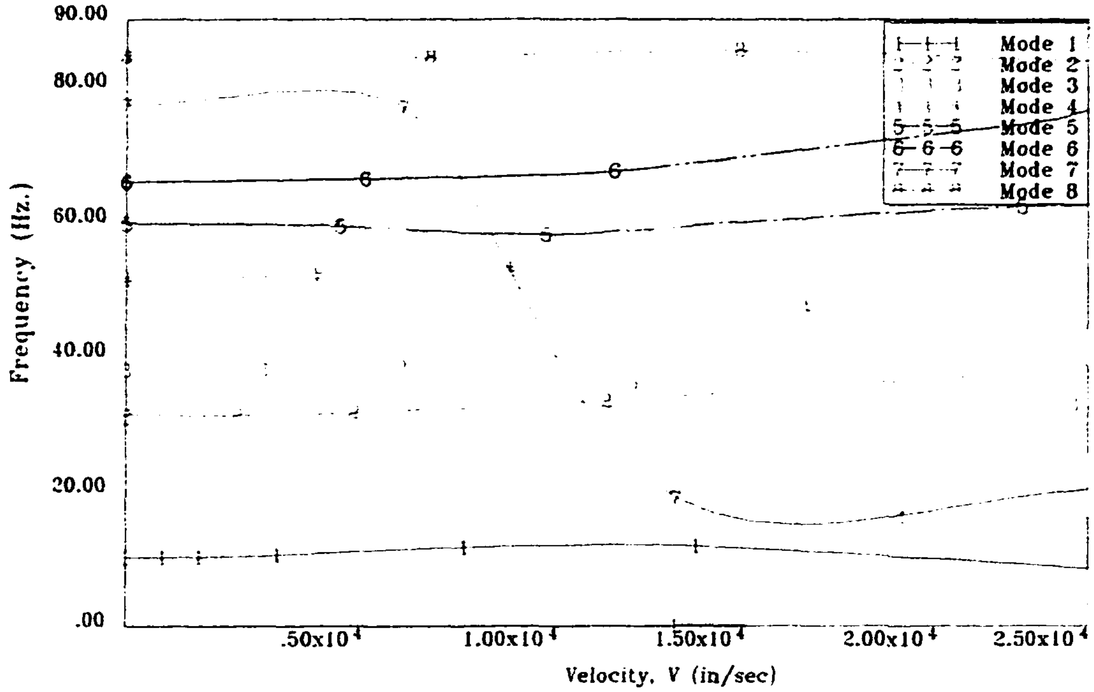

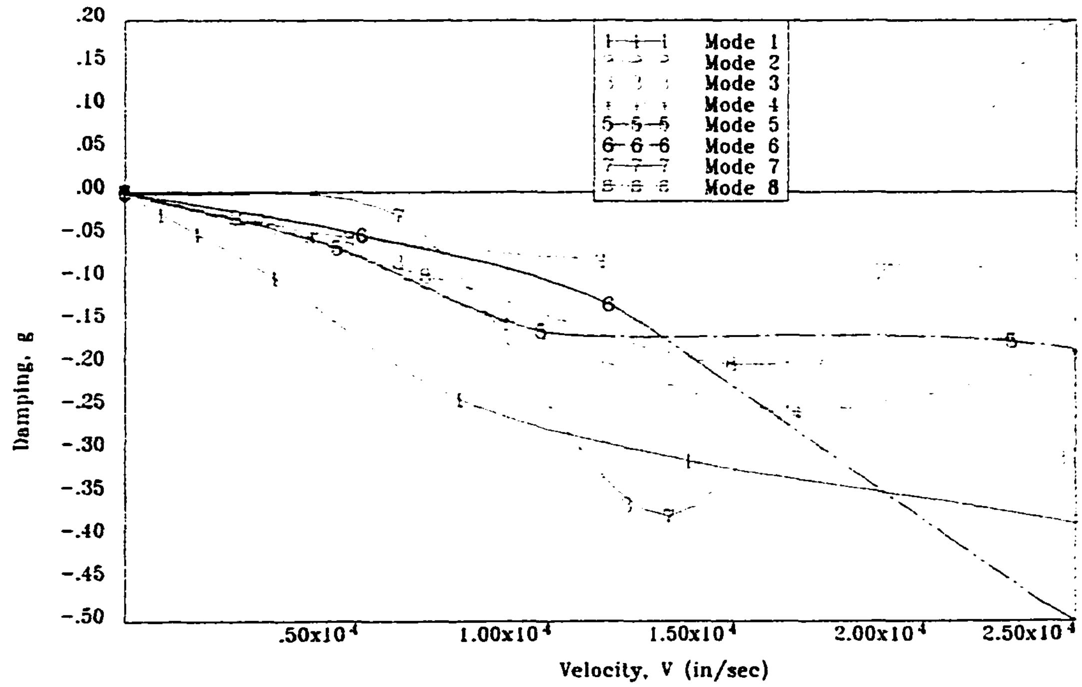

Figure 7.16 V-f and V-g Plots of GAF Model: $M = 1.15$, by ZONA7 of ASTROS*
(Flutter Speed = 20,776 *in/sec*, Flutter Frequency = 19.8 *Hz.*)

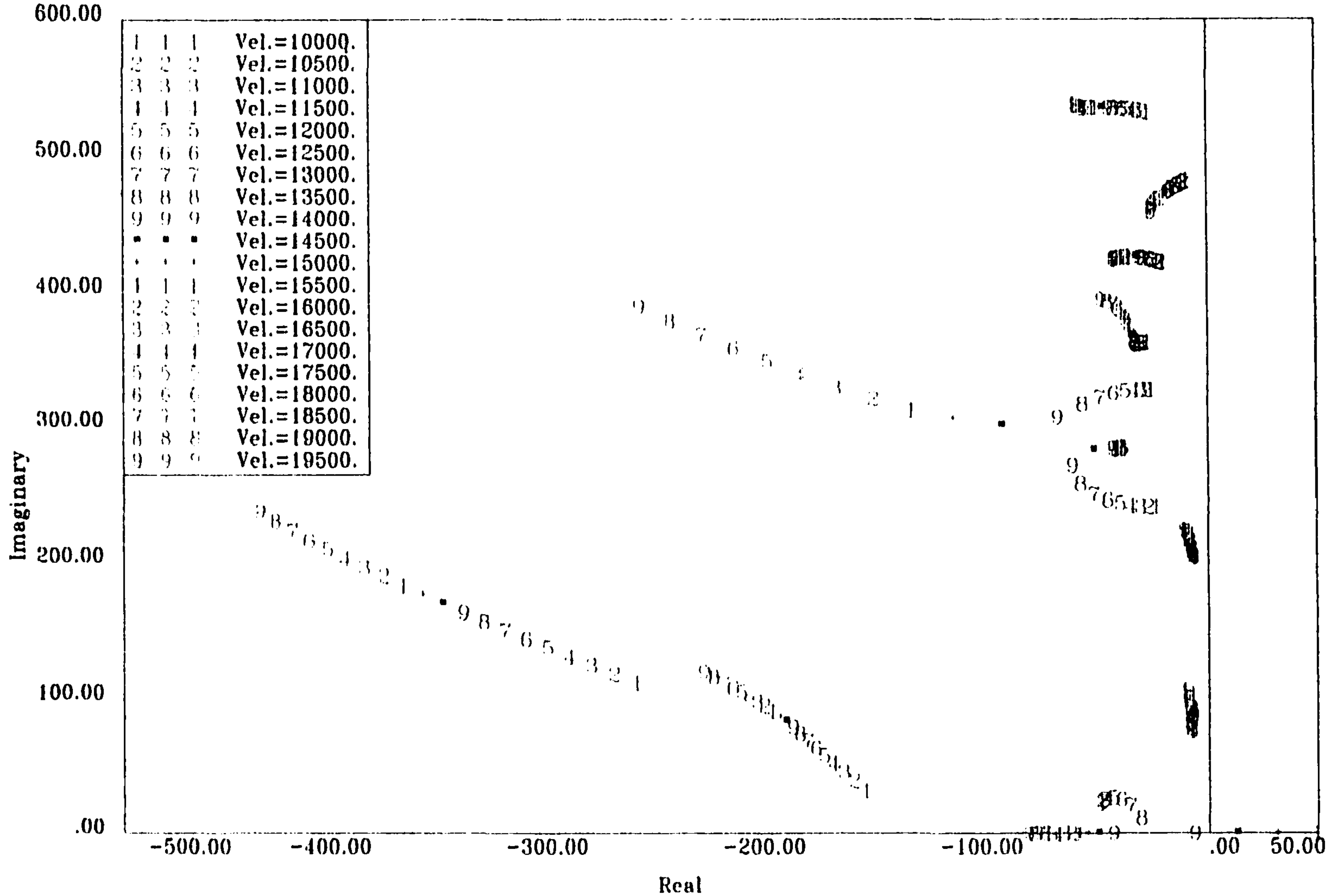

Figure 7.17 Root-Locus Plot of GAF Model: M = 1.15, by ZONA7 of ASTROS*
(Divergence Speed = 14,170 in/sec)

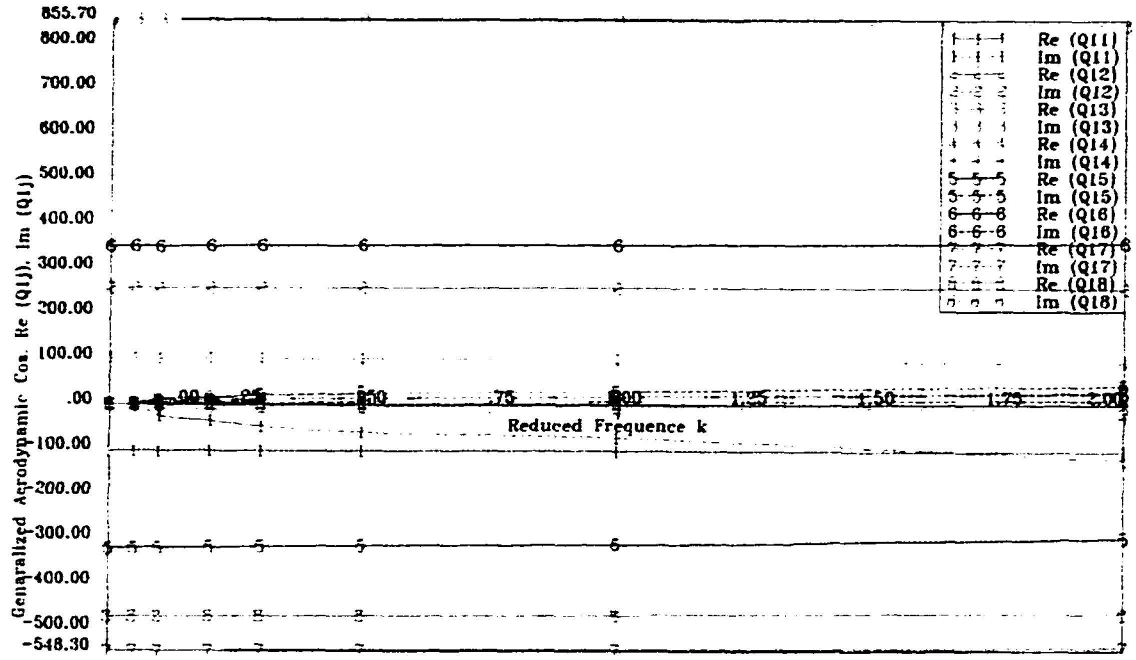

Figure 7.18 Generalized Unsteady Aerodynamic Coefficients Q_{1j} of GAF Model: $M = 3.0$, by ZONA7U of ASTROS*

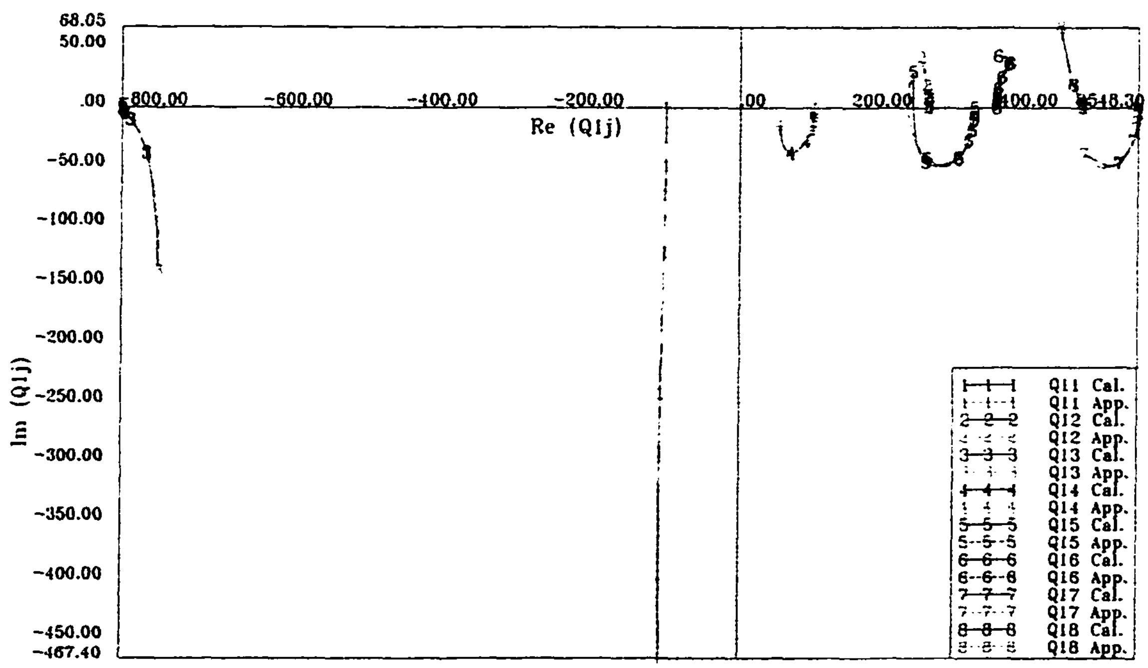

Figure 7.19 Generalized Unsteady Aerodynamic Coefficients Q_{1j} of GAF Model: $M = 3.0$, by ZONA7U of ASTROS* and Approximated by Minimum-State Method

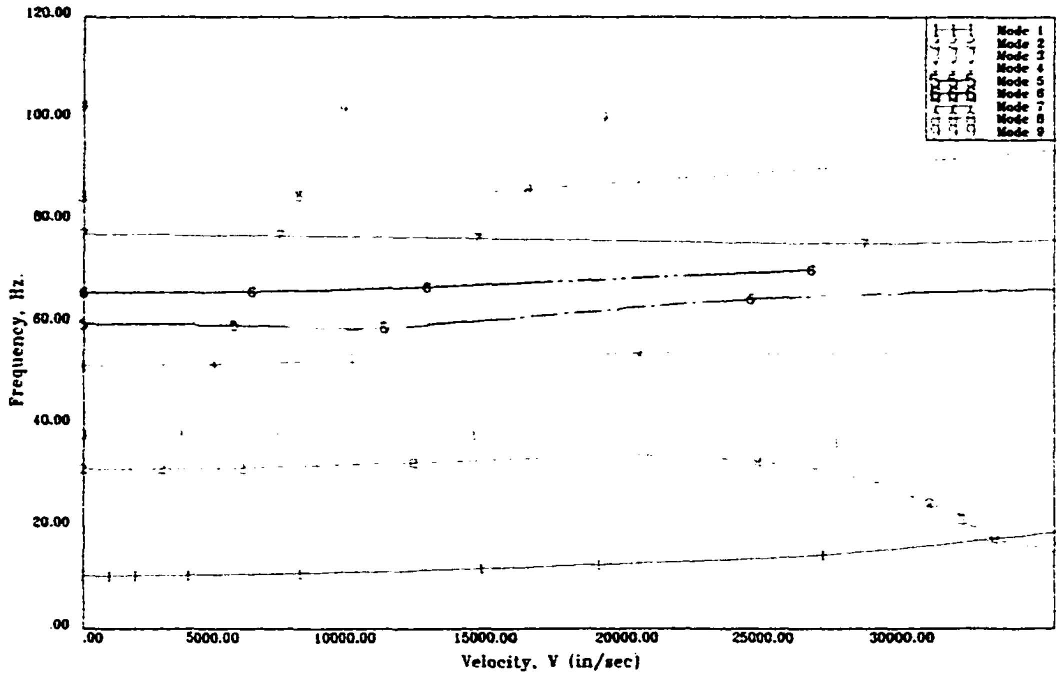

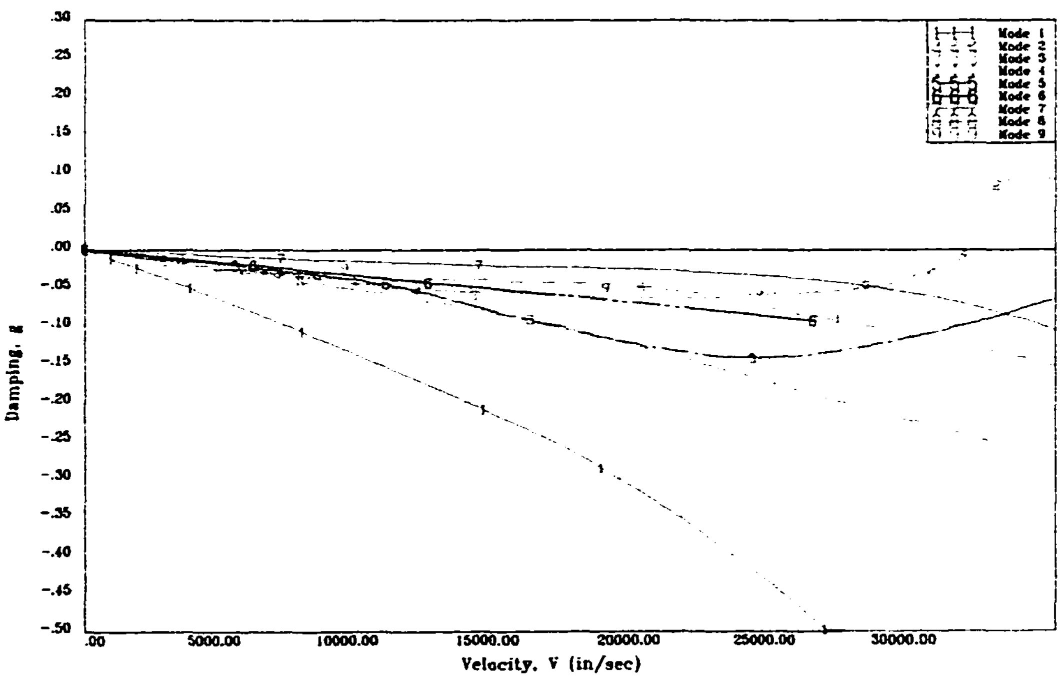

Figure 7.20 V-f and V-g Plots of GAF Model: $M = 3.0$, by ZONA7U of ASTROS*
(Flutter Speed = 31,743 *in/sec*, Flutter Frequency = 21.1 *Hz.*)

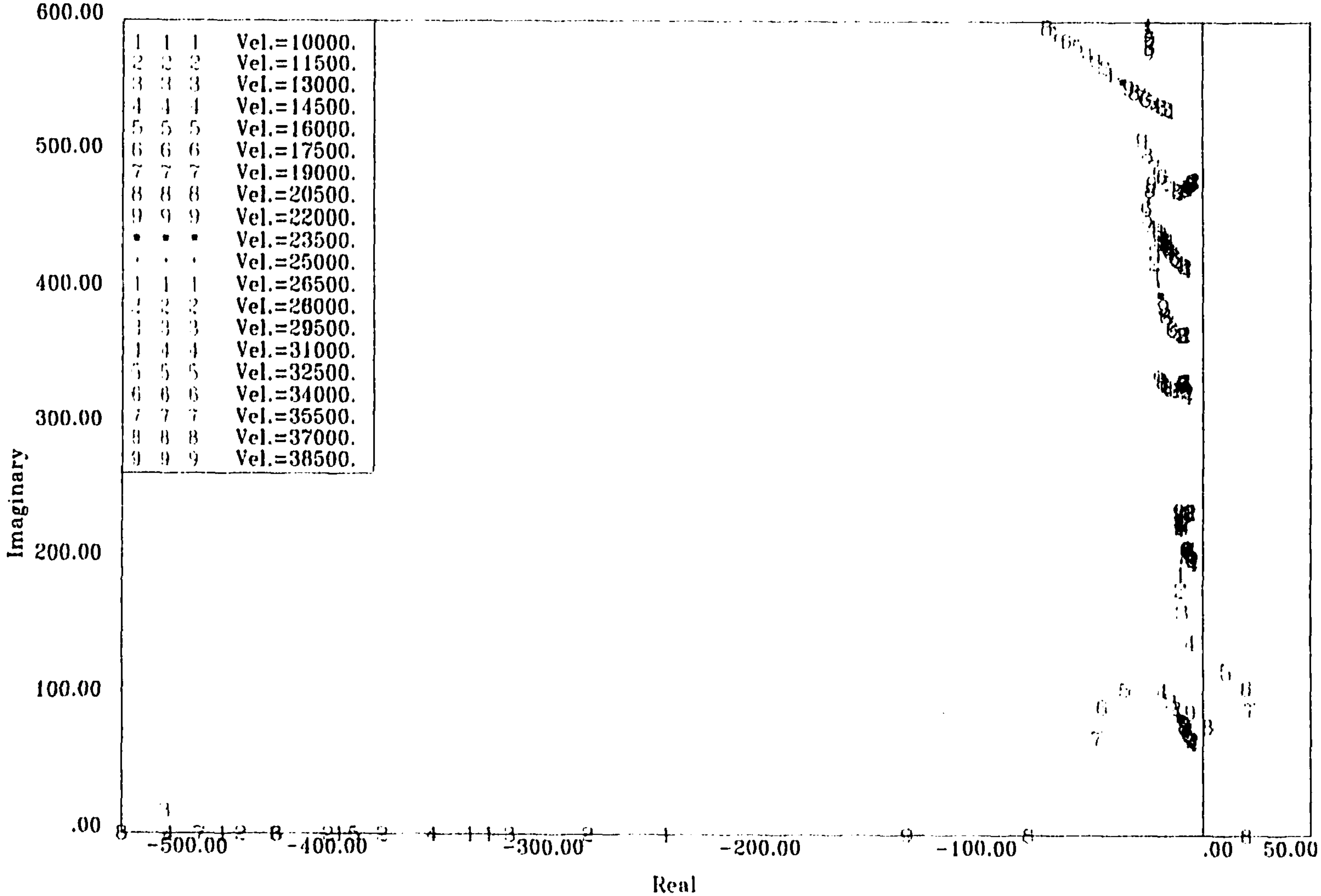

Figure 7.21 Root-Locus Plot of GAF Model: M = 3.0, by ZONA7U of ASTROS*
(Flutter Speed = 33,536 in/sec, Flutter Frequency = 21.3Hz.)

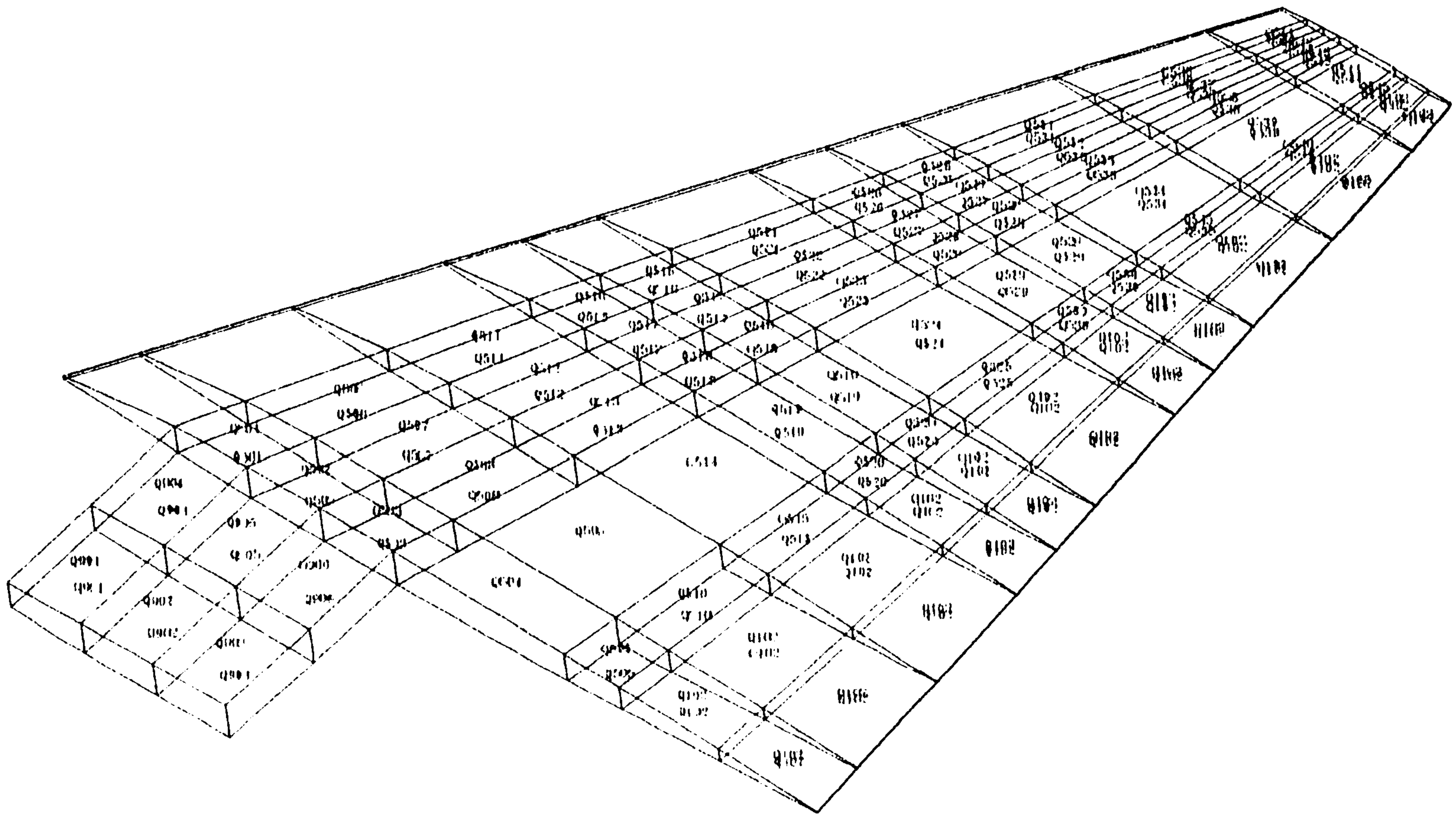

Figure 7.22 Design Variables and Numbering of GAF Model

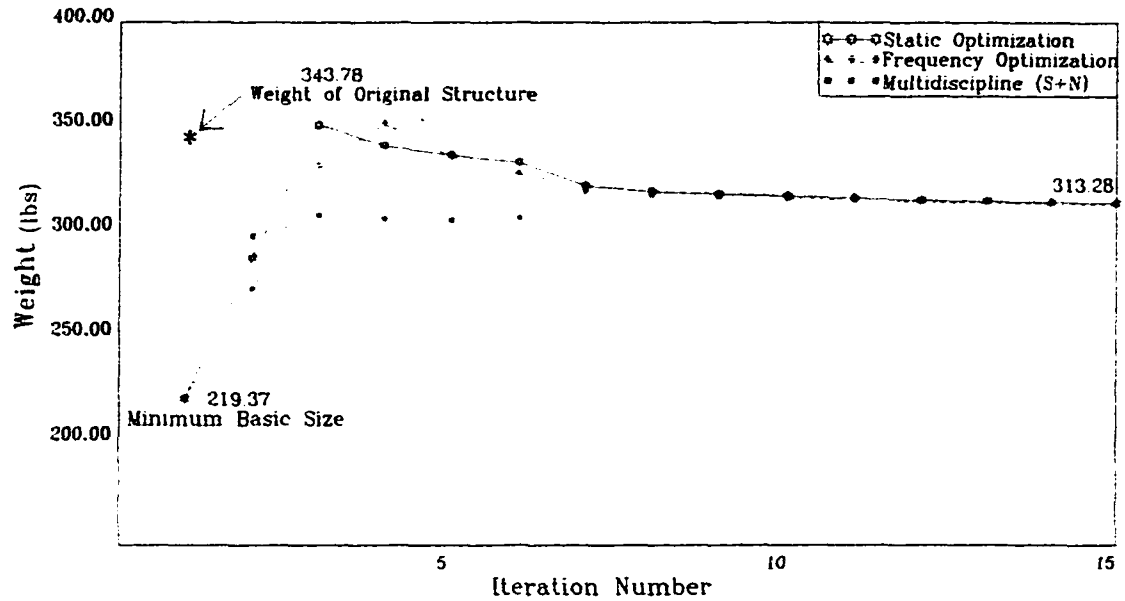

Figure 7.23 Iteration History of Structural Design Optimization of GAF Model: Statics, Normal Modes, and Both Disciplines (S + N) by ASTROS*

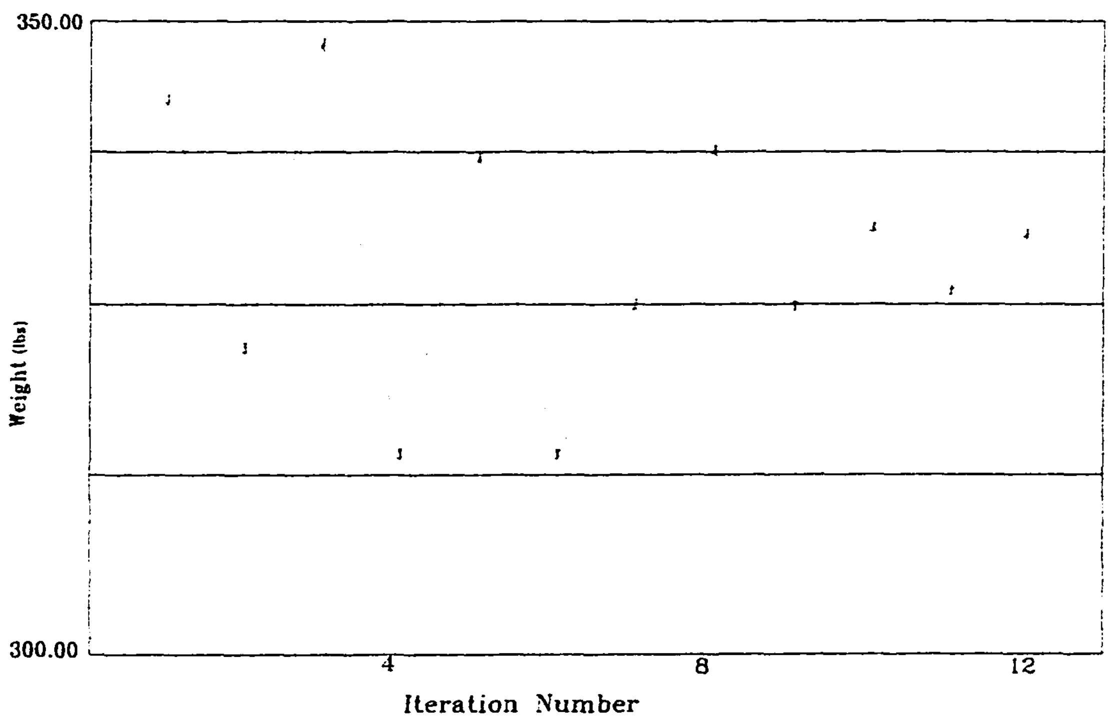

Figure 7.24 Iteration History of Structural Design Optimization of GAF Model: Flutter Discipline at $M = 0.85$, by Root-Locus Method

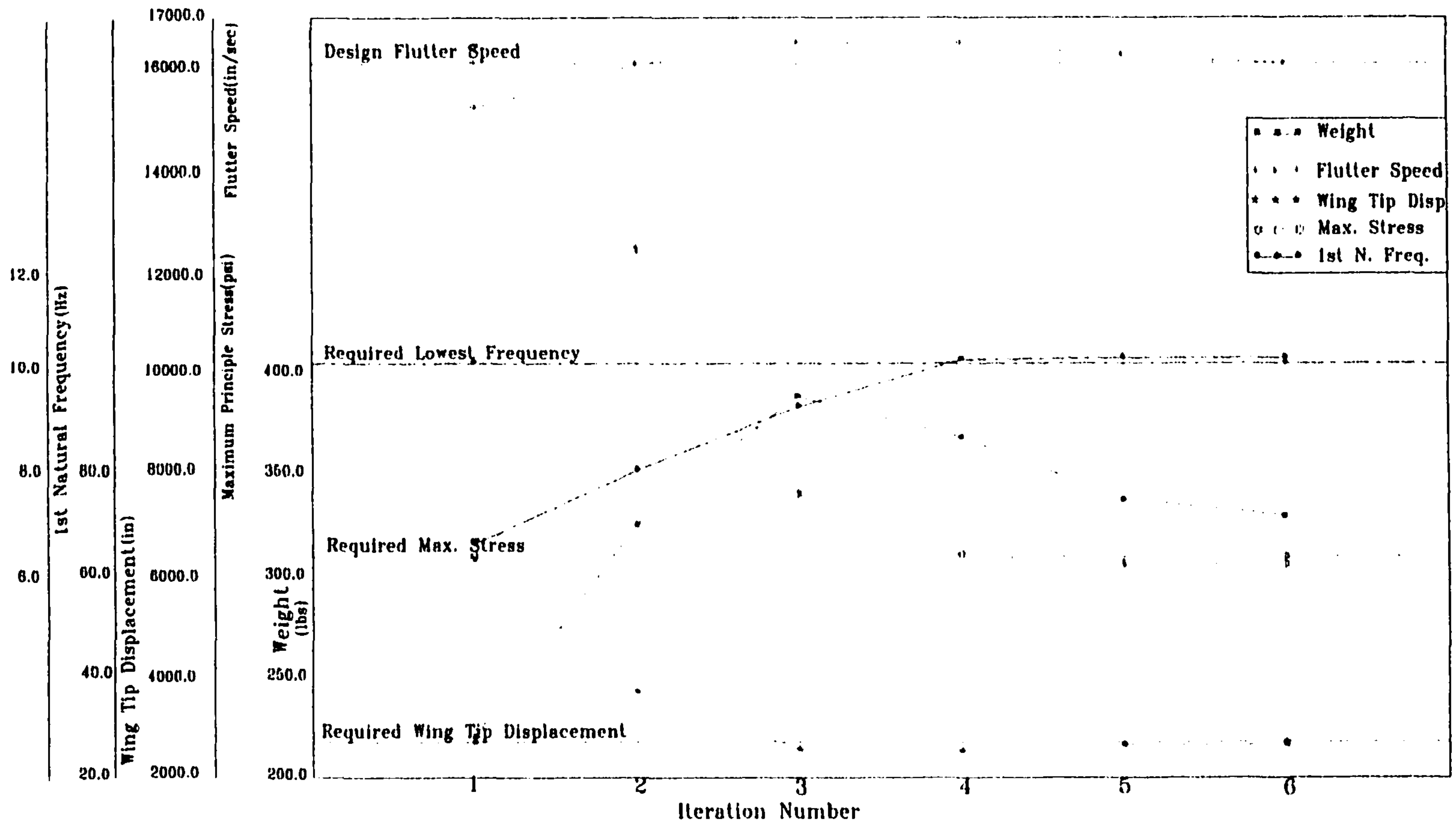

Figure 7.25 Design Iteration History of GAF: Multidisciplinary Design Optimization (With Constraints on Stress, Displacement, Natural Frequency, and Flutter Speed)

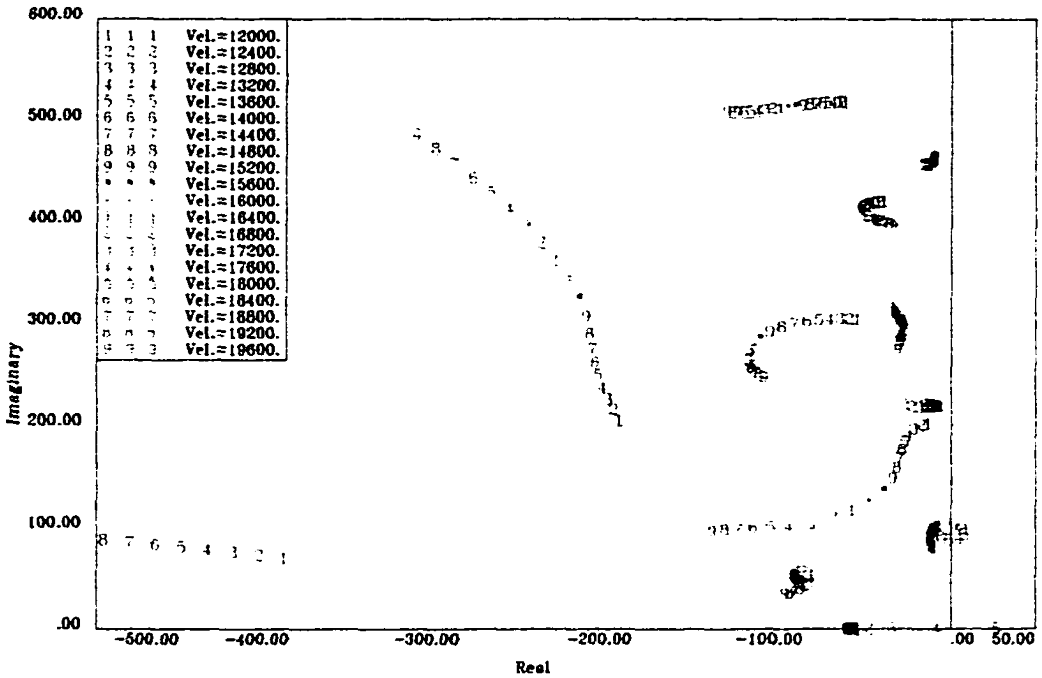

Figure 7.26 Root-Locus Plot for Final Designed GAF Model in Open Loop Configuration (Flutter Speed = 16,107 *in/sec*, Flutter Frequency = 18.8 *Hz.*)

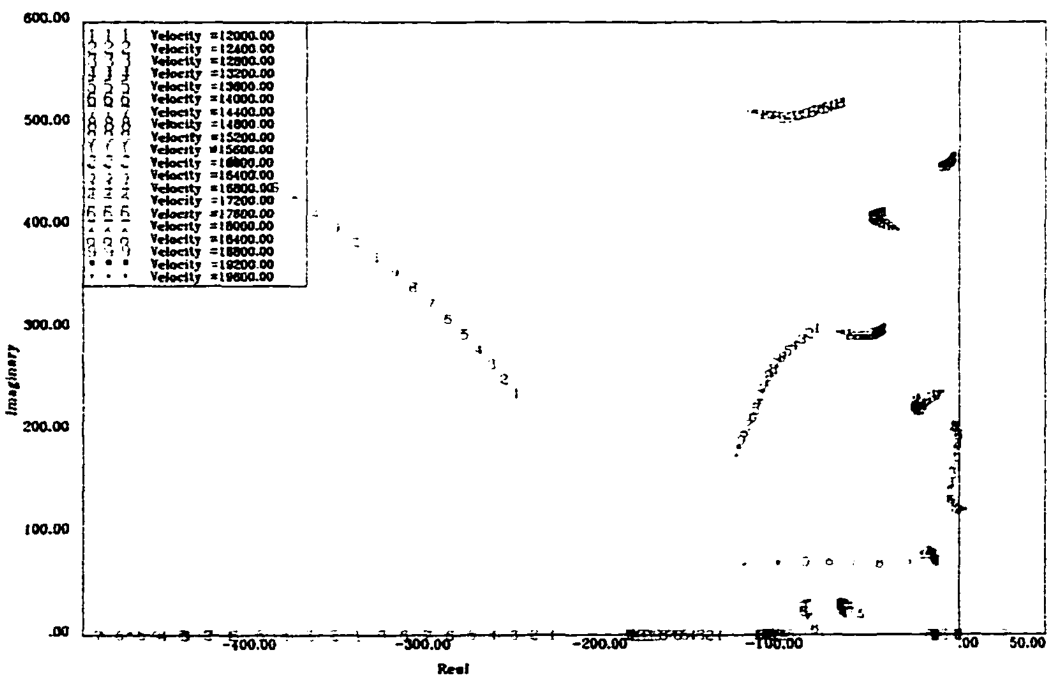

Figure 7.27 Root-Locus Plot for Final Designed GAF Model in Closed Loop Configuration (Divergence Speed = 17,756 *in/sec*, no Flutter)

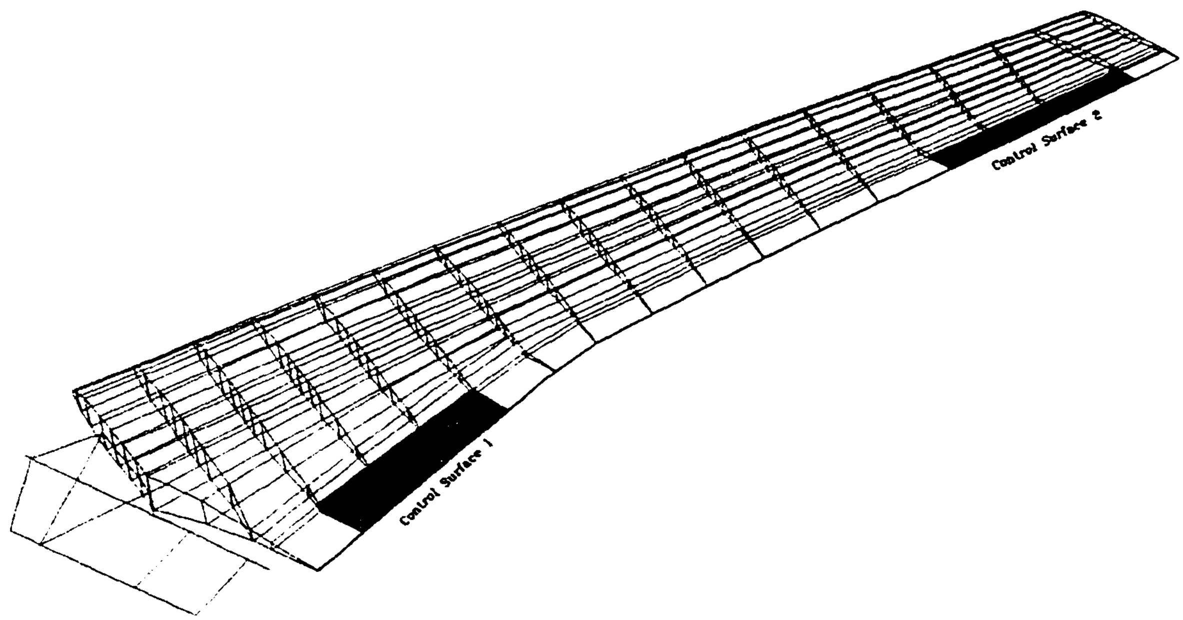

Figure 7.28 Structural Configuration of DAST Model by FEM

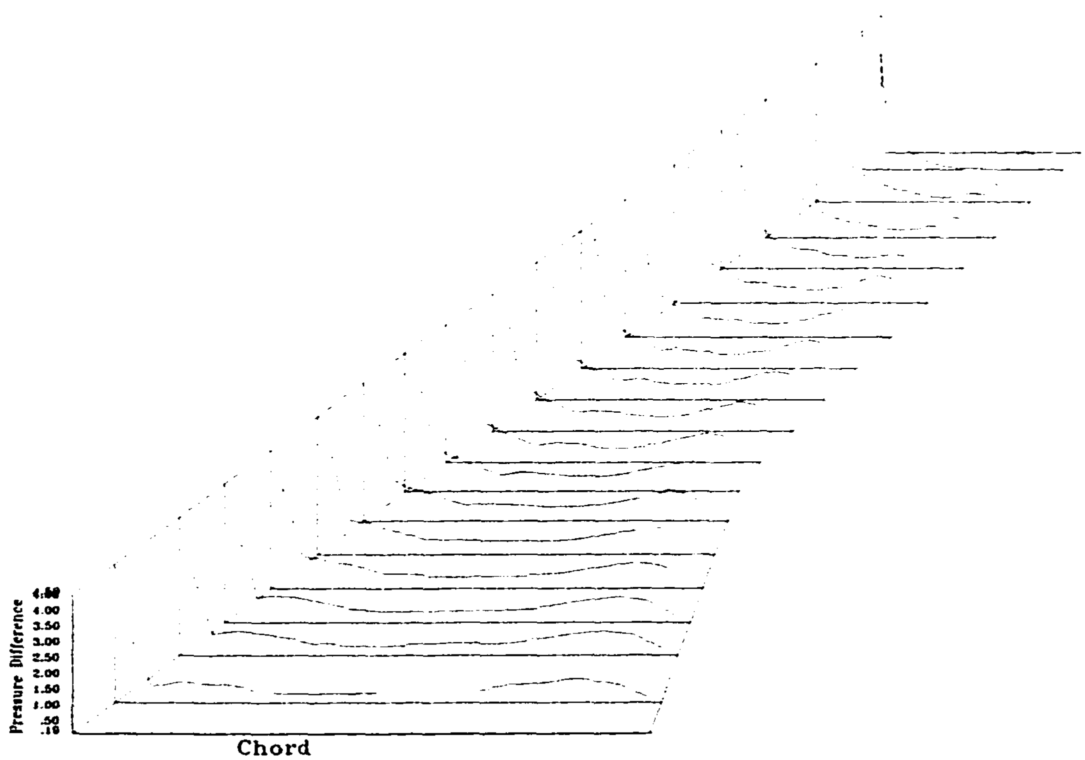

Figure 7.29 Pressure Distribution of DAST Model: 10g Pull-up Trim Condition, $M = 0.80$, by ZONA6 of ASTROS*

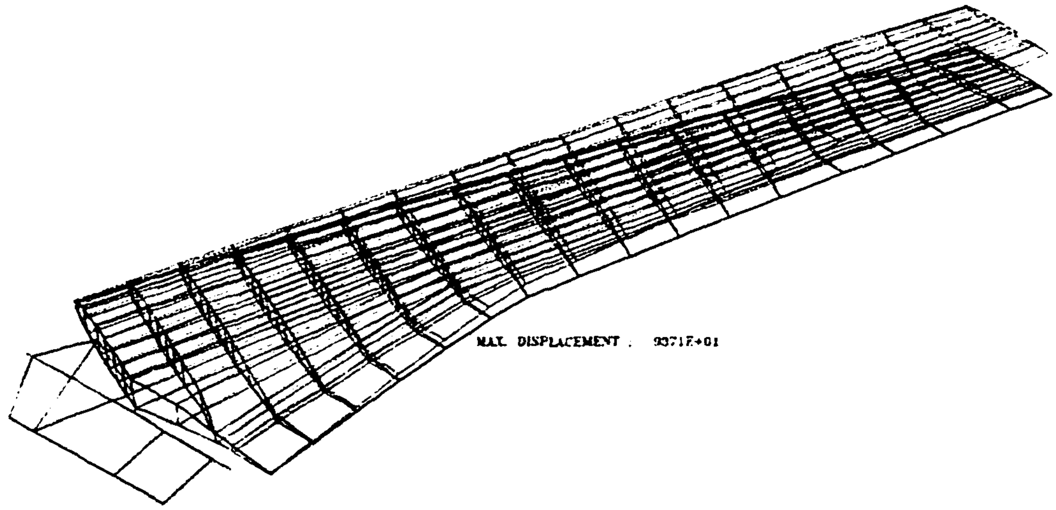

Figure 7.30 Deflection Shape of DAST Model: 10*g* Trim Condition, $M = 0.80$, by ZONA6 of ASTROS*

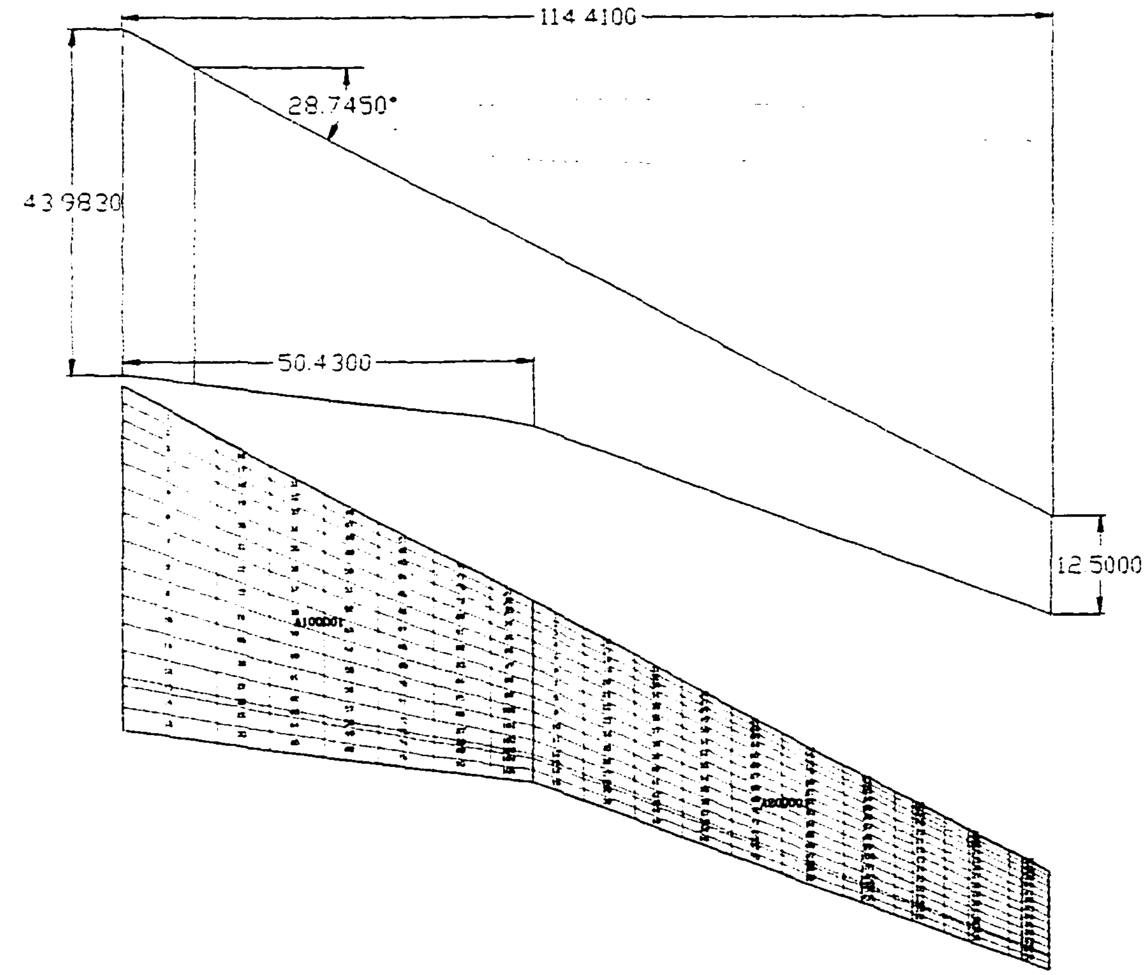

Figure 7.31 Aerodynamic Planform Configuration of DAST Model

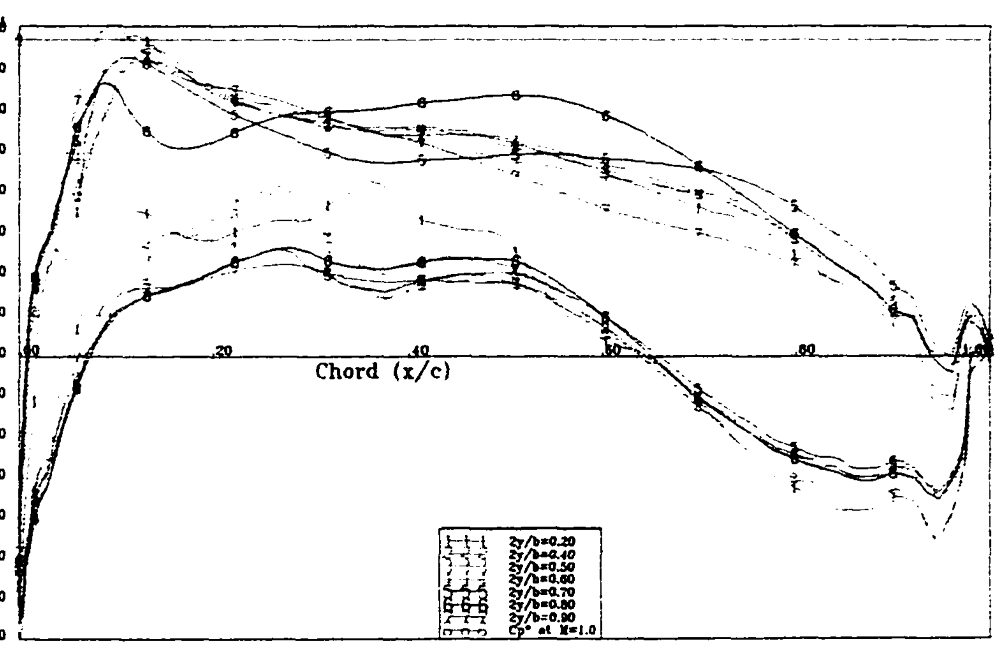

Figure 7.32a Aerodynamic Pressure Coefficients of DAST Model for Navier-Stokes Flow: $M = 0.70$, AoA = 0.0°, by ENSAERO

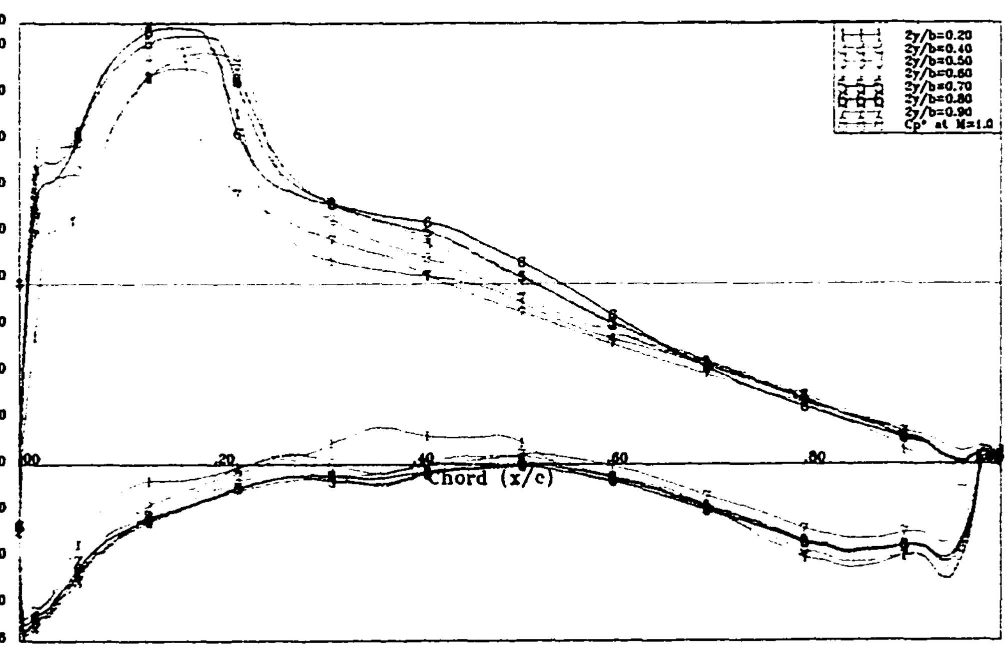

Figure 7.32b Aerodynamic Pressure Coefficients of DAST Model for Navier-Stokes Flow: $M = 0.70$, AoA=5.0°, by ENSAERO

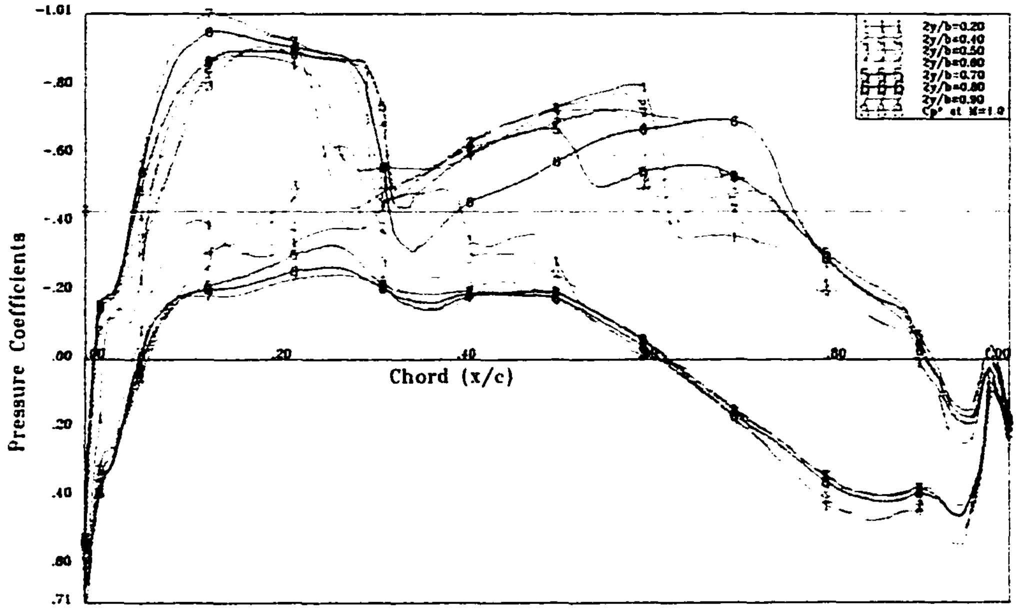

Figure 7.32c Aerodynamic Pressure Coefficients of DAST Model for Euler Flow: $M = 0.80$, AoA=0.0°, by ENSAERO

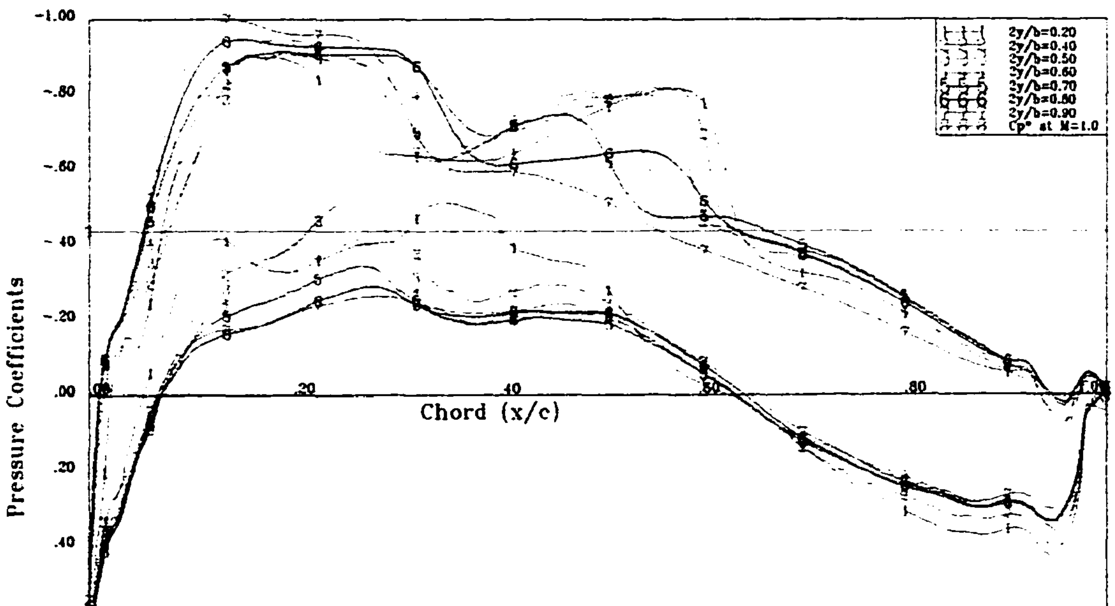

Figure 7.32d Aerodynamic Pressure Coefficients of DAST Model for Navier-Stokes Flow: $M = 0.80$, AoA=0.0°, by ENSAERO

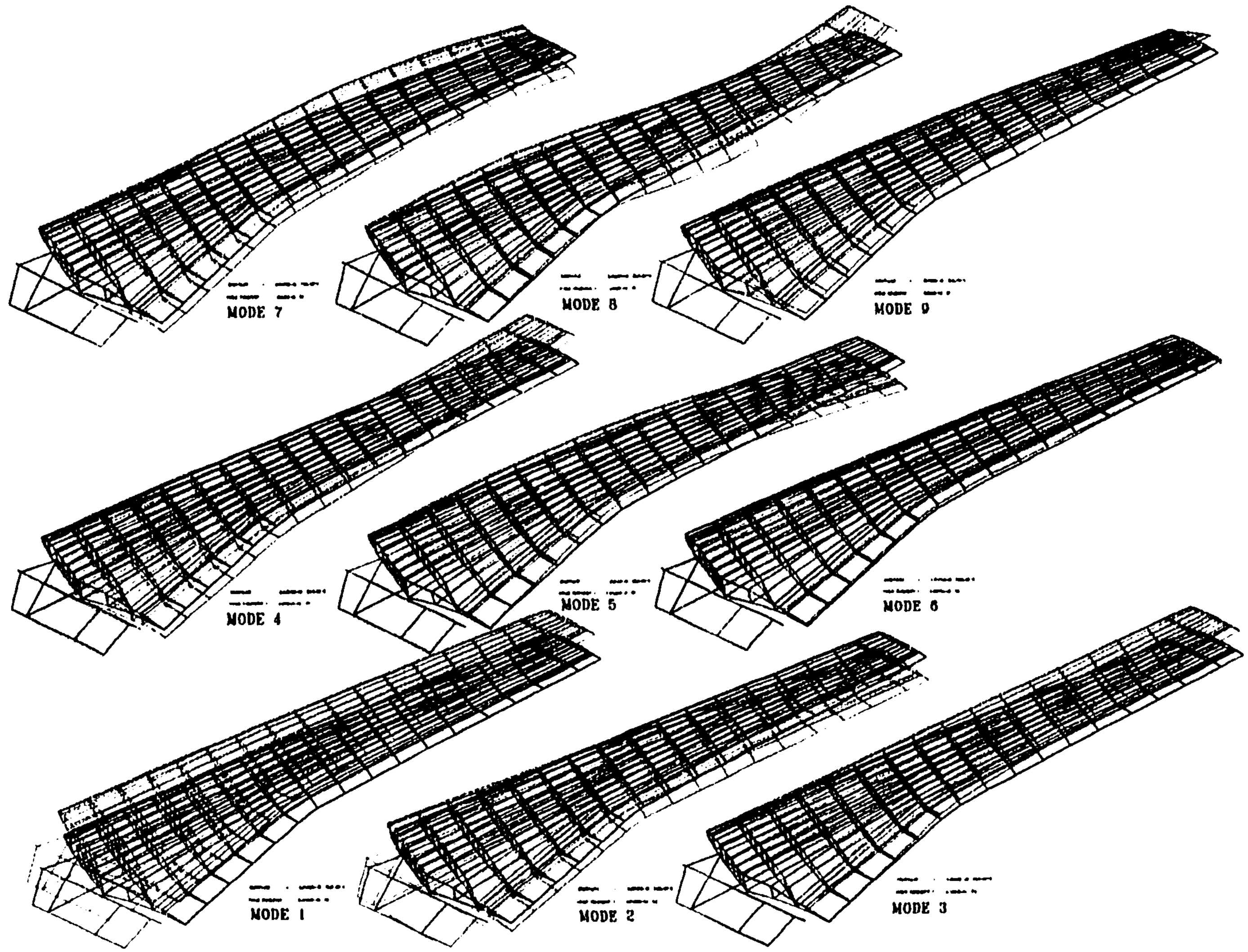

Figure 7.33 Normal Modes of DAST Model

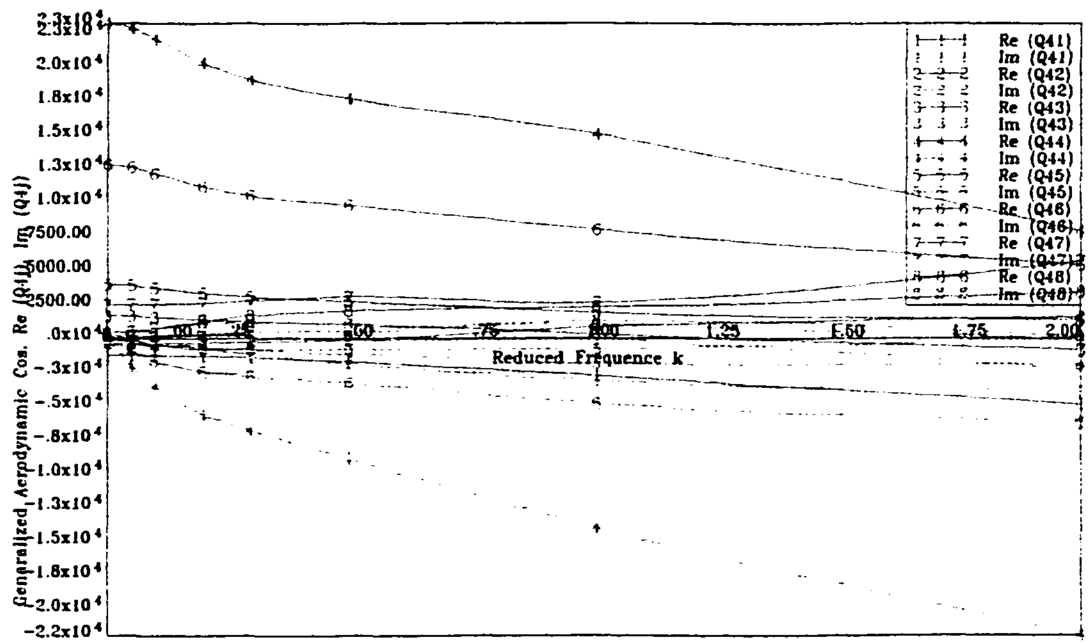

Figure 7.34 Generalized Unsteady Aerodynamic Loads of DAST Model: $M = 0.80$, by ZONA6 of ASTROS*

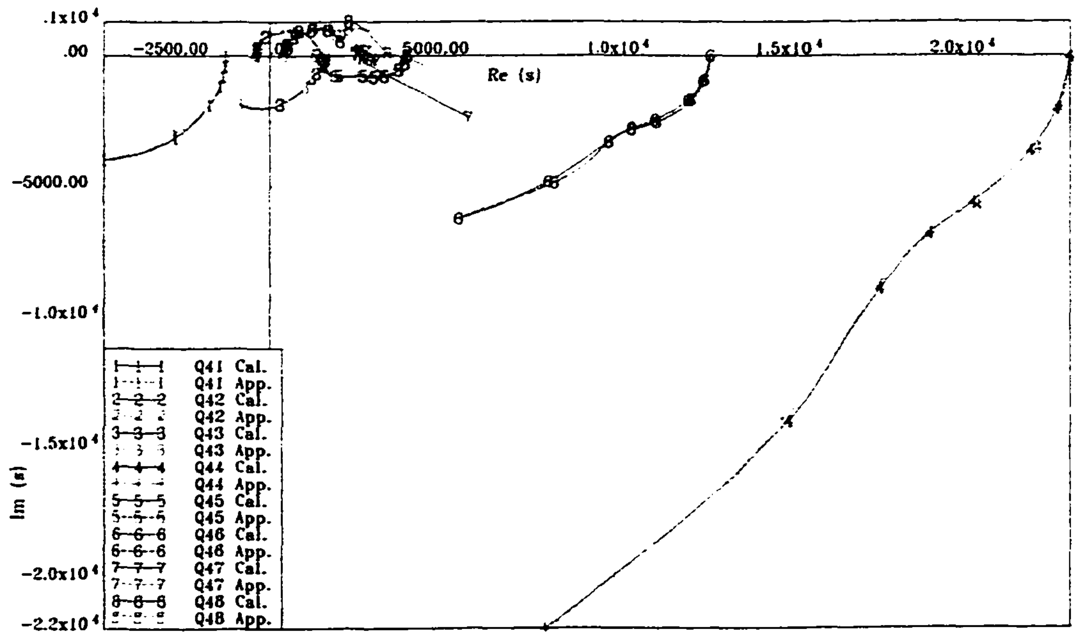

Figure 7.35 Generalized Unsteady Aerodynamic Coefficients Q_{4j} of DAST Model: $M = 0.80$, by ZONA6 of ASTROS* and Approximated by Minimum-State Method

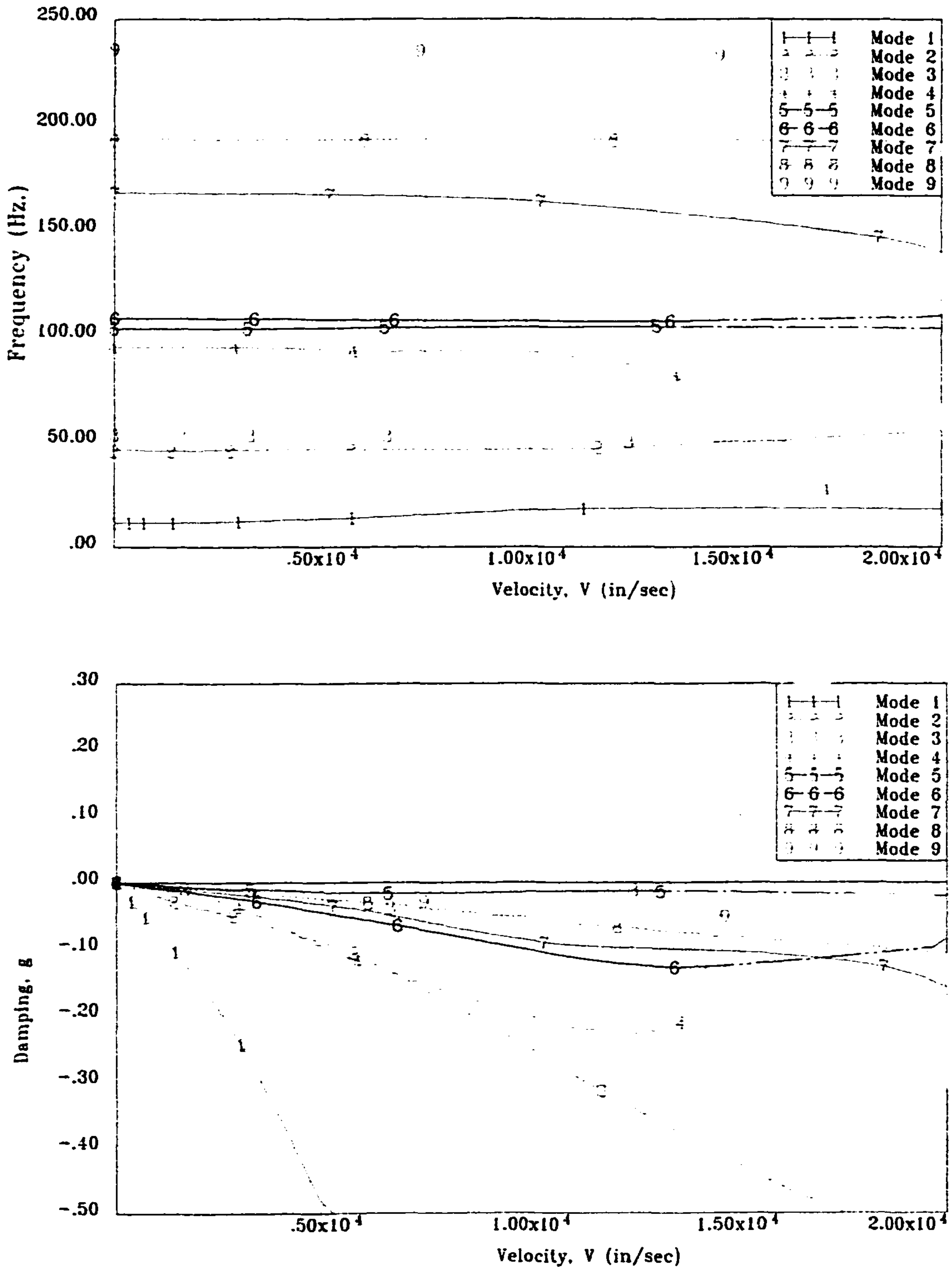

Figure 7.36 V-f and V-g Plots of DAST Model: $M = 0.80$, by ZONA6 of ASTROS*
(Flutter Speed = 14,358 *in/sec*, Flutter Frequency = 48.67 *Hz.*)

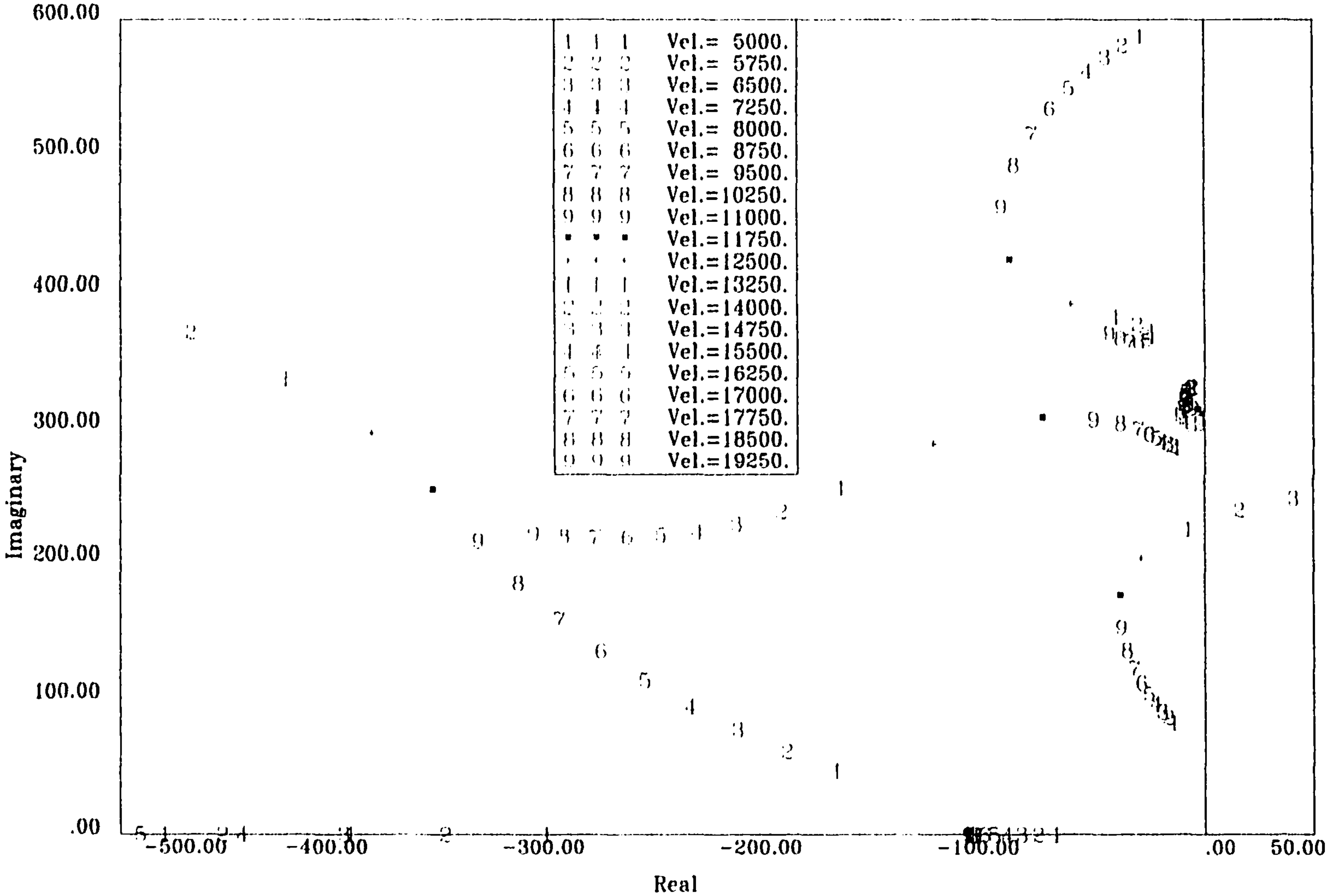

Figure 7.37 Root-Locus Plot of DAST Model: M = 0.8, by ZONA6 of ASTROS*
(Flutter Speed = 13,490 in/sec, Flutter Frequency = 36.3 Hz.)

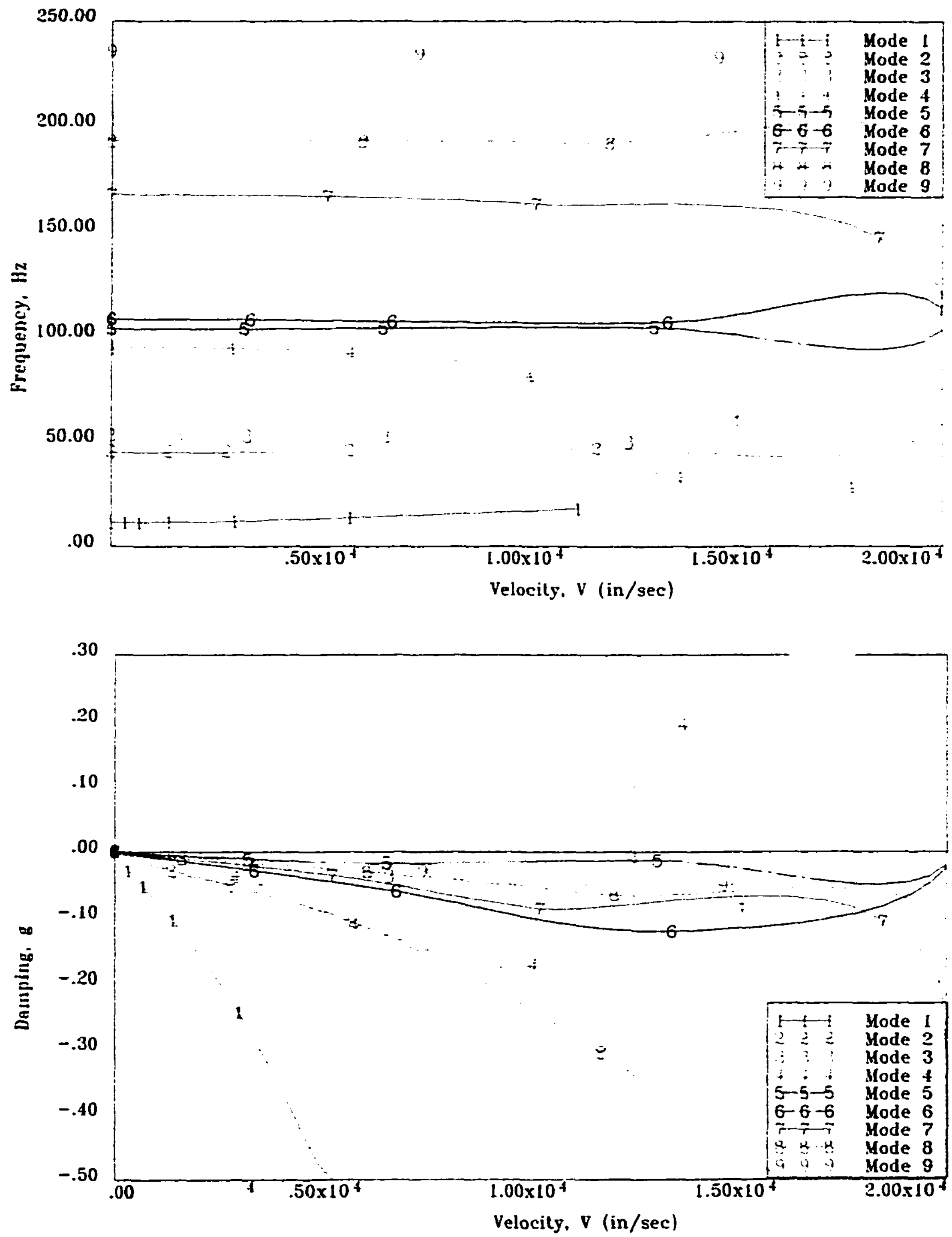

Figure 7.38 V-f and V-g Plots of DAST Model: $M = 0.80$, by ZTAIC of ASTROS*
(Flutter Speed = 11,800 *in/sec*, Flutter Frequency = 56.0 *Hz*.)

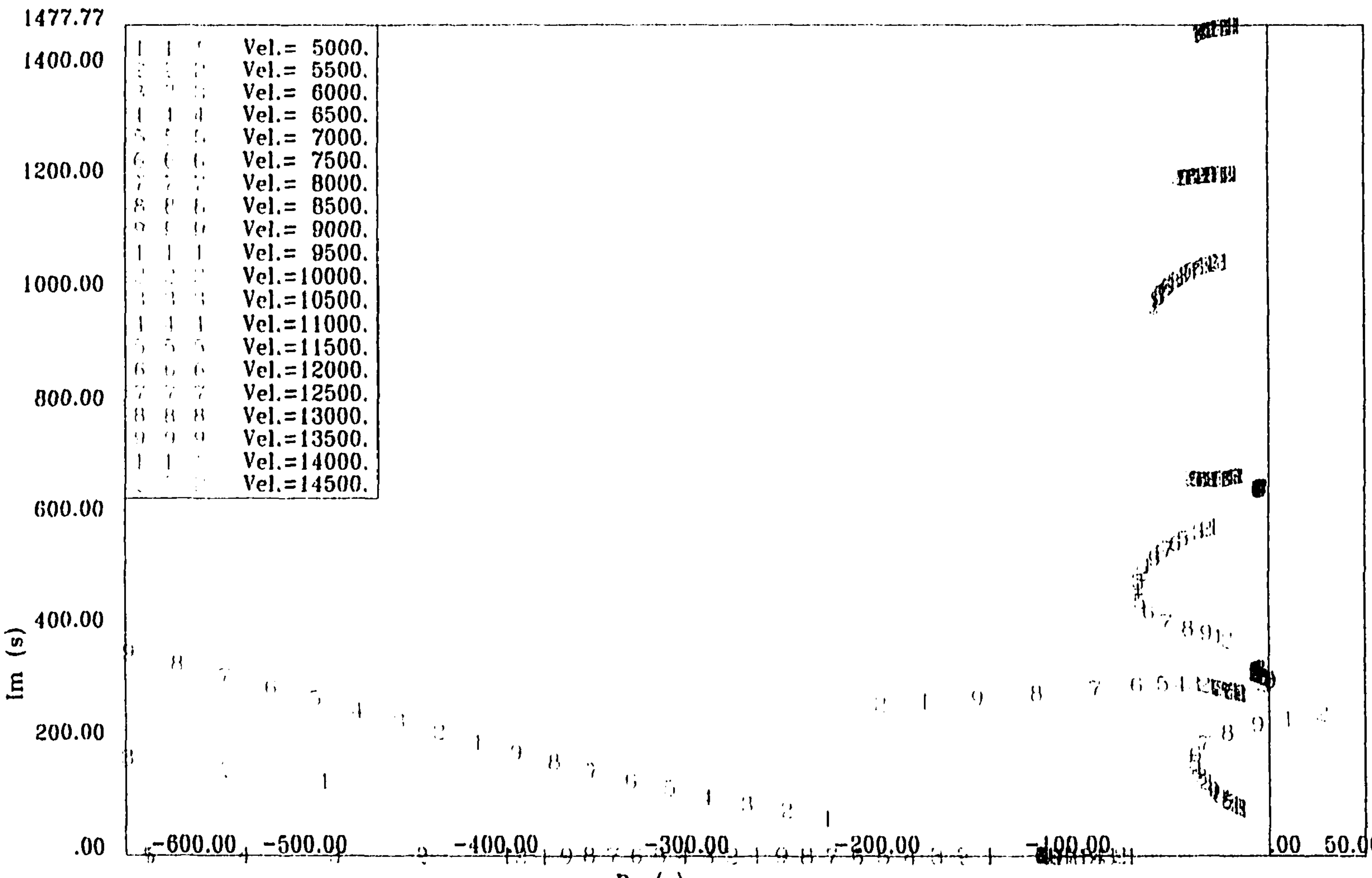

Figure 7.39 Root-Locus Plot of DAST Model: M = 0.80, by ZTAIC of ASTROS*
(Flutter Speed = 12,893 in/sec, Flutter Frequency = 49.3 Hz.)

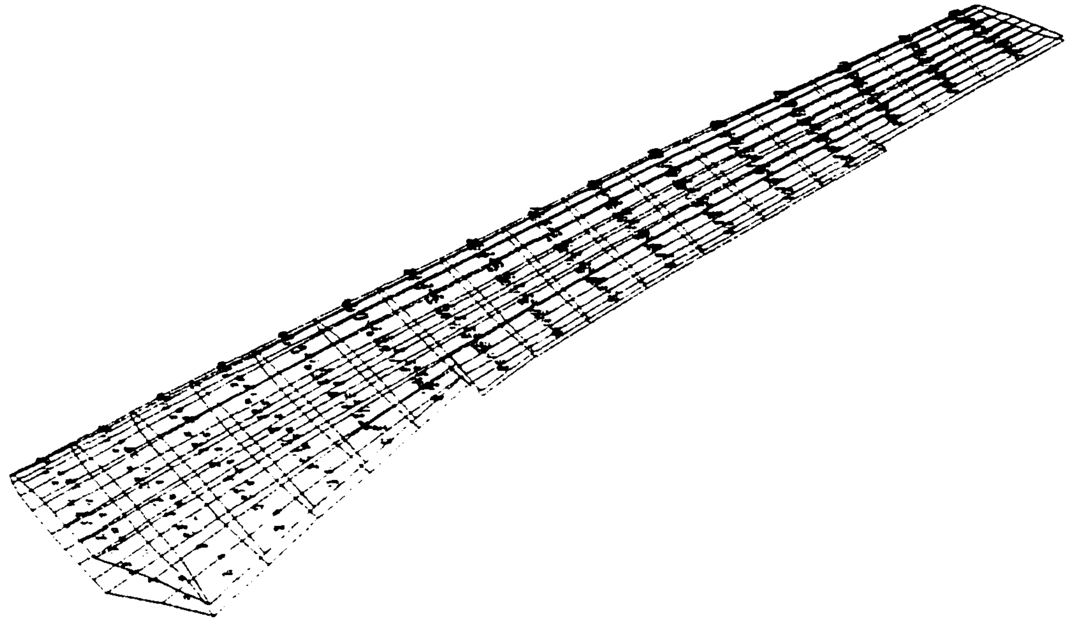

Figure 7.40 Structural Design Variables and Numbering of DAST Model

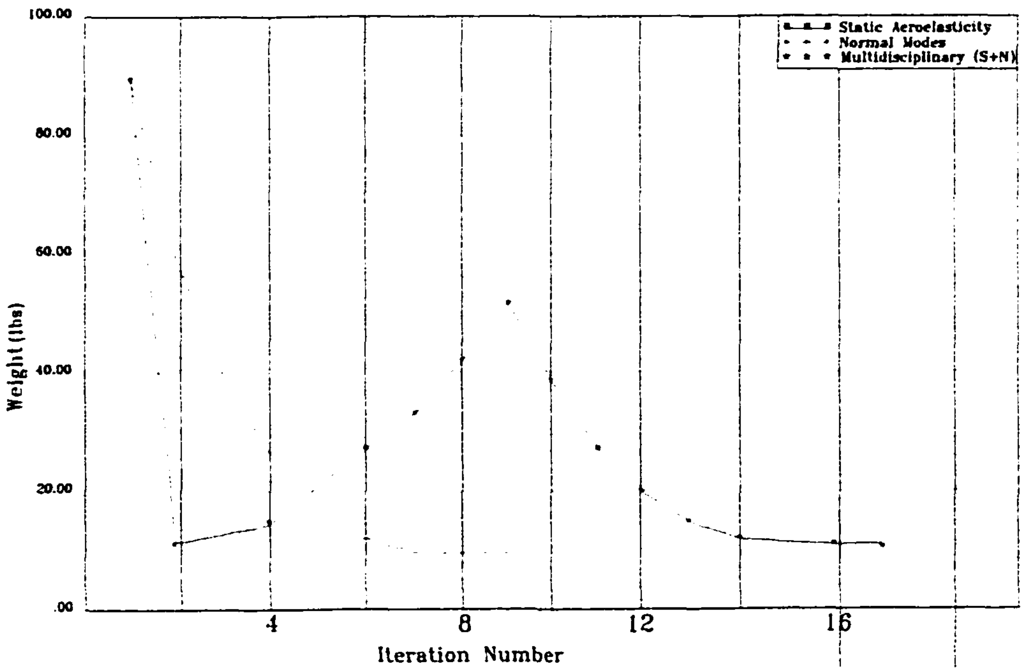

Figure 7.41 Iteration History of Design Optimization of DAST Model for Static Aeroelasticity, Normal Modes, and Multiple Disciplines (S + N)

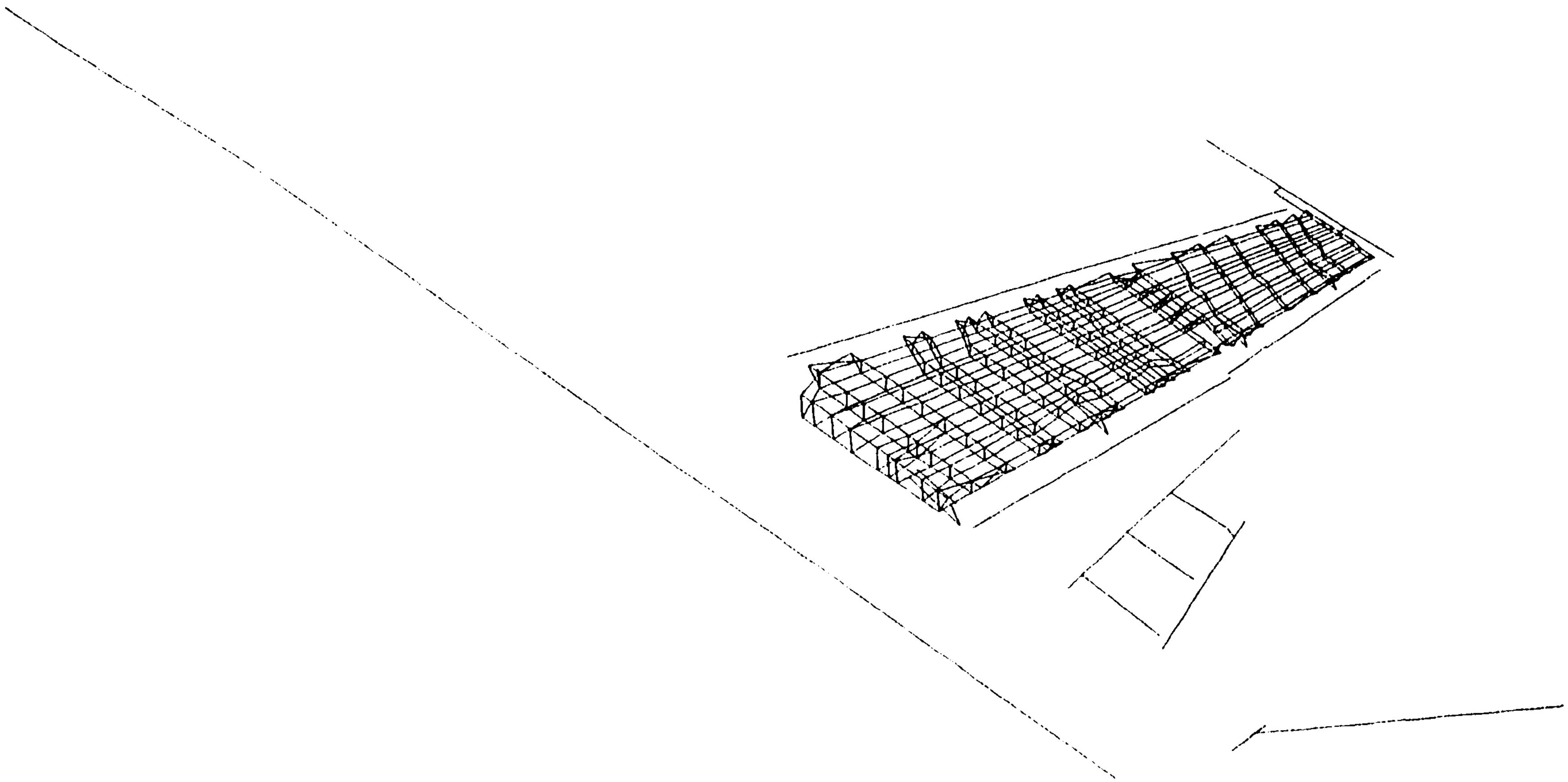

Figure 7.42 Structural Configuration of AAW Model by FEM

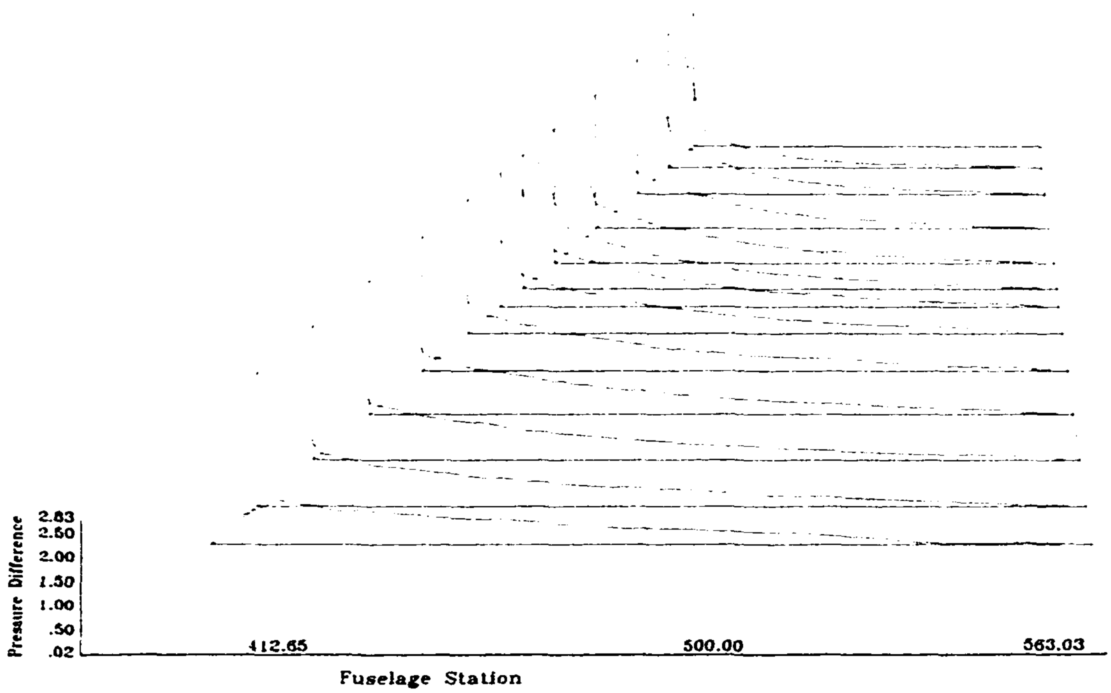

Figure 7.43 Aerodynamic Pressure Distribution of AAW Main Wing Model: $7g$ Pull-up Trim Condition, $M = 0.85$, AoA = 6.974°, by ZONA6 of ASTROS*

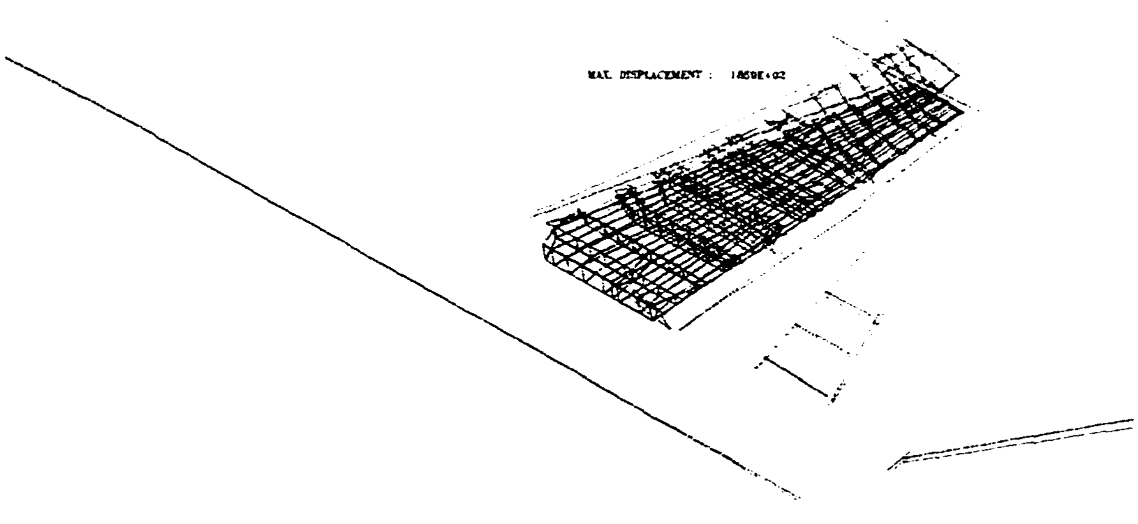

Figure 7.44 Deflection Shape of AAW Model: $7g$ Pull-up Trim Condition, $M = 0.85$, by ZONA6 of ASTROS*

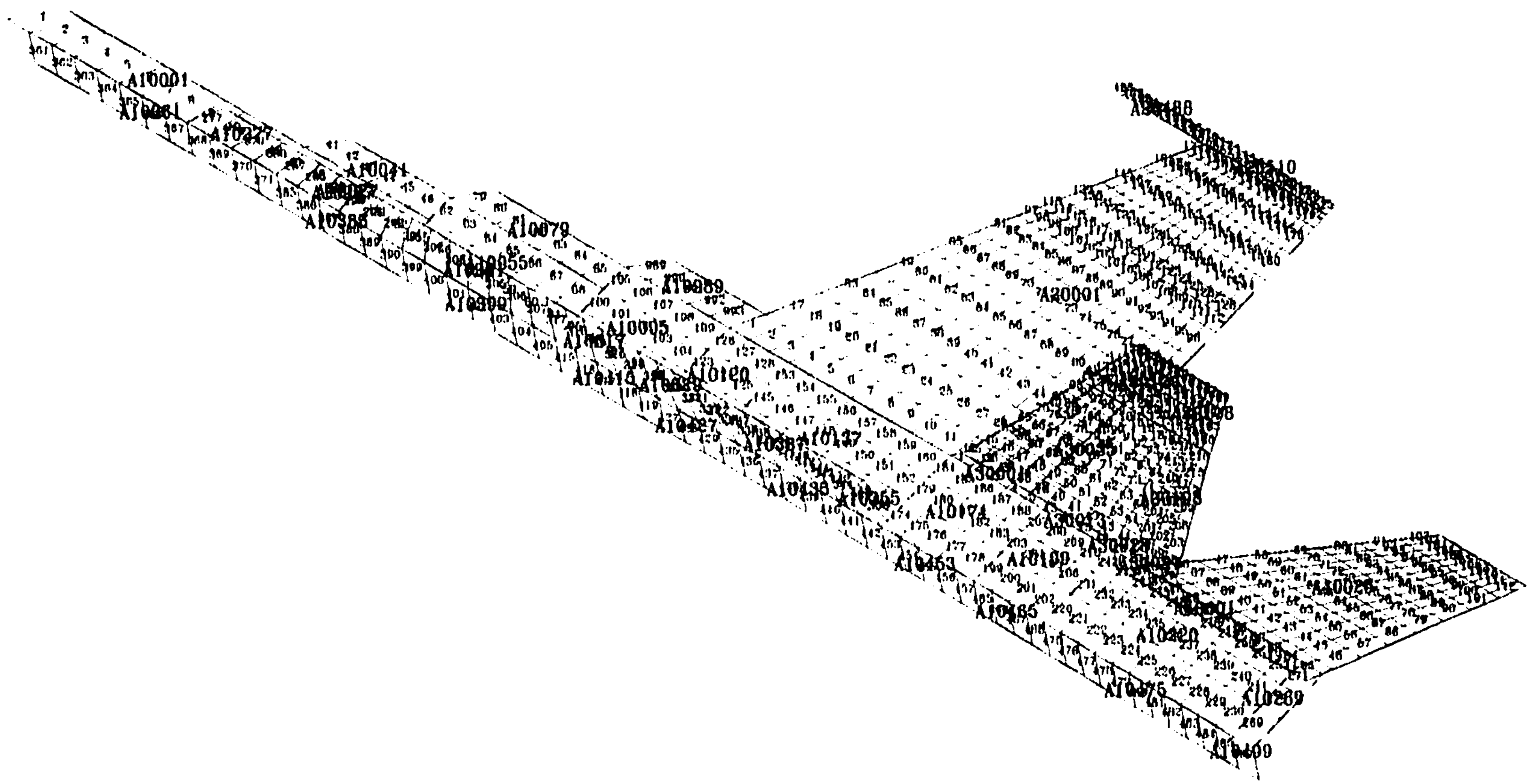

Figure 7.45 Aerodynamic Panels of AAW Model by ASTROS

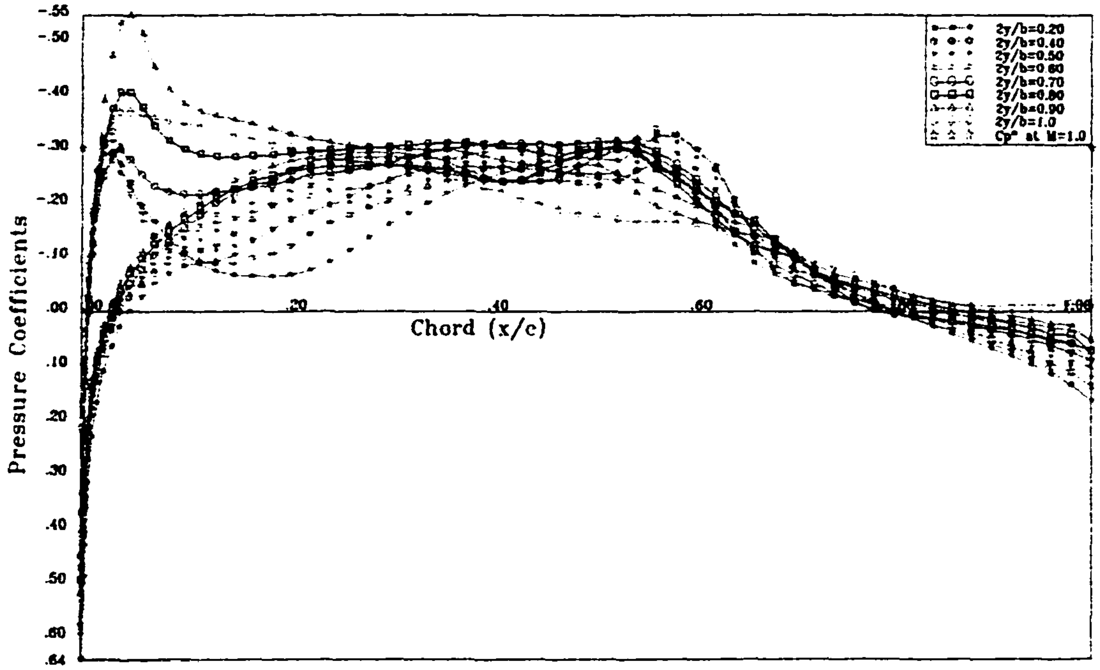

Figure 7.46a Aerodynamic Pressure Coefficients of AAW Model for Navier-Stokes Flow: $M = 0.85$, AoA = 0.0°, by ENSAERO

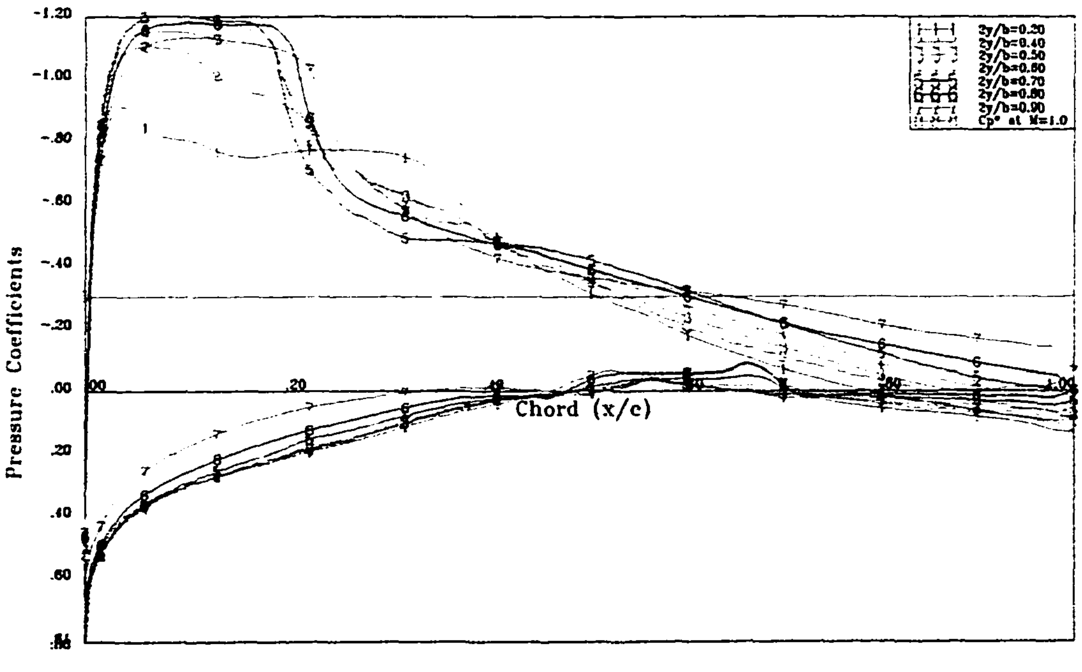

Figure 7.46b Aerodynamic Pressure Coefficients of AAW Model for Navier-Stokes Flow: $M = 0.85$, AoA = 8.6°, by ENSAERO

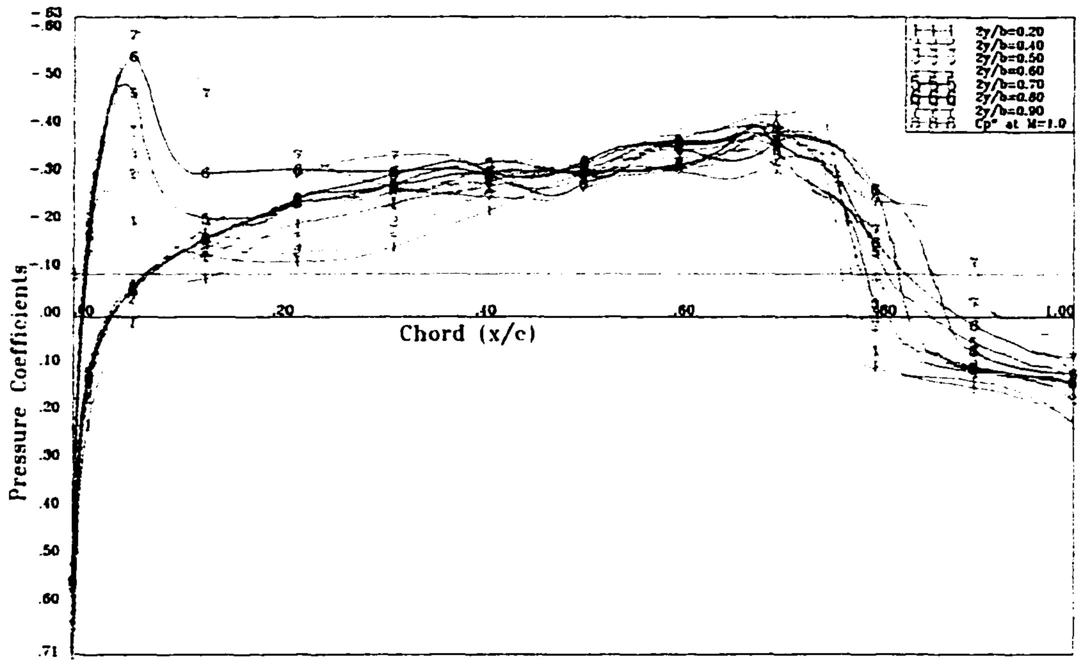

Figure 7.46c Aerodynamic Pressure Coefficients of AAW Model for Navier-Stokes Flow: $M = 0.95$, AoA = 0.0°, by ENSAERO

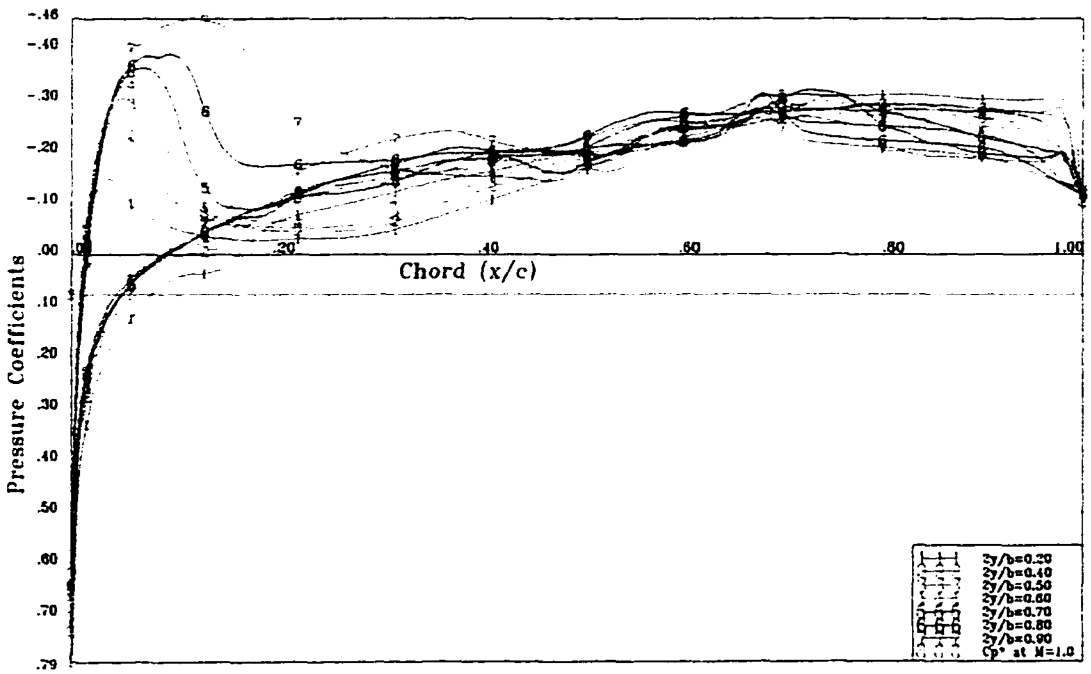

Figure 7.46d Aerodynamic Pressure Coefficients of AAW Model for Navier-Stokes Flow: $M = 1.05$, AoA = 0.0°, by ENSAERO

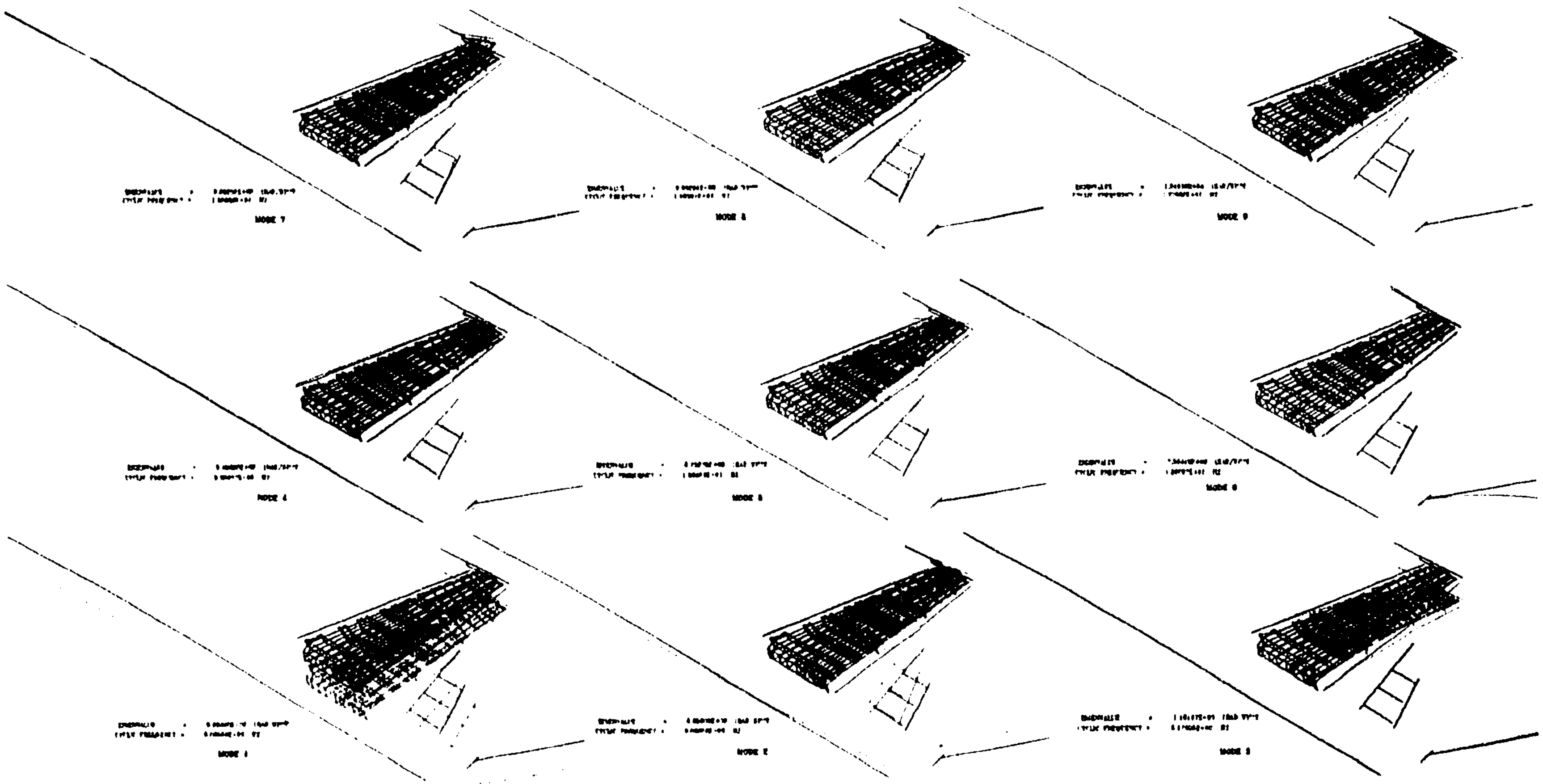

Figure 7.47 Normal Modes of AAW Model

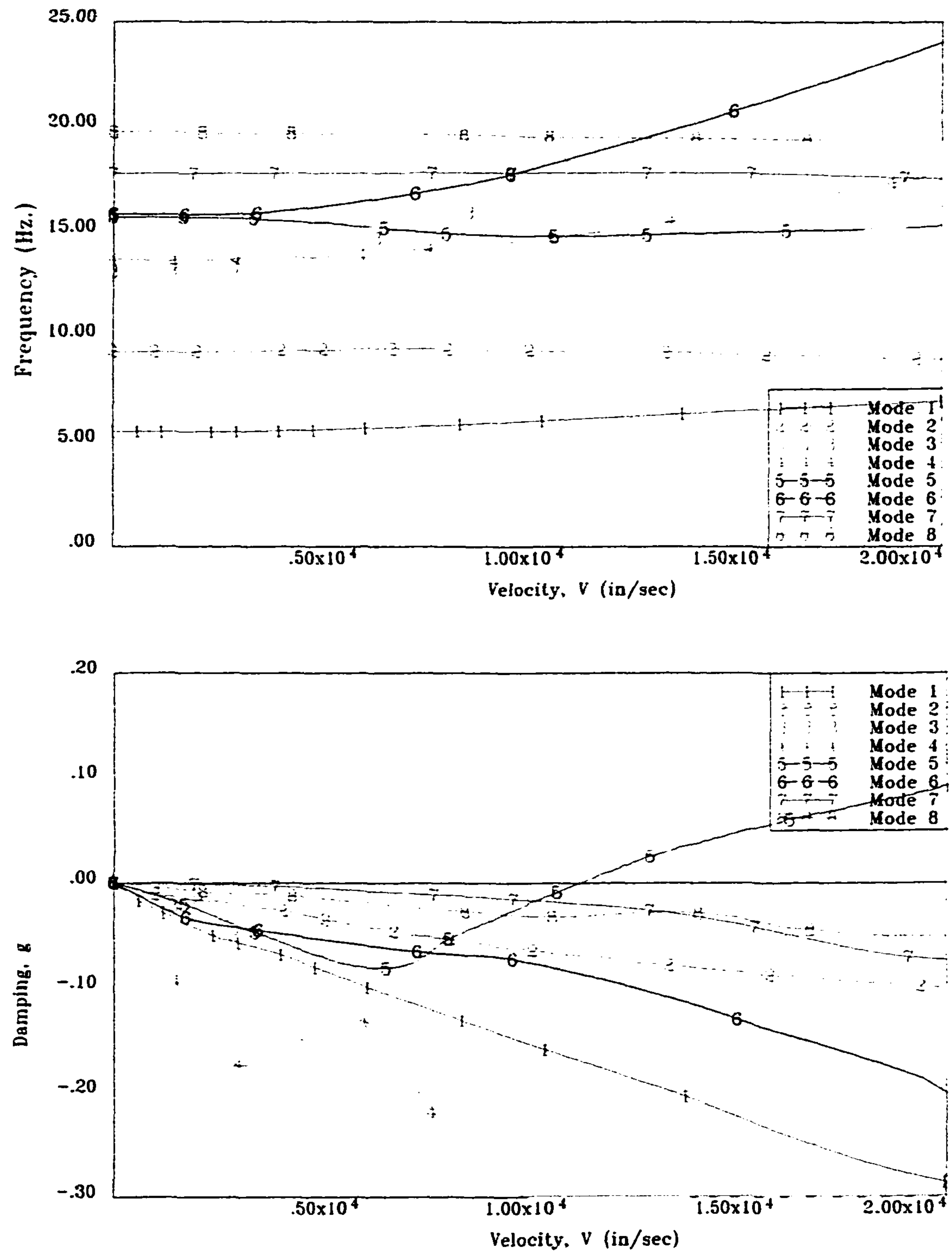

Figure 7.48 V-f and V-g Plots of AAW Model: $M = 0.85$, by ZONA6 of ASTROS*
(Flutter Speed = 11,281 *in/sec*, Flutter Frequency = 14.80 *Hz.*)

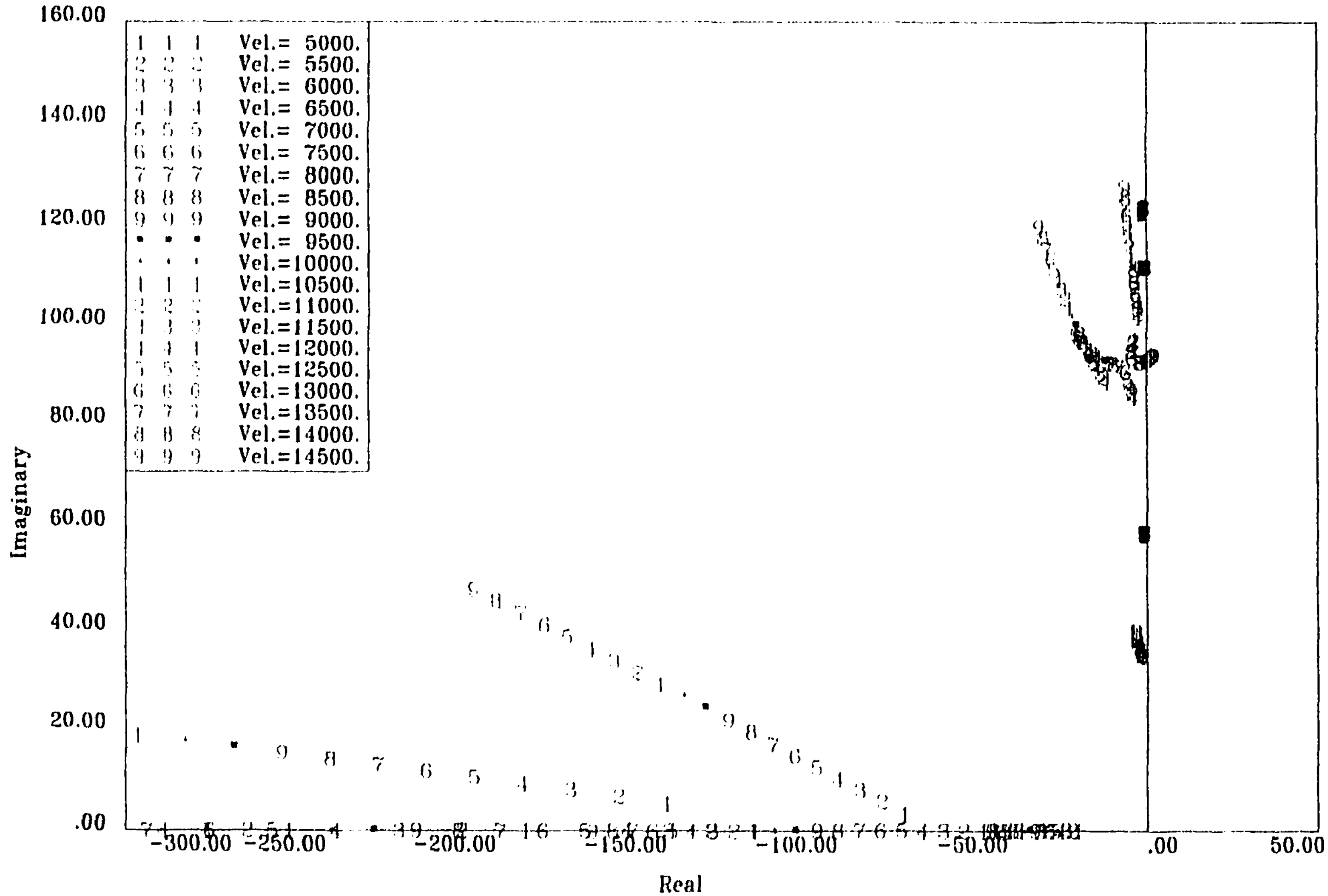

Figure 7.49 Root-Locus Plot of AAW Model: M = 0.85, by ZONA6 of ASTROS*
(Flutter Speed = 10,979 in/sec, Flutter Frequency = 14.77 Hz.)

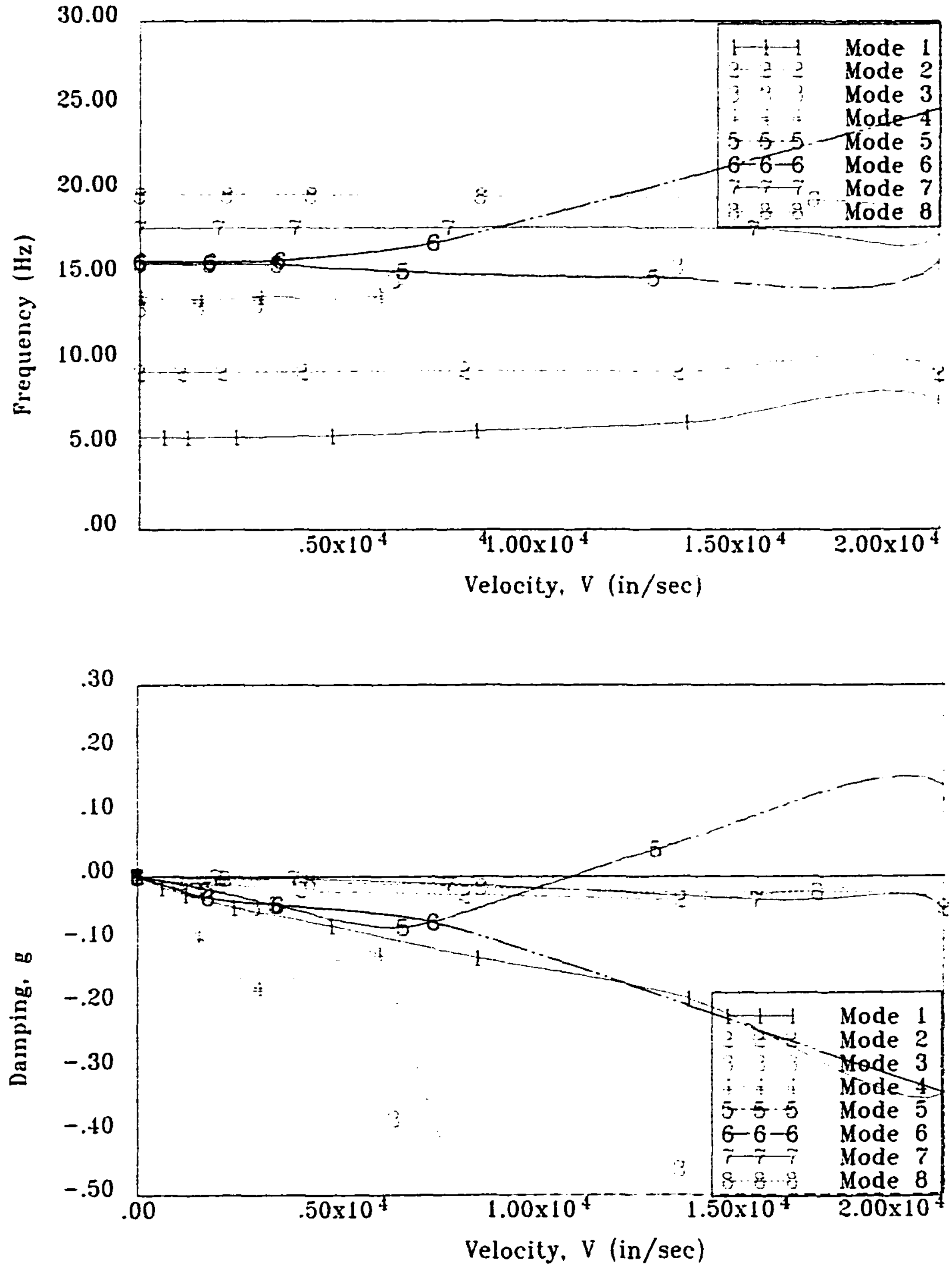

Figure 7.50 V-f and V-g Plots of AAW Model: $M = 0.85$, by ZTAIC of ASTROS*
(Flutter Speed = 10,714 *in/sec*, Flutter Frequency = 14.94 *Hz*.)

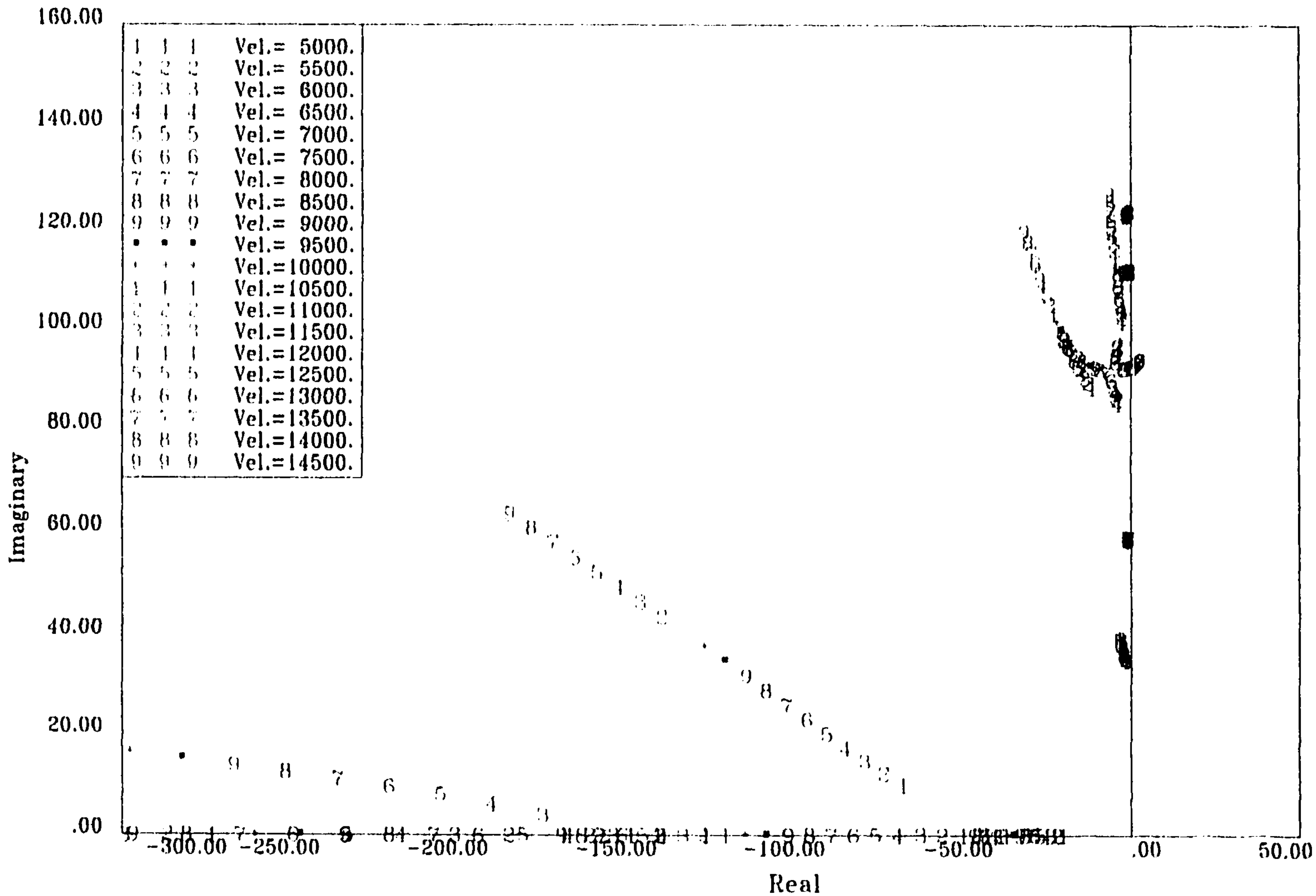

Figure 7.51 Root-Locus Plot of AAW Model: M = 0.85, by ZTAIC of ASTROS*
(Flutter Speed = 10,538 in/sec, Flutter Frquency = 14.73 Hz.)

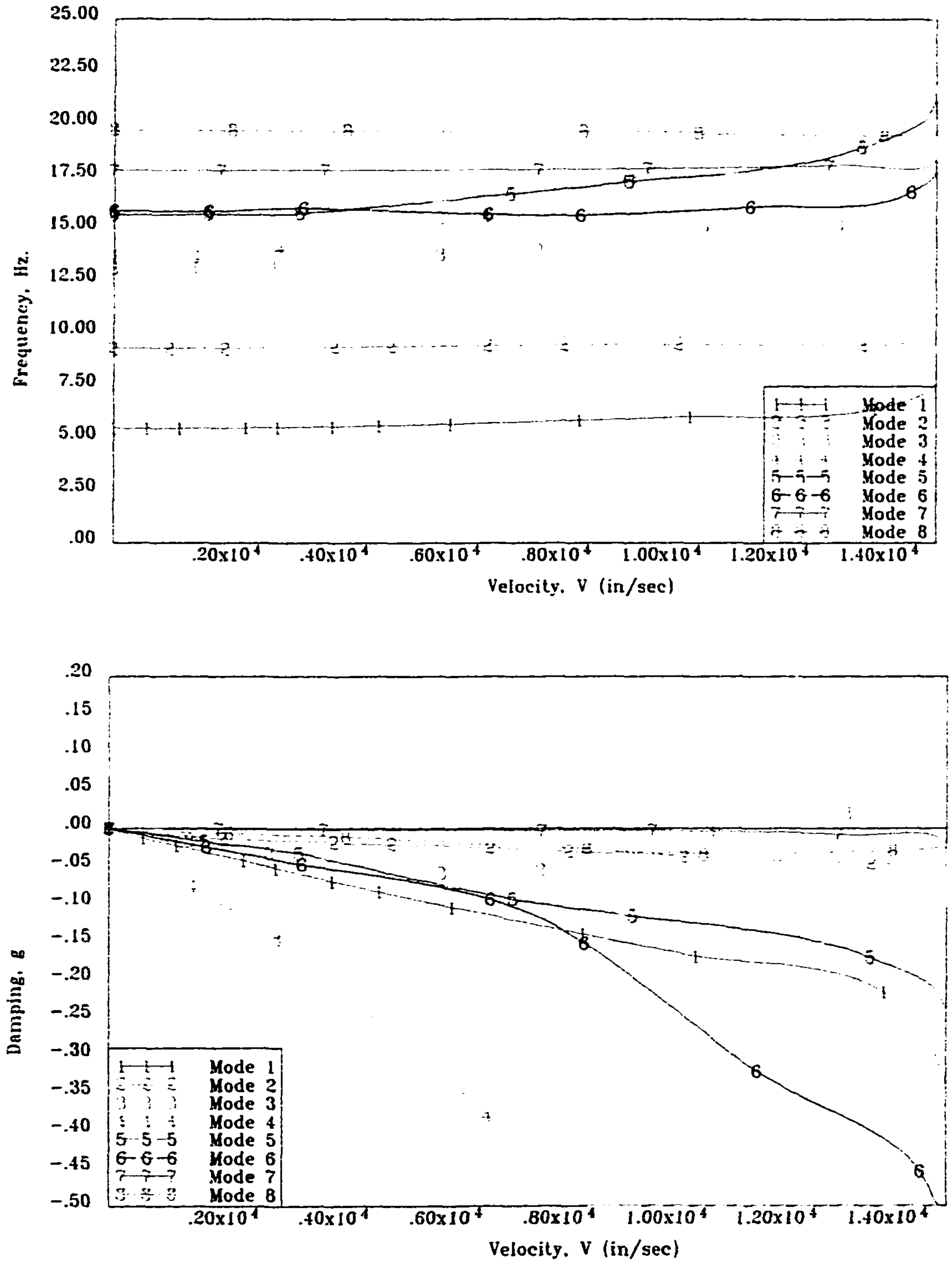

Figure 7.52 V-f and V-g Plots of AAW Model: $M = 1.15$, by ZONA7 of ASTROS*
(Flutter Speed = 11,088 *in/sec*, Flutter Frequency = 14.90 *Hz.*)

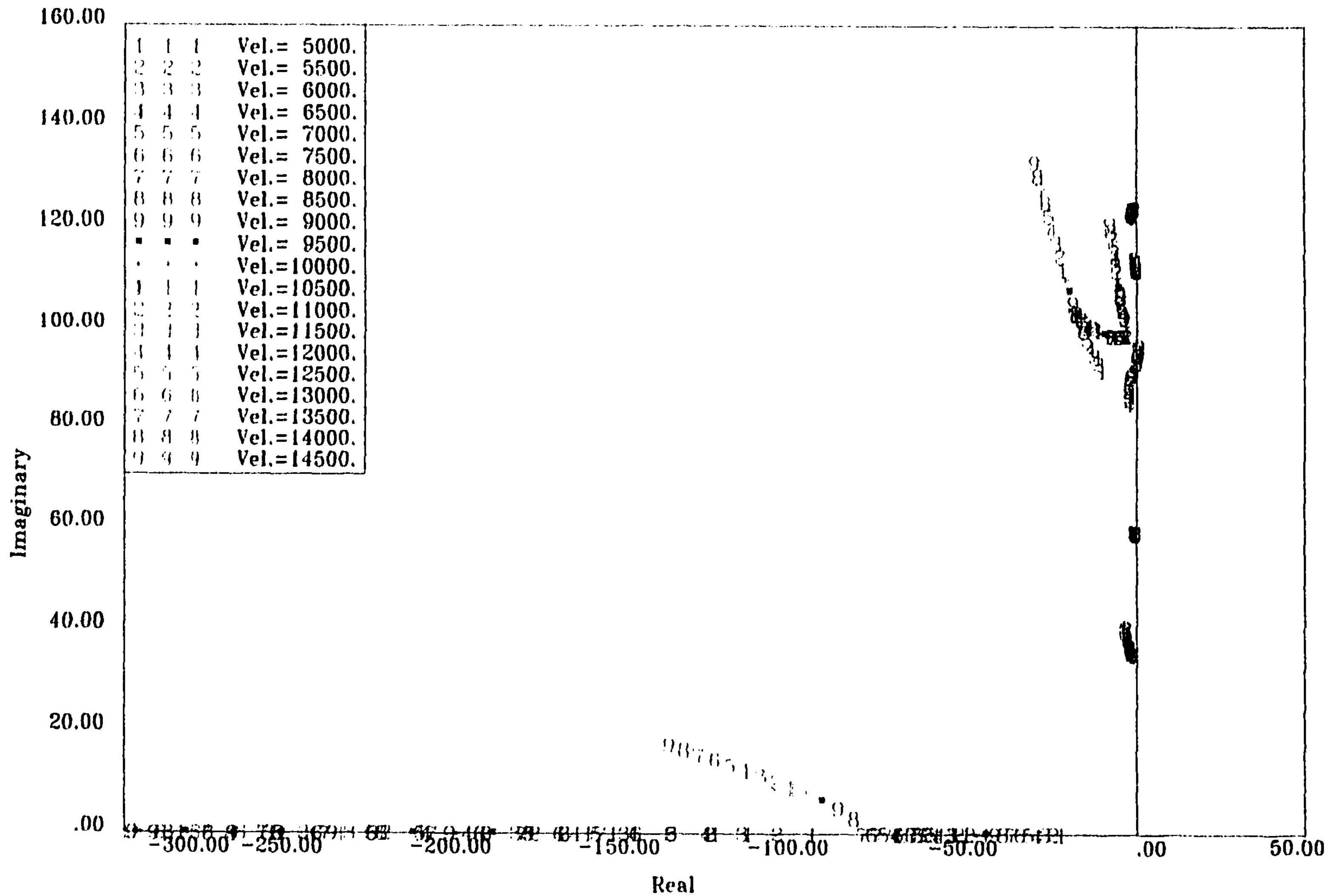

Figure 7.53 Root-Locus Plot of AAW Model: M = 1.15, by ZONA7 of ASTROS* (Flutter Speed = 11,308 in/sec, Flutter Frequency = 14.93 Hz.)

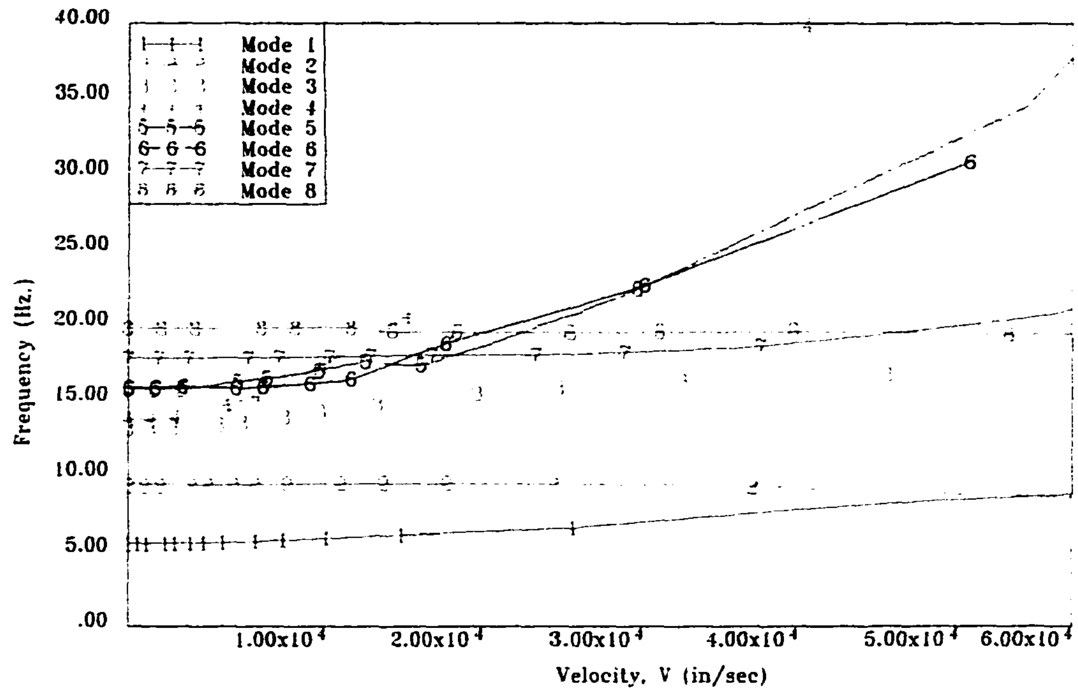

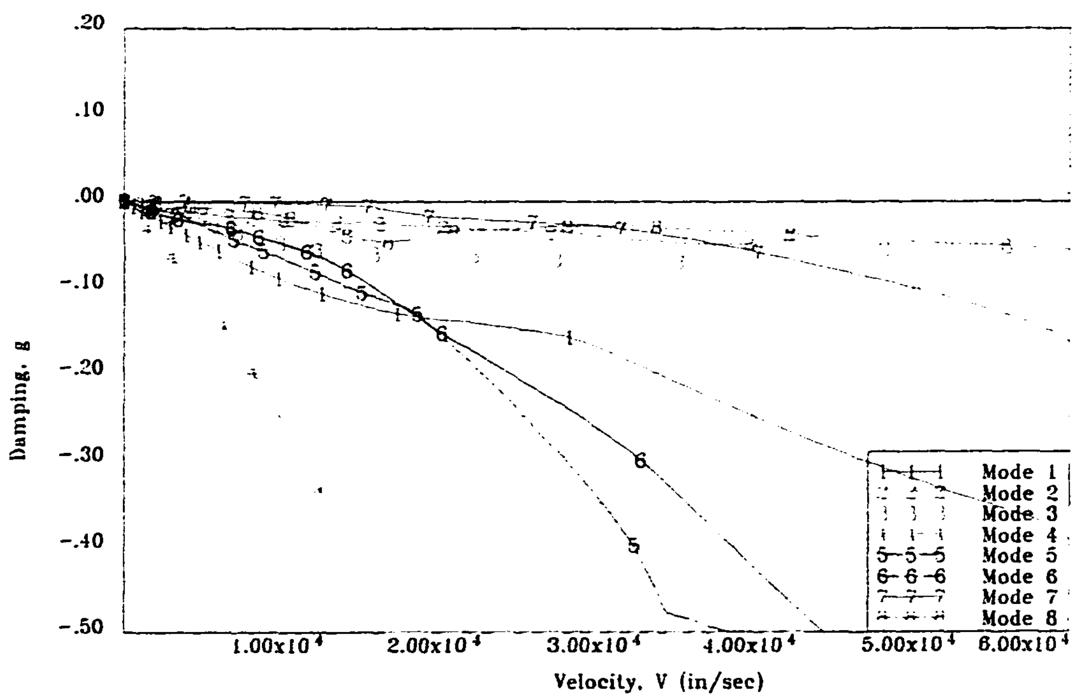

Figure 7.54 V-f and V-g Plots of AAW Model: $M = 3.0$, by ZONA7U of ASTROS*
(Flutter Speed = 58,768 *in/sec*, Flutter Frequency = 8.55 *Hz.*)

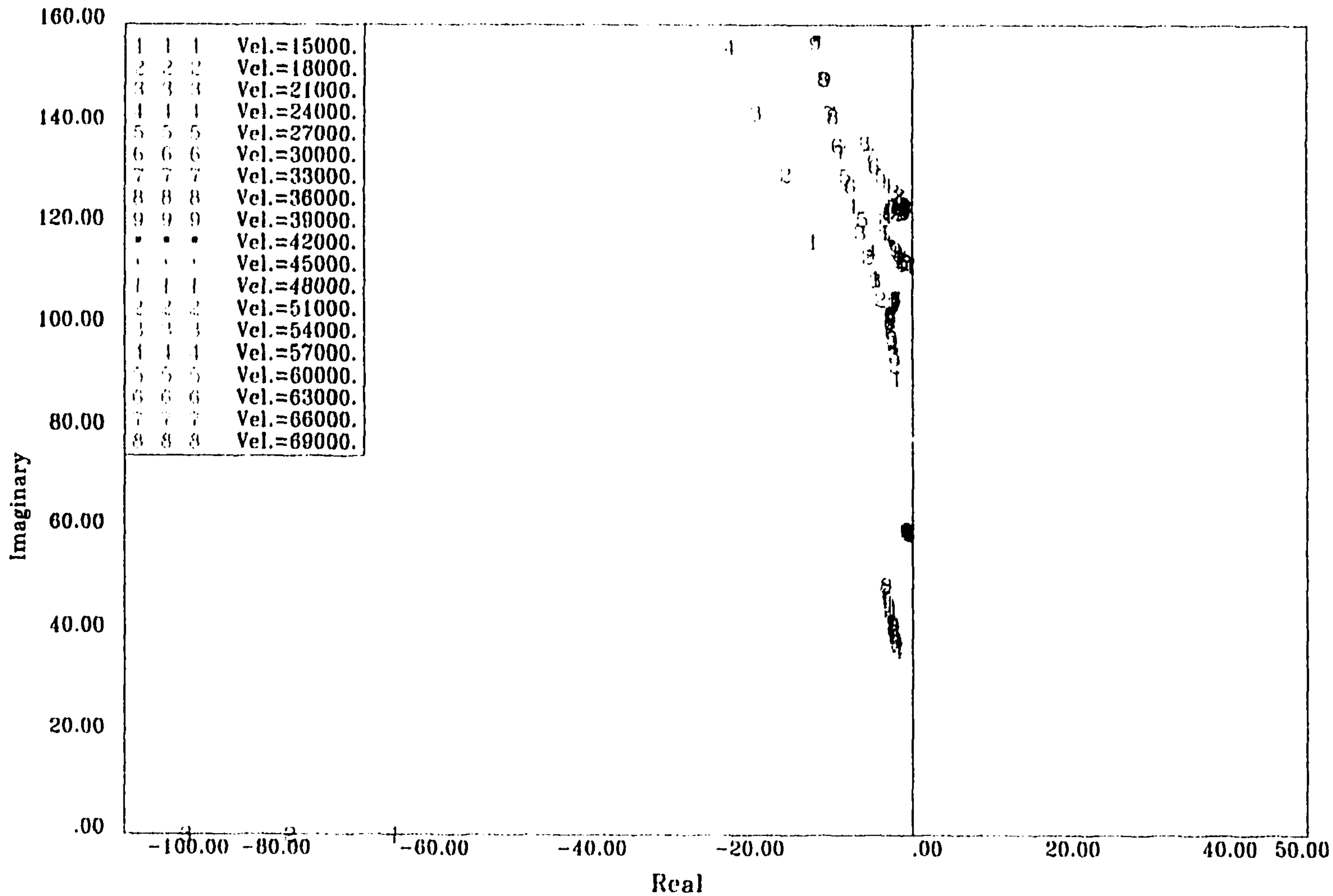

Figure 7.55 Root-locus Plot of AAW Model: M = 3.0, by ZONA7U of ASTROS* (No Flutter)

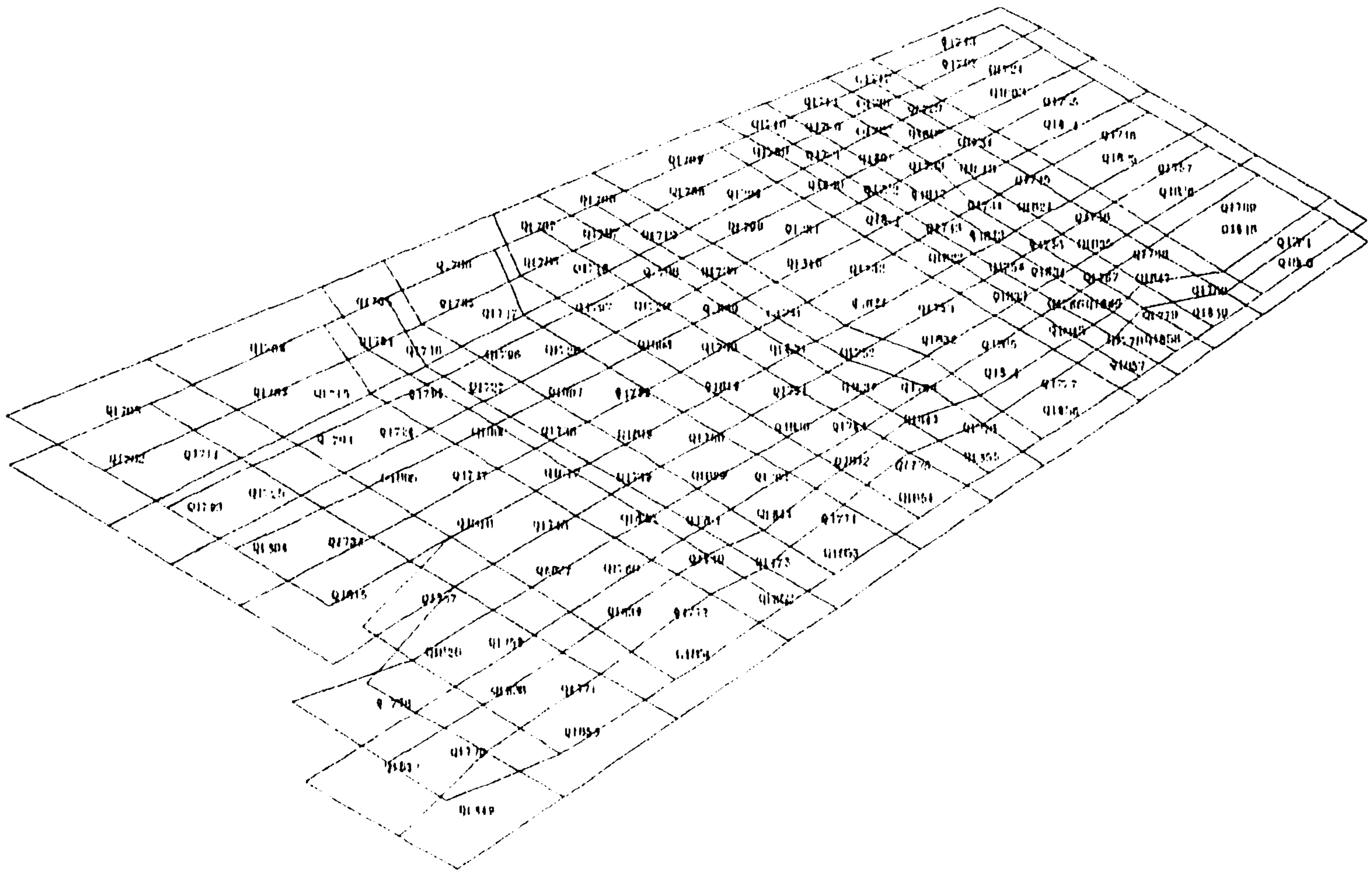

Figure 7.56 Design Variables and Numbering of AAW Inboard Wing Model

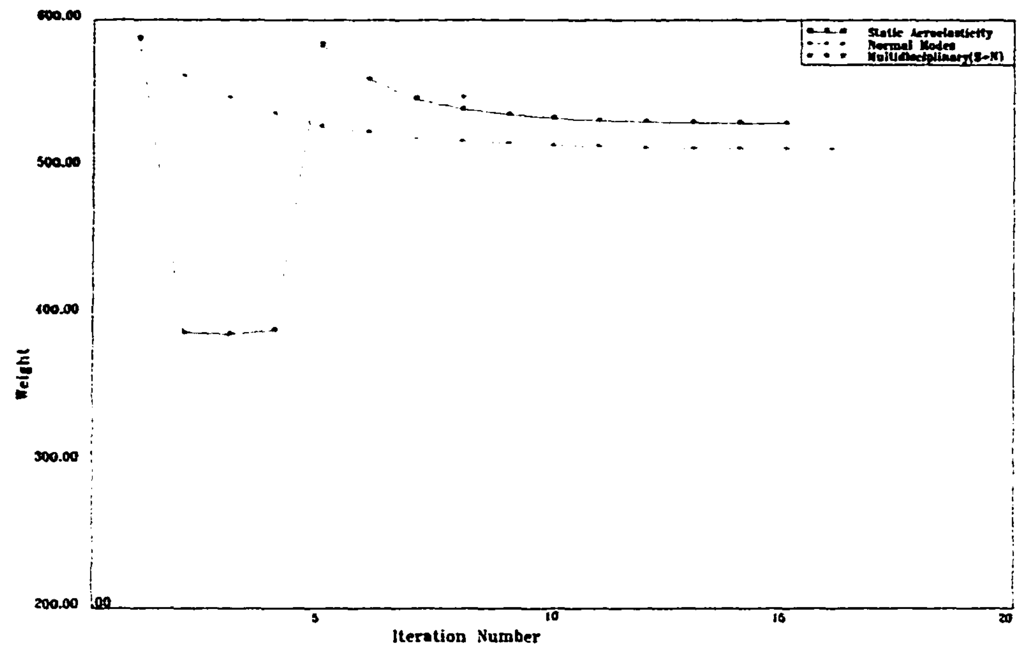

Figure 7.57 Iteration History of Design Optimization of AAW Model for Static Aeroelastcity, Normal Modes, and Multiple Disciplines (S+N): $M = 0.85$, by ZONA6 of ASTROS*

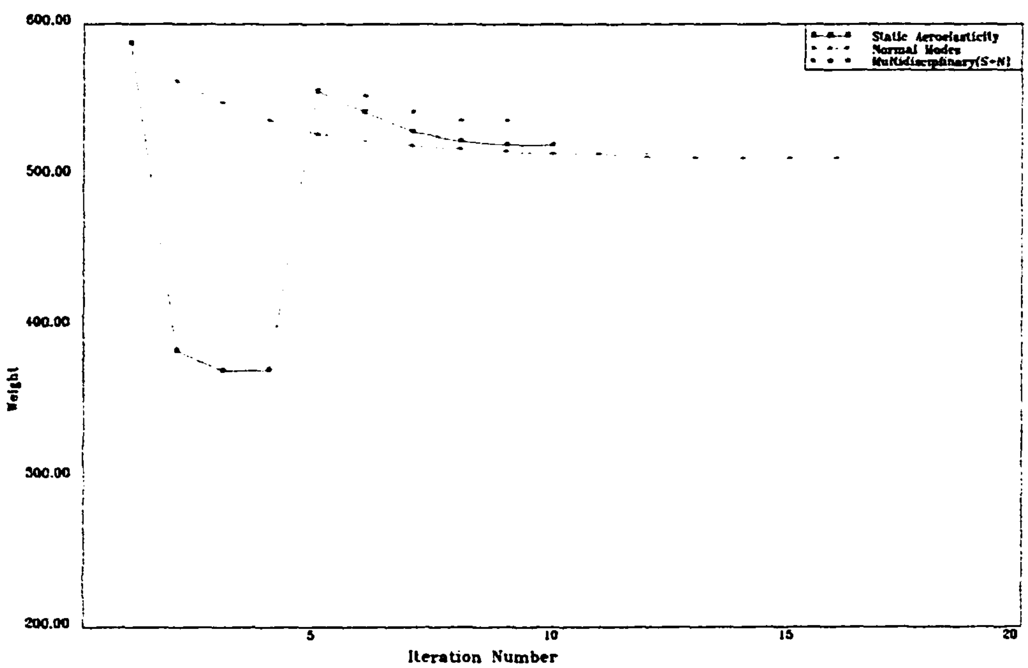

Figure 7.58 Iteration History of Design Optimization of AAW Model for Static Aeroelastcity, Normal Modes, and Multiple Disciplines (S+N): $M = 1.15$ by ZONA7 of ASTROS*

Chapter 8

CONCLUSIONS AND RECOMMENDATIONS

8.1 Conclusions

Most research in Multidisciplinary Design Optimization (MDO) to date has been dealing with somewhat specific and simplified problems. To apply MDO to practical design problems, in which many different fields or categories are combined, a process of integration to a solid application is essential. Thus, Multidisciplinary Design Optimization considering several disciplines simultaneously, the testing of the capabilities of aeroelastic analysis and optimization in the recently modified code ASTROS* throughout the unified speed regime from subsonic to hypersonic flow, and the direct application of such analyses and optimizations to complex airplane wing structures are the main characteristics of the present research. It can then be used as an example for the practical optimized design of aircraft wings in industry.

More specifically, a unified aerodynamic module has recently been developed for aeroelastic analysis, aeroservoelastic analysis, and Multidisciplinary Design Optimization applications in the whole Mach number range, and has been installed in ASTROS*. For verification and benchmarking of these new capabilities, three models, the GAF, DAST, and AAW wing models, were selected and modified as required, the new ASTROS* code was applied to these models, and its accuracy, ease of use, and applicability to practical complex aircraft wing models was tested.

The GAF model is a fighter wing model, the DAST model is a flight test wing model made of composites, and the AAW model is an airplane wing model including a fuselage and vertical and horizontal tails. These models were thought to be sufficiently complex to test the new ASTROS*. ASTROS* data for the GAF model were generated from MSC/NASTRAN data. ASTROS* and MSC/NASTRAN data for the DAST model were generated from Engineering Analysis Language (EAL, Ref. 7.3) data. The AAW model was a derivative of a MSC/NASTRAN model. For benchmarking and testing of ASTROS* with these models, static and normal modes analyses were performed by ASTROS*, and some of the analysis results and the calculated weight data were compared to those by MSC/NASTRAN where appropriate. The two sets of results compared well for the GAF model. The DAST model was modified by adding ribs and equivalent fuselage mass to the original structural model, and results could be obtained in static, normal modes, static aeroelastic, and flutter analyses that were consistent with this type of wing.

For flutter analysis, ZONA6, ZTAIC, ZONA7, and ZONA7U in ASTROS* were tested by comparison of the results to those by the root-locus method for the GAF and AAW models and to k-method results by MSC/NASTRAN for the GAF model. ZONA6 and ZTAIC were checked at M = 0.85, ZONA7 at M=1.15, and ZONA7U at M = 3.0. The DAST model only was checked at M = 0.80. The obtained flutter analysis results were reasonable for the respective types of aircraft for all the unsteady aerodynamic methods in ASTROS*.

Static aeroelastic analyses were performed for the DAST and AAW models. The stresses in the elements, the displacement at the grid points, the longitudinal stability derivatives, and the trim parameters were calculated in a pitching trim condition. ZONA6 and ZTAIC in ASTROS* were checked at $M = 0.85$, ZONA7 at $M = 1.15$, and ZONA7U at $M = 3.0$. The static aeroelastic analysis results for all steady aerodynamic methods in ASTROS* were consistent and reasonable.

Structural design optimizations for the individual disciplines of statics and normal modes were performed by ASTROS* and some by MSC/NASTRAN, and like results compared well.

Structural design optimization was performed for static aeroelasticity by ZONA6, ZTAIC, ZONA7, and ZONA7U in ASTROS* for the DAST and AAW models. The total weight was optimized with the constraints of strength, displacement, and the lowest natural frequency for the given trim condition.

Structural design optimizations with the multiple disciplines of static loads, normal modes, and static aeroelasticity were performed by ASTROS*. For multiple disciplines, the results could not be compared to those from MSC/NASTRAN because the latter code did not have multidisciplinary design optimization capability until Version 70. However, in the design optimization problems by ASTROS*, the computed accuracy could be checked by a final analysis even though it is not known whether the obtained answer is a global optimum

Structural design optimizations with a flutter constraint and multidisciplinary structural design optimization including a flutter constraint could not be performed by ASTROS* or MSC/NASTRAN due to problems with the pk-algorithm. These optimizations were performed by the approximate design optimization method for the GAF model. The sensitivity derivatives and aerodynamic loads were obtained by ZONA6 in ASTROS*. The aerodynamic loads were approximated by the minimum-state method, and flutter analyses were performed by the root-locus method. The approximate optimum problems were solved by NPSOL. The results were consistent with this type of aircraft.

Flutter suppression was achieved by obtaining control system parameters, i.e., actuator parameters and the gain margin, to maximize the flutter speed for the GAF model at $M = 0.85$. The root-locus method was used to calculate the flutter speed, and the sensitivities of the flutter dynamic pressure with respect to the design variables were calculated analytically using FORTRAN coding. The mathematical optimization problem was solved by IMSL of MS-FORTRAN Power-Station rather than by NPSOL because this case is a simple unconstrained optimization problem. The developed code performed well. The speed of the lowest aeroelastic instability was increased by about 10%.

It was shown that structural design optimization can be performed by using either powerful analysis codes or by combining them with approximate design optimization methods, for any multiple disciplines that the analysis codes can handle.

Sensitivity derivatives usually can be calculated by these analysis codes. If the analysis codes do not have the capability to perform sensitivity analysis for any discipline, however, the derivatives can nevertheless be obtained by analytical or finite difference methods, and structural design optimization can be performed for these disciplines.

8.2 Recommendations and Future Work

Benchmarking and testing of the new aerodynamic analysis modules in ASTROS* was accomplished for the developed models only for symmetric boundary conditions and the static, normal modes, static aeroelastic, and flutter disciplines. For a more realistic structural design optimization of an aircraft wing, the models should also be checked for anti-symmetric boundary conditions in roll and flutter and for other failure modes such as buckling. For these cases, the task becomes more complex; however, the methodologies are similar to the ones used here.

Modeling a control system is another difficult research field. When the forms of the transfer functions for actuators, controllers, and sensors, and the underlying relations are determined, the coefficients can be calculated by the method used here to compute flutter sensitivities and maximize flutter speed.

In the TES (Transonic Equivalent Method) used in ZTAIC of ASTROS*, the shock strength and position in the steady aerodynamics is assumed to remain stationary when the flow becomes unsteady. This is only an assumption; however, ZTAIC represents an advanced method compared with linear theories, which do not even consider shock strength. For complete consideration of the shock and any tip vortex problems, the time domain approach can be considered.

The GAF and AAW models are only marginally suitable for hypersonic flow, however, those models were, nevertheless, used for verification of ZONA7U in ASTROS* at $M = 3.0$. True hypersonic wing models should be used for testing in this flow regime.

REFERENCES

Chapter 1 Introduction

1.1 *Automated Structural Optimization System (ASTROS) User's Manual*, Ver. 10.0

1.2 Reymond, M. and Miller, M., *MSC/NASTRAN Quick Reference Guide*, Ver. 70, The MacNeal-Schwendler Corporation, 1996.

1.3 Guruswamy, G. P., "User's Guide for ENSAERO - A Multidisciplinary Program for Fluid/Structural/Control Interaction Studies of Aircraft (Release 1)", *NASA TM* 108853, Oct. 1994.

1.4 Bisplinghoff, R. L., Ashley, H., and Halfman, R. L., *Aeroelasticity*, Addison-Wesley Publishing Company, USA, 1955.

1.5 Karpel, M., "Design for Active and Passive Flutter Suppression and Gust Alleviation", *NASA CR*-3482, 1981.

1.6 Chen, P. C., Sarhaddi, D., Liu, D. D., Karpel, M., Striz, A. G., and Jung, S. Y., "A Unified Unsteady Aerodynamic Module for Aeroelastic, Aeroservoelastic, and MDO Applications", Proceedings, Confederation of European Aerospace Societies International Forum on Aeroelasticity and Structural Dynamics, 1997, Rome, Italy, June 1997.

1.7 Fung, Y. C., *An Introduction to the Theory of Aeroelasticity*, Dover Publications, Inc., New York, 1969.

1.8 Bisplinghoff, R. L., and Ashley, H., *Principles of Aeroelasticity*, Wiley Publishing Company, New York, 1962.

1.9 Johnson, E. H., and Venkayya, V. B., "Automated Structural Optimization System (ASTROS) Vol. I - Theoretical Manual:, Ver. 5.0, AFWAL-TR-88-3028, Flight Dynamics Laboratory, Wright-Patterson Air Force Base, Ohio, Dec. 1988.

Chapter 2 Structural Dynamics

2.1 Meirovitch, M., *Analytical Methods in Vibrations*, The Macmillan Company, Collier-Macmillan Limited, London, 1967.

2.2 Blakely K., *Basic Dynamic Analysis, Optimization, MSC/NASTRAN User's Guide*, Ver. 68, MacNeal-Schwendler Corporation, 1993.

2.3 Gibson, R. F., *Principles of Composite Material Mechanics*, McGraw-Hill, Inc., Singapore, 1994.

Chapter 3 Aerodynamic Analysis

3.1 Theodorsen, T., "General Theory of Aerodynamic Instability and the Mechanism of Flutter", *NACA Rept.* 496, 1935.

3.2 Garrick, I. E., and Rubinow, S. I., "Flutter and Oscillating Air Force Calculation for an Airfoil in a Two-dimensional Supersonic Flow", *NACA Rep.* 846, 1946.

3.3 Jones, R. T., "The Unsteady Lift of a Wing of Finite Aspect Ratio", *NACA Rept.* 681, 1940.

3.4 Mazelsky, B., and Drischler, J. A., "Numerical Determination of Indicial Lift and Moment Functions for a Two-Dimensional Sinking and Pitching Airfoil at Mach Numbers 0.5 and 0.6", *NACA TN* 2739, 1952.

3.5 Drischler, J. A., "Calculation and Compilation of the Unsteady Lift Functions for a Rigid Wing Subjected to Sinusoidal Gusts and to Sinusoidal Sinking Oscillations", *NACA TN* 3748, Oct. 1956.

3.6 Miles, J. W., "Transient Loading of Wide Delta Airfoils at Supersonic Speeds", *Journal of Aeronautical Science*, Vol. 18, No. 8, Aug. 1951, pp. 543-554.

3.7 Djojodihardjo, R. H., and Widnall, S. E., "A Numerical Method for the Calculation of Nonlinear Unsteady Lifting Potential Flow Problems", *AIAA Journal*, Vol. 7, No. 10, Oct. 1969, pp. 2001-2009.

3.8 Cunningham. A. M.. Jr., "Unsteady Subsonic Collocation Method for Wings with and without Control Surfaces", *Journal of Aircraft*, Vol. 9, No. 6, June. 1972, pp. 413-419.

3.9 Chen, P. C., and Liu. D. D., "A Harmonic Gradient Method for Unsteady Supersonic Flow Calculations", *Journal of Aircraft*, Vol. 22, No. 5, May 1985, pp. 371-379.

3.10 Chen, P. C., and Liu, D. D., "Unsteady Supersonic Computation of Arbitrary Wing-Body Configurations Including External Stores", *Journal of Aircraft*, Vol. 27, No. 2, Feb. 1990, pp. 108-116.

3.11 Albano, E., and Rodden, W. P., "A Doublet-Lattice Method for Calculating Lift Distribution on Oscillating Surfaces in Subsonic Flows", *AIAA Journal*, Vol. 7, No. 2, Feb. 1969, pp. 270-285.

3.12 Borland, C. J., and Rizzetta, D. P., "Nonlinear Transonic Flutter Analysis", *AIAA Journal*, Vol. 20, No. 11, Nov. 1981 pp. 1606-1615.

3.13 Guruswamy, G. P., "Computations and Aeroelastic Applications of Unsteady Transonic Aerodynamics About Wings", *Journal of Aircraft*, Vol. 21, No. 1, Jan. 1984, pp. 37-43.

3.14 Batina, J. T., Siedel, D. A., Bland, S. R., and Bennett, R. M., "Unsteady Transonic Flow Calculations for Realistic Aircraft Configurations", *Journal of Aircraft*, Vol. 26, No. 1, Jan. 1989, pp. 21-28.

3.15 Batina, J. T., "Unsteady Transonic Algorithm Improvement for Realistic Aircraft Applications", *Journal of Aircraft*, Vol. 26, No. 2, Feb. 1989, pp. 131-139.

3.16 Ballhaus, W. F., and Goorjian,P. M., "Implicit Finite-Difference Computations of Unsteady Transonic Flows about Airfoils", *AIAA Journal*, Vol. 15, No. 12, Dec. 1977, pp. 1728-1735.

3.17 Ballhaus, W. F., and Goorjian, P. M., "Computation of Unsteady Transonic Flows by the Indicial Method", *AIAA Journal*, Vol. 16, No. 2, Feb. 1978, pp. 117-124.

3.18 Ballhaus, W. F., and Jameson, A., "Implicit Approximate-Factorization Schemes for Steady Transonic Flow Problems", *AIAA Journal*, Vol. 16, No. 6, June 1978, pp. 573-579.

3.19 Nixon, D., "Calculation of Unsteady Transonic Flows Using the Integral Equation Method", *AIAA Journal,* Vol. 16, No. 9, Sep. 1978. pp. 573-579.

3.20 Fung, K. Y., and Chung, A. W., "Computations of Unsteady Transonic Aerodynamics using Prescribed Steady Pressures", *Journal of Aircraft*, Vol. 20, No. 12, Dec. 1983, pp. 1058-1061.

3.21 Landahl, M. T., *Unsteady Transonic Flow*, 2nd Edition, Cambridge University Press, New York, 1989.

3.22 Liu, D. D., Kao, Y. F., and Fung, K. Y., "An Efficient Method for Computing Unsteady Transonic Aerodynamics of Swept Wings with Control Surfaces", *Journal of Aircraft*, Vol. 25, No. 1, Jan. 1988, pp. 25-31.

3.23 Guruswamy, G. P, "Unsteady Aerodynamic and Aeroelastic Calculations for Wings Using Euler Equations", *AIAA Journal*, Vol. 28, No. 3, Mar. 1990, pp. 461-469.

3.24 Obayashi, S., and Guruswamy, G. P., "Unsteady Shock-Vortex Interaction on a Flexible Delta Wing", *Journal of Aircraft,* Vol. 29, No. 5, Sep. 1992, pp. 790-798.

3.25 Holst, T. L., Kaynak, U., Gundy, K. L., Thomas, S. D., Flores, J., and Chaderjian, N. M., "Transonic Wing Flows Using an Euler/Navier-Stokes Zonal Approach", *Journal of Aircraft,* Vol. 24, No. 1, Jan. 1987, pp. 17-24.

3.26 Volpe, G., "Inverse Airfoil Design: A Classical Approach Updated for Transonic Application", Chapter 7 of *Applied Computational Aerodynamics* Edited by Henne, P. A., Progress in Astronautics and Aeronautics, Vol. 125, AIAA, Inc., Washington, 1989.

3.27 Anderson, G. , Kolonay, R., and Eastep, F., "Control Surface Reversal in the Transonic Regime", *AIAA*-97-1385, *38th AIAA/ASME/ASCE/AHS/ASC, Structures, Structural Dynamics and Materials Conference*, Kissimmee, FL, Apr. 7-10, 1997; pp. 769-778.

3.28 Nixon, D., "Basic Equations for Unsteady Transonic Flow", Chapter 2 of *Unsteady Transonic Aerodynamics*, Edited by David Nixon, Progress in Astronautics and Aeronautics, Volume 120, AIAA, Washington, 1989.

3.29 Beam, R., and Warming, R. F., "An Implicit Finite Difference Algorithm for Hyperbolic Systems in Conservation-law Form", *Journal of Computational Physics*, Vol. 22, 1976, pp. 87-110.

3.30 Pulliam, T. H., and Chaussee, D. S., "A Diagonal Form of an Implicit Approximate Factorization Algorithm", *Journal of Computational Physics*, Vol. 39, 1981, pp. 347-363.

3.31 Obayashi, S., Guruswamy, G. P., and Goorjian, P. M., "Streamwise Upwind Algorithm for Computing Unsteady Transonic Flows past Oscillating Wings", *AIAA Journal*, Vol. 29, No. 10, Oct. 1991, pp. 1668-1677.

3.32 Baldwin, B. S., and Lomax, H., "Thin Layer Approximation and Algebraic Model for Separated Turbulent Flows", *AIAA*-78-257, 1978.

3.33 Degani, D., and Schiff, L. B., "Computations of Turbulent Supersonic Flows Around Pointed Bodies Having Crossflow Separation", *Journal of Computational Physics*, Vol. 66, No. 1, 1986, pp. 173-196.

3.34 Flores, J., "Simulation of Transonic Viscous Wing and Wing-Fuselage Flows using Zonal Method", *NASA TM*-8941, 1987.

Chapter 4 Flutter Analysis

4.1 Smilg, B., and Wasserman L. S., "Application of Three Dimensional Flutter Theory to Aircraft Structures", *ACTR* No. 4798, Material Div., Army Air Corps, Jul. 9, 1942.

4.2 Garrick, I. E., and Rubinow, S. I., "Flutter and Oscillating Air Force Calculation for an Airfoil in a Two-Dimensional Supersonic Flow", *NACA Rep.* 846, 1946.

4.3 Edwards, J. W., "Unsteady Aerodynamic Modeling and Active Aeroelastic Control", *NASA CR*-148019, Feb. 1977.

4.4 Yang, T. Y., Striz, A. G., and Guruswamy, P., "Flutter Analysis of Two-Dimensional and Two-Degree-of-Freedom Airfoils in Small Disturbance Unsteady Transonic Flow", *AFFDL-TR*-78-202, Dec. 1978.

4.5 Yang, T. Y., Guruswamy, P., and Striz, A. G., "Flutter Analysis of a *NACA* 64A006 Airfoil in Small Disturbance Transonic Flow", *Journal of Aircraft*, Vol. 17, No. 4, April 1980, pp. 225-232.

4.6 Yang, T. Y., Guruswamy, P., and Striz, A. G., "Application of Transonic Codes to Flutter Analysis of Conventional and Supercritical Airfoils", *Journal of Aircraft*, Vol. 19, April 1982, pp. 211-220.

4.7 Karpel, M., "Physically Weighted Approximations of Unsteady Aerodynamic Forces using the Minimum-State Method", *NASA TP*-3025,1991.

4.8 Karpel, M., "Extensions to the Minimum-State Aeroelastic Modeling Method", *AIAA Journal*, Vol. 29, No. 11, Nov. 1991, pp. 2007-2009.

4.9 Karpel, M., "Reduced-Order Aeroelastic Models via Dynamic Residualization", *Journal of Aircraft*, Vol. 27, No. 5, May 1990, pp. 449-455.

4.10 Vepa, R., "Finite State Modeling of Aeroelastic Systems", *NASA CR*-2779, Feb. 1977.

4.11 Tiffany, M. S. H., and Adams, W. M. Jr., "Nonlinear Programming Extensions to Rational Function Approximations of Unsteady Aerodynamics", *AIAA*-87-0854, AIAA/ASCE/AHS/ASC 28th Structures, Structural Dynamics, and Materials Conference, Monterey, CA., April 9-12, 1987, pp. 406-420.

4.12 Leishman, J., and Crouse, G., "A State-Space Method of Unsteady Aerodynamics in a Compressible Flow for Flutter Analyses", *AIAA*-89-0022, 27th Aerospace Sciences Meeting, Reno, Nevada Jan. 9-12, 1989, pp. 1-11.

4.13 Yates, E. C. Jr., Wynne, E. C., Farmer, M. G., and Desmarais, R. N., "Prediction of Transonic Flutter for a Supercritical Wing by Modified Strip Analysis", *Journal of Aircraft*, Vol. 19, No. 11, Nov. 1982, pp. 999-1004.

4.14 Guruswamy, G. P., "Transonic Aeroelastic Analysis of the B-1 Wing", *Journal of Aircraft*, Vol. 23, No. 7, July 1986, pp. 547-553.

4.15 Cunningham, H. J., Batina, J. T., and Bennet, R. M., "Mordern Wing Flutter Analysis by Computational Fluid Dynamics Methods", *Journal of Aircraft*, Vol. 25, No. 10, Oct. 1988, pp. 962-968.

4.16 Guruswamy, G. P., "Unsteady Aerodynamic and Aeroelastic Calculations for Wings Using Euler Equations", *AIAA Journal*, Vol. 28, No. 3, Mar. 1990, pp. 461-469.

4.17 Lee-Rausch, E. M., and Batina, J. T., "Wing Flutter Boundary Prediction Using Unsteady Euler Aerodynamic Method", *Journal of Aircraft*, Vol. 32, No. 2, March-April 1995, pp. 416-422.

4.18 Rodden, W. P. and Johnson, E. H., *Aeroelastic Analysis, User's Guide of MSC/NASTRAN,* Ver. 68, The MacNeal-Schwendler Corporation, Oct. 1994.

Chapter 5 Aeroservoelasticity

5.1 Abel, I., Perry, B. III, and Murrow, H. N., "Two Synthesis Techniques Applied to Flutter Suppression on a Flight Research Wing", *Journal of Guidance & Control*, Vol. 1, 1977, pp. 303-333.

5.2 Roger, K. L., Hodges, G. E., and Felt, L., "Active Flutter Suppression - A Flight Test Demonstration", *Journal of Aircraft*, Vol. 12, No. 6, June 1975, pp. 551-556.

5.3 Murrow H. N., and Eckstrom C. V., "Drones for Aerodynamic and Structural Testing (DAST) - A Status Report", *Journal of Aircraft*, Vol. 16, No. 8, Aug. 1979, pp. 521-526.

5.4. Newsom, J. R., "A Method for Obtaining Practical Flutter-Suppression Control Laws Using Results of Optimal Control Theory", *NASA TP*-1471, Aug. 1979.

5.5. Newsom, J. R., Abel, I., and Dunn, H. J., "Application of Two Design Methods for Active Flutter Suppression and Wind-Tunnel Test Results", *NASA TP*-1653, 1980.

5.6 Mukhopadhyay, V., Newsom, J. R., and Abel, A., "A Method for Obtaining Reduced-Order Control Laws for High-Order Systems Using Optimization Techniques", *NASA TP*-1876, Aug. 1981.

5.7 Karpel, M., "Design for Active Flutter Suppression and Gust Alleviation using State-Space Aeroelastic Modeling", *Journal of Aircraft*, Vol. 19, No. 3, March 1982, pp. 221-227.

5.8 Karpel, M., "Time-Domain Aeroservoelastic Modeling using Weighted Unsteady Aerodynamic Forces", *Journal of Guidance, Control & Dynamics*, Vol. 13, No. 1, Jan. 1990, pp. 30-37.

5.9 Karpel, M., "FASER - Computer Program for Aeroservoelastic Design", *TAE Report* 733, Jan. 1995.

5.10 Guruswamy, G. P., "Transonic Aeroelasticity of Fighter Wings with Active Control Surfaces", *Journal of Aircraft*, Vol. 26, No. 7, July 1989, pp. 682-684.

5.11 Adams, W. M., Jr., Christhilf, D. M., Waszak, M. R., and Srinathkumar, S., "Design, Test, and Evaluation of Three Active Flutter Suppression Controllers", *NASA TM*-4338, 1992.

5.12 Gupta, K. K., and Brenner, M. J., "Development of an Integrated Aeroservoelastic Analysis Program and Correlation With Test Data", *NASA TP*-3120, 1991.

5.13 Srinathkumar, S., "Eigenvalue/Eigenvector Assignment Using Output Feedback", *NASA TP*-1118, 1978.

5.14 Mukhopadhyay, V., "An Interactive Software for Conceptual Wing Flutter Analysis and Parametric Study", *NASA TM*-110276, NASA Langley Research Center, Hampton, Virginia, Aug. 1996.

5.15 Noll, T. E., Perry III, B. Tiffany, S. H., Cole, S. R., Buttrill, C. S., Adams, W. M., Jr., Houck, J. A., Srinathkumar, S., Mukhopadhyay, V., Pototzky, A. S., Heer. J., MacGraw, S. M., Miller, G., Ryan, R., Brosnan, M., Havert, J., and Klepl, M., "Aeroservoelastic Wind-Tunnel Investigations Using the Active Flexible Wing Model – Status and Recent Accomplishments", *NASA TM*-101570, NASA Langley Research Center, Hampton, Virginia, Apr. 1989.

5.16 Mukhopadhyay, V., Perry III, B., and Noll, T. E., "Flutter Suppression Control Law Synthesis for the Active Flexible Wing Model", *NASA TM*-101584, NASA Langley Research Center, Hampton, Virginia, May 1989.

5.17 Noll, T. E., Perry III, B., and Gilbert, M. G., "Recent Activities in Aeroservoelasticity at the NASA Langley Research Center", *NASA TM*-101582, NASA Langley Research Center, Hampton, Virginia, Aug. 1996.

5.18 Noll, T. E., "Aeroserveelasticity", *NASA TM*-102620, NASA Langley Research Center, Hampton, Virginia, Mar. 1990

5.19 Karpel, M., "Sensitivity Derivatives of Flutter Characteristics and Stability Margins for Aeroservoelastic Design", *Journal of Aircraft*, Vol. 27, No. 4, Apr. 1990, pp. 368-375.

Chapter 6 Sensitivity Analysis and Structural Design Optimization

6.1 Logan, T. R., "Strategy for Multilevel Optimization of Aircraft", *Journal of Aircraft*, Vol. 27. No. 12, Dec. 1990, pp. 1068-1072.

6.2 Malone, B., and Mason W. H., "Multidisciplinary Optimization in Aircraft Design Using Analytic Technology Models", *Journal of Aircraft*, Vol. 32, No. 2, March 1995, pp. 431-438.

6.3 Sobieszczanski-Sobieski, J., "Structural Optimization by Multilevel Decomposition", *AIAA Journal*, Vol. 23, No. 11, Nov. 1985, pp. 1775-1782.

6.4 Sobieszczanski-Sobieski, J., "Sensitivity of Complex, Internally Coupled Systems", *AIAA Journal*, Vol. 28, No. 1, Jan. 1990, pp. 153-160.

6.5 Turner, M. J., "Optimization of Structures to Satisfy Flutter Requirements", *AIAA Journal*, Vol. 7, No. 5, May 1969, pp. 945-951.

6.6 Rudisill, S., and Bhatia, K. G., "Optimization of Complex Structures to Satisfy Flutter Requirements", *AIAA Journal*, Vol. 9, No. 8, Aug. 1971, pp. 1487-1491.

6.7 Wilkinson, K., and Lerner, E., "Practical Design of Minimum-Weight Aircraft Structures for Strength and Flutter Requirements", *Journal of Aircraft*, Vol. 13, No. 8, Aug. 1976, pp. 614-624.

6.8 Wilkinson, K., Markowitz, J., Lerner, E., and George, D., "FASTOP: A Flutter and Strength Optimization Program for Lifting-surface Structures", *Journal of Aircraft*, Vol. 14, No. 6, June 1977, pp. 561-587.

6.9 Karpel, M., "Multidisciplinary Optimization of Aeroservoelastic Systems using Reduced-Size Models", *Journal of Aircraft*, Vol. 29, No. 5, Sept. 1992, pp. 939-946.

6.10 Karpel, M., "Multidisciplinary Optimization of Aeroservoelastic System", *NASA CR*-191255, Nov. 1992.

6.11 Livne, E., Schmit, L. A., and Friedman, P. P., "Towards Integrated Multidisciplinary Synthesis of Actively Controlled Fiber Composite Wings", *Journal of Aircraft*, Vol. 27, No. 12, Dec. 1990, pp. 979-992.

6.12 Karpel, M., "Structural Optimization for Aeroelastic Control Effectiveness", *Journal of Aircraft*, Vol. 26, No. 5, May 1989, pp. 493-495.

6.13 Miura, H., and Neil, D. J., "Applications of Structural Optimization Methods to Fixed-Wing Aircraft and Spacecraft in the 1980s", *NASA TM*-103939, May 1992.

6.14 Karpel, M., "Time Simulation of Flutter with Large Stiffness Changes", *NASA TM*-107650, July 1992.

6.15 Gabriele, G. A., and Ragsdell, K. M., "Large Scale Nonlinear Program Using the Generalized Reduced Gradient Method", *Journal of Mechanical Design*, Vol. 102, July 1980, pp. 566-573.

6.16 Vanderplaats, G. N., "An Efficient Feasible Direction Algorithm for Design Synthesis", *AIAA Journal*, Vol. 22, No. 11, Nov. 1984, pp. 1633-1640.

6.17 Schmit, L. A., Jr. and Miura, H., "Approximate Concept for Efficient Structural Synthesis", *NASA CP*-2552, March 1976.

6.18 Jin, I. M., and Schmit, L. A., "Control Design Variable Linking for Optimization of Structural/Control Systems", *NASA CR*-4493, 1993.

6.19 Haftka, R. T., and Gürdal, Z., *Elements of Structural Optimization*, 3rd Edition, Kluwer Academic Publishers, Dordrecht, The Netherlands, 1992.

6.20 Arslan, A. E., and Carlson, L. A., "Integrated Determination of Sensitivity Derivatives for an Aeroelastic Transonic Wing", *Journal of Aircraft*, Vol. 33, No. 1, Jan. 1996, pp. 224-231.

6.21 Moore G. J., *Design Sensitivity and Optimization, MSC/NASTRAN User's Guide*, Version 68, MacNeal-Schwendler Corporation, 1994.

Chapter 7 Applications to Models

7.1 Chen, P. C., Private Communication, ZONA Technology, Inc., 1997.

7.2 Liu, D. D., Chen, P. C., Yao, Z. X., and Sarhaddi, D., "Recent Advances in Lifting Methods", Paper No. 4, *Proceedings at International Forum on Aeroelasticity and Structural Dynamics*, U.K., June 1995.

7.3 Whetstone, W. D., *Engineering Analysis Language Reference Manual (EAL)*, Vol. 1, General Rules and Utility Processing, Engineering Information System, Inc., San Jose, CA., July, 1983.

7.4 Pendleton, E., Bessette, D., Field, P., Miller, G., and Griffin, K., "The Active Aeroelastic Wing Flight Research Program", *AIAA-98-1972, 39th AIAA/ASME/ASCE/AHS/ASC Structures, Structural Dynamics, and Materials Conference and Exhibit*, and *AIAA/ASME/AHS Adaptive Structures Forum*, Long Beach, CA, Apr. 20-23, 1998, pp. 2518-2530.

7.5 Pendleton, E., Griffin, K., Kehoe, M., and Perry, B., "A Flight Research Program for Active Aeroelastic Wing Technology", *AIAA-96-1574, Proceedings of the 37th AIAA Structures, Structural Dynamics, and Materials Conference*, Salt Lake City, Utah, April 15-17, 1996, pp. 2263-2273.

7.6 Liu, D. D., Yao, Z. X., Sarhaddi, D., and Chavez, F., "From Piston Theory to a Unified Hypersonic-Supersonic Lifting Surface Method", *Journal of Aircraft*, Vol. 34, No. 3, May-June 1997, pp. 304-313.

Computer and Graphics Bibliography

o Gill, P. E., Murray, W., Saunders, M. A., and Wright, M. H., *User's Guide for NPSOL (Version 4.0) : A FORTRAN Package for Nonlinear Programming*, Stanford University, Stanford, CA., Jan. 1986.

o *FORTRAN Power-Station Programmer's Guide*, Version 4.0, Microsoft Corporation, 1995.

o *Fortran Power-Station Reference*, Version 4.0, Microsoft Corporation, 1995.

o Omura, G., *Mastering Autocad 13 for Windows*, Sybex, San Francisco, 1995.

IMAGE EVALUATION TEST TARGET (QA-3)

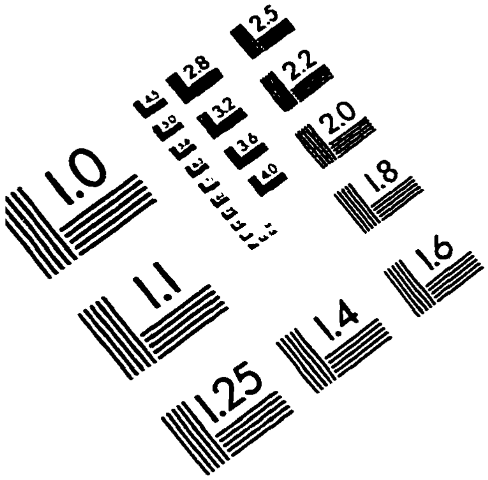

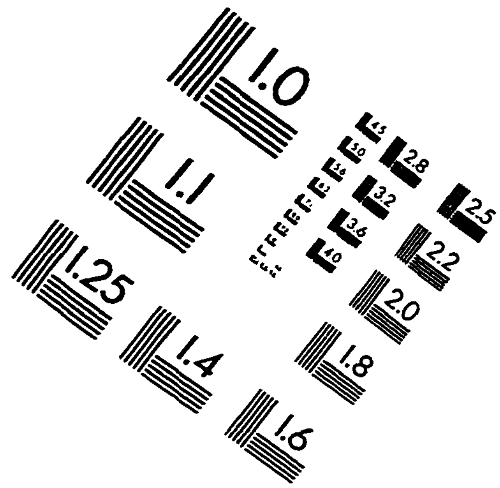

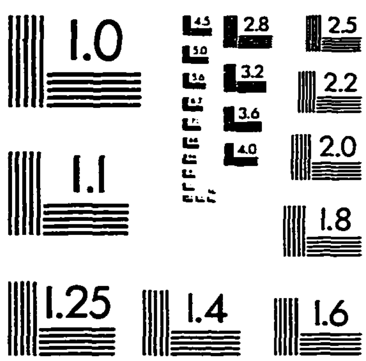

150mm

6"

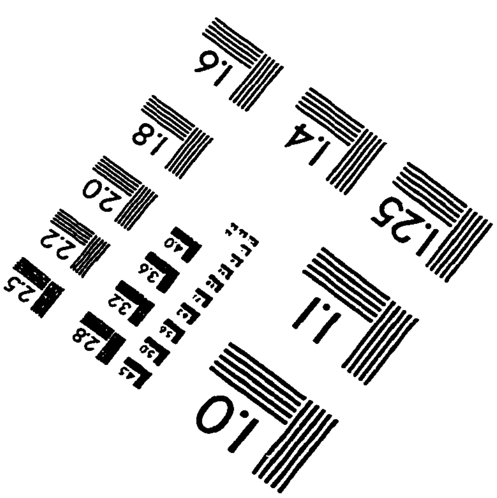

APPLIED IMAGE . Inc
1653 East Main Street
Rochester, NY 14609 USA
Phone: 716/482-0300
Fax: 716/288-5989